COMSOL MODELLING OF UNIFORM CORROSION OF USED NUCLEAR FUEL CANISTERS

MOHD MOINUDDIN

A THESIS SUBMITTED TO

THE FACULTY OF GRADUATE STUDIES

IN PARTIAL FULFILLMENT OF THE REQUIREMENTS FOR THE DEGREE OF

MASTER OF APPLIED SCIENCE

GRADUATE PROGRAM IN
CIVIL ENGINEERING

YORK UNIVERSITY
TORONTO, CANADA

April 2018

ABSTRACT

Uniform corrosion of copper can occur in spent nuclear fuel canisters placed in deep geological repositories (DGR). To estimate the minimum thickness for safe design of canisters, it is necessary to analyze the corrosion rate. Copper Corrosion Model (CCM) has been used to model the corrosion process taking into account processes including adsorption/desorption, precipitation/dissolution, oxidation, and parameters including oxygen concentration, chloride, moisture and associated rate constants. In this work, CCM has been incorporated in COMSOL and validated with CCM. Once validated, the COMSOL model was used to examine the sensitivity of various parameters with respect to copper corrosion. It was found that initial chloride concentration, adsorption/desorption of cupric ions are parameters that most effect copper corrosion. The developed model can be used to simulate the uniform corrosion process under DGR conditions with more complexity including variation in temperature, saturation and pressure, and aid in the design of copper canisters.

DEDICATION

I dedicate this thesis to my parents, Noor Begum and Yousuf Harun. I hope this thesis will be a stepping stone to the dreams you had for me for all those years ago when you chose to provide me the best resources you could.

ACKNOWLEDGEMENTS

First of all, I would like to thank Dr. Magdalena Krol for her energetic encouragements and invaluable support throughout the project. I would also like to offer special thanks to Dr. Scott Briggs for his patient guidance in moving the tasks far. I would also like to thank Fraser King for his invaluable suggestions in the development of this project. I would also like to extend my thanks to NWMO for all their support in this project. Lastly, I would like to thank all the people involved in making this project a success and considering to leave the world a better place for the future generations.

TABLE OF CONTENTS

LIST OF TABLES

LIST OF FIGURES

CHAPTER ONE: BACKGROUND

1.1 Introduction

There are over four hundred nuclear reactors worldwide under operation for power generation and sixty new nuclear plants are under construction as of April 2017 (NEI, 2017). In Canada, 16% of electricity is generated from nuclear power with eighteen nuclear reactors located in Ontario and one in New Brunswick (WNA, 2017). These reactors are responsible for more than 50% of Ontario's power (OPG, 2017) and therefore are an important part of Ontario's energy production. Nuclear power generation requires the use of radioactive fuel. After the nuclear fuel in these reactors is used, the spent fuel needs to be properly disposed of, such that the radioactivity remaining in the UFC does not come into contact with the biosphere.

Canada has more than 32 million kg of spent nuclear fuel (SNF) with more than 1 million kg generated every year (NWMO, 2016). There are different types of nuclear waste which are categorized based on the level of radioactivity:

- LLW - Low Level Waste (e.g. Mops, clothes used in vicinity of nuclear reactors)
- ILW - Intermediate Level Waste (e.g. heat exchangers)
- HLW - High Level Waste (e.g. fuel bundles)

For HLW, the radioactivity levels of the SNF may not be safe for up to 100,000 years, whereas LLW has a half-life of less than 500 years (NEI, 2014)

After the removal of the SNF from the reactor, it is placed in pools for up to 10 years where their heat and radioactivity decreases. The cooled SNF is then placed in thick concrete containers to contain the radiation which have a minimum design life of 50 years. The SNF can then be placed in a new concrete container until a permanent solution is designed. This is a temporary solution for the current situation (NWMO, 2017a).

A permanent solution to storing SNF has been proposed by many countries, including Canada, which typically involves the burial of the SNF in deep geological repositories (DGRs).

1.1.1 Examples of Current or Previously Operational DGRs

Waste Isolation Pilot Plant (WIPP) (USA):

The WIPP repository began its operation in 1999 with a design capacity of more than 170,000 m^3 (equivalent to 30 blimps). The wastes are stored in plastic lined steel drums and wooden boxes. The repository is over 650 m deep and stores intermediate level radioactive wastes (actinides) from USA's defense program (NRC, 1996).

Morsleben Repository (Germany):

The Morsleben repository was a potash and rock salt mine which was later used for storing LLW and ILW. This repository was in operation for 25 years, storing over 35,000 m^3 of radioactive waste (BfS, 2016). The repository was shut down in 1991 due to structural collapse (WISE, 1991).

Asse II Mine (Germany):

The Asse II repository is 765 m deep and, similarly to the Morseleben repository, it was previously a rock salt and potash mine. This repository was used for LLW and ILW storage but was shut down due to brine contamination (BfS, 2017).

Yucca Mountain Nuclear Waste Repository (USA):

Yucca Mountain is located in Nevada, USA. This repository was under construction for many decades and was supposed to be used for HLW and ILW. However, due to funding and regulatory concerns, construction was halted (Eureka, 2017).

1.1.2 Testing areas and planned repositories

Mont Terri Rock Laboratory is an underground repository lab being used by the Swiss nuclear agency (NAGRA) for various tests including the analysis of corrosion of carbon steel. It is a 50 m long test tunnel with a diameter of 3 m located at a depth of 300 m. This tunnel has dummy containers backfilled with bentonite to analyze the effects of corrosion. The dummy containers had heating elements to mimic radioactive conditions. It was found that the corrosion rate decreases with time due to the formation of protective corrosion layer of oxides in geological conditions. The average corrosion rate was found to be between 1-5 um/year (Nagra, 2014; Necib et al., 2017; Thury and Bossart, 1999). Moreover, another laboratory, GRIMSEL test site (GTS), in Switzerland developed by

NAGRA, has extensive research and development works ongoing for safe disposal of nuclear waste (Kallio, 1997).

Onkalo spent nuclear fuel repository is being constructed by Posiva (Finland) and will extend up to 450 m in depth. The disposal of radioactive materials is based on the KBS-3 concept developed by SKB (Sweden) and Posiva, where the radioactive materials will be placed inside copper canisters that are deposited in vertical tunnels and surrounded by bentonite (Posiva, 2018).

The French nuclear waste agency, Andra, is planning to dispose highly radioactive waste produced from generating 75% of the country's electric power, near the village of Bure (Broomby, 2014).

Site selection in Switzerland is currently ongoing for deep geological repository (Le News, 2017). The required containment period is around two hundred thousand years for disposal of the HLW. Retrieval of the HLW after placement in DGR is also taken into account as the spent fuel containing uranium and plutonium can be used in energy production by future generations with advanced technology (Nagra, 2018).

Spent fuel repository is being planned to be constructed at Forsmark, Sweden by SKB. Construction is expected to take around 10 years, starting at 2020. This repository can store over 6000 canisters at a depth of 500 m covering an area of three to four square kilometers (SKB, 2018).

Countries including Czech, China and Switzerland are considering carbon steel for the use of canister material (Rani and Shrivastava, 2016; Zhang et al., 2017), whereas Russia and Japan are considering the use various materials, including vitrified glass, in the disposal of spent nuclear fuel (Kitamura et al., 2016; Poluektov et al., 2017).

1.1.3 Canadian Deep Geological Repository

In Canada, the Nuclear Waste Management Organization (NWMO) is responsible for designing the Canadian DGR. The plan is for the repository to be 500 m below the earth's surface away from the surface biosphere.

To prevent the interaction of SNF with the surface biosphere, a multi-barrier system is planned for the DGR which would provide different levels of protection to prevent exposure of radioactive materials to the biosphere. The system consists of:

1) the hardened ceramic pellet of uranium
2) zirconium alloy tubes
3) copper-coated steel canister (UFC)
4) bentonite layer
5) bedrock

Each item in the multi-barrier system has a specific purpose. The ceramic uranium pellets are inserted inside Zirconium alloy tubes (corrosion resistant) which are then inserted inside the steel canister (structurally durable), coated with copper (corrosion resistant) surrounded by bentonite layer (NWMO, 2017b). Bentonite consists mainly of montmorillonite which has the ability to swell upon contact with water. This property, along with the low permeability of the material, adds to the protection of the UFC (Suorsa, 2017). This clay layer will be surrounded by a natural geological sedimentary or crystalline rock layer (bedrock). The container, bentonite, and copper coating (items 3&4) make up the Engineered Barrier system (EBS).

1.2 Copper coating

UFCs are coated with copper to form a corrosion barrier, however when copper is exposed to moisture, oxygen, or chloride, it can deteriorate or undergo corrosion. This can potentially lead to UFC failure and therefore it is necessary to find out the maximum amount of copper that could corrode, given the repository conditions, in order to establish a minimum thickness for the UFC copper coating.

The main purpose of the copper barrier is to ensure that the fuel inside the container remains intact for up to a period of million years (Canadian design life) and to prevent the structural steel support from being exposed to groundwater. Studies on the feasibility of copper being used as canister material has been considered for nearly 40 years by several nuclear agencies, including the Swedish and Finnish agencies. Copper is considered for the UFC because of its thermodynamic ability to have immunity against spontaneous corrosion in anoxic oxygen free water conditions of DGR. In addition, it is a cheaper material than noble metals which also have these corrosion-resistant properties (Scully and Edwards, 2013; King et al., 2012).

Oxygen-free phosphorus doped (OFP) copper can be used for the outer UFC coating in cases where deformation is expected under mechanical stresses. OFP can contain oxygen up to 3 ppm and phosphorus in the range of 40-60 ppm. This grade of copper is both structurally and thermally stable (Aalto et al., 1996) and the addition of phosphorus increases the creep strength of copper (Pettersson, 2010).

In the case of Canada, the copper is used as a coating and the steel canister provides the structural support, therefore OFP copper is not required.

1.2.1 Mark II UFC Design

The previous Canadian UFC design (Mark I) consisted of 100 mm thick steel coated with 25 mm thick copper. Mark II, has 3 mm copper coating making it thinner, lighter and thereby with a higher degree of flexibility in handling (Scully et al., 2016) (Figure 1.1). Mark II also has a semi-spherical cap end, as opposed to the flat end of the Mark I design. The switch to the Mark II design was based on improvements in manufacturing technologies (Standish et al., 2016). The thickness of 3mm copper was chosen since NWMO's current corrosion allowance is 1.27 mm for 1 million years – based on preliminary studies (Scully and Edwards, 2013). This allowance is continually being reviewed based on site-specific data and modelling efforts.

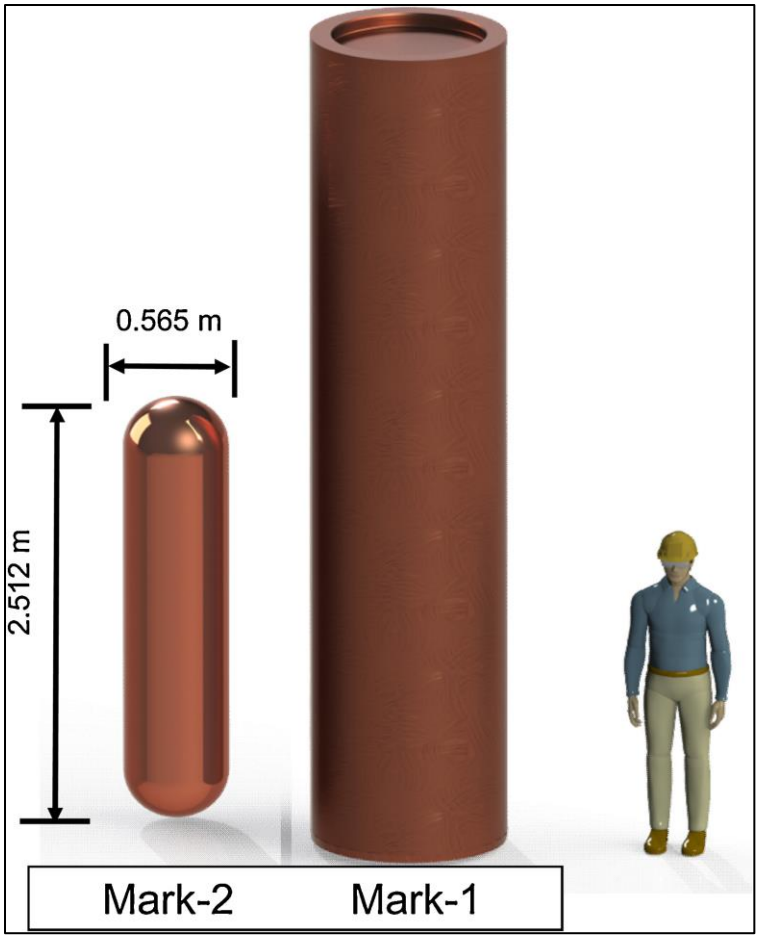

Figure 1.1: Comparison of Mark I and Mark II designs (Courtesy of NWMO)

1.3 Conditions in Canadian DGR

The conditions in the DGR will be different from that of the surface. The temperature can be higher by as much as 7^{o}C from the surface temperature (Carvalho et al., 2013). Initially this will not affect the conditions near the vicinity of the radioactive waste as the canisters temperature will be quite high due to radioactivity (as much as 80^{o}C during the first hundred years. The oxygen levels in the repository may accumulate during excavation and construction. In general, the DGR will experience an initial warm oxidation period followed by a cool anoxic period. The presence of oxygen and high temperature may enhance the corrosion process initially which would decrease gradually with time (Standish et al., 2016).

1.3.1 Possible copper corrosion processes

Several processes lead to different types of corrosion such as uniform corrosion, pitting corrosion, stress corrosion, and microbial influenced corrosion (MIC).

Pitting or localized corrosion refers to pits or holes developed on the surface due to chemical reactions or mechanical damage e.g. stainless steel in chloride solutions can develop pits. Some studies including the ones done by King and Lilja (2014) and Scully and Edwards (2013) indicate that pitting is less likely to occur in DGR conditions.

Stress corrosion occurs when the metal is subjected to tensile stress in a corrosive environment (e.g. stainless steel in hydrogen sulfide media). However, in the DGR system, the canister will likely experience compressive stress due to bentonite and rock surrounding the copper canister. Therefore, stress corrosion will have limited effect on the canister.

Microbial influenced corrosion (MIC) of copper occurs when sulfides and sulfide reducing bacteria are present. This kind of corrosion can occur during anaerobic conditions which might occur after 100 years in DGR (Standish et al., 2016).

Uniform corrosion of copper occurs in DGR environments containing oxygen and chlorides (King, 2016). Previous NWMO studies have shown that the UFC will be primarily subjected to uniform corrosion (Kwong, 2011). Therefore, this study focuses on uniform corrosion modelling.

To date, predictions of corrosion have been based on a custom-designed code known as the Copper Corrosion Model (CCM) (King et al., 2008; King and Kolar, 2000). This study considers the uniform corrosion version of CCM i.e. CCM-UC for predicting the extent of corrosion in the DGR. However, CCM is limited in use due to its single dimensionality, lack of support (it is non-commercial) and difficulty to parameterize. Therefore, this project focuses on developing a COMSOL version of the CCM, validating and verifying the code, and using it to understand the effect of various parameters on UFC corrosion.

1.4 Conclusion

There is a growing amount of spent nuclear fuel generated from nuclear power plants that needs appropriate disposal. Permanent solution of disposal involves burying the spent nuclear fuel 500 m deep underground in copper canisters surrounded by bentonite. Under deep repository conditions, the copper canister is susceptible to corrosion which may be uniform, pitting and/or microbial. Uniform corrosion will likely have the most impact during the initial period of canister burial and therefore it is important to understand the effects of uniform corrosion on the canister. This study aims to do that, with the use of a numerical model.

CHAPTER TWO: LITERATURE REVIEW

2.1 Introduction and background

Copper is among the first metals used by civilization. Artifacts dating back to 9000 BC made of copper have been excavated from Mesopotamian civilization - now Egypt (De Ryck et al., 2005). Copper has been used for sea water application due to its ability to form a complex surface film which protects the metal layers below thereby leading to low corrosion potential (Huh et al., 2014). Due to the stability of copper metal evidenced by its electrochemistry and the availability of data from past copper artifacts, among other properties, copper is considered a suitable material for the protection of long-lived nuclear fuel canisters by many nuclear agencies (Kitamura et al., 2016), including the Canadian Nuclear Waste Management Organization (NMWO).

NWMO is implementing Adaptive Phased Management (APM), the approach selected by the Government of Canada in 2007 for long-term management of used nuclear fuel. The goal of APM is long-term containment and isolation of used nuclear fuel in a Deep Geological Repository (DGR) constructed in a suitable formation in either sedimentary or crystalline rock at a depth of approximately 500 meters. The design of a DGR includes an engineered barrier system (EBS) consisting of a suitably low permeability rock to act as a natural barrier. Within the EBS, a steel used fuel container (UFC) is coated in copper and encapsulated within an engineered bentonite clay buffer (Figure 2.1).

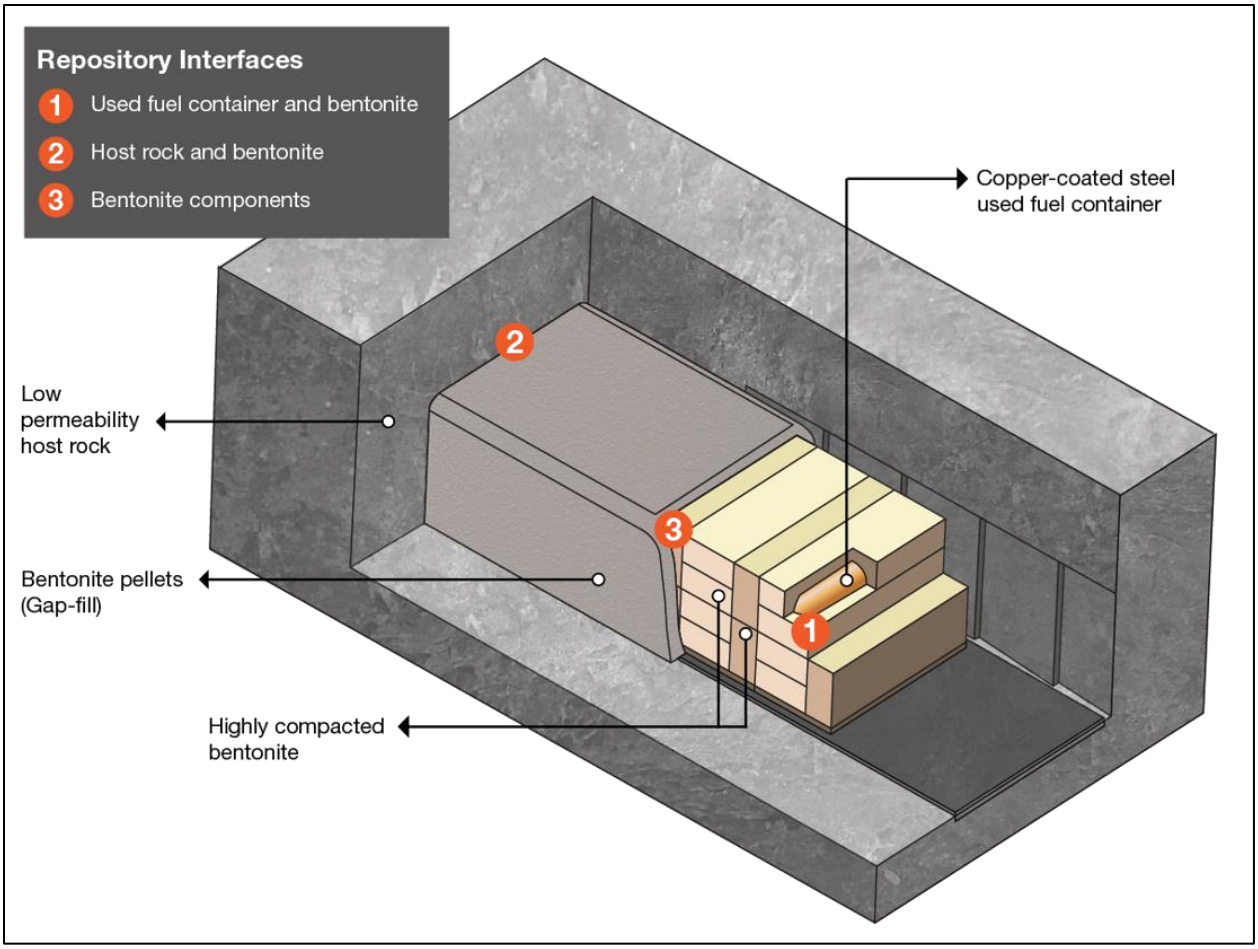

Figure 2.1: Canadian deep geological repository design concept for the long-term management of used nuclear fuel (Courtesy of NWMO, 2018).

While stable in many environments, copper can still be susceptible to corrosion in the DGR due to the presence of oxygen, chloride, and water. Of interest, therefore, is various reactions that could take place and their respective reaction rates. In the DGR, corrosion will be limited by the amount of oxidant present and the mass transfer restrictions by highly compacted bentonite. However, during the construction and emplacement period, there will be oxygen present in the DGR which would enter the repository. The oxygen content of groundwater in DGR is expected to be less than 0.1 mg/l which would be negligible compared to the oxygen trapped during construction (Mattsson, 1980). In addition, shortly after emplacement of the used fuel containers, there will be elevated temperature in the repository due to the heat generated from radioactivity. This warm oxidation period can extend up to hundreds of years favoring aerobic corrosion

processes. The trapped oxygen is gradually consumed during the corrosion process and as oxygen is depleted, copper corrosion will decrease unless sulfide is present which could lead to microbially influenced corrosion (MIC) (Johansson et al., 2017). Radiolysis of water could also produce oxidants, however these oxidants will be limited by the low humidity environment in the vicinity of the canister because of high temperature (King et al. 2002, Standish et al. 2016).

2.1.1 Corrosion allowance

Different corrosion processes may occur in DGR namely uniform, pitting, stress and microbial influenced corrosion. Preliminary estimate for uniform corrosion in the DGR was estimated to be 0.17 mm based on initial oxygen content expected in the repository (King, 2005; Kwong, 2011) . For pitting corrosion, the initial estimate of 0.1 mm is predicted based on surface roughening in the form of under-deposit corrosion over distinct pitting (King, 2005). Stress corrosion cracking occurs due to tensile stress and is not considered the to be a significant contributor to corrosion since the canister is more likely to be under compressive stress in the DGR (King and Kolar, 2005). Preliminary corrosion allowance for microbial corrosion is based on sulfate reducing bacteria producing a continuous concentration of 3 ppm of hydrogen sulfide which is estimated to result in a corrosion rate of 1 mm for 1 million years (King and Kolar, 1996).

The total copper corrosion allowance would therefore amount to: 1.27 mm (0.17 mm from uniform corrosion, 0.1 mm for pitting corrosion, and 1 mm for microbial corrosion) (Kwong, 2011). This value is a preliminary estimate based on different assumptions.

2.2 Copper Corrosion Model

To better understand the different mechanisms that can lead to uniform corrosion, the Copper Corrosion Model (CCM) was developed by King and Kolar (2000). This model calculates the corrosion potential under different conditions and considers reactions such as redox, precipitation/dissolution, adsorption/desorption and mass transport of different species.

Uniform corrosion is when the surface of the metal is covered by a thin layer of corrosion which may include compounds of oxides, sulfides, hydroxides and chlorides.

When modelling uniform corrosion, CCM considers ten chemical species including oxygen, chloride, cuprite, paratacamite and iron. To determine the corrosion rate or the extent of corrosion, it is necessary to determine the speed of the individual reactions. In other words, the kinetics of the reactions involved in corrosion processes which can aid in the estimation of corrosion extent. The rate constants used in CCM for the DGR environment have been obtained based on previous qualitative or quantitative analysis. These are described in this chapter.

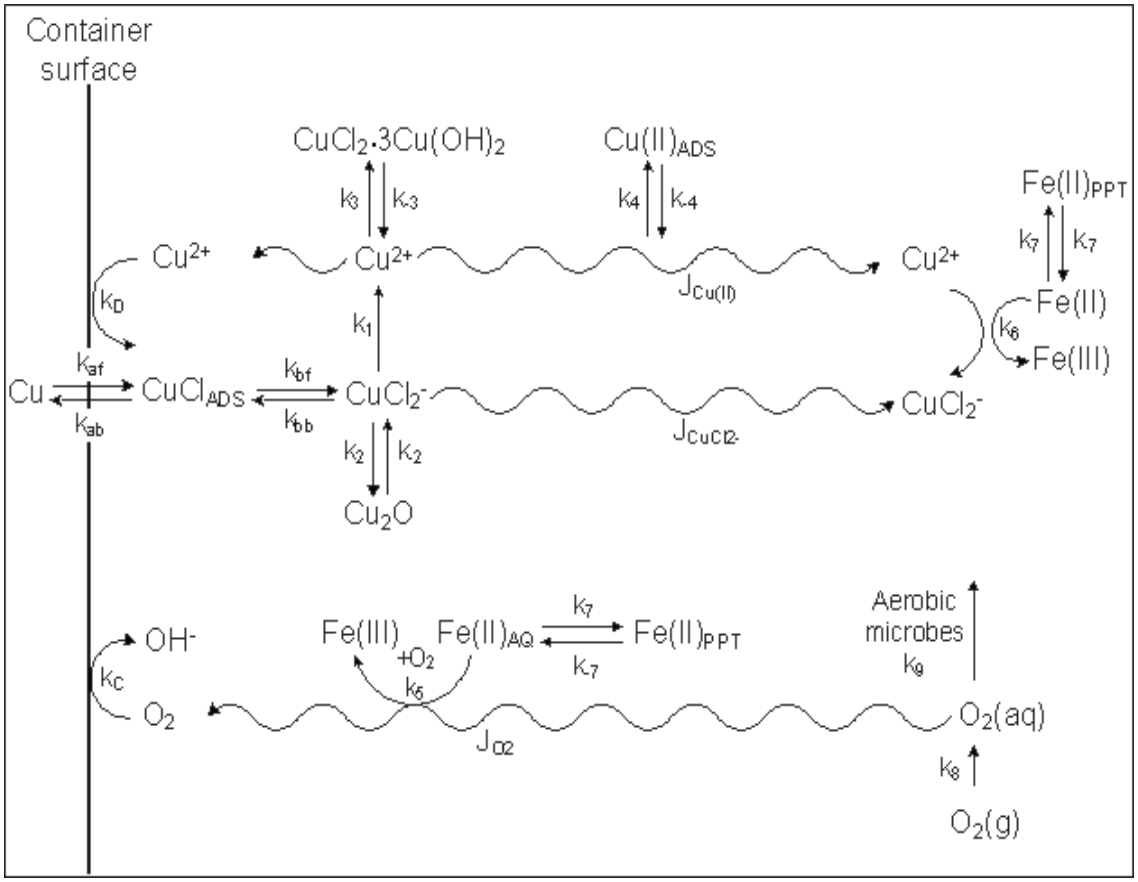

Figure 2.2: Uniform Corrosion Schematic (King et al, 2008). The above diagram shows the different reactions along with their associated rate constants (k_i).

2.3 Kinetics

The rate of corrosion depends on the kinetics of several reactions including adsorption/desorption, precipitation/dissolution and oxidation/reduction as shown in Figure 2.2. These are described below.

2.3.1 Homogenous Oxidation of Copper Chloride by Oxygen (k_1)

The homogenous reaction of copper chloride oxidation by O_2 is included in the CCM reaction scheme:

$$4CuCl_2^- + O_2 + 2H_2O \rightarrow 4Cu^{2+} + 8Cl^- + 4OH^- \qquad 2.1$$

The rate of consumption of oxygen can be expressed as:

$$-\frac{\partial c_0}{\partial t} = \frac{k_1}{4} c_0 c_1 \qquad 2.2$$

This rate constant is dependent upon the formation of copper chloride ions and the presence of oxygen. This constant influences the formation of cupric ions which can undergo adsorption or interfacial reductions which can significantly affect the corrosion process.

A study conducted by Jhaveri and Sharma (1967) indicates that cuprous ions have high affinity for forming chloride compounds over oxychlorides in aerated chloride media. The rate constant involved depends upon the ionic strength and the pH of the media. As seen from the reaction and equation, this rate constant affects the availability of copper ions and oxygen. This in turn can have chain effect on other products formed including atacamite and adsorption of copper on bentonite thereby affecting the corrosion process significantly, as seen in the CCM.

From experiments on Red Sea water conducted by Sharma and Millero (1988a), the following equation for k_1 has been derived (King, 2016):

$$\log k_1 = 11.38 - 2064/T - 3.69\sqrt{\frac{c_6}{1 - 0.1103\, c_6}} + 0.73\sqrt{\frac{c_6}{1 - 0.1103\, c_6}} \qquad 2.3$$

where,

c_0	Dissolved O_2
c_1	Dissolved $CuCl_2^-$
c_6	Dissolved Cl^-
T	Temperature

The value of k_1 is dependent upon the concentration of chloride and temperature of the system. Moreover, at a constant chloride solution, the presence of ions of magnesium and calcium reduces the rate of reaction (Sharma and Millero, 1988b). The temperature in the simulation is assumed to be at 25^{o}C though the temperature in the DGR will be higher at the beginning of the DGR lifecycle and decrease with time (Guo, 2011).

2.3.2 Precipitation and Dissolution of Solid Cuprite (k_2/k_{-2})

The precipitation and dissolution of cuprite is given by King (2016):

$$2CuCl_2^- + H_2O \underset{k_{-2}}{\overset{k_2}{\rightleftharpoons}} Cu_2O + 4Cl^- + 2H^+ \qquad 2.4$$

There is uncertainty in the mechanism of the formation of cuprous oxide. In presence of chloride ions, the anodic reaction will involve the formation of CuCl and $Cu(OH)_{ads}$. With high pH, the adsorbed copper ions can react to form monolayer of Cu_2O. Moreover, the formation of Cu_2O is independent of chloride and is dependent on pH (Elsner et al., 1988). Furthermore, in an experiment conducted by Hutchison et al. (2017), Cu_2O and CuCl were the primary corrosion product when copper and its alloys are exposed to artificial human perspiration (pH 6.5).

The rate of precipitation of cuprite can be expressed as:

$$\frac{\partial(Sc_2)}{\partial t} = \varepsilon_a S \frac{k_2}{2} \max(0, c_1 - c_1^{sat}) \qquad 2.5$$

The rate of dissolution can be shown as (King, 2016):

$$-\frac{\partial(Sc_2)}{\partial t} = k_{-2}c_2 \qquad 2.6$$

where,

c_1	Dissolved $CuCl_2^-$
c_1^{sat}	Concentration of $CuCl_2^-$ at saturation
c_2	Precipitated Cu_2O
ε_a	Accessible porosity
S	Water Saturation

Since there are no known reported values of k_2 and k_{-2}, precipitation and dissolution of cuprite in the CCM model was taken as 1 s^{-1} and 0.1 s^{-1}, respectively based on limited experimental works conducted by King and Légère (King, 2016).

Using these values, it was found that no Cu_2O is formed in the CCM model (Chapter 3). These results are reasonable since pH was not taken into account (i.e. pH was assumed to be neutral). In addition, the experiments conducted by Cano et al. (2005) indicate that the formation of cuprite is observed at 160^{o}C. The temperature in the CCM and COMSOL simulations was taken as 25^{o}C. Furthermore, another study indicates that the formation of Cu_2O occur generally in atmospheric environments containing hydrogen sulfide (Tran et al., 2003; Watanabe et al., 2009b; Watanabe et al., 2009a). In sea water and marine atmosphere, cuprite and paratacamite were the major components of copper corrosion (patina). In this case, where copper was completely immersed in marine environments, cuprite formation decreased with time until the patina component was predominantly paratacamite (Veleva and Farro, 2012). Therefore, the temperature, pH and absence of sulfide assumption can affect the prediction of formation of Cu_2O in CCM.

2.3.3 Dissolution and Precipitation of Paratacamite (k_3/k_{-3})

Paratacamite/atacamite is named after the Atacama Desert in northern Chile. It normally occurs as powdery light green corrosion on copper (Scott, 2000). The precipitation of paratacamite ($CuCl_2.3Cu(OH)_2$) occurs from a supersaturated solution of dissolved Cu(II) (King et al., 2001; King et al., 2002b) while atacamite formation is dependent on the concentration of chloride. With the presence of chloride and in low

sulfate concentration, atacamite was found to precipitate from chalcopyrite (mineral of copper). This was observed under low acidity of pH > 2.8 (McDonald and Muir, 2007). In the DGR model considered, sulfur is not considered during the warm oxidizing period and the pH is taken as neutral. The precipitation/dissolution of paratacamite is represented by the kinetic rate constants k_3/k_{-3} and expressed as:

$$4Cu^{2+} + 6OH^- + 2Cl^- \rightarrow CuCl_2.3Cu(OH)_2 \qquad 2.7$$

where the rate of precipitation (k_3) is given by:

$$\frac{\partial c_4}{\partial t} = \varepsilon_a S \frac{k_3}{4} \max(0, c_3 - c_3^{sat}) \qquad 2.8$$

and the expression for dissolution (k_{-3}) from (King, 2016) is:

$$-\frac{\partial c_4}{\partial t} = k_{-3} c_4 \qquad 2.9$$

where

c_3	Dissolved Cu^{2+}
c_3^{sat}	Dissolved Cu^{2+} at saturation
c_4	Precipitated $CuCl_2.3Cu(OH)_2$
ε_a	Accessible porosity
S	Saturation

Atacamite is formed from interaction of copper ions with bentonite based on unpublished work of King and Strandlund. Moreover, it was found that coverage of the copper surface by paratacamite would form a passive film ((King et al., 2001).

Others have found that under tropical atmospheric conditions, paratacamite was present as one of the components of corrosion of copper (Mendoza et al., 2004). Under marine conditions, cuprite (Cu_2O) changes to paratacamite with time (Veleva et al., 1996). In a study conducted by Kosec et al. (2015), cuprous oxide and paratacamite was found to be the products of corrosion. Here the copper was placed in aerated saline solutions to study the extent of corrosion. The corrosion rate decreased from 15 um/yr (initially) to less than 1 um/yr for a four-year exposure period. In the simulation, paratacamite is formed and not cuprous oxide. Moreover, according to this study the copper in bentonite

underwent pitting corrosion. This might be attributed to different methods (or sources of error) of measurement i.e. the sensors used in this experiment were themselves susceptible to localized corrosion.

Few dissolution and precipitation rates for atacamite/paratacamite are found in literature. The dissolution rate of atacamite was reported to be $10^{-7.55}$–$10^{-5.14}$ mol dm^{-2} s^{-1} for pH 5.5-4 (Le Roux et al., 2016). This range is based on experiments conducted in arid conditions. The absolute value for the corresponding rate constant (k_{-3}) for the CCM model was taken as 10^{-6} s^{-1} based on King (2016).

2.3.4 Adsorption and Desorption of Copper Ions (k_4/k_{-4})

How an element adsorbs to a surface is typically a function of temperature, species type, and surface type. For example, Cu^{2+} can adsorb strongly onto sodium bentonite (Ryan and King, 1994) and possibly other mineral surfaces within the repository and geosphere. Conversely, Cu^{2+} species in the form of anionic species like $CuCl_2^-$ do not adsorb strongly onto bentonite (King et al. 1992, 2001, 2002b).

Sorption isotherms are used to quantify the amount of sorption occurring. Linear isotherms are commonly used when describing the adsorption of radionuclides on clay (Cook 1988), since the concentration of species is small compared with the cation-exchange capacity (CEC) of the clay and sorption and desorption are assumed to be fast relative to the rate of diffusion (King 2016). However, buffer material experiments have shown that the copper concentration close to the corroding surface can actually exceed the CEC of the bentonite and therefore a linear isotherm does not capture the exchange accurately (King et al. 1992, Litke et al. 1992). A Langmuir-type isotherm has been suggested by Ryan and King (1994) after conducting equilibrium adsorption studies on loose and compacted Na-bentonite. In addition, a study conducted by Bhattacharyya and Gupta (2006) showed that copper adsorption onto montmorillonite and kaolinite followed a Langmuir isotherm. They found the rate constant to be 7.7 x 10^{-2} to 15.4 x 10^{-2} g/mg-min. This implies that based on the constituents of different clays, there will be different adsorption characteristics. The adsorption characteristics of copper in bentonite is dependent upon several factors including pH, temperature and surface area (Gupta and G. Bhattacharyya, 2012).

The rate of adsorption and desorption of copper ions can be described by the equation

$$Cu^{2+} + 2Y^{-} \underset{k_{-4}}{\overset{k_4}{\rightleftharpoons}} CuY_2 \qquad 2.10$$

where Y represents a monovalent adsorption site

Assuming a Langmuir isotherm, the rate of the forward reaction for adsorption mechanism can be expressed as:

$$\frac{\partial c_5}{\partial t} = \varepsilon_a S k_4 c_3 (c_5^{max} - c_5) \qquad 2.11$$

and the rate of reverse reaction (adsorption) from King (2016):

$$-\frac{\partial c_5}{\partial t} = k_{-4} c_5 \qquad 2.12$$

where

c_3	Dissolved Cu^{2+}
c_5	Adsorbed Cu(II)
c_5^{max}	Maximum adsorption capacity of bentonite for Cu(II)

Ryan and King (2016) calculated the rate constant, k_4 to be 2 x 10^{-3} $dm^3 \cdot mol^{-1} \cdot s^{-1}$ and the rate of desorption, k_{-4}, to be 1 x 10^{-6} s^{-1}.

Experiments conducted by Al-Qunaibit et al. (2005) indicate that the rate constant observed for different bentonite masses (0 – 2 g) for copper adsorption was observed to be in the range of 10^{-4} to 10^{-3} min^{-1}. This experiment was conducted for 80 ppm Cu^{2+} with copper nitrate solution with dry bentonite. The amount adsorbed was calculated using initial and final concentration of copper ions in the solution. Desorption was estimated by placing the clay pellets in water and calcium chloride solution. This was calculated from equilibrium concentration obtained from sorption. No desorption was observed in case of deionized water. In calcium chloride solution, the exchange of copper ions was around 1% for 24 hours of shaking. The maximum adsorption obtained was 0.9 g/g clay. The corresponding value for c_5^{max} was 0.3 mol/kg i.e. 0.02 g/g clay (King, 2016). The difference might be attributed to the fact that the clay types are different (as clay from Saudi Arabia was used for former and Saskatchewan for latter). Regardless, all experiments showed

the desorption was low compared to adsorption (Al-Qunaibit et al., 2005). This is also reflected in the CCM.

With a decrease in pH, the adsorption of copper decreases in sodium bentonite based on a study conducted by Abollino et al. (2003). Moreover, another study with natural bentonite indicate that the removal of copper is increased with increasing pH with optimum efficiency for copper removal at pH 7 (Veli and Alyüz, 2007). pH was not considered in the CCM but may influence the adsorption and desorption of Cu(II).

Experiments conducted on bentonite with temperature variations (20-50^{o}C) indicated that the adsorption of copper decreases with increase in temperature (Bereket et al., 1997). The temperature considered in the CCM was 25^{o}C. The initial temperature in the DGR will be high extending up to 80^{o}C during the first hundred years. With time, this temperature would decrease, and the adsorption of copper would increase.

2.3.5 Interfacial Reactions (k_a, k_{bb}, k_{af}, k_{bf}, k_{ab}, k_c, k_d)

There are several species that can react on the UFC surface including O_2(aq), $CuCl_2^-$, Cu^{2+} and Cl^-. These reactions are called interfacial and are made up of anodic dissolution of copper (Equation 2.13 and 2.14) and cathodic reduction of dissolved oxygen (Equation 2.17).

The anodic reactions between copper and chlorides can be represented by:

$$Cu + Cl^- \underset{k_{ab}}{\overset{k_{af}}{\rightleftharpoons}} CuCl_{ADS} + e^- \qquad 2.13$$

$$CuCl_{ADS} + Cl^- \underset{k_{bb}}{\overset{k_{bf}}{\rightleftharpoons}} CuCl_2^- \qquad 2.14$$

A combined electrochemical rate constant (k_a) can be used when expressing the anodic current as shown in the equation below:

$$k_a = \frac{k_{af}k_{bf}}{k_{ab}} \qquad 2.15$$

King et al. (1995) found that k_a has a value of 3.3 x 10^{-8} m^4/mol-s based on experiments conducted on copper covered in bentonite placed in copper chloride solutions of different concentrations in the range of 0.1 – 1.0 mol/dm^{-3}. The reverse

reaction rate, for the conversion of $CuCl_2^-$ to adsorbed CuCl, k_{bb}, has value of 1.42 x 10^{-4} m/s. The corresponding anodic current generated can be expressed as (King and Litke (unpublished data); King (2016)):

$$i_a = n_a F \left\{ k_a [Cl^-]^2 \exp \frac{F}{RT} (E - E_a) - k_{bb} [CuCl_2^-] \right\} \qquad 2.16$$

where,

$[Cl^-]$	Concentration of chloride
$[CuCl_2^-]$	Concentration of cuprous chloride ions
i_a	Current for anodic dissolution of Cu
F	Faraday's constant (96487 C/mol)
R	Universal gas constant
E_a	Anodic potential under standard conditions
E	Potential in the system

The reduction of oxygen can occur in steps involving the formation of intermediate peroxide under acidic conditions. This was observed with experiments conducted with sulfuric acid where oxygen was bubbled through (Hsueh et al., 1983). The formation of intermediate peroxide is not considered in the CCM model since a neutral pH was assumed within the repository.

The reducing reaction can be stated as follows:

$$O_2 + 2\ H_2O + 4\ e^- \xrightarrow{k_c} 4\ OH^- \qquad 2.17$$

A value for the electrochemical constant for the reduction of oxygen (k_c) was found to be 1.7 x 10^{-9} dm/s, is based on the reduction of copper in 1 mol/dm^3 of NaCl under standard conditions of unit activity with 1 atmospheric pressure and 25^oC (King et al., 1995). The reaction can lead to increase in the value of pH which can favor the formation of Cu_2O. This reduction of oxygen at the copper bentonite interface can influence the cathodic current (i_c). This can be expressed as the following form of Nernst equation (King et al., 1994; King et al., 1995; King, 2016):

$$i_c = -n_c F k_c [O_2] \exp \frac{\alpha_c F}{RT} (E - E_c) \qquad 2.18$$

where,

i_c	Cathodic reduction of O_2
n_c	Number of electrons involved in reduction of O_2
$[O_2]$	Concentration of oxygen
α_c	Cathodic mass transfer coefficient
E_c	Cathodic potential at standard conditions
E	Potential in the system

The other cathodic reaction that can occur at the bentonite-UFC interface is the reduction of Cu^{2+}:

$$Cu^{2+} + 2\ Cl^- + e^- \xrightarrow{k_d} CuCl_2^- \qquad 2.19$$

Experiments conducted by Morel et al. (1979) indicate that copper placed in chloride media had copper (II) from the bulk solution reduced at the electrode surface to copper (I). This is then stabilized by forming complexes with chloride. Moreover, another study by Oglesby et al. (1977) indicates that the potentiometric response of copper(II) ions in chloride media increases with ionic activity. This indicates that the potential increases with more chloride activity.

The value of k_d was found out to be 2×10^{-8} dm·s^{-1} at 25 ^oC based on studies conducted by Hurlen (1961). This value was derived from current potential curves obtained from dissolution of copper in chloride solution.

The corresponding cathodic current for this reaction can be expressed as (King, 2016):

$$i_d = -n_d F k_d [Cu^{2+}] \exp\left(-\frac{\alpha_d F}{RT} (E - E_d)\right) \qquad 2.20$$

where,

i_d	Current for reduction of Cu^{2+}
n_d	Number of electrons involved in reduction of Cu^{2+}
$[Cu^{2+}]$	Concentration of cupric ions

α_d	Cathodic mass transfer coefficient
E_d	Cathodic potential at standard conditions
E	Potential in the system

2.4 Copper in different environments

For the prediction of corrosion behavior of copper, several experiments have been analyzed taking into consideration the behavior in aqueous solutions, atmospheric conditions and bentonite. These are discussed below.

2.4.1 Copper in aqueous solutions

Experiments conducted by Lal and Thirsk (1953) indicate that in neutral and alkaline chloride solutions, the anodic behavior of copper generates cuprous chloride film through dissolution and precipitation processes. Copper metal gets dissolved in the electrolyte as ions. These ions precipitate and reversibly get deposited forming cuprous chloride film. It was observed that with the increase in the chloride concentration, there is an increase in current density. Moreover, it was also found that the potentials obtained from neutral chloride solutions were slightly lower than that of alkaline solutions.

Under acidic conditions, copper in the presence of chloride solutions results in the formation of complexes including $CuCl_2^-$ and $CuCl_3^-$. The process is controlled by activation or concentration polarization rather than by diffusion indicating that the rate of chemical reactions is faster compared to the transport of chemical species present (Hurlen, 1961).

Extensive studies conducted by Ives and Rawson (1962) show that copper has a strong tendency to react with dissolved oxygen to form cuprite (Cu_2O) - the primary product in acidic aqueous media (k_2 in CCM). A thin layer (20 Å) of this cuprous oxide is produced which can easily break up with mechanical strains. Therefore, this layer does not provide a corrosion protective surface. The change in potential (in volts) due to the presence of Cu-Cu_2O couple in an acidic medium can be expressed as:

$$E_{Cu|Cu2O,\ H+} = 0.471 - 0.0592\ pH \qquad 2.21$$

As the film grows, it breaks up and can lead to the formation of CuO. The change in potential due to Cu-CuO couple can be expressed in a similar way as:

$$E_{Cu|CuO,\ H+} = 0.570 - 0.0592\ pH \qquad 2.22$$

This formation of copper (I) oxide may be thermodynamically favored. This compound then dissolves to provide copper (II) ions. The change in potential can be given as:

$$E_{Cu2O,\ Cu2+,\ H+} = 0.203 + 0.0592\ pH + 0.0592 \log [Cu^{2+}] \qquad 2.23$$

where

$[Cu^{2+}]$ = concentration of copper (II) ions

This study by Ives and Rawson (1962) proposed a duplex film corrosion model. In this model, the copper metal is surrounded by a layer of Cu_2O followed by a porous film which is formed by the disruption of the oxide film below it. The disruption of the oxide film occurs as the oxide, which is insulated from the metal, falls off or dissolves into the solution. The kinetics of the reactions for the formation of Cu_2O is first order with respect to the dissolved oxygen (Ives and Rawson, 1962). Moreover, as seen from previous equations, the pH of the solution is one factor in determining the potentials. Other factors may include environment, presence of oxygen or other redox active species, temperature, etc.

The passivation of the surface of copper in 3% NaCl solution (with applied external potential) consisted of Cu_2O and CuCl. The surface film is weak and is easily displaced by mechanical abrasion. With the increase in potential, the cuprous ions react with chloride ions resulting formation of $CuCl_2^-$ ions (Sugawara et al., 1965). This supports the CCM model for the rate constants k_{bf} and k_{bb}.

Copper can exist in both monovalent and divalent states. Experiments conducted on copper tubes with aerated supply water shows that chloride can react with cuprous ions to form CuCl (Cornwell et al., 1973). As expected, increase in the chloride led to an increase in the corrosion rate as these chlorides can hydrolyze to form Cu_2O precipitates (k_2/k_{-2}) in neutral pH media. The stability of the Cu_2O scales was found to be dependent upon both pH and chloride concentrations (Palit and Pehkonen, 2000). Furthermore, tests conducted by Boulay and Edwards (2001) in alkaline soft water containing dissolved

oxygen of about 9 mg/L, indicate that pH of 7 results in five times higher corrosion rate (high copper corrosion by-products) than pH of 9.5 (high copper particulates).

In case of long-term stagnation experiments for tap water in copper pipes indicate that the consumption of oxygen can be described by 1st order kinetic law. Moreover, the corrosion scales formed consisted primarily of Cu_2O and a carbonate compound of copper (Merkel et al., 2002).

Experiments conducted in neutral tap water indicate that initially the surface of copper is covered by cuprous, cupric oxides and cupric hydroxide. With the passage of time, the copper surface is covered by a uniform layer of cuprous oxide which is stable and retards the corrosion process (Shim and Kim, 2004). This indicates that the stability of cuprous oxide is influenced by the presence of hard water (contain calcium and magnesium minerals) or soft water (contains sodium) (Diffen, 2014) .

Another experiment conducted by Vargas et al. (2009) state that the corrosion due to DO (Dissolved Oxygen) for tap water can be described by zeroth-order kinetic rate law. The oxidation of copper is limited by pH which is controlled by the nature of the corrosion scale. Transport diffusion is negligible for experiments conducted with dissolved oxygen in tap water in copper pipes. The main parameters that control the oxidation of copper kinetics are pH and temperature (Vargas et al., 2010).

Studies conducted by González-Dávila et al. (2009) in seawater and NaCl solution indicate that oxidation of Cu(II) to Cu(I) is dependent upon both the chloride concentration and the pH. The rate can be expressed as

$$\frac{\mathrm{d[Cu(I)]}}{\mathrm{dt}} = -\mathrm{k}\,[\mathrm{Cu(I)}][\mathrm{O_2}] \qquad 2.24$$

where k is in kg/mol-min

In case of the presence of excess oxygen, the reaction may follow pseudo 1st order kinetics. The expressions obtained for the rate constant for the oxidation of Cu(I) for sodium chloride (0.1-0.7 M ionic strength) solution and seawater are as follows:

$$\log k_{NaCl} = 5.221 + 0.609\ pH - 1915\ T - 1.818\sqrt{I} + 0.408\ I \quad 2.25$$

$$\log k_{sea\ water} = 5.036 + 0.514\ pH - 1765\ T - 1.101\sqrt{I} + 0.233\ I \quad 2.26$$

A similar experiment was conducted earlier by Sharma and Millero (1988) and the rate constant was expressed as:

$$\log k = 12.32 + 0.12\ pH - 2064\ /\ T - 3.69\sqrt{I} + 0.73\ I \quad 2.27$$

This above equation was modified in terms of chloride concentration (King, 2016). This is expressed as:

$$\log k_1 = 11.38 - 2064/\ T - 3.69\sqrt{\frac{[Cl^-]}{1 - 0.1103\ [Cl^-]}} + 0.73\sqrt{\frac{[Cl^-]}{1 - 0.1103\ [Cl^-]}} \quad 2.28$$

Investigations conducted on the anodic dissolution of copper in flowing sodium chloride solutions with a temperature range between 25 - 175 ^oC indicate that the process is diffusion controlled with primary product being $CuCl_2^-$. This study indicates that the anodic process depended on the square of the chloride concentration and independent of the pH (Bacarella and Griess, 1973). The corresponding reaction can be expressed as:

$$Cu + 2\ Cl^- = CuCl_2^- \quad 2.29$$

This supports the equations obtained from King 2016. The corresponding current for the anodic process in terms of reaction rates was expressed as:

$$i_a = n_a\ F\left\{k_a\ [Cl^-]^2 \exp\frac{F}{RT}\ (E - E_a)\ - k_{bb}\ [CuCl_2^-]\right\} \quad 2.30$$

A study conducted with copper in O_2 free water indicate that a monolayer of Cu_2O is formed after 6 months of exposure. Hydrogen gas was produced as per the following reaction:

$$Cu + H_2O \rightarrow Cu_2O + H_2 \qquad 2.31$$

The copper present in the aqueous solution had a concentration range of 4-5 ug/L (Boman et al., 2014).

The major products of Cu corrosion are Cu_2O (s) and Cu (II) (aq) for tap water. Mass and charge balance indicated that most Cu (II) species are soluble in water leaving behind a film of Cu_2O. The kinetic investigation demonstrated that the mechanism involves simultaneous dissolution and formation of the film rather than a stepwise mechanism (Zhou et al., 2016).

2.4.2 Copper in atmospheric conditions

According to a study conducted by Odnevall and Leygraf (1995), the atmospheric corrosion of copper is highly dependent upon the relative humidity. With the increase in relative humidity, there is an increase in the thickness of the cuprite layer. This means that increasing moisture can lead to increase in growth of cuprite.

Moreover, under atmospheric conditions, a layer of only a few nanometers thick forms on the surface of copper which is greenish in color consisting of mainly copper (I) oxide. This reaction proceeds if sufficient oxygen is available (Clarelli et al., 2014).

2.4.3 Copper in bentonite

Bentonite is considered for surrounding the copper canisters in the DGR by many countries including Canada, Sweden, Finland and Korea (KAERI; NMWO, 2018). It is composed primarily of hydrous magnesium-calcium-aluminum silicate called montmorillonite which is under a clay group known as smectite. It is formed in nature from volcanic ash.

A study conducted by Finnish nuclear disposal program for 10 months (Huttunen-Saarivirta et al., 2016) indicate that when copper is placed in an abiotic system (sterilized artificial groundwater) Cu_2O is the major corrosion product. The anodic reaction proceeds as follows:

$$2\ Cu + H_2O \rightarrow Cu_2O + 2\ H^+ + 2\ e^- \qquad 2.32$$

In case of presence of oxygen, the mechanisms of cathodic reactions could be:

$$O_2 + 4\ H^+ + 4\ e^- \rightarrow 2\ H_2O \qquad 2.33$$

or

$$O_2 + H_2O + 4\ e^- \rightarrow 4\ OH^- \qquad 2.34$$

The former cathodic reaction has been used to describe the formation of cuprite where the hydrogen ions produced in the anodic reactions gets consumed. There were two layers of Cu_2O film produced: an inner protective thin layer which was surrounded by a porous outer layer (Huttunen-Saarivirta et al., 2016; Vargas et al., 2009). This observation is consistent with the studies of copper in aqueous solutions *'duplex film corrosion model'* (Ives and Rawson 1962).

With organo-bentonite, adsorption of copper ions followed the Sips adsorption model over Langmuir or Freundlich models. The adsorption process was found to occur through chemisorption with the process being endothermic, irreversible and non-spontaneous. With the increase in pH from 1 to 3, there was an increase in adsorption. Moreover, the kinetic data followed pseudo-second-order over a pseudo-first order model (Sandy et al., 2012). This indicates that the initial conditions of DGR with high temperature, there would be high adsorption which would gradually decrease with a decrease in temperature. Moreover, since the process is irreversible, the desorption rate would be low or negligible compared to the adsorption rate. According to a study by Glatstein and Francisca (2015), copper adsorption follows both linear and Freundlich models for experiments conducted on copper (nitrate compound) with sodium bentonite which show that ionic strength does not influence the adsorption process. The equilibrium was reached in this laboratory experiment within few hours for the solution concentration of 1-500 mg/L. Reaction kinetics over diffusion kinetics was the main driver for adsorption (Glatstein and Francisca, 2015).

For pH 1.5-2, no adsorption of Cu(II) was observed by Gok et al. (2008). This changes as the pH is increased from 2-5.5 indicating that with higher pH there is more adsorption of copper onto bentonite (Gok et al., 2008). Moreover, another study indicated that Cu^{2+} ions with bentonite show higher adsorption with an increase in pH. Langmuir isotherm corresponded to the adsorption trend over Freundlich with adsorption kinetics following pseudo-second order (Melichová and Hromada, 2013).

With the increase in pH, there are more Cu (II) ions adsorbed onto bentonite clay. However, with a decrease in pH, there is hydration of the metal followed by hydrolysis giving acidic properties to the metal solution (Uddin, 2017). Under acid activated conditions, there is more adsorption Cu(II) onto bentonite. This is indicated by Koyuncu and Kul (2014) who state that acid activation condition results in the formation of smaller pores in solid particles resulting in higher adsorption. A study conducted by Anna et al. (2015) indicated that in case of Ca-bentonite, similar to that of Na-bentonite, increasing pH favors more adsorption of Cu^{2+}.

A study conducted in case of binary solutions of Cu(II)/Cr(III) on GMZ bentonite indicate that Cr(III) have greater tendency to be adsorbed than Cu(II). This leads to Cu(II) remaining in the solution. This shows that in presence of other ions, the adsorption of Cu(II) can be preferred or inhibited depending upon their nature (Chen et al., 2015).

2.5 Corrosion models

CCM was developed to aid in understanding of copper corrosion mechanisms under DGR conditions. It is one of the only computer models capable of estimating the corrosion potentials, current densities, and species concentrations. There are other computational models that include corrosion in their calculations, although none are as robust and detailed as CCM. These other models are described in the following sections.

2.5.1 STEADYQL model

This model was developed initially for study of soil solutions by Furrer et al. (1989) for SKB. This model is used considering the thermodynamic boundary conditions of copper in bentonite under anoxic conditions. This model uses *partial or quasi steady state assumption* for the development of kinetic model based on thermodynamic and kinetic information (Werme et al., 1992). The basics of this model is shown in Figure 2.3, where the domain is represented by a “box”. The interaction of water along with the dissolved solutes and the materials within the box can be represented by slow and fast processes. Fast reactions include equilibrium reactions between dissolved solid and surface constituents. Slow reactions include diffusion and kinetic reactions. This algorithm of this model takes into account mass, flux and mole balance. This steady state model can be used for single ‘box’. This model was later modified to multi-box model to take into account diffusion processes as shown in Figure 2.5.

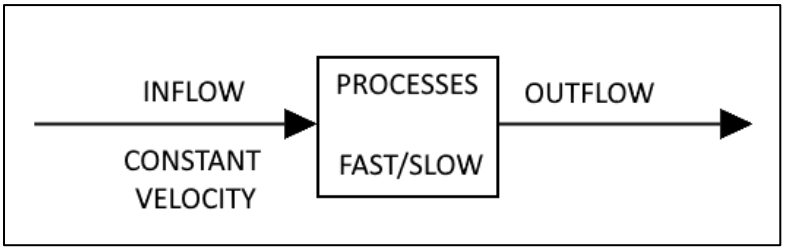

Figure 2.3: The basics used in STEADYQL model
(Reproduced from Wersin et al., 1993)

In the case of copper corrosion, this model considers the equilibrium reactions of copper, iron, hydrogen, hydrogen sulfide, calcium and carbonates (Figure 2.5). A steady state approach can approximate the slow kinetically driven processes in the DGR but does not allow for simulating changes from an aerobic to anaerobic environment. Therefore, corrosion is evaluated under anoxic and oxic cases separately but the

transition between the two conditions is not modelled (Wersin et al., 1994). For oxic and anoxic conditions, reactions are divided into fast and slow processes. For the anoxic case, fast processes include complexation reactions between porewater and solid matrix, while slow processes include transport related processes such as diffusion through bentonite and corrosive oxidation of copper by Fe(III) (Wersin et al., 1994). Oxic fast processes include interactions of dissolved species with the solid matrix and CuS precipitation, while copper corrosion (oxidation) and diffusion to the bentonite and canister are assumed to be slow processes.

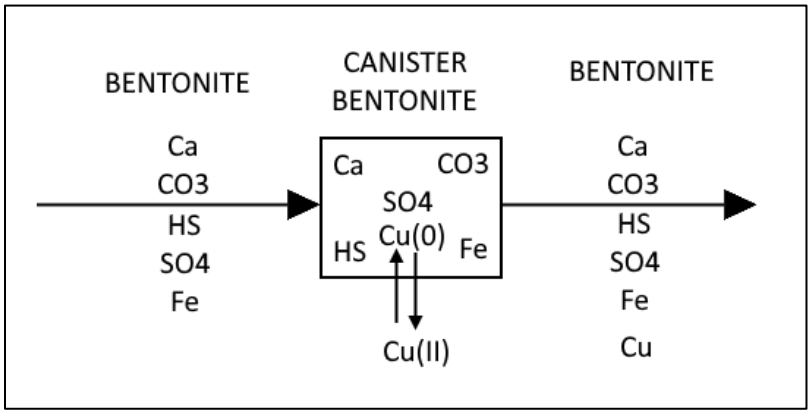

Figure 2.4: Single box model of canister bentonite interaction (Reproduced from Wersin et al., 1993)

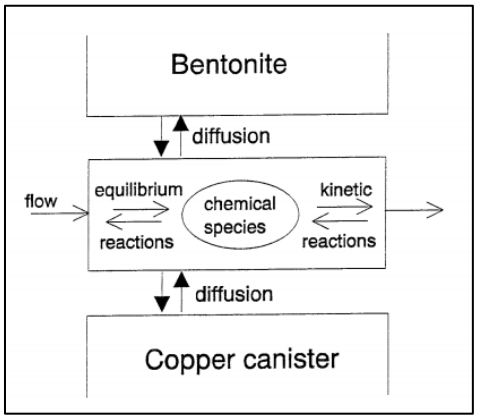

Figure 2.5: Multi-box model of copper bentonite interaction (Reproduced from Wersin et al., 1994)

2.5.2 T2GGM model

T2GGM is a numeric model developed for gas generation and transport in the DGR. This model is a combination of gas generation model (GGM) which calculates water consumption and gas generation due to corrosion and microbial degradation, and TOUGH2 flow code which models the two-phase transport through the DGR shafts and geosphere. Pressure, temperature, saturation, etc. are passed in GGM compartment which calculates gas and water generation rates. These are sent to TOUGH2 elements as sources (Avis et al., 2014). The flow of data within this model is shown in Figure 2.6.

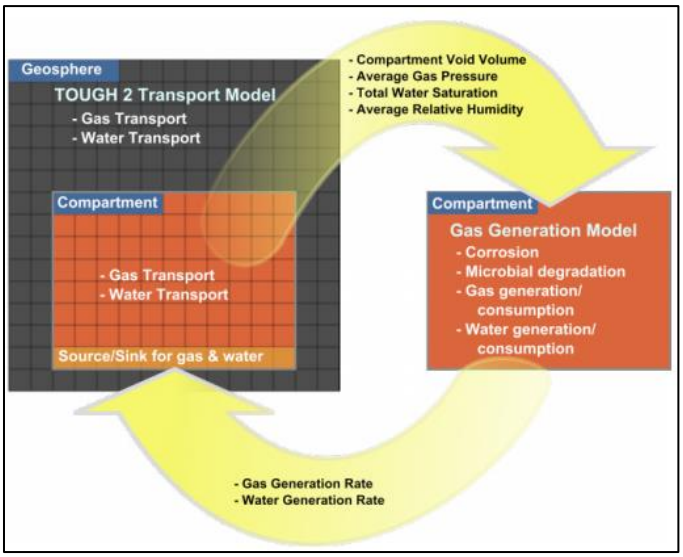

Figure 2.6: Flow of data within T2GGM code (Reproduced from Avis et al. 2014)

This model is not applied for copper canister corrosion but can take into account enhanced steel corrosion due to high CO_2 partial pressure, oxidation-reduction reactions for the consumption of oxygen, nitrates, iron (III), sulfates. T2GGM can simulate some corrosion and microbial degradation processes including: corrosion product and hydrogen gas generation from steel corrosion and other alloys under aerobic and anaerobic conditions; CO_2 and CH_4 gas generation from degradation of organic materials under aerobic and anaerobic conditions; H_2 gas generation, including methanogenesis from CO_2; biomass generation, decay and recycling; limitation of microbial and corrosion reactions by the availability of water; exchange of gas and water between the repository and surrounding geosphere; and two phase flow of water and gas inside geosphere (Suckling et al., 2012; Humphreys, 2011). All microbial and corrosion processes are

modelled as kinetic reactions. The data used for this model are gathered from site and waste characterization and repository engineering programs. This model is applied in the repository, considering saturation, and oxidation conditions.

2.5.3 DRINK model

DRINK stands for DRIgg Near field Kinetic. Drigg is a low level radioactive waste repository located in UK. Unlike DGR which will accommodate ILW/HLW, this site stores LLW and has been in operation since 1959 (Jason Nisse, 2005). DRINK code is used to simulate the evolution of biogeochemical processes for long term in Drigg. This code considers the microbial activity, radionuclide chemistry, ambient chemistry with the changing/development of pH, redox potential and bulk geochemistry which are directly influenced by microbial activity. It is technically a 2D geochemical transport code which includes modules for steel corrosion, sorption, microbiology, radioactive decay, mineral precipitation/dissolution and gaseous release. The geochemistry in DRINK is modified version of PHREEQE code. The main role of PHREEQE in DRINK is to modelling of mineral precipitation/dissolution, speciation of dissolved species and calculation of pH (Humphreys et al., 1997).

2.5.4 Other models/experiments/simulations

Experiments in laboratory and field scale were conducted in Germany to analyze the effects of chloride rich solutions of magnesium and sodium on cemented low (L) and ILW. Laboratory experiments were conducted over a period of 3 years with powdered hydrated cement paste and full-scale field experiments were conducted for 20 years in the Asse II salt mine located in Saxony using uranium doped cemented L/ILW. Geochemist's Workbench (GWB) software package was used for simulation. It was inferred that the corrosion with magnesium ion rich solutions was greater than that of sodium ion rich solutions. This might be attributed to the extensive exchange of magnesium with calcium in the cementitious solid (Bube et al., 2013). Equilibrium conditions were achieved after ~14 years for the full-scale experiments as indicated from the laboratory data. The laboratory and simulation were found to be in agreement with one another. This experiment demonstrated the applicability of thermodynamic

methods/simulations to describe the effects of L/ILW with cementitious materials (Bube et al., 2013).

In Japan, effects of pH and redox conditions on corrosion of subsurface disposal systems were analyzed. Simulations were performed at different pH using a finite difference computer code using PHREEQC-TRANS and then the consumption of residual oxygen in the backfill was calculated. The dissolved oxygen in the groundwater which could result in corrosion in the engineered barrier was also estimated. It was found that basic pH level of 12.5 would remain for more than 100 years in the system. Moreover, the rate of oxygen supply from groundwater was low due to the low permeability and low diffusivity layer of backfill. It was found that the residual oxygen would be consumed within 13 years by corrosion reactions. The aerobic corrosion rate was found to be limited at $1x10^{-3}$ um/year. Thus, it was inferred that the aerobic condition influence on corrosion was limited and long-term effects on corrosion would be due to anaerobic conditions. So, the engineered barriers have to be designed accordingly (Ooma et al., 2014).

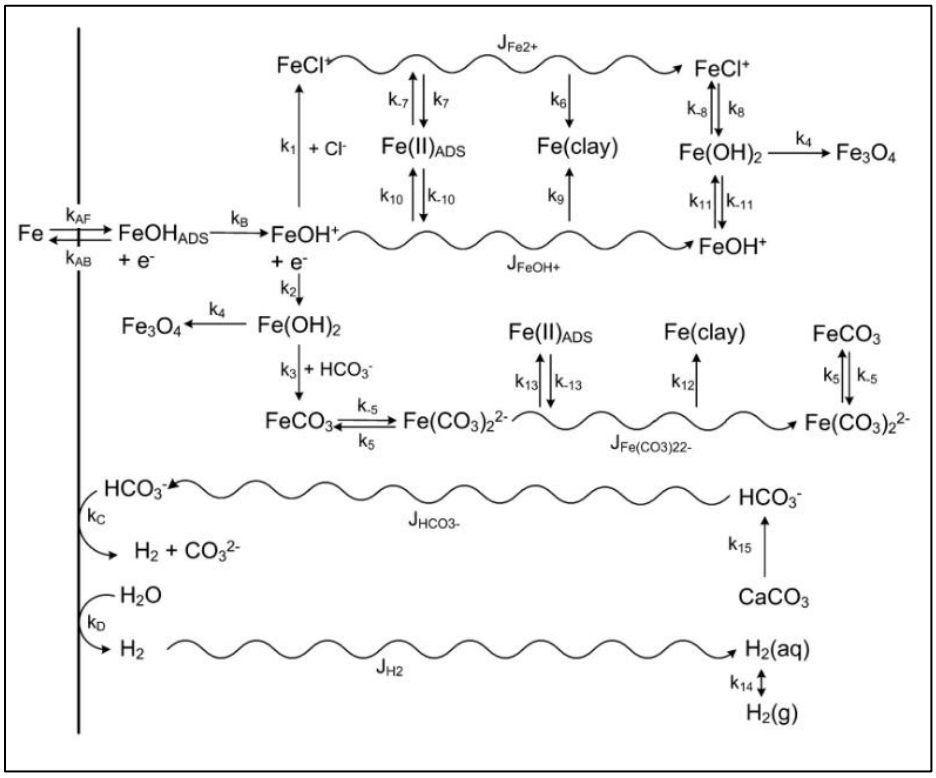

Figure 2.7: Reaction scheme for Steel Corrosion Model (SCM). Here k indicates the rate constants and J indicates the diffusive fluxes (King et al. 2014)

In Canada, a model for anaerobic corrosion of steel in carbon-steel containers to be used for DGR was developed by King et al. (2014). This model deals with interfacial reactions occurring in buffer, backfill material and host rock. Simulations were performed for sedimentary rock with a groundwater chloride concentration of 4.75 mol/L. This model takes into account the periodic build up and release of hydrogen. Moreover, the precipitation of Fe_3O_4 and the conversion of montmorillonite to a non-swelling clay is also taken into consideration. The steel corrosion model (SCM) is summarized in Figure 2.7. According to King et al. (2014), oxygen gets consumed in approximately 5,000 years and then commences anaerobic corrosion. Another study by Ooma et al. (2014) shows that anaerobic corrosion begins just after 13 years. The significant difference in result can be attributed to the methods and conservatism assumed and is an area of ongoing research.

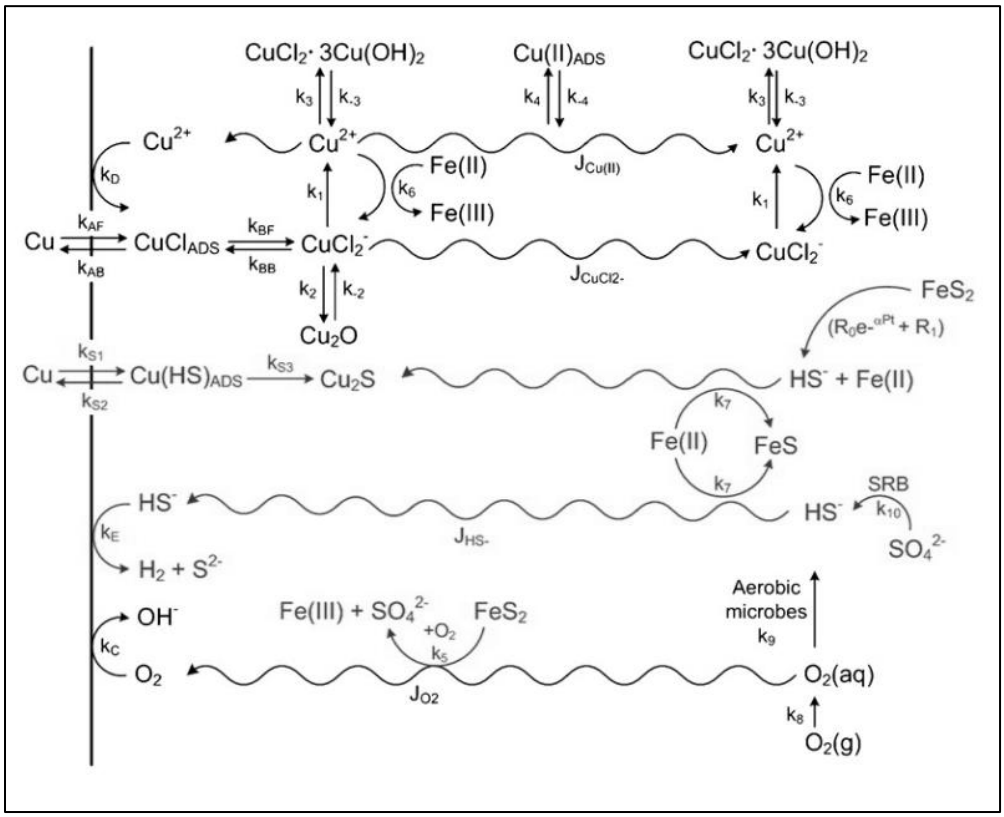

Figure 2.8: Reaction scheme for Copper Sulphide Model (CSM). Here k indicates the rate constants and J indicates the diffusive fluxes. This is an extension to CCM -UC (Reproduced from King et al., 2011)

A copper sulfide model (CSM) was developed by King et al (2011) to examine the reactions taking place in repositories that use copper lined UFCs during anaerobic phases

(Figure 2.8). This model examines the influence of corrosion with sulfide, chloride, saturations, and microbial scenarios is described by King et al. (2011). The predicted depth of corrosion over a period of 1 million years was found to be less than 1 mm. Most of the depth is achieved during the anaerobic period rather than the aerobic period because of the formation of Cu_2S

2.6 Implication for corrosion modelling in a DGR

- Since early times, copper has been used for making tools. This has led to the availability of data from archaeological artifacts indicating its corrosion resistance and stability making it suitable for use in disposal of spent nuclear fuel.
- Presence of oxygen, chloride, and water can lead to copper corrosion in the DGR. Laboratory experiments conducted under different conditions can give an indication of the estimation of corrosion rate.
- Increase in chloride concentration leads to increase in corrosion current density indicating the concentration of chloride is a major factor in corrosion. A similar scenario is observed for oxygen concentration.
- Alkaline conditions have lesser tendency to corrode copper over acidic conditions. In the DGR, the nature of the pH of the surrounding environment around copper would affect the corrosion rate. Furthermore, adsorption of copper onto bentonite is affected by pH. Low pH shows less adsorption compared to high pH.
- High temperature leads to increase in corrosion of copper. During the initial period, there will be a high temperature in DGR due to radioactivity. This implies that the corrosion rate may be initially high.

2.7 Conclusion

There is a lot of data regarding copper obtained from archaeological artifacts. Different kinetic studies of interaction of copper with chloride, oxygen and water in different environments have been conducted which can lead to the formation compounds including cuprite, paratacamite and copper chloride. Moreover, different models including STEADYQL, CSM, CCM have been developed in the past for modelling corrosion phenomena on copper.

CHAPTER THREE: MODEL DEVELOPMENT

3.1 Introduction

Prediction of copper canister behavior in the DGR requires the development and use of computer models. The models consider the impact of different species (i.e. chloride, oxygen) and DGR conditions (i.e. moisture, temperature) on the canister to aid in design. The Copper Corrosion Model (CCM) developed by King and Kolar (1995) is has been widely used to predict copper corrosion of UFCs. This model uses the TRANSIENT Solver, written in C, to solve the partial differential equations involved in calculating the transport of species through the engineered barrier system (EBS) to the copper container. CCM is a one-dimensional (1D) model and is limited in terms of usability. Therefore, the objective of this study was to develop the CCM model in COMSOL which overcomes these drawbacks. To ensure accuracy of the new COMSOL model, validation and verification activities were performed. Firstly, the COMSOL model was verified against CCM for a variety of parameters (Chapter 4). Secondly, laboratory experiments, that were conducted for the development of the CCM model, were used to validate the accuracy of the COMSOL model (Chapter 5). This chapter describes how the CCM model was developed in COMSOL and the experiments performed to validate the COMSOL model.

The CCM model is based on experiments conducted by King et al. (1995) which are described in Section 5.1. There are several versions of the CCM model including microbial influenced corrosion (MIC), stress corrosion cracking (SCC), uniform corrosion (UC), etc. The CCM – UC is used in this study.

3.2 Description

COMSOL is a finite element software with predefined engineering and mathematical equations for solving multiphysics based systems of partial and ordinary differential equations. This software can also add/customize physical phenomena based on user requirements. COMSOL can simulate electrochemical equations using the Electroanalysis Module which was used herein to simulate the corrosion of copper canisters. This module has built-in physics for the corrosion and transport processes. Moreover, there is a multi-dimension capability in COMSOL (i.e. the corrosion model is currently modeled in 1-D) which allows for the extension of CCM to 2D and 3D.

A step-wise approach was taken in the development of the CCM-UC model in COMSOL. This approach was developed by King (2016) The steps progress with increasing complexity by addition of species, rate constants, dimensions and other variables. The reactions occurring in the interface are the determining factors for the corrosion process. The components/species available for the interfacial reactions are influenced by the reactions involving diffusion, precipitation, adsorption, etc.

Details of the steps are shown in Table 3.1. The steps involved can be summarized as:

Step 1: Simplified steady-state model

Step 2: Simplified transient state model

Step 3a-f: Transient model with progressive complexity for reaction schemes

Step 4: Non-isothermal model

Step 5: Variable saturation model

Step 6: Multi-dimensional model

Steps 4 to 6 include temperature, saturation, and dimensionality variation and are outside the scope of the current work.

Table 3.1: Steps involved in modelling process (King, 2016)

Step	Additional processes	Additional Species
1	• Steady State	O_2, Cl^-, $CuCl_2^-$
2	• Transient	O_2, Cl^-, $CuCl_2^-$
3a	• Homogeneous oxidation of $CuCl_2^-$ (k_1) • Interfacial reduction of Cu^{2+} (k_D)	Cu^{2+}
3b	• Precipitation/dissolution of solid Cu(II) (k_3/k_{-3})	$CuCl_2.3Cu(OH)_2$
3c	• Precipitation/dissolution of solid Cu_2O (k_2/k_{-2})	Cu_2O
3d	• Adsorption/desorption of Cu^{2+} (k_4/k_{-4})	$Cu(II)_{ADS}$
3e	• Aerobic respiration (k_9)	–
3f	• Reactions involving dissolved and precipitated Fe(II) (k_5, k_6, k_7/k_{-7})	$Fe(II)_{AQ}$ $Fe(II)_{PPT}$
4	• Spatial and temporal variation in temperature • Temperature dependence of rate constants, diffusion coefficients, and other input data	–
5	• Oxygen dissolution (k_8) • Spatial and temporal variation in saturation • Effects of saturation on interfacial reactions • Effective diffusion coefficients, and solute concentration	Gaseous O_2
6	• 2D/3D dimensionality of Mark II DGR	–

Using the step wise approached discussed above, the model was developed up to and including Step 3d, the precipitation and dissolution of Cu_2O. It does not model later steps involving microbial activity (Step 3e), iron reactions (Step 3f) which are left for future work.

The current implementation of the model in COMSOL consists of a 1D system with the copper electrode on the left-hand side, saturated and isothermal conditions (25°C) as shown in Figure 3.1.

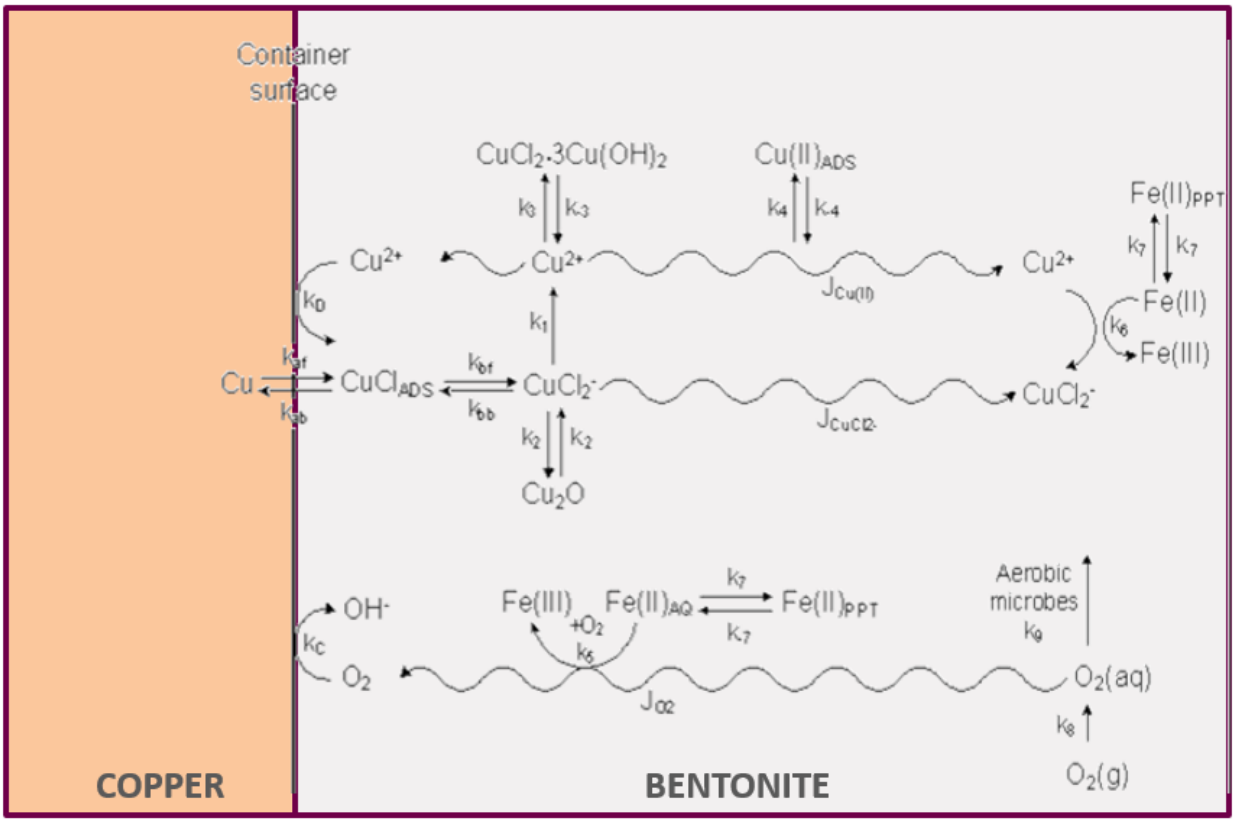

Figure 3.1: Schematic diagram for the interface between copper and bentonite along with associated corrosive reactions (Adapted from King, 2016).

The COMSOL Multiphysics Electroanalysis Module was used with adaptive time stepping methods and a maximum element size of 10^{-7} m. The initial corrosion potential is taken as -0.25 V_{SCE} (Voltage with respect to Standard Calomel Electrode). The experimental value is -0.2 V_{SCE}. Taking the initial corrosion potential close to the experimental value aids in faster convergence or avoidance of numerical error in COMSOL simulation.

Since the model incorporates transport of different species including chloride and oxygen through a bentonite layer, which is a low permeability soil, mass transfer is assumed to be diffusion dominated (no advection). The diffusion coefficient is a function of free species-specific diffusion coefficient (D_0), tortuosity (τ_f) and effective porosity (ε_e).

The effective diffusion coefficient is given by:

$$D_{EFF} = \varepsilon_e \tau_f D_0 \qquad 3.1$$

Typically, a multi-porosity model is assumed in which the total porosity (ε) is divided into accessible (ε_a) and non-accessible (ε_{na}) porosity, representing connected and isolated pores, respectively. The accessible porosity is further divided into a storage porosity (ε_s) and the effective porosity for mass transport (ε_e). The values of tortuosity and porosities would change based on the soil layers' properties while the free diffusion coefficient is species-specific. Currently, this model only simulates one layer, bentonite, in which both the effective and storage porosity are taken as 0.205. Moreover, the tortuosity is taken as 0.05. These values are based on the properties of bentonite (King, 2016).

3.2.1 Step 1: Steady State Model with Simplified Reaction Scheme

In Step 1, three species are initially considered: dissolved O_2, Cl^- and $CuCl_2^-$. These species are free to diffuse to and from the left-hand boundary which represents the container surface (Figure 3.2). There are two interfacial electrochemical reactions (Equation 3.3 and 3.4) and no homogeneous reactions. Corrosion of the copper surface is considered under isothermal and saturated conditions.

The cathodic reduction of O_2, which diffuses from the right boundary, results in copper corrosion of the copper container. In addition, dissolution of copper consumes Cl^- ions (in the form of $CuCl_2^-$ complex ions). In this step, chloride is generally in excess (i.e., the concentration of Cl^- is much greater than the concentration of $CuCl_2^-$), but in general it is also supplied by diffusion from the source at the right-hand boundary (Figure 3.1).

$CuCl_{ADS}$ is the intermediate species which is consumed in the interface and not explicitly modelled. The OH^- species are also not modelled as they are the product of the cathodic reduction of O_2 (Equation 3.2) that is irreversible (i.e., the rate does not depend on the reverse reaction involving the oxidation of OH^-).

In this step, the cathodic reaction is the reduction of oxygen:

$$O_2 + 2\ H_2O + 4\ e^- \xrightarrow{k_c} 4\ OH^- \qquad 3.2$$

The rate constant associated with the above reaction is k_c with an assumed value of 1.7 x 10^{-10} m/s (King et al., 1995) (see Chapter 2 for rate constant review).

The anodic reaction for the dissolution of copper is:

$$Cu + Cl^- \underset{k_{ab}}{\overset{k_{af}}{\rightleftharpoons}} CuCl_{ADS} + e^- \qquad 3.3$$

$$CuCl_{ADS} + Cl^- \underset{k_{bb}}{\overset{k_{bf}}{\rightleftharpoons}} CuCl_2^- \qquad 3.4$$

The reversible reaction of adsorption of copper and chloride has rate constants of k_{af} and k_{ab} for forward and reverse reactions respectively. Similarly, the formation of cuprous chloride ions has rate constants of k_{bf} and k_{bb}.

A combined rate constant, k_a, is used to denote k_{af} x k_{bf} / k_{ab}. This has a value of 3.3 x 10^{-8} m^4/mol-s (King et al., 1995) while the value of k_{bb} is assumed to be 1.42 x 10^{-4} m/s (Hurlen, 1961).

The relationship between current and potential can be expressed using Butler-Volmer equations for both anodic and cathodic reactions as follows:

$$i_a = n_a F \left\{ k_a [Cl^-]^2 \exp \frac{F}{RT} (E - E_a) - k_{bb} [CuCl_2^-] \right\} \qquad 3.5$$

$$i_c = -n_c F k_c [O_2] \exp \frac{\alpha_c F}{RT} (E - E_c) \qquad 3.6$$

Where the various coffieicients are defined in the glossary.

The length of the bentonite layer on the copper electrode in the experiment was 1mm and 10mm. The boundary condition for concentration was taken as constant for O_2 and Cl^- at the right-hand boundary with the concentration of O_2 (range between 0.2-0.0007 mol/m^3) as summarized in Table 5.1, and the concentration of Cl^- as taken 1000 mol/m^3 (with activity coefficient of 0.657). Moreover, the concentration for $CuCl_2^-$ was taken as zero for the same lengths and boundary.

3.2.2 Step 2: Transient Model with Simplified Reaction Scheme

Step 2 is identical to Step 1 except that a transient solution is calculated. The time simulated is for 250 hours and 2500 hours for 1 mm and 10 mm respectively.

3.2.3 Step 3a: Homogeneous oxidation of Cu(I) and Interfacial Reduction of Cu(II)

In Steps 3a-d, additional chemical species, reactions, and/or processes are introduced. Step 3a includes one additional species (Cu^{2+} (concentration c_3)), diffusion of Cu^{2+} towards and away from the container surface, oxidation of $CuCl_2^-$ (concentration c_1) by dissolved O_2 (concentration c_0) and an additional cathodic reaction. These processes are described below and shown in Figure 3.2. In the figure, the new species/processes are shown in red font while the existing species and processes from Steps 1 are shown in black.

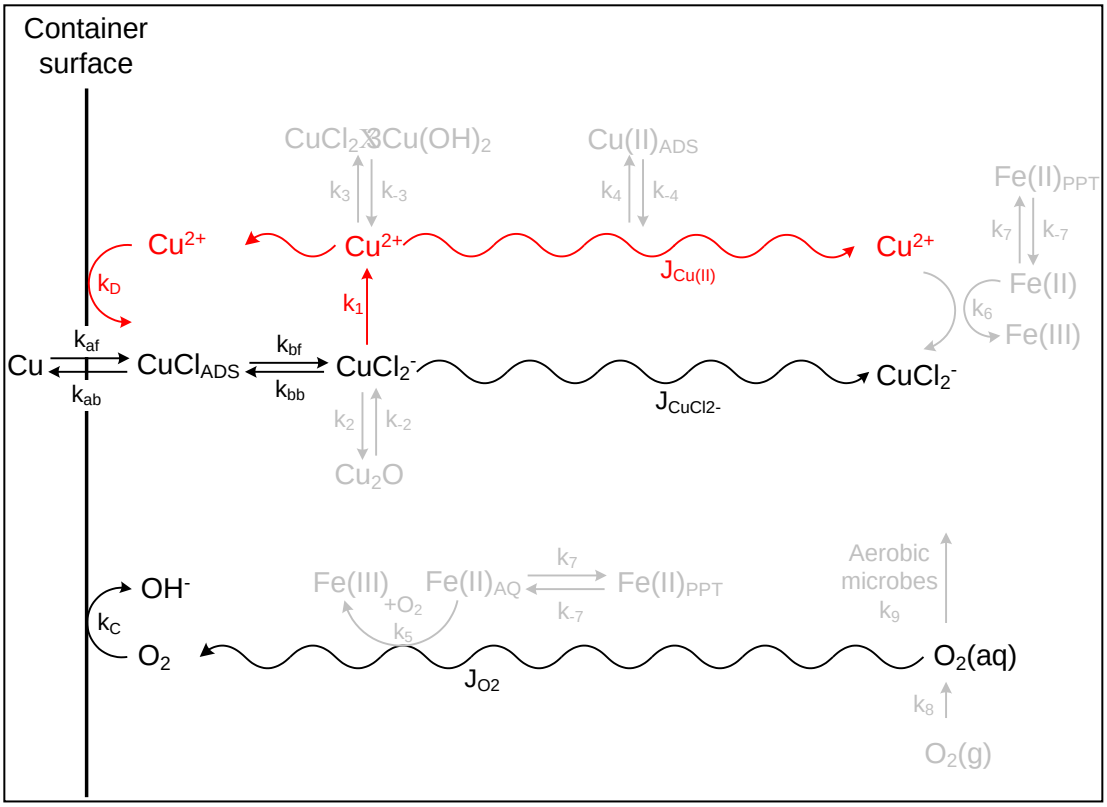

Figure 3.2: Reaction scheme for Step 3a in CCM-UC model (King, 2016)

In Step 3a, the interfacial reactions are influenced by homogeneous reactions in the bulk solution. In this step an additional chemical species is considered, namely cupric

ions, along with the rate constants for the homogeneous oxidation of copper chloride ions (k_1) and the reduction of cupric ions at the interface of copper bentonite (k_d).

$$Cu^{2+} + 2\,Cl^- + e^- \xrightarrow{k_d} CuCl_2^- \qquad 3.7$$

Evans diagrams can be used for analyzing the corrosion process. These diagrams represent the relation between an electrode's kinetic behavior i.e. current density and thermodynamics i.e. potential (Corrosionpedia, 2018).

An example presented by Tavakoli et al, (2017) considers a system containing chloride, chromium and magnesium. There can be two anodic reactions and one cathodic reactions as shown in the Evans diagram (Figure 3.3). The intersectional point of cathodic and anodic reaction represents the corrosion potential (E_{corr}). In the absence of magnesium, the intersectional point is higher indicating the influence of the anodic reactions is greater. The corresponding currents are represented by i_{corr} (Tavakoli et al., 2017).

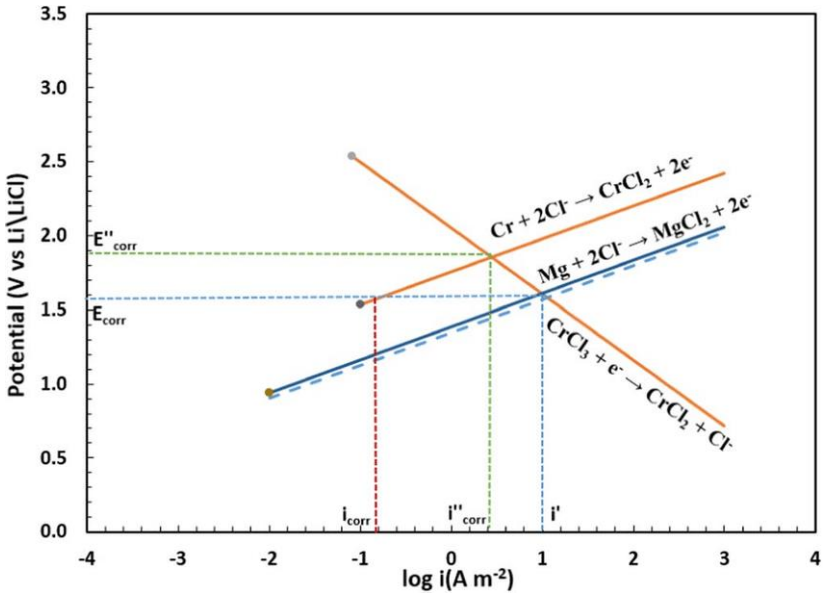

Figure 3.3: Corrosion potential for chloride, copper and magnesium system (Tavakoli et al., 2017)

As in case of Step 1, Butler-Volmer expressions are used for determining the current at the interface. Another cathodic reaction is included in addition to the previous ones from Step 1 and 2:

$$i_d = -n_d F k_D [Cu^{2+}] \exp\left(-\frac{\alpha_d F}{RT}(E - E_d)\right) \quad 3.8$$

At the left-hand boundary condition, at the copper surface, the sum of the anodic and cathodic reaction is set to zero in order to solve for the corrosion potential.

$$i_a + i_c + i_d = 0 \quad 3.9$$

The boundary condition of zero net current condition is considered on the left side boundary. From this condition, the corrosion potential (E_{corr}) can be determined from the equation involving relation of i_{corr} and E_{corr}.

This corrosion potential can be used to determine the corrosion current which can be used to calculate the corrosion rate through the following expression:

$$Corrosion\ Rate = \frac{i_{corr} M_{Cu}}{F \rho_{Cu}} \quad 3.10$$

where i_{corr} is the corrosion current density determined from the model, M_{Cu} is the atomic mass of copper and ρ_{Cu} is the density of copper (see Appendix A for the derivation of this equation).

Step 3a also includes a homogeneous oxidation reaction of $CuCl_2^-$ by O_2:

$$4CuCl_2^- + O_2 + 2H_2O \xrightarrow{k_1} 4Cu^{2+} + 8Cl^- + 4OH^- \quad 3.11$$

The consumption rate of O_2 can be expressed as:

$$-\frac{\partial c_0}{\partial t} = \frac{k_1}{4} c_0 c_1 \quad 3.12$$

This expression is dependent on the expression of both oxygen and copper chloride.

The expression for the rate constant, k_1 (Equation 3.13) is derived from experiments conducted by Sharma and Millero (1988), where c_6 is the aqueous concentration of chloride.

$$\log k_1 = 11.38 - 2064/T - 3.69 \sqrt{\frac{c_6}{1 - 0.1103\, c_6}} + 0.73 \sqrt{\frac{c_6}{1 - 0.1103\, c_6}} \quad 3.13$$

The reaction-diffusion equations for Step 3a are:

$$\varepsilon_a \frac{\partial(Sc_0)}{\partial t} = \frac{\partial}{\partial x}\left(\tau_f \varepsilon_e S D_0 \frac{\partial c_0}{\partial x}\right) - \varepsilon_a S \frac{k_1}{4} c_0 c_1 \qquad 3.14$$

$$\varepsilon_a \frac{\partial(Sc_1)}{\partial t} = \frac{\partial}{\partial x}\left(\tau_f \varepsilon_e S D_1 \frac{\partial c_1}{\partial x}\right) - \varepsilon_a S k_1 c_0 c_1 \qquad 3.15$$

$$\varepsilon_a \frac{\partial(Sc_3)}{\partial t} = \frac{\partial}{\partial x}\left(\tau_f \varepsilon_e S D_3 \frac{\partial c_3}{\partial x}\right) + \varepsilon_a S k_1 c_0 c_1 \qquad 3.16$$

$$\varepsilon_a \frac{\partial(Sc_6)}{\partial t} = \frac{\partial}{\partial x}\left(\tau_f \varepsilon_e S D_6 \frac{\partial c_6}{\partial x}\right) + 2k_1 c_0 c_1 \varepsilon_a S \qquad 3.17$$

These equations are incorporated into the COMSOL model.

3.2.4 Step 3b: Precipitation/dissolution of Solid Cu(II)

In this step, precipitation of paratacamite ($CuCl_2$. $3Cu(OH)_2$) and dissolution of copper (II) with their respective rate constant (k_3/k_{-3}) are considered.

The rate constant, k_3, is assumed to be 1 x 10^{-5} s^{-1} at 25^{o}C. Moreover, the value of k_{-3} is taken as 1/10^{th} of the k_3 value based on a limited number of measurements (King 2016, King and Strandlund - unpublished data). The associated reactions are highlighted in red in *Figure 3.4*.

The reaction is:

$$4Cu^{2+} + 6\ OH^- + 2Cl^- \underset{k_{-3}}{\overset{k_3}{\rightleftharpoons}} CuCl_2.3Cu(OH)_2 \qquad 3.18$$

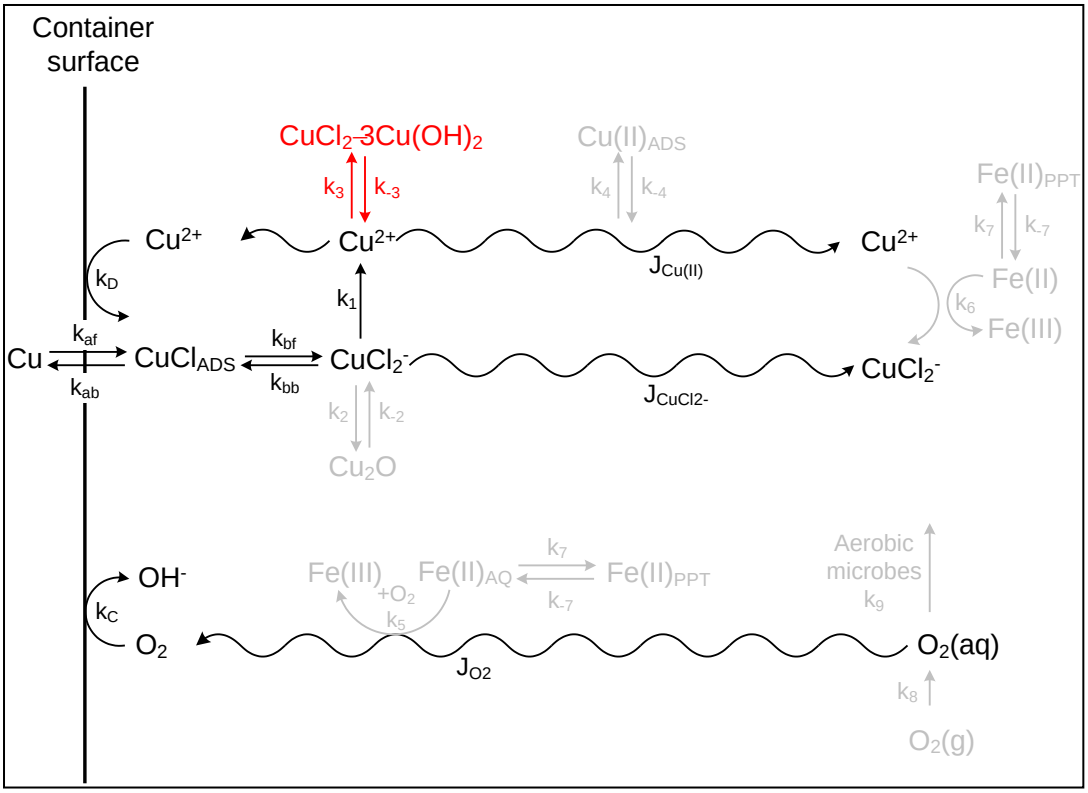

Figure 3.4: Reaction scheme for Step 3b in CCM-UC model (King, 2016)

The rate of precipitation can be given by:

$$\frac{\partial c_4}{\partial t} = \varepsilon_a S \frac{k_3}{4} max(0, c_3 - c_3^{sat}) \qquad 3.19$$

The 'max' function takes into account that the solution is not supersaturated with Cu^{2+} ions. The expression for the rate of dissolution can be given by:

$$-\frac{\partial c_4}{\partial t} = k_{-3} c_4 \qquad 3.20$$

The modified and the extended equations for the reaction-diffusion equations are as follows:

$$\varepsilon_a \frac{\partial(Sc_0)}{\partial t} = \frac{\partial}{\partial x}\left(\tau_f \varepsilon_e S D_0 \frac{\partial c_0}{\partial x}\right) - \varepsilon_a S \frac{k_1}{4} c_0 c_1 \quad 3.21$$

$$\varepsilon_a \frac{\partial(Sc_1)}{\partial t} = \frac{\partial}{\partial x}\left(\tau_f \varepsilon_e S D_1 \frac{\partial c_1}{\partial x}\right) - \varepsilon_a S k_1 c_0 c_1 \quad 3.22$$

$$\varepsilon_a \frac{\partial(Sc_3)}{\partial t} = \frac{\partial}{\partial x}\left(\tau_f \varepsilon_e S D_3 \frac{\partial c_3}{\partial x}\right) + \varepsilon_a S[k_1 c_0 c_1 - k_3 max(0, c_3 - c_3^{sat})] + 4k_{-3} c_4 \quad 3.23$$

$$\frac{\partial c_4}{\partial t} = \varepsilon_a S \frac{k_3}{4} max(0, c_3 - c_3^{sat}) - k_{-3} c_4 \quad 3.24$$

$$\varepsilon_a \frac{\partial(Sc_6)}{\partial t} = \frac{\partial}{\partial x}\left(\tau_f \varepsilon_e S D_6 \frac{\partial c_6}{\partial x}\right) + \varepsilon_a S \left[2k_1 c_0 c_1 - \frac{k_3}{2} max(0, c_3 - c_3^{sat})\right] + 2k_{-3} c_4 \quad 3.25$$

The equations are appended with the ones included in the previous step into the COMSOL model.

3.2.5 Step 3c: Precipitation/dissolution of Solid Cu_2O

The precipitation and dissolution of cuprous oxide (Cu_2O) is considered in this step, with a rate constant of k_2/k_{-2}, respectively. The rate constant (k_2) is assumed to be 1 s^{-1} at 25°C based on limited measurements (see Chapter 2). The reaction is dependent on pH and independent of chloride concentration. The reverse reaction rate constant, k_{-2}, is assumed to be 0.1 s^{-1} which is based on limited measurements (King 2016, King and Legere -unpublished data). The associated reactions are highlighted in red in *Figure 3.5*.

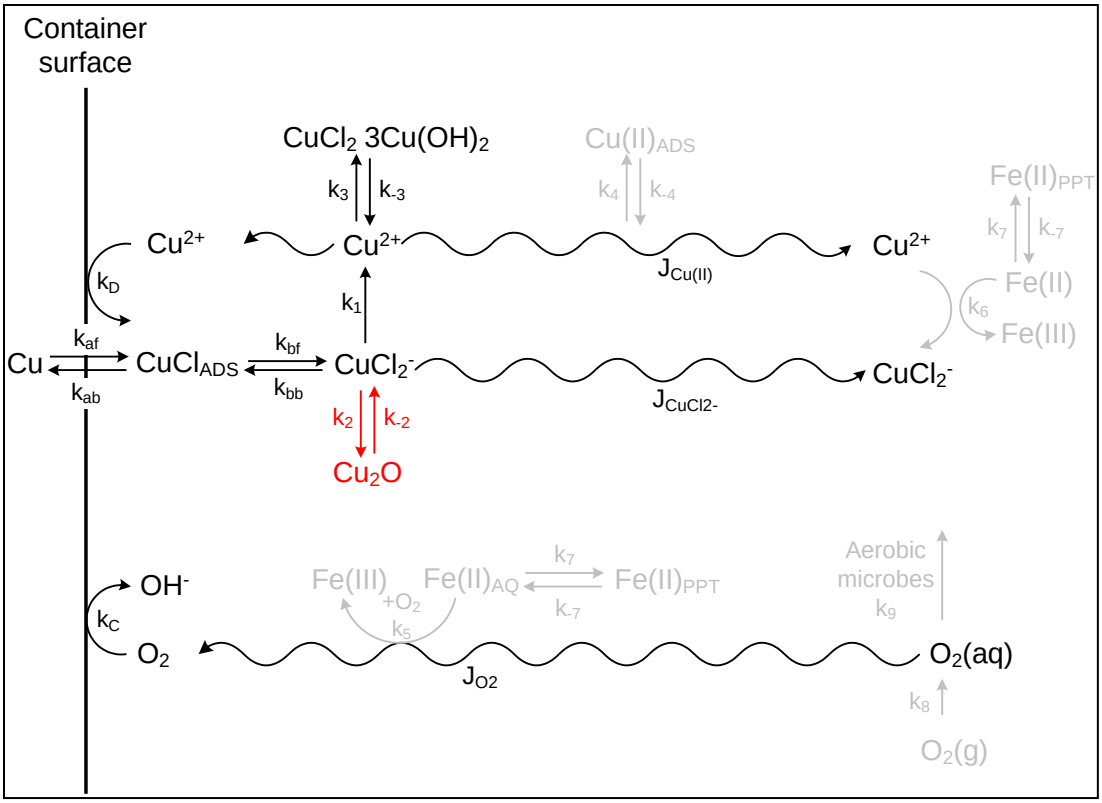

Figure 3.5: Reaction scheme for Step 3c in CCM-UC model (King, 2016)

The concentration of Cu_2O can be expressed as:

$$2CuCl_2^- + H_2O \underset{k_{-2}}{\overset{k_2}{\rightleftharpoons}} Cu_2O + 4Cl^- + 2H^+ \qquad 3.26$$

The rate expression can be given by:

$$\frac{\partial(Sc_2)}{\partial t} = \varepsilon_a S \frac{k_2}{2} max(0, c_1 - c_1^{sat}) \qquad 3.27$$

The c_1^{sat} term ensures the rate is valid for the cuprous oxide precipitating from saturated solutions and no supersaturation occurs. This reduces the numerical errors in solving the equations.

$$-\frac{\partial(Sc_2)}{\partial t} = k_{-2} c_2 \qquad 3.28$$

$$\varepsilon_a \frac{\partial(Sc_0)}{\partial t} = \frac{\partial}{\partial x}\left(\tau_f \varepsilon_e S D_0 \frac{\partial c_0}{\partial x}\right) - \varepsilon_a S \frac{k_1}{4} c_0 c_1 \quad 3.29$$

$$\varepsilon_a \frac{\partial(Sc_1)}{\partial t} = \frac{\partial}{\partial x}\left(\tau_f \varepsilon_e S D_1 \frac{\partial c_1}{\partial x}\right) + \varepsilon_a S[-k_1 c_0 c_1 - k_2 max(0, c_1 - c_1^{sat})] + 2k_{-2} c_2 \quad 3.30$$

$$\frac{\partial(Sc_2)}{\partial t} = \varepsilon_a S \frac{k_2}{2} max(0, c_1 - c_1^{sat}) - k_{-2} c_2 \quad 3.31$$

$$\varepsilon_a \frac{\partial(Sc_3)}{\partial t} = \frac{\partial}{\partial x}\left(\tau_f \varepsilon_e S D_3 \frac{\partial c_3}{\partial x}\right) + \varepsilon_a S[k_1 c_0 c_1 - k_3 max(0, c_3 - c_3^{sat})] + 4k_{-3} c_4 \quad 3.32$$

$$\frac{\partial c_4}{\partial t} = \varepsilon_a S \frac{k_3}{4} max(0, c_3 - c_3^{sat}) - k_{-3} c_4 \quad 3.33$$

$$\varepsilon_a \frac{\partial(Sc_6)}{\partial t} = \frac{\partial}{\partial x}\left(\tau_f \varepsilon_e S D_6 \frac{\partial c_6}{\partial x}\right) + \varepsilon_a S\left[2k_1 c_0 c_1 + 2k_2 max(0, c_1 - c_1^{sat}) - \frac{k_3}{2} max(0, c_3 - c_3^{sat})\right] + 2k_{-3} c_4 - 4k_{-2} c_2 \quad 3.34$$

As in the previous steps, these equations were implemented into COMSOL.

3.2.6 Step 3d: Adsorption/desorption of Cu(II)

The adsorption and desorption process of Cu(II) to and from bentonite is included in this step. The associated rate constants considered are k_4/k_{-4}.

The rate constant k_4 is assumed to be 2 x 10^{-6} m^3/mol-s based on experiments conducted on loose clay (King 2016, King and Ryan -unpublished data). The reverse rate constant (k_{-4}) which is the desorption of Cu^{2+} ion from bentonite is taken as 1/10^{th} of the forward reaction. The associated reactions are highlighted in red in *Figure 3.6*.

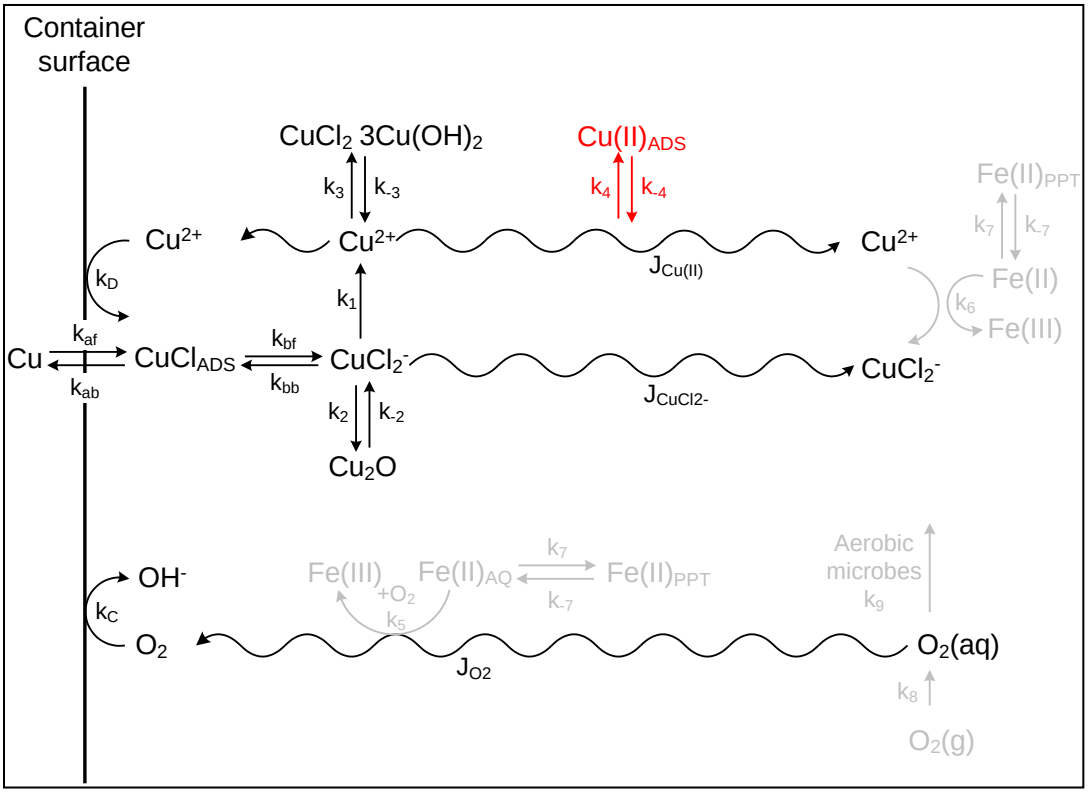

Figure 3.6: Reaction scheme for Step 3d in CCM-UC model (King, 2016)

The reaction is as follows:

$$Cu^{2+} + 2Y^{-} \underset{k_{-4}}{\overset{k_4}{\rightleftharpoons}} CuY_2 \qquad 3.35$$

where Y indicates a charged adsorption site on bentonite

The rate of the forward reaction:

$$\frac{\partial c_5}{\partial t} = \varepsilon_a S k_4 c_3 (c_5^{max} - c_5) \qquad 3.36$$

for $c_5 < c_5^{max}$

c_5^{max} indicates the maximum surface coverage of copper.

$$-\frac{\partial c_5}{\partial t} = k_{-4} c_5 \qquad 3.37$$

The associated reaction-diffusion equations are defined as follows:

$$\varepsilon_a \frac{\partial (S c_0)}{\partial t} = \frac{\partial}{\partial x}\left(\tau_f \varepsilon_e S D_0 \frac{\partial c_0}{\partial x}\right) - \varepsilon_a S \frac{k_1}{4} c_0 c_1 \qquad 3.38$$

$$\varepsilon_a \frac{\partial(Sc_1)}{\partial t} = \frac{\partial}{\partial x}\left(\tau_f \varepsilon_e S D_1 \frac{\partial c_1}{\partial x}\right) + \varepsilon_a S[-k_1 c_0 c_1 - k_2 max(0, c_1 - c_1^{sat})] + 2k_{-2} c_2 \quad 3.39$$

$$\frac{\partial(Sc_2)}{\partial t} = \varepsilon_a S \frac{k_2}{2} max(0, c_1 - c_1^{sat}) - k_{-2} c_2 \quad 3.40$$

$$\varepsilon_a \frac{\partial(Sc_3)}{\partial t} = \frac{\partial}{\partial x}\left(\tau_f \varepsilon_e S D_3 \frac{\partial c_3}{\partial x}\right) + \varepsilon_a S[k_1 c_0 c_1 - k_3 max(0, c_3 - c_3^{sat}) - k_4 c_3 (c_5^{max} - c_5)\rho_d] + 4k_{-3} c_4 + k_{-4} c_5 \rho_d \quad 3.41$$

$$\frac{\partial c_4}{\partial t} = \varepsilon_a S \frac{k_3}{4} max(0, c_3 - c_3^{sat}) - k_{-3} c_4 \quad 3.42$$

$$\rho_d \frac{\partial c_5}{\partial t} = \varepsilon_a S k_4 c_3 (c_5^{max} - c_5)\rho_d - k_{-4} c_5 \rho_d \quad 3.43$$

$$\varepsilon_a \frac{\partial(Sc_6)}{\partial t} = \frac{\partial}{\partial x}\left(\tau_f \varepsilon_e S D_6 \frac{\partial c_6}{\partial x}\right) + \varepsilon_a S\left[2k_1 c_0 c_1 + 2k_2 max(0, c_1 - c_1^{sat}) - \frac{k_3}{2} max(0, c_3 - c_3^{sat})\right] + 2k_{-3} c_4 - 4k_{-2} c_2 \quad 3.44$$

As in the previous steps, these equations were implemented in COMSOL.

The rate constants used in the development of CCM-UC in COMSOL has been summarized in Table 3.2.

Table 3.2: Rate constant values or expressions used in the development of copper corrosion model in COMSOL

RATE CONSTANT	UNITS	REACTION	ASSUMPTIONS	EXPRESSION	REFERENCES
k_1	For c6 [Cl^-] unit: mol. dm^{-3}, k1 has unit: dm^3. mol^{-1}. s^{-1}	Oxidation of $CuCl_2^-$ by O_2	*Value based on experiment *pH 6-9 *5-45°C *Activation energy, Ea: 39.5-45.4 kJ·mol^{-1} *seawater and Red Sea waters ***Derivation from Sharma & Millero's 1988 equation**	$\log k_1 = 11.38 - \frac{2064}{T} - 3.69\left(\frac{c_6}{1-0.1103c_6}\right)^{1/2} + 0.73\left(\frac{c_6}{1-0.1103c_6}\right)$	(King, 2016) Referenced as (Sharma and Millero, 1988a)
	For c6 unit: mol. m^{-3}, k1 has unit: m^3. mol^{-1}. s^{-1}			$\log k_1 = 8.38 - \frac{2064}{T} - 3.69\left(\frac{c_6}{1000-0.1103c_6}\right)^{1/2} + 0.73\left(\frac{c_6}{1000-0.1103c_6}\right)$	Personal correspondence (King, 2016 (SI Units)
				$\log k_1 = 12.32 + 0.12(pH) - \frac{2064}{T} - 3.69I^{1/2} + 0.73I$	**Originally in** (Sharma and Millero, 1988a)

RATE CONSTANT	UNITS	REACTION	ASSUMPTIONS	EXPRESSION	REFERENCES
k_2	s^{-1}	Rate of hydrolysis of $CuCl_2^-$	*25°C ***Assumed value**	k_2=1. There is uncertainty in the mechanism of formation of Cu_2O. This value of k_2 assumes of hydrolysis of $CuCl_2^-$. It is set 10 higher than k_{-2} to simulate experimentally observed formation of Cu_2O	(King, 2016)
k_{-2}	s^{-1}	Rate of dissolution of Cu_2O	*25°C ***Assumed value**	k_{-2}=0.1. This value is based on some experimental data on the dissolution rate of Cu_2O in Cl^- solutions as function of pH. Considered independent of $[Cl^-]$. Dependent upon specific surface area of Cu_2O which is unknown and is dependent upon environmental conditions under which precipitation occurs.	King and Legere, **unpublished data**
k_3	s^{-1}	Rate constant for the precipitation of $CuCl_2 \cdot 3Cu(OH)_2$	*25°C ***Assumed value**	k_3=1 x 10^{-5}. No kinetic data available. Taken as 10 times higher than the dissolution rate constant to account for the experimental observation of precipitated $CuCl_2 \cdot 3Cu(OH)_2$.	(King, 2016)
k_{-3}	s^{-1}	Rate constant for the dissolution of $CuCl_2 \cdot 3Cu(OH)_2$	*25°C ***Assumed value**	k_{-3}=1 x 10^{-6}. Based on limited number of experimental measurements. Dependent on specific surface area (similar to k_{-2} for Cu_2O).	King and Strandlund, **unpublished data**

RATE CONSTANT	UNITS	REACTION	ASSUMPTIONS	EXPRESSION	REFERENCES
k_4	$dm^3.mol^{-1}.s^{-1}$	Rate constant for the adsorption of Cu^{2+} on Na-bentonite	25°C	k_4= 2 x 10^{-3}. Based on kinetic studies of loose clay. According to Fraser's TM file, this value is consistent with Langmuir adsorption data of paper of Ryan and King 1994	King and Ryan, **unpublished data**
k_{-4}	s^{-1}	Rate constant for the desorption of Cu^{2+}	25°C	k_{-4}=1 x 10^{-6}. Based on desorption of loose clay systems	King and Ryan, **unpublished data**
k_5	$dm^3.mol^{-1}.s^{-1}$	Rate constant for the reaction between O2 and dissolved Fe(II)	*25°C (Temp. unquoted in Wehrli paper. So, **assumed**) *[O_2] = 1.26 x 10^{-3} mol. dm^{-3} *reaction is 1st order wrt [O_2]	k_5=2.9. Based on pH=7 experiment of Wehrli with k=3.7 x 10^{-3} s^{-1}. It is stated the reaction is highly pH dependent.	Wehrli (1990)
k_6	$dm^3.mol^{-1}.s^{-1}$	Rate constant for the reaction between Cu^{2+} and Fe(II)	*25° *No experimental data *Based on the assumption homogenous kinetics are rapid ***Assumed value**	k_6=10	King (2016)

RATE CONSTANT	UNITS	REACTION	ASSUMPTIONS	EXPRESSION	REFERENCES
k_7	s^{-1}	Rate constant for the rate of precipitation of Fe(II) solid	*25°C *No experimental data ***Assumed value**	k_7=1. Based on precipitation of Cu_2O	King (2016)
k_{-7}	s^{-1}	Rate constant for the dissolution of a Fe(II)	*25°C ***Assumed value**	k_{-7}=0.1. Based on dissolution of Cu_2O	King (2016)
k_8	s^{-1}	Rate constant for the dissolution of O_2(g)	25°C	k_8=0.0122	King (2016)
k_9	s^{-1}	Rate constant for microbial aerobic respiration	25°C	$k_9=2.2 \times 10^{-9}$.	King (2016), King and Kolar 2006

RATE CONSTANT	UNITS	REACTION	ASSUMPTIONS	EXPRESSION	REFERENCES
k_a	dm. s^{-1}	Combined electrochemical rate constant for anodic dissolution of Cu	*25°C *Based on mean value for 0.1 mol.dm^{-3} and 1.0 mol. dm^{-3} Cl^- solution	$k_a = k_{af}k_{bf}/k_{ab} = 3.3 \times 10^{-4}$.	King et al. (1995)
k_{bb}	$dm \cdot s^{-1}$	Rate constant for the reverse reaction involving $CuCl_2^-$	25°C	$k_{bb} = 1.42 \times 10^{-3}$.	King et al. (1995)
k_c	dm. s^{-1}	Electrochemical rate constant for O_2 reduction	25°C	$k_c = 1.7 \times 10^{-9}$	King et al. (1995)
k_d	$dm \cdot s^{-1}$	Electrochemical rate constant for the reduction of Cu^{2+}	*25 °C *Based on i/E curves	$k_d = 2 \times 10^{-8}$	Hurlen (1961)

3.3 Conclusion

The development of CCM-UC model has been divided into several steps (Step 1 to Step 6) with increasing complexity. These steps were used to develop CCM using COMSOL Multiphysics, incorporating interfacial current equations (Butler-Volmer) along with diffusion equations. The COMSOL model has been completed up to Step 3d which includes reduction of copper ions, oxidation of copper chloride ions, precipitation and dissolution of paratacamite.

CHAPTER FOUR: COMSOL MODEL VERIFICATION

4.1 Description

The CCM model was used to verify the COMSOL model. In order to do that, the CCM model was modified to align with the step-wise approach taken in this work. The same parameters were used, as input for both COMSOL and CCM. Although most of the results matched extremely well between the two models, some variation was observed in Step 2, as well as, the current density outputs. This may be due to various reasons. First, COMSOL is solved using finite elements method while CCM is solved using finite difference methods. Although the two models have similar outputs and have been tested to be independent of both time and space discretization, the solvers are different, and it is possible for this to be reflected in the results. For example, both models use approximately the same initial time step, 10^{-7} hours. However, each model uses a different method for determining dynamic time stepping throughout the run of each simulation (CCM results are only reported starting at 10^{-4} hours). Similarly, while the smallest space discretization is also the same between each model, the CCM model uses an increasing grid size moving away from the copper surface where the COMSOL model uses a constant grid size. Other factors (i.e. time dependent boundary conditions) could lead to a difference in solution and while the COMSOL code is controlled for many of these factors, the CCM code is not controlled by or run by the author of this work directly.

To verify the COMSOL model, all the specie concentrations were compared, as well as, the current density and corrosion potential. For the species concentrations, excellent agreement was obtained between the two models. All parameters in the COMSOL code are able to reproduce the same behavior and trend compared to CCM, and in most cases the absolute values of species concentration are also reproduced. However, the species concentration plots of Step 2 for 1 mm bentonite layer differs slightly during the initial time (0-10 hours) although the same step for 10 mm matches up well.

Similarly, although the trend is similar, there is slight deviation with the current density absolute value shown for both Step 2 and 3d. The following chapter shows the comparison between the two models for only Step 2 and 3d, the rest of the steps are shown in the *Appendix B.*

4.1.1 Assumptions

Several assumptions were taken when running the CCM and COMSOL models:

I. The tortuosity was taken as 0.12195 instead of 0.05 as indicated in Fraser (2016) document. Moreover, the maximum Cu (II) adsorbed (c_{5max}) was taken as zero instead of 0.3 mol/kg as indicated in the same reference document. This was done to match all the CCM input parameters.

II. The temperature of the system is taken to be 25 ^{o}C, unlike in the DGR where the temperature will be initially high (up to 80 ^{o}C) and gradually decrease with time.

III. The system is assumed to be completely saturated. This is not the case for the DGR, as saturation will be low initially.

IV. Pressure of the DGR is not taken into account

V. The system has been designed based on CCM-UC until Step 3d. Future steps overcomes the following shortcomings:

   a. The system considered to be in 1 D
   b. Influence of microbes are absent
   c. There is no sulfide in the system

4.2 Comparison of CCM and COMSOL Plots

The concentration profiles of different species (O_2, Cl^-, $CuCl_2^-$, Cu_2O, $CuCl_2.3Cu(OH)_2$) with time have been plotted along with the variation of current density with distance from the interface of copper and bentonite. Moreover, the variation of corrosion potential with time has been plotted for both CCM and the COMSOL model. In all plots the solid line represents the COMSOL results while the dots represent CCM results.

- Figure 4.1 to Figure 4.6 shows the profile for Step 2 for the 1mm bentonite case. Although there is some deviation from the CCM profile, the later complex steps involving more reactions matches accurately.
- Figure 4.7 to Figure 4.14 shows the profile for Step 3d for 1 mm layer of bentonite and Figure 4.15 to Figure 4.22 shows the profile for Step 3d for 10 mm layer. It can be seen that the concentration profiles of CCM and COMSOL match accurately for both the layers of bentonite.

- The current density profiles (Figure 4.3, Figure 4.11 and Figure 4.19) show a slight deviation from the CCM profiles, but there is perfect overlap of corrosion potential profile (Figure 4.6, Figure 4.14 and Figure 4.22) in all the cases.
- The reason for deviations of current profiles and Step 2 is not fully clear even though numerous debugging were done.

4.2.1 1 mm Bentonite Layer

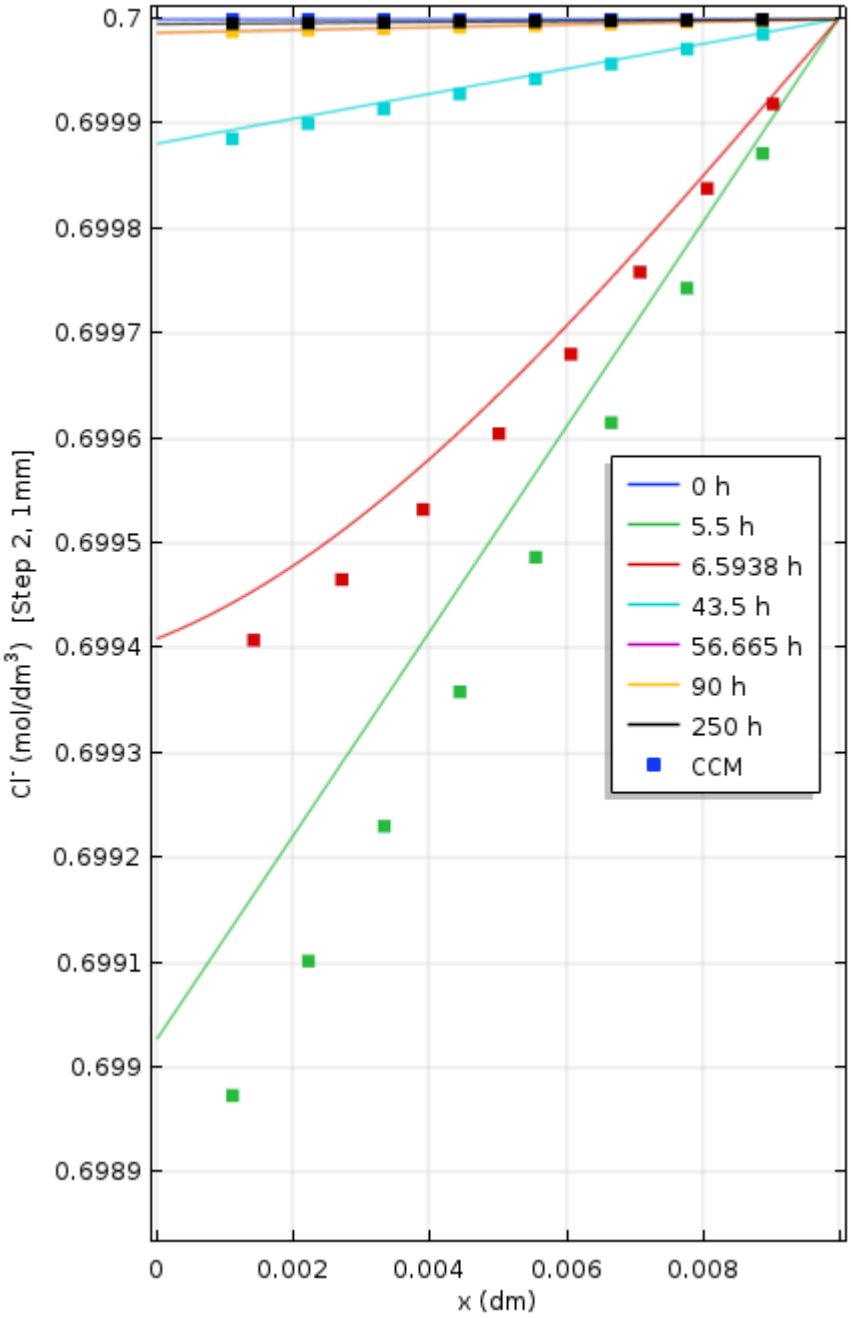

Figure 4.1: Concentration profile of chloride over bentonite thickness (1 mm), Step 2

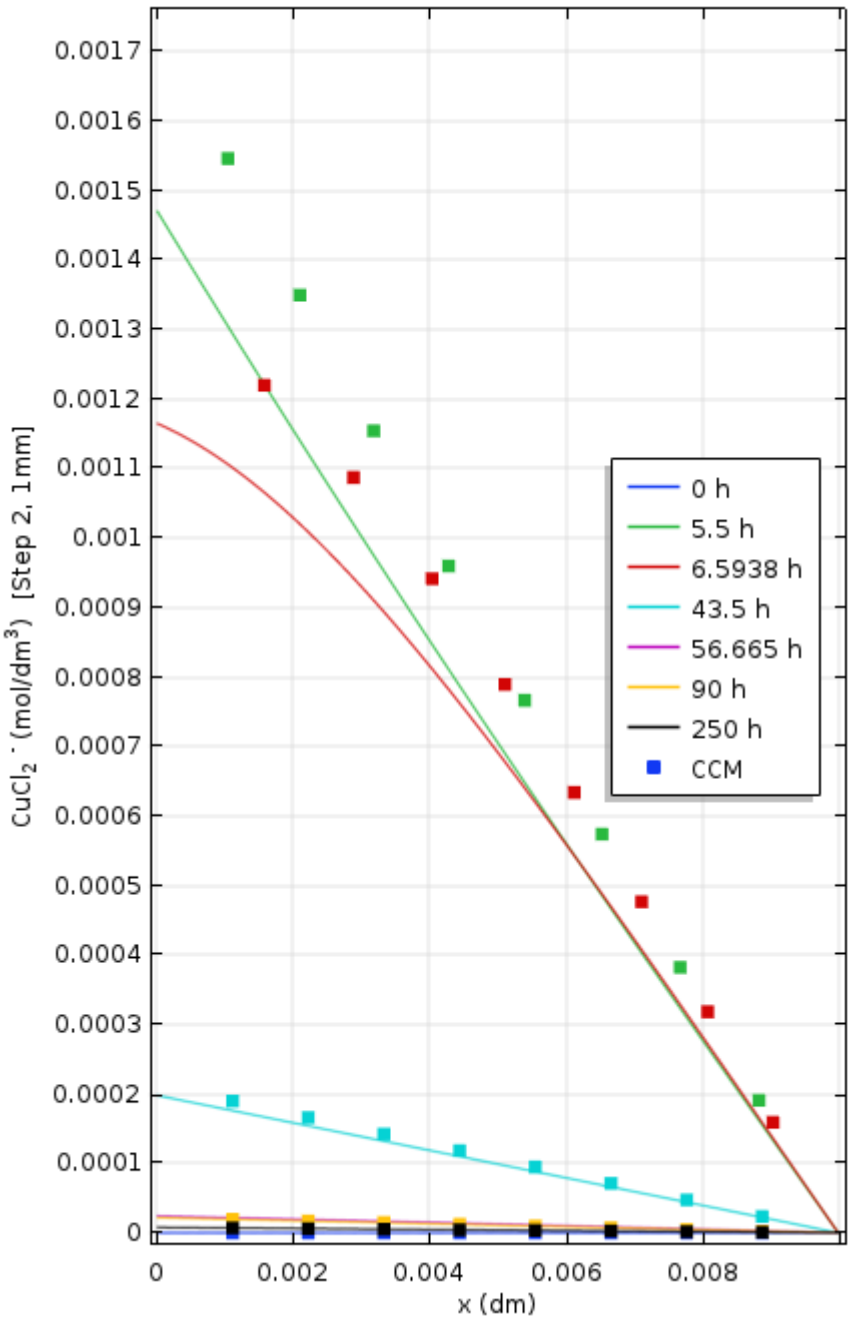

Figure 4.2: Concentration profile of copper chloride ions over bentonite thickness (1 mm), Step 2

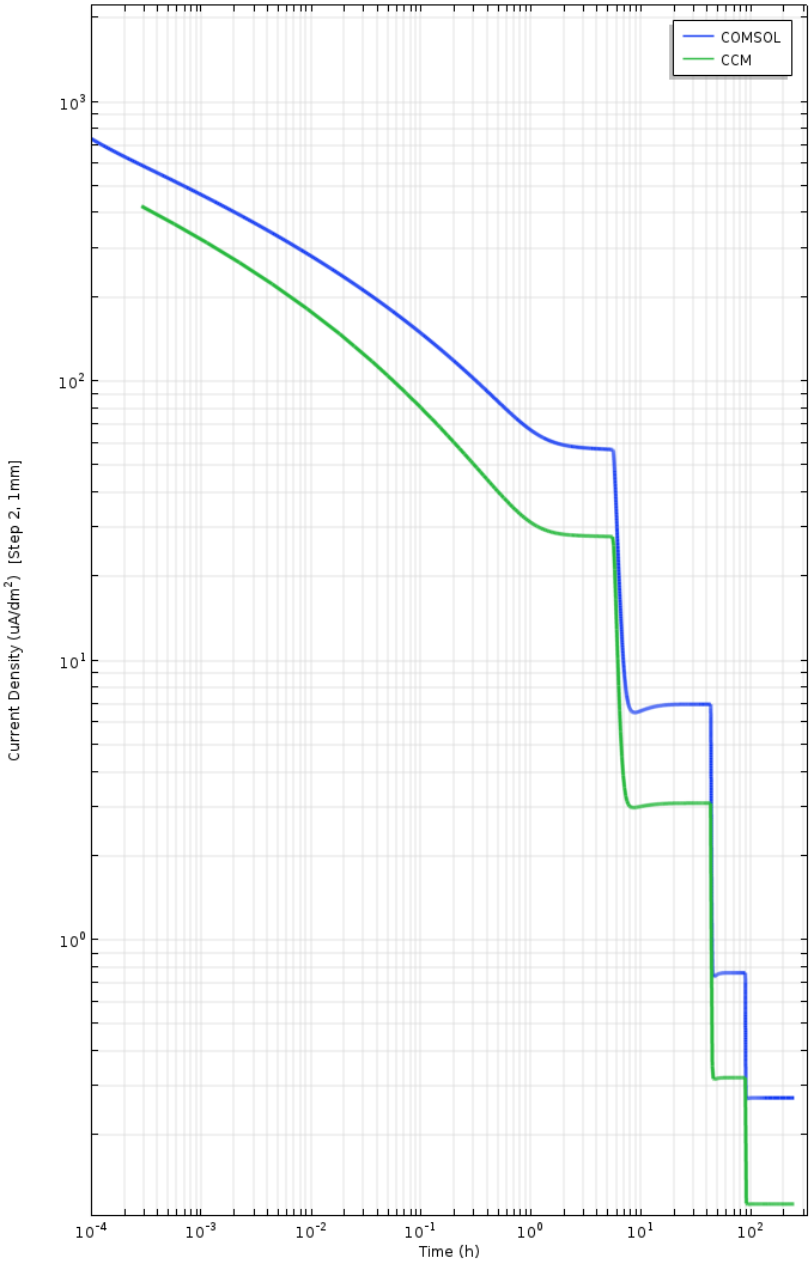

Figure 4.3: Current density profile over time for 1 mm bentonite thickness, Step 2

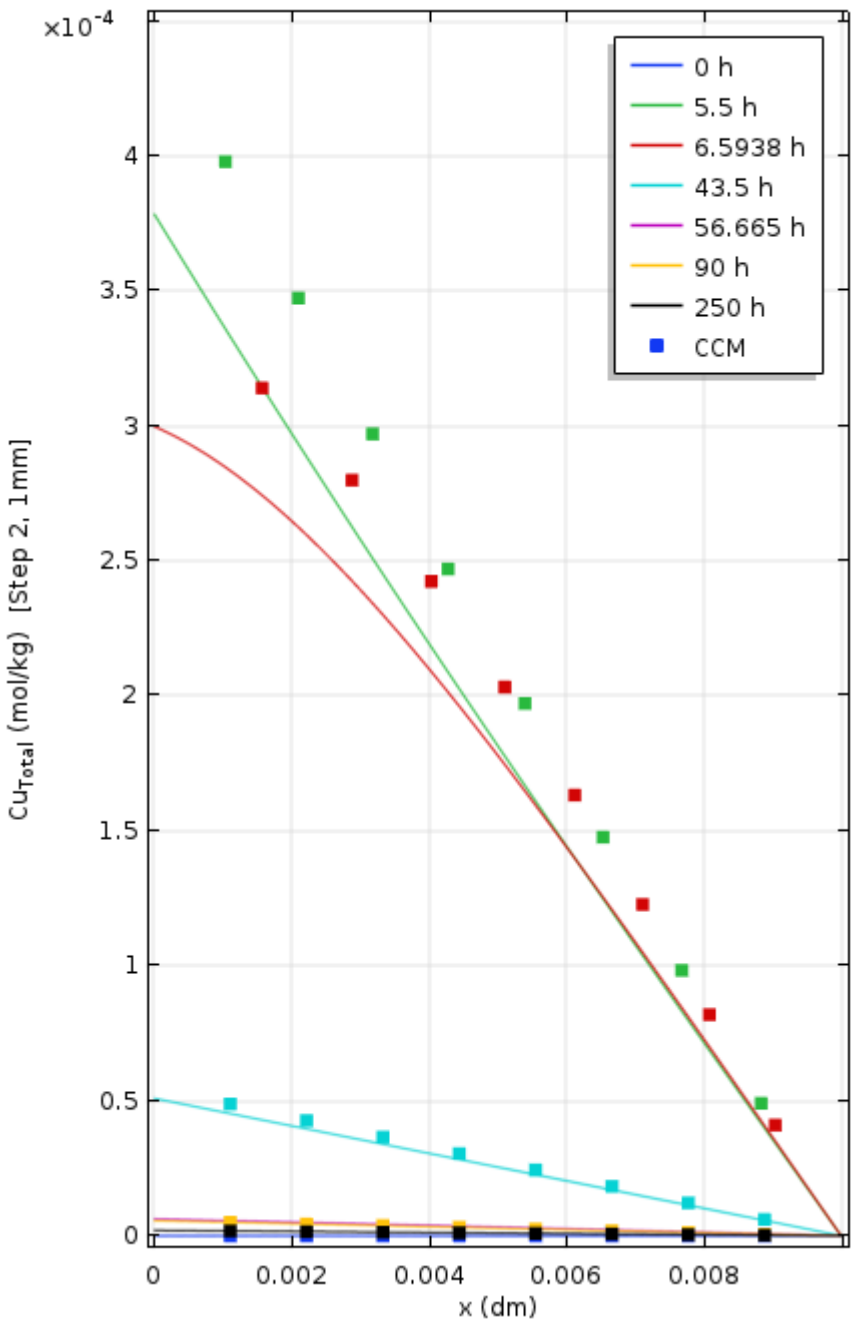

Figure 4.4: Concentration profile of total amount of copper ($CuCl_2^-$, Cu^{2+}, Cu_2O, $CuCl_2.3Cu(OH)_2$ over bentonite thickness (1 mm), Step 2

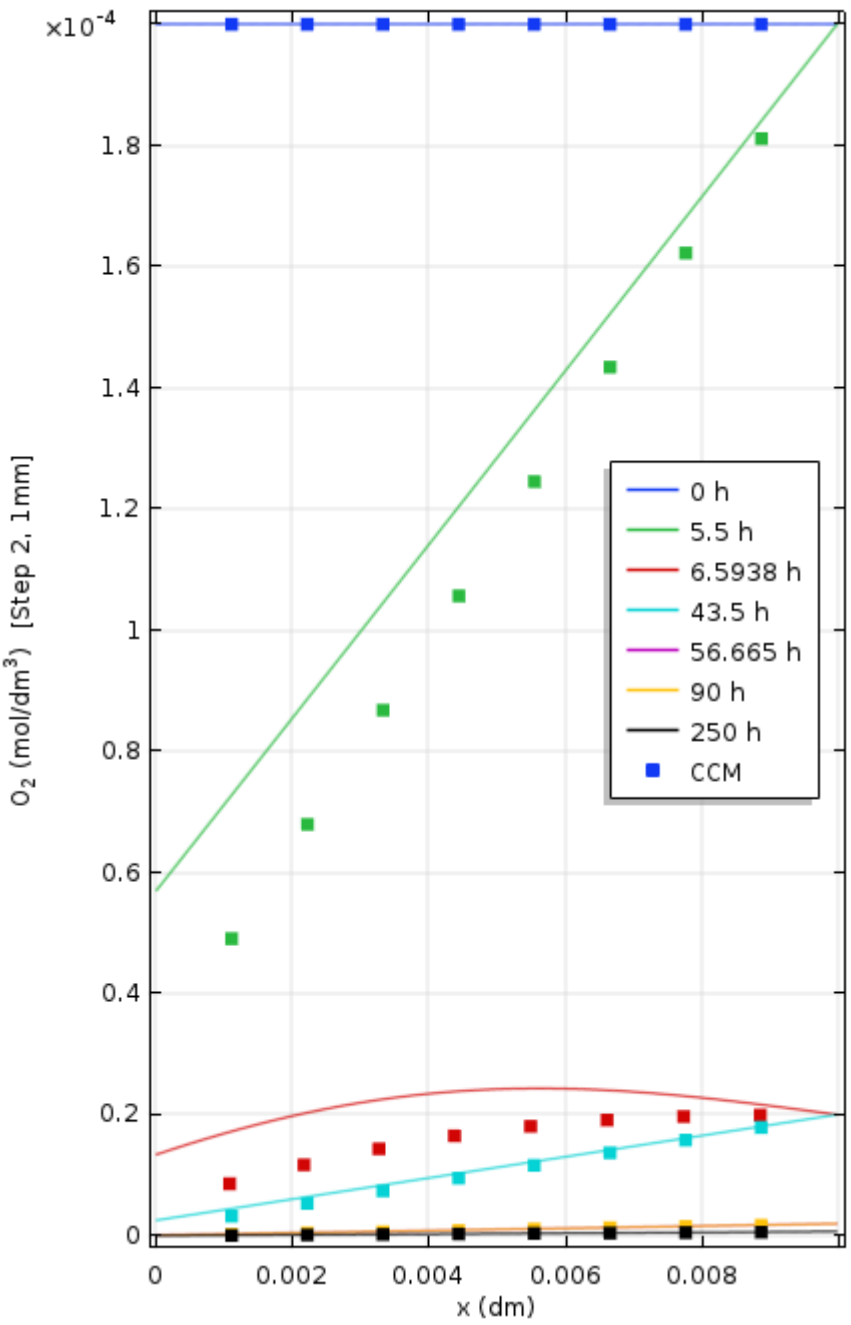

Figure 4.5: Concentration profile of oxygen over bentonite thickness (1 mm), Step 2

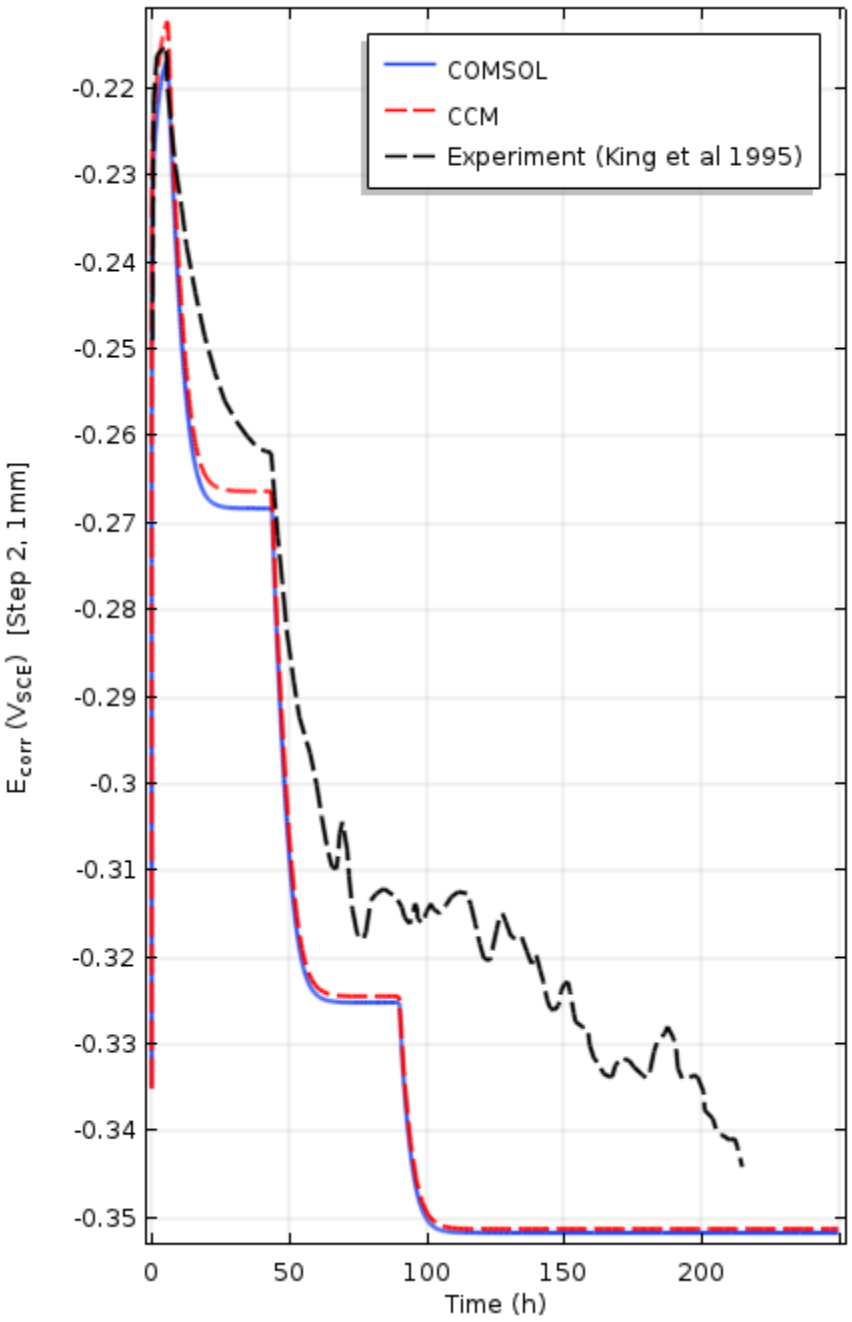

Figure 4.6: Variation of corrosion potential with time for 1 mm bentonite thickness with changing oxygen concentration for Step 2

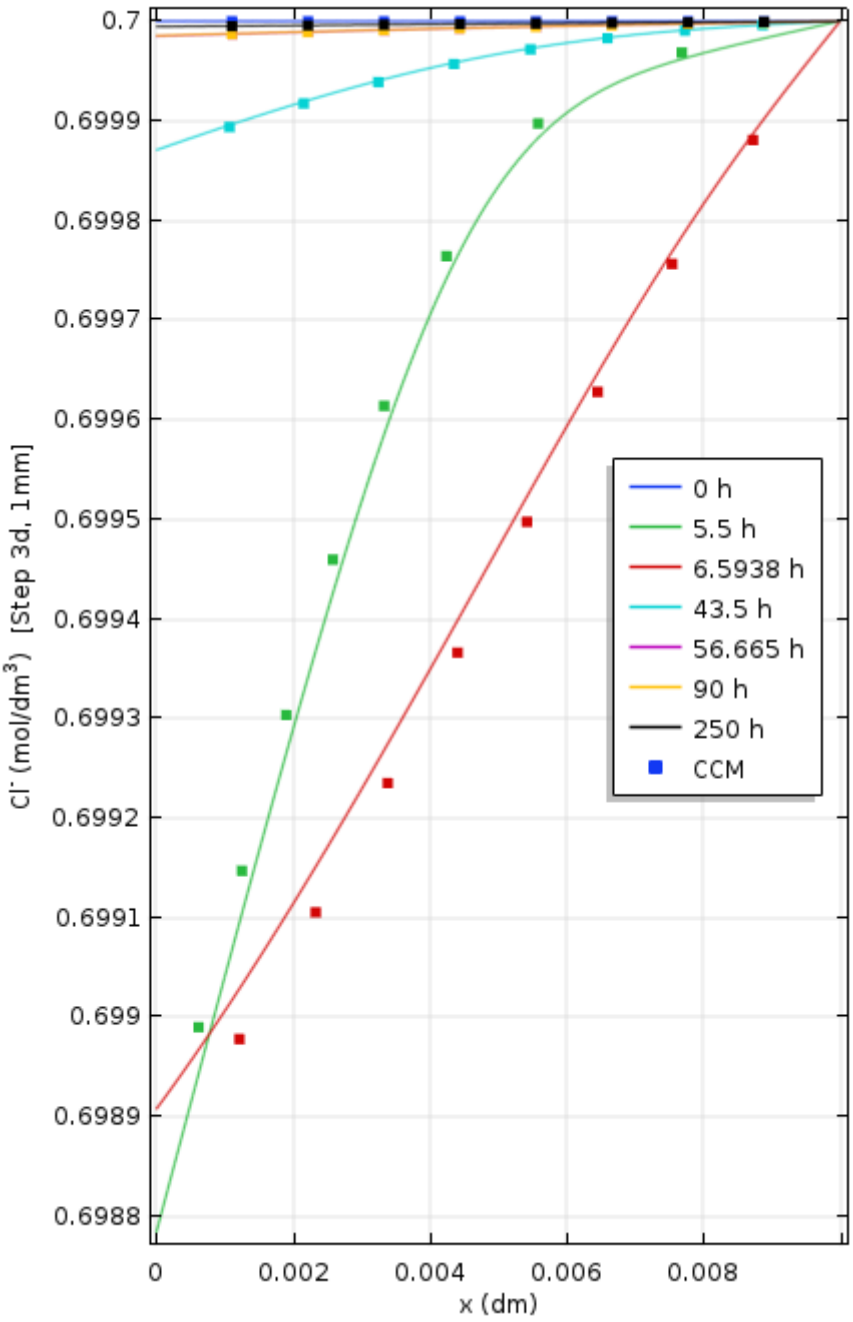

Figure 4.7: Concentration profile of copper chloride ions over bentonite thickness (1 mm), Step 3d

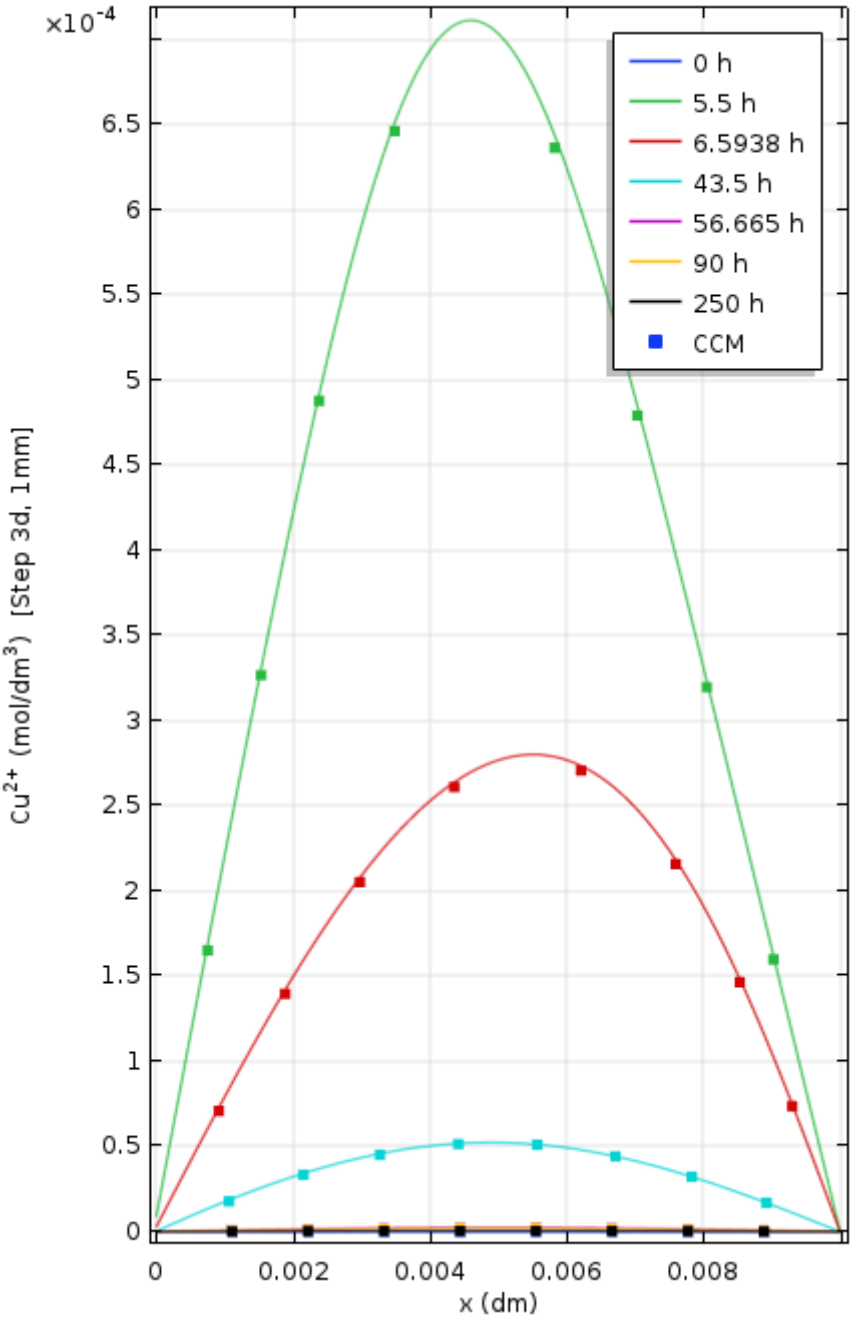

Figure 4.8: Concentration profile of copper ions over bentonite thickness (1 mm), Step 3d

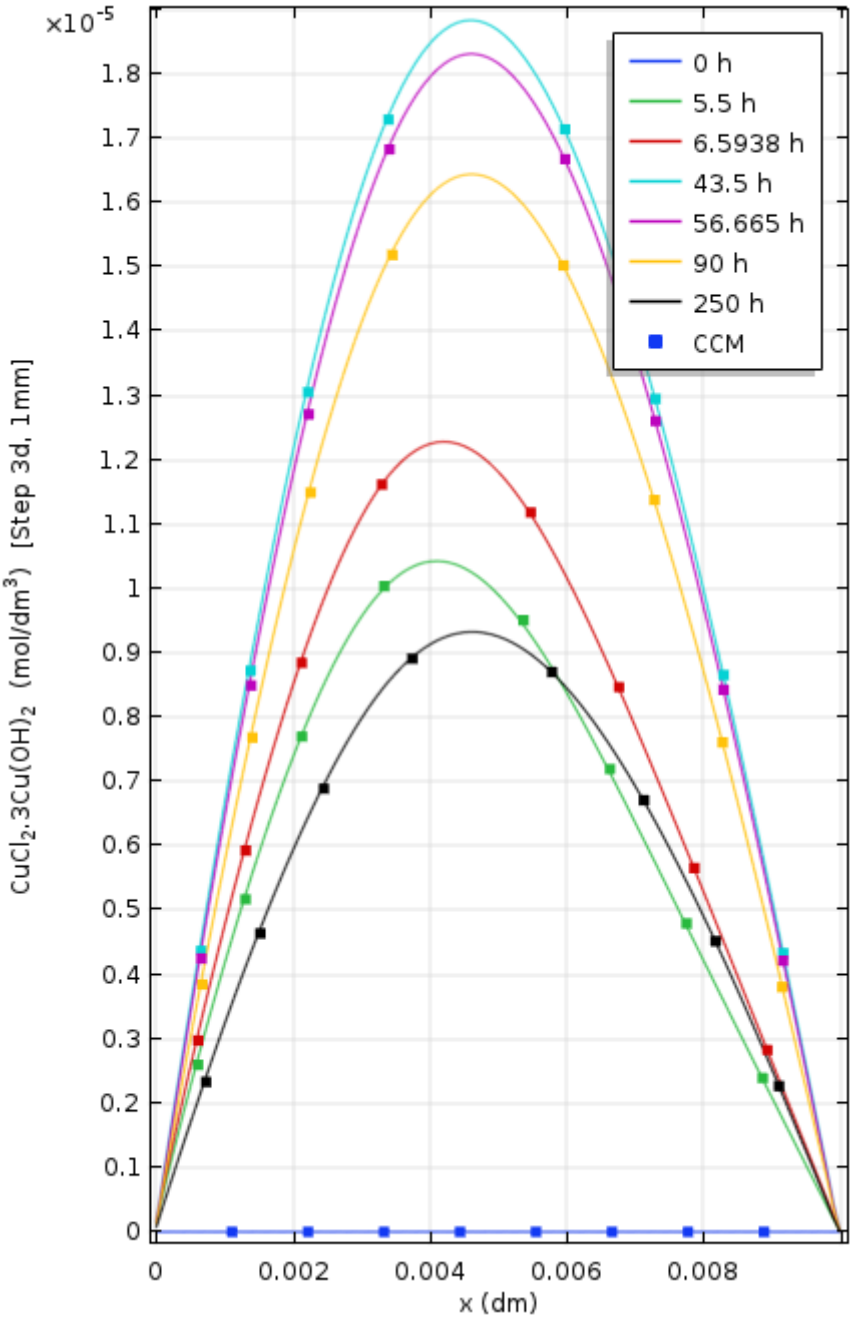

Figure 4.9: Concentration profile of paratacamite over bentonite thickness (1 mm), Step 3d

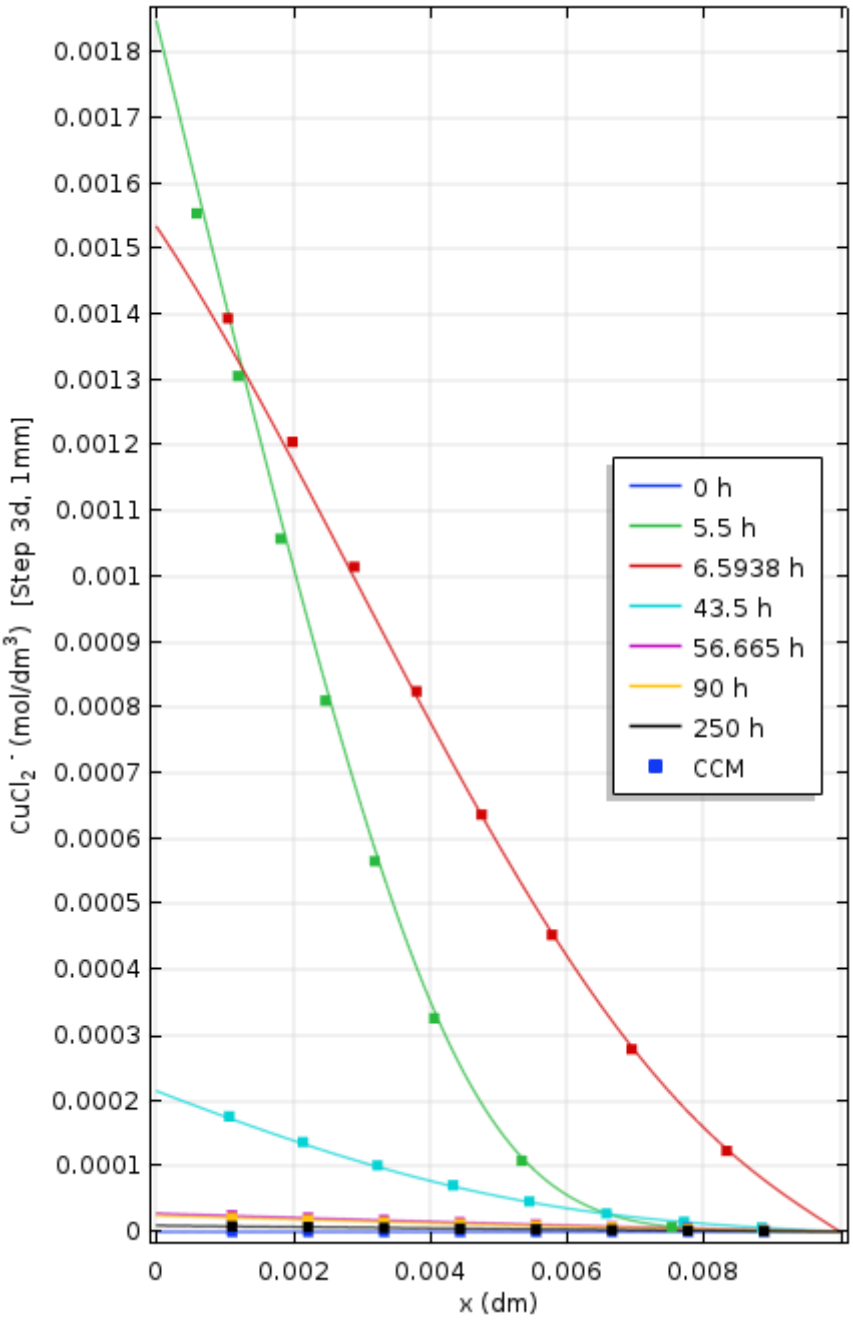

Figure 4.10: Concentration profile of copper chloride ions over bentonite thickness (1 mm), Step 3d

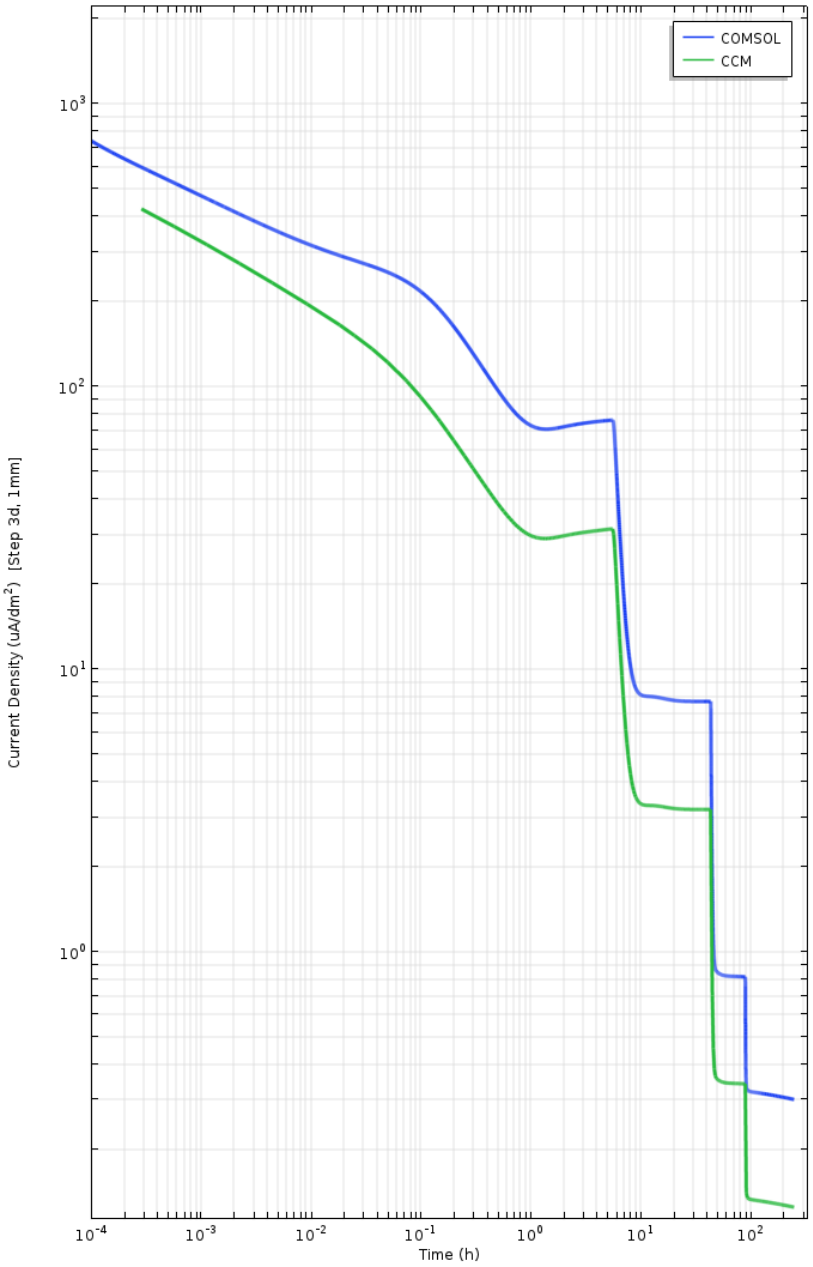

Figure 4.11: Current density profile over time for 1 mm bentonite thickness, Step 3d

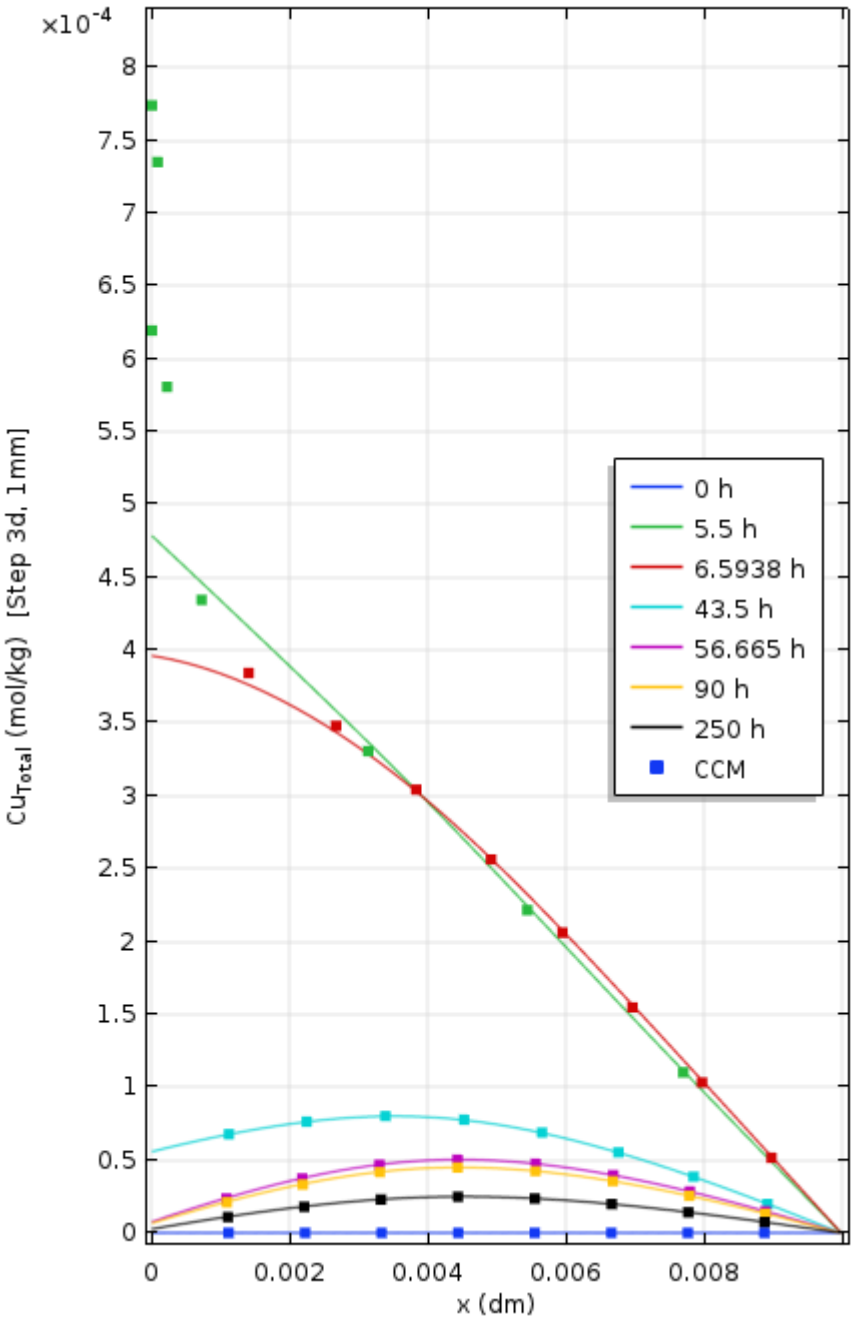

Figure 4.12: Concentration profile of total amount of copper ($CuCl_2^-$, Cu^{2+}, Cu_2O, $CuCl_2.3Cu(OH)_2$) over bentonite thickness (1 mm), Step 3d

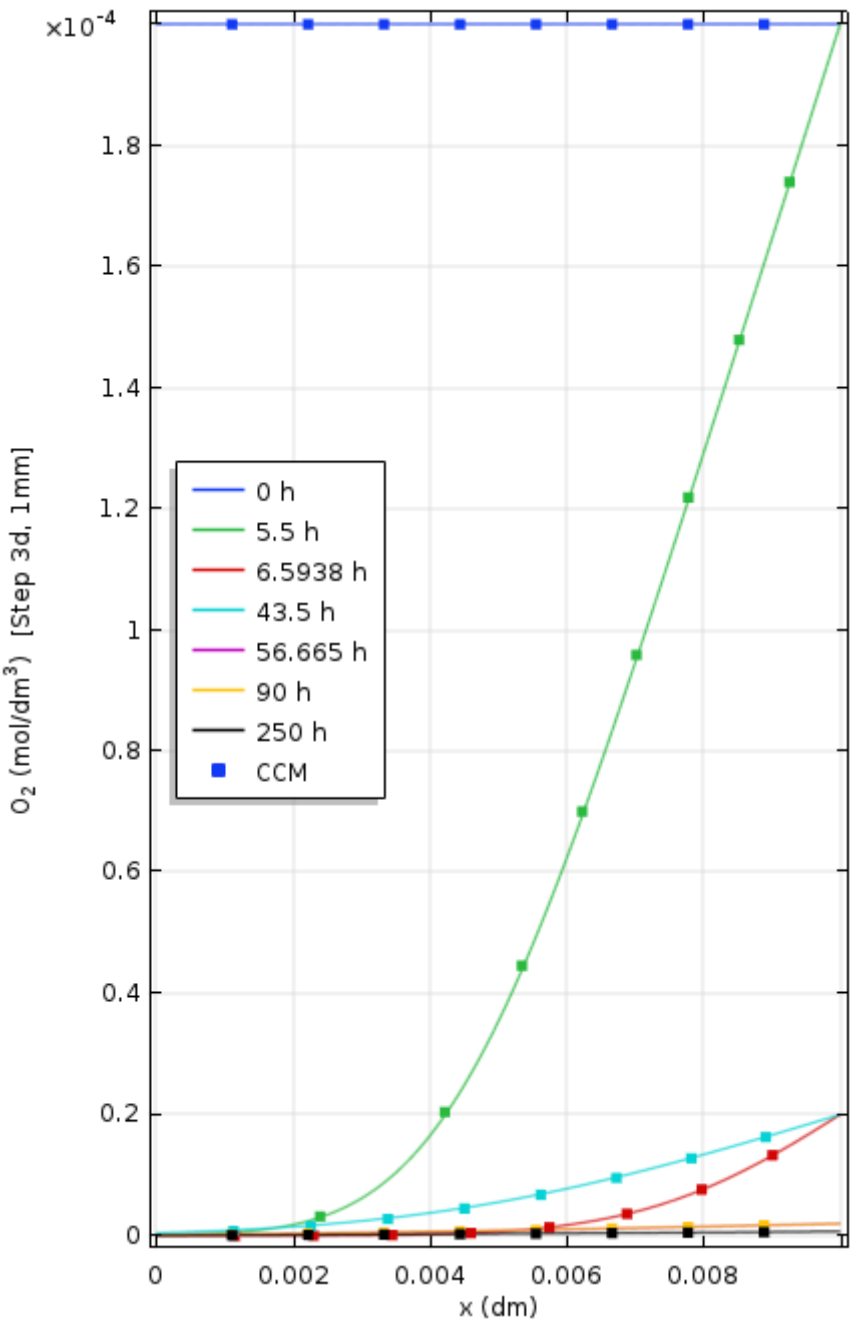

Figure 4.13: Concentration profile of oxygen over bentonite thickness (1 mm), Step 3d

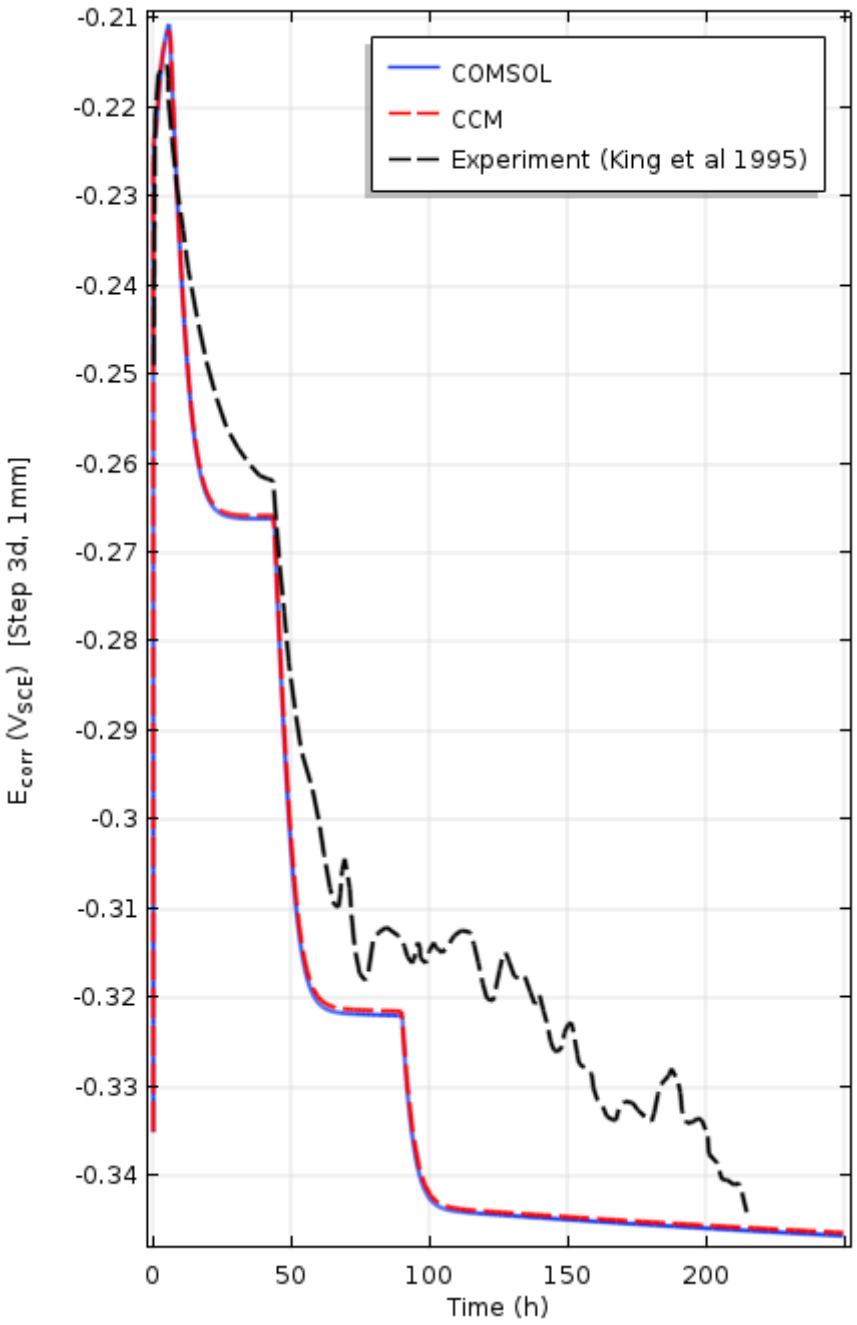

Figure 4.14: Variation of corrosion potential with time for 1 mm bentonite thickness with changing oxygen concentration for Step 3d

4.2.2 10 mm Bentonite thickness

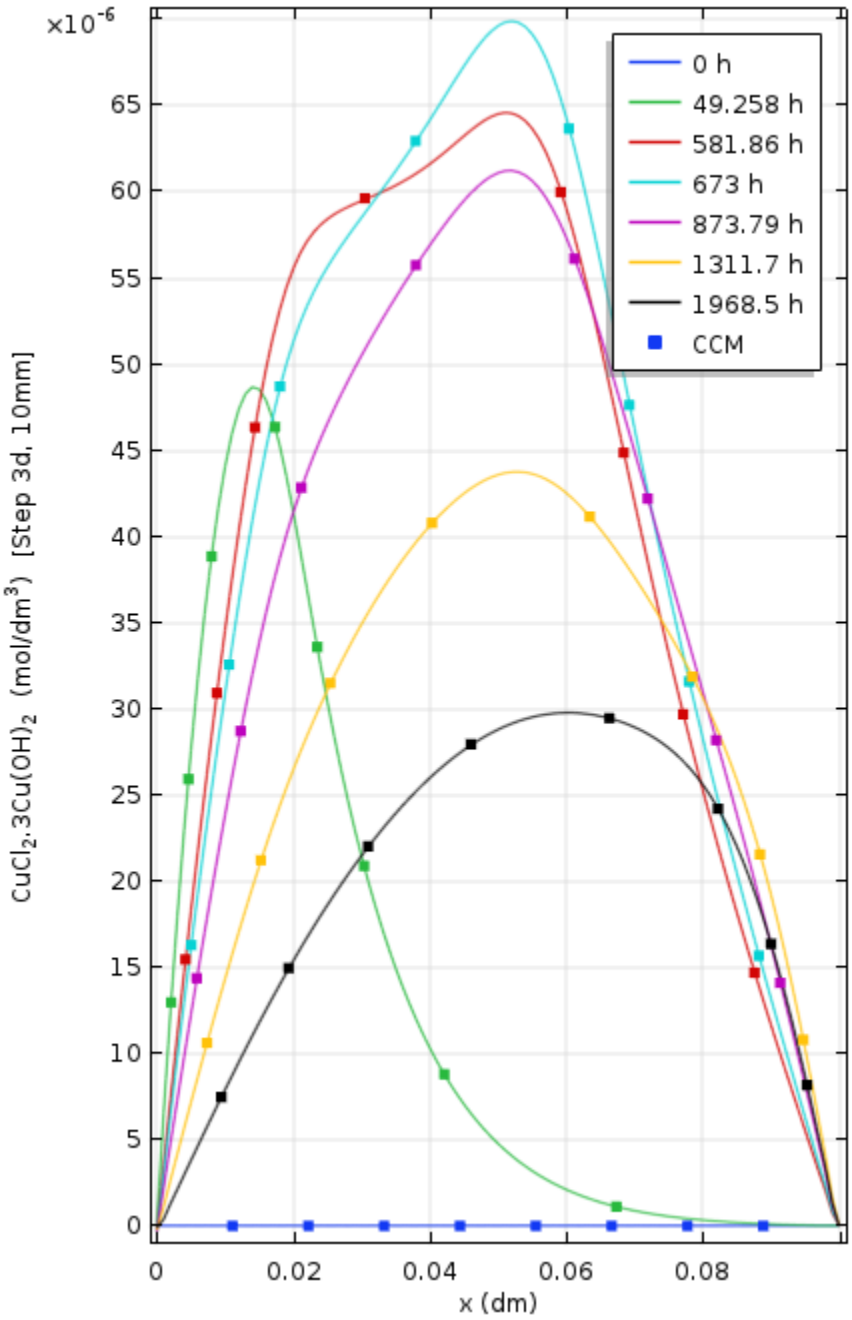

Figure 4.15: Concentration profile of paratacamite over bentonite thickness (10 mm), Step 3d

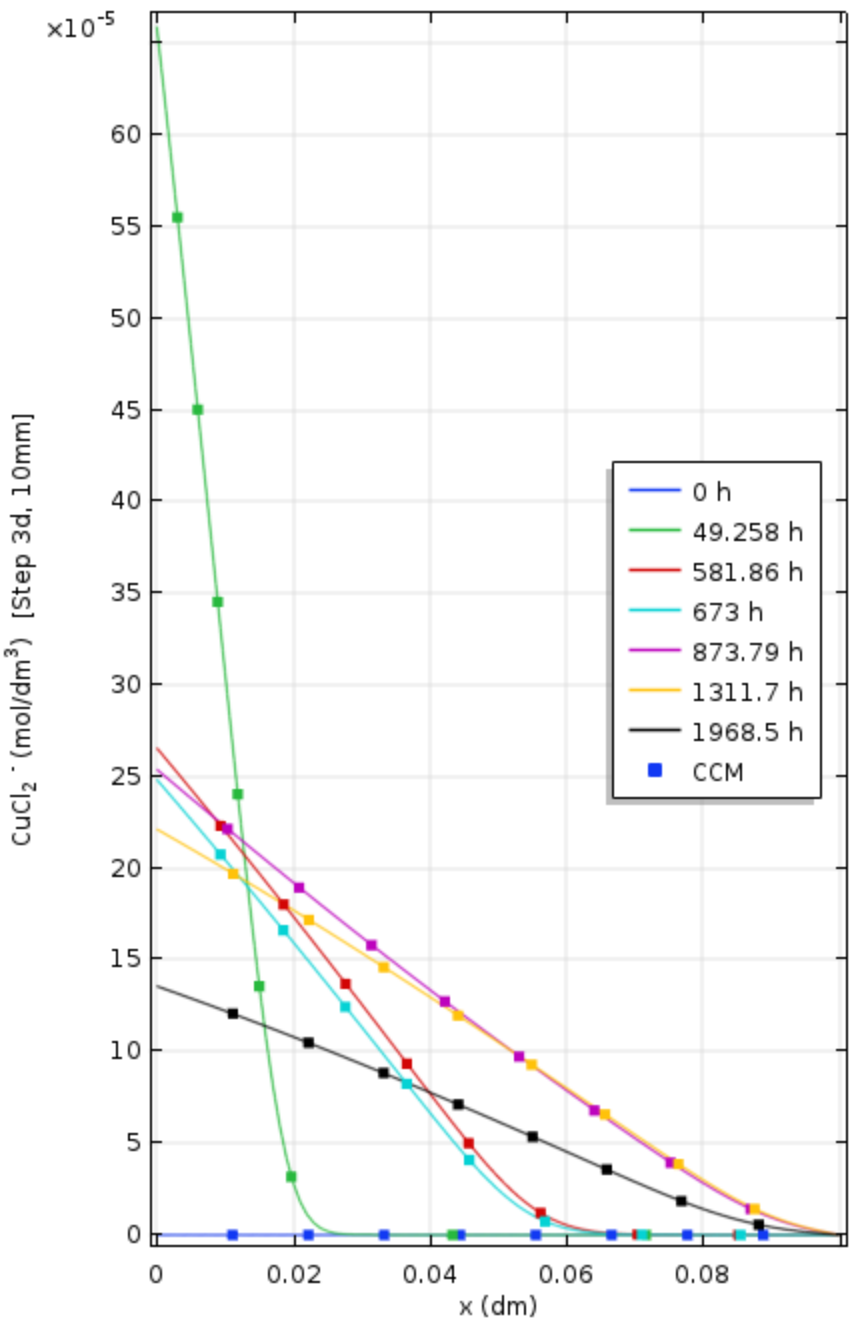

Figure 4.16: Concentration profile of copper chloride ions over bentonite thickness (10 mm), Step 3d

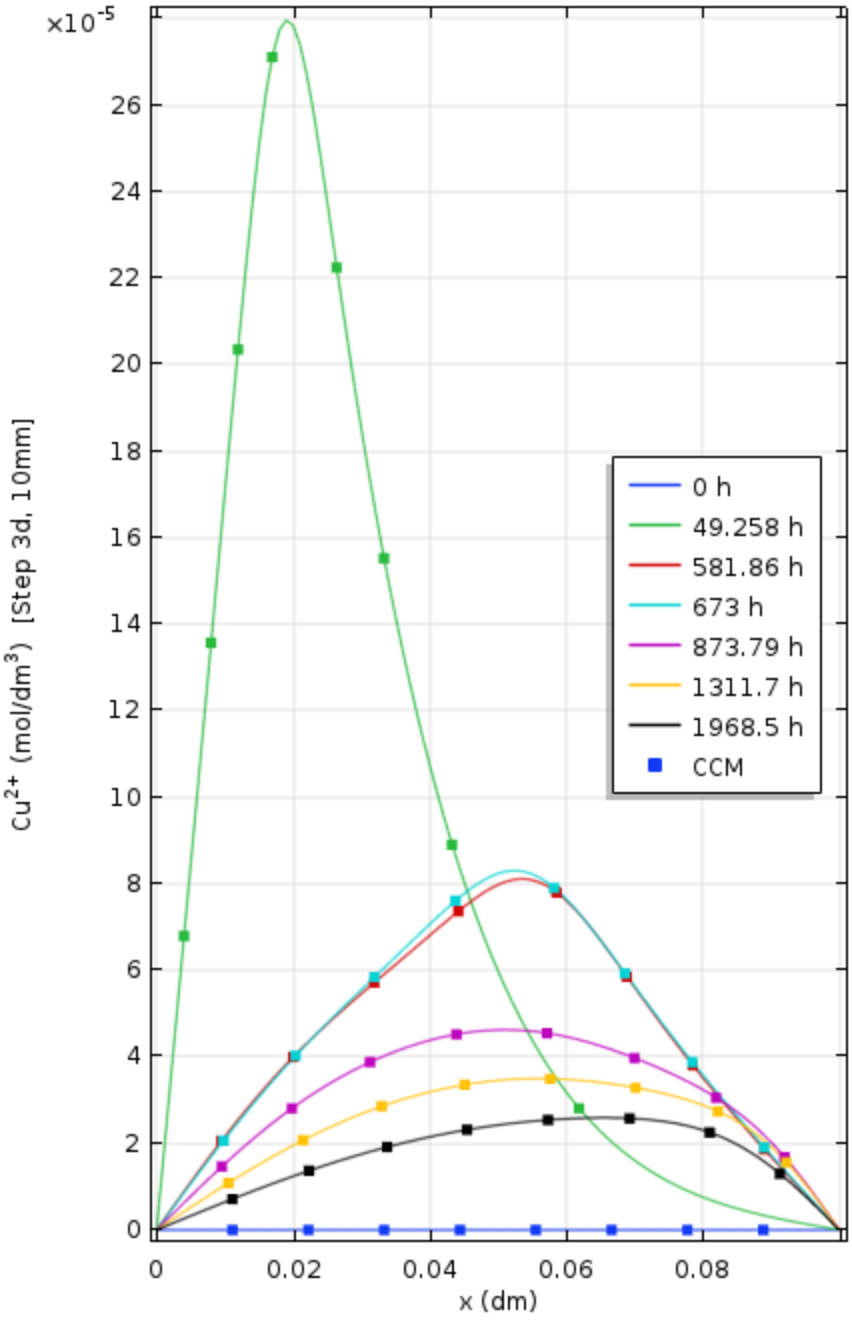

Figure 4.17: Concentration profile of copper ions over bentonite thickness (10 mm), Step 3d

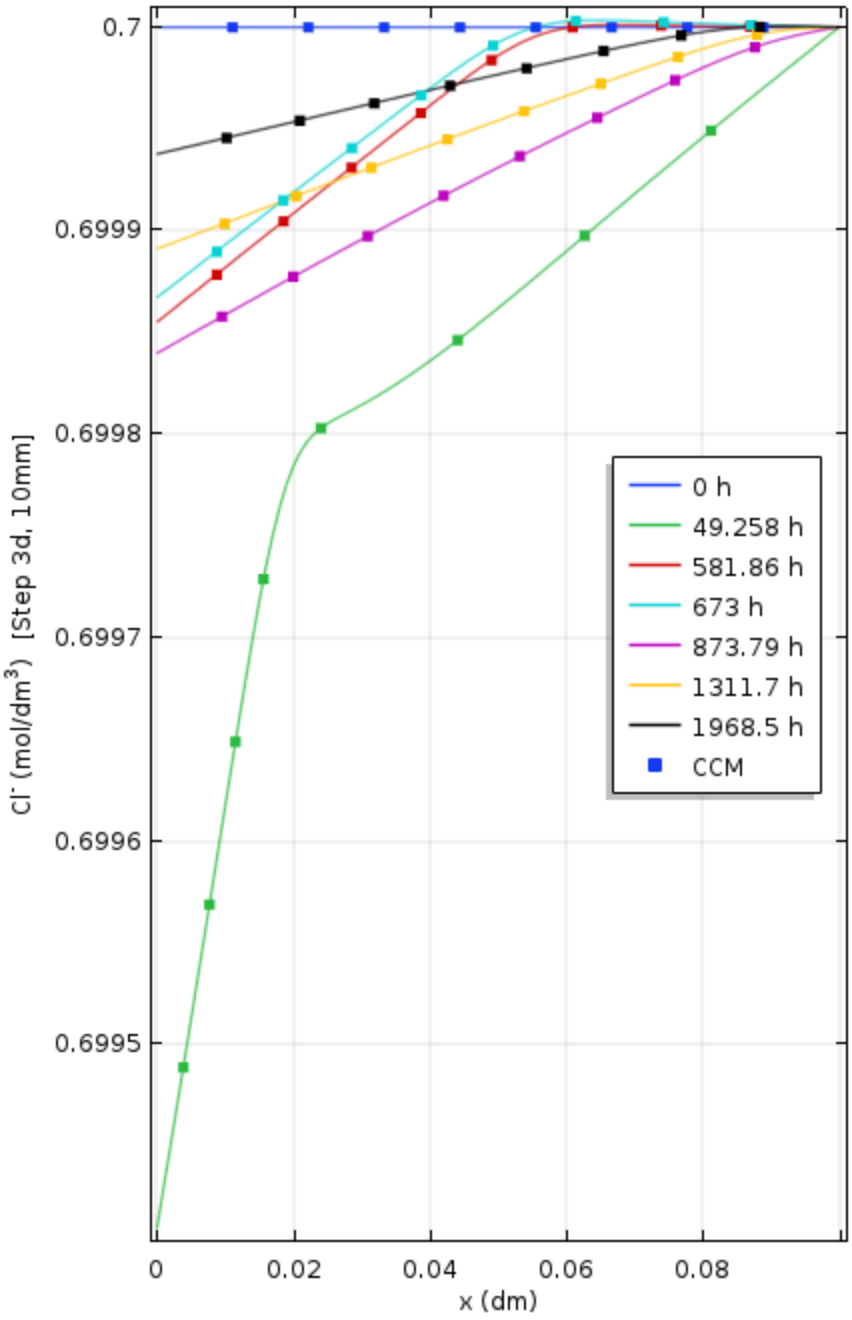

Figure 4.18: Concentration profile of chloride ions over bentonite thickness (10 mm), Step 3d

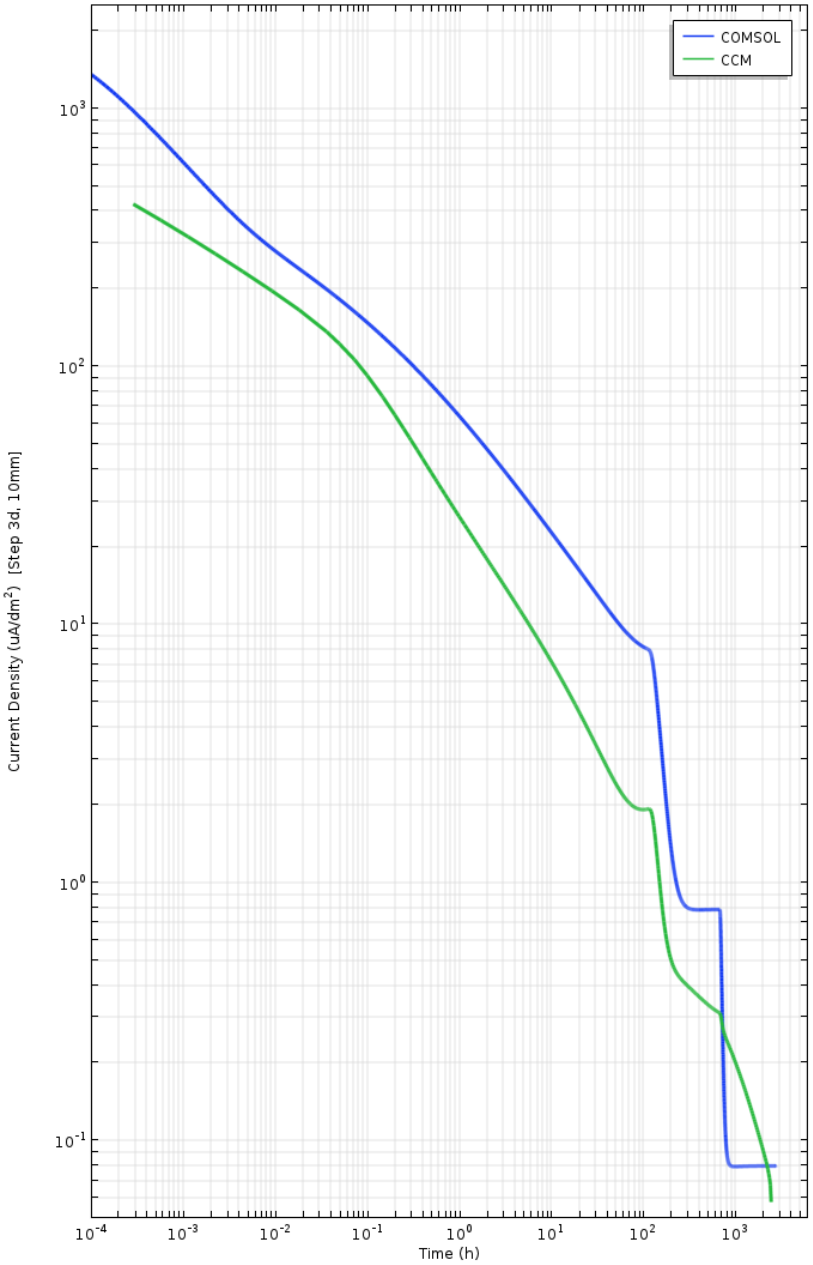

Figure 4.19: Current density profile over time for 10 mm bentonite thickness, Step 3d

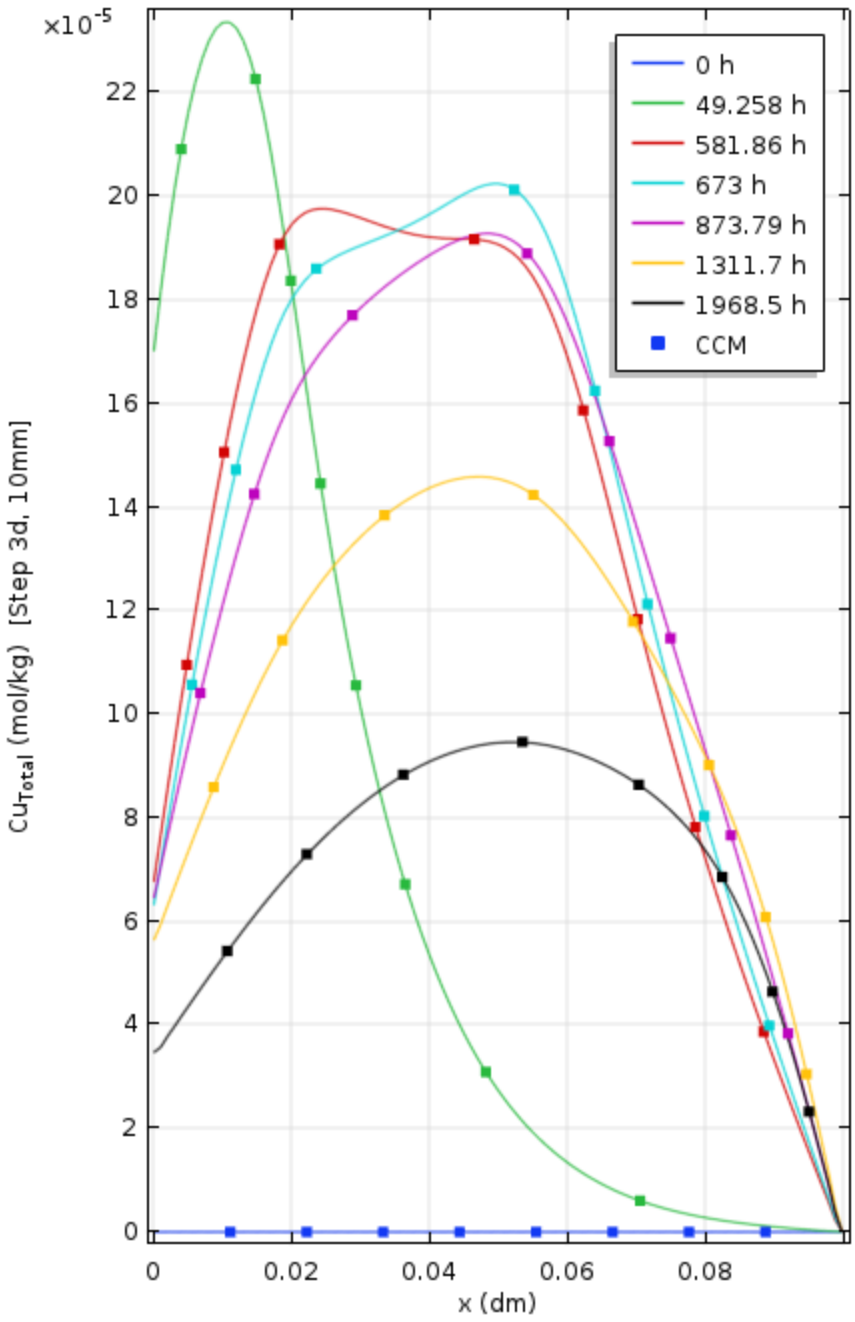

Figure 4.20: Concentration profile of total amount of copper ($CuCl_2^-$, Cu^{2+}, Cu_2O, $CuCl_2.3Cu(OH)_2$) over bentonite thickness (10 mm), Step 3d

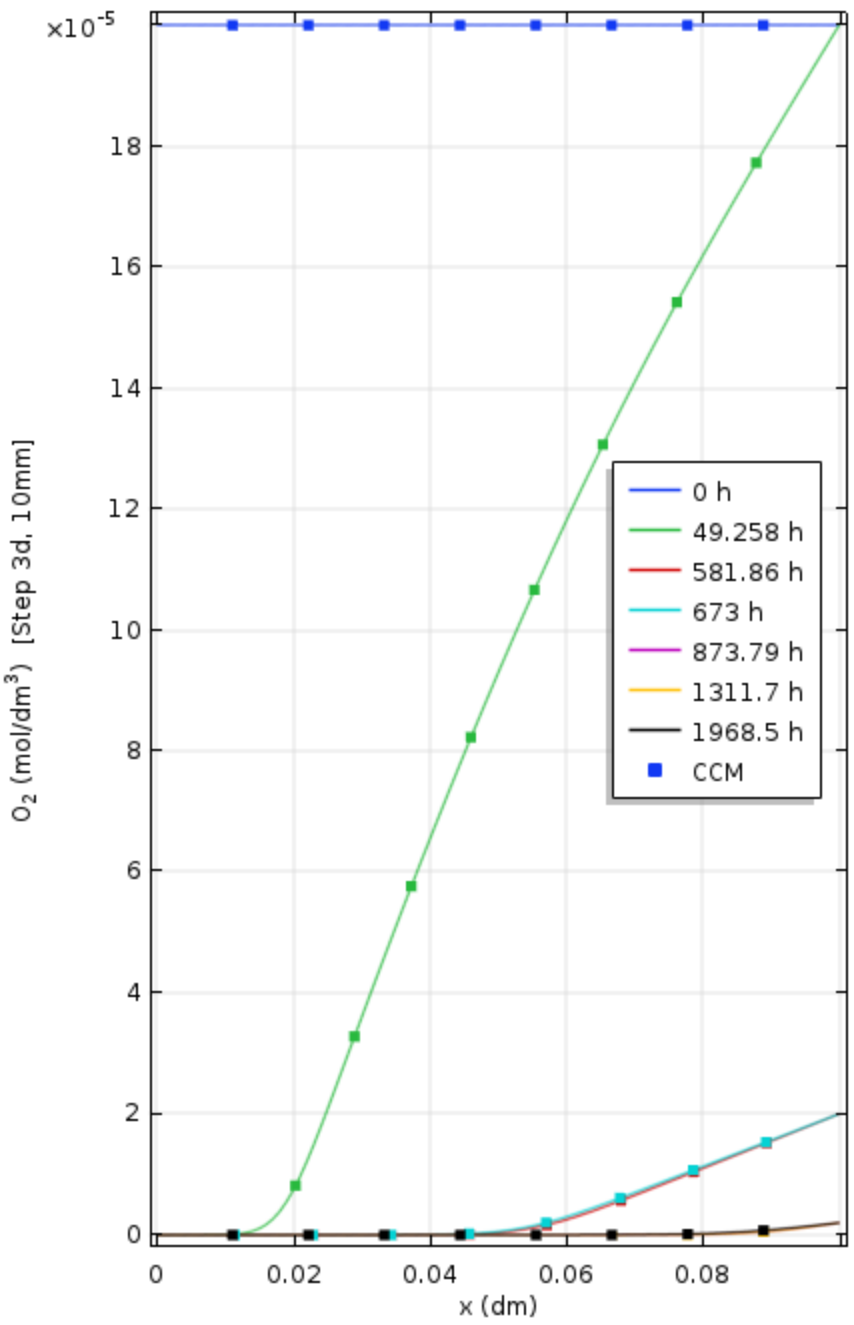

Figure 4.21: Concentration profile of oxygen over bentonite thickness (10 mm), Step 3d

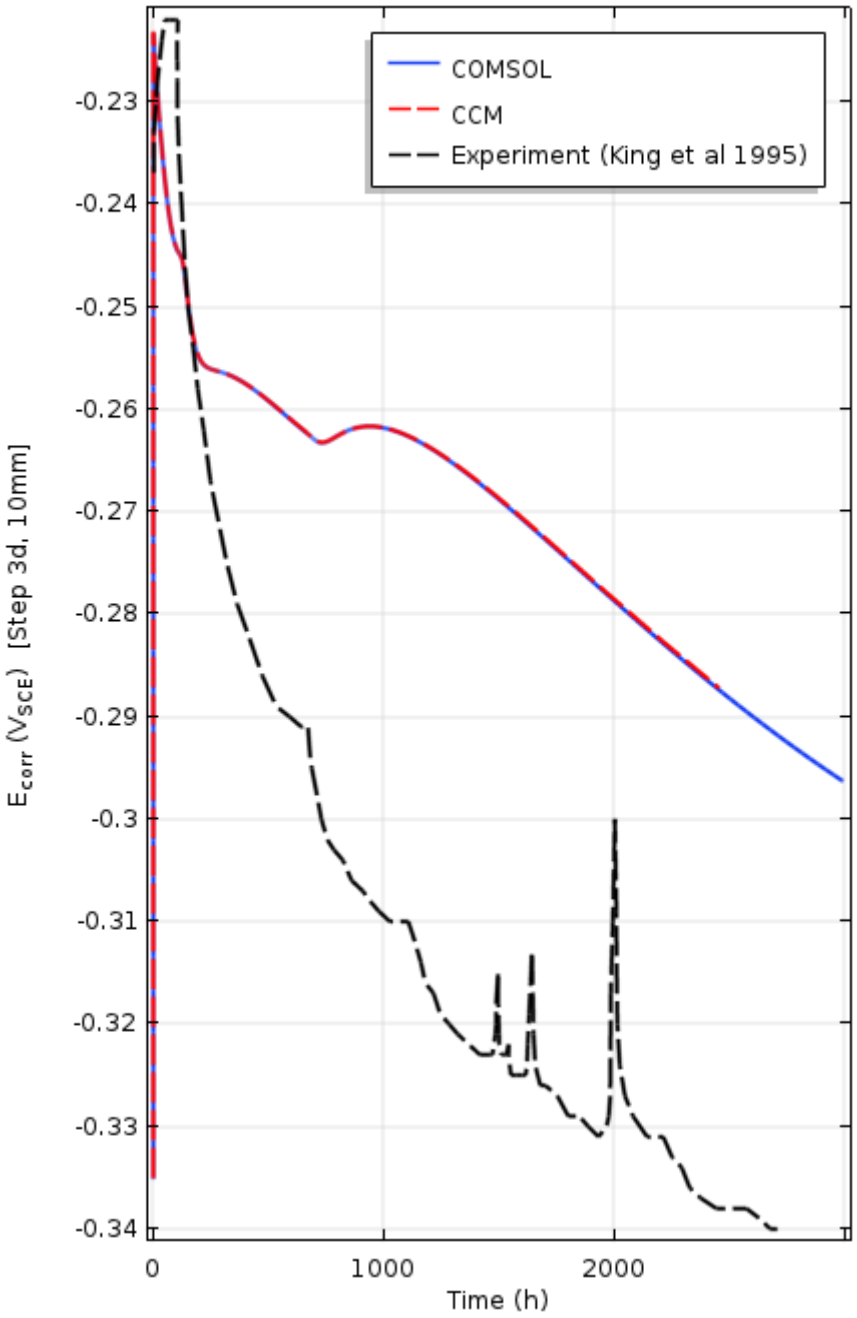

Figure 4.22: Variation of corrosion potential with time for 10 mm bentonite thickness with changing oxygen concentration for Step 3d

4.3 Conclusion

Outputs from COMSOL was verified against CCM outputs for the same input parameters. A slight deviation for Step 2 was observed for the two models as well as in the current density profile. Numerous debugging was done but the matching was still not ideal. The concentration profiles with distance and corrosion potential profile with time match the outputs of that of CCM with high accuracy. Since the latter, more complex steps matched the CCM model, it was determined that the COMSOL model has been verified.

CHAPTER FIVE: MODEL VALIDATION

5.1 Description

Once the COMSOL model was verified, it was validated by comparing it with an experiment conducted by King et al. (1995). This experiment consisted of two copper samples covered in a 1 mm and 10 mm layer of bentonite respectively. These were placed in separate NaCl bulk solutions (with an initial NaCl concentration 1000 mol/m^3 with an activity coefficient of 0.657) and equilibrated with compressed air with an initial concentration of 20 vol% O_2/N_2. This was progressively reduced to 2 vol% O_2/N_2 and 0.2 vol% O_2/N_2 and finally resulting in deaerated conditions using ultra-high purity Ar or N_2. In the 1 mm experiment, there was an accidental overpurge of oxygen at 70 hours, which led to E_{corr} fluctuations as shown in Figure 5.2. This indicates that the corrosion potential is significantly sensitive to oxygen concentration.

Table 5.1: Change in oxygen concentration with time for both 1 mm and 10 mm bentonite layers dipped in NaCl (King et al., 1995)

Oxygen concentration (mol/m^3)	**Time (h)**	
	1 mm	**10 mm**
0.2	0-5.5	0-107.4
0.02	5.5-43.5	107.4-673
0.002	43.5-90	673-2500
0.0007	>90 (till ~250 h)	>2500 (till ~2700 h)

Figure 5.1 shows the experimental setup. The copper sample was covered by a bentonite layer of 1 mm or 10 mm and then covered by a platinum mesh which also allowed for contact with the bulk solution of NaCl. The solution was aerated with oxygen through the inlet as shown in the figure. The potential in the copper sample was measured with a saturated calomel reference electrode (SCE).

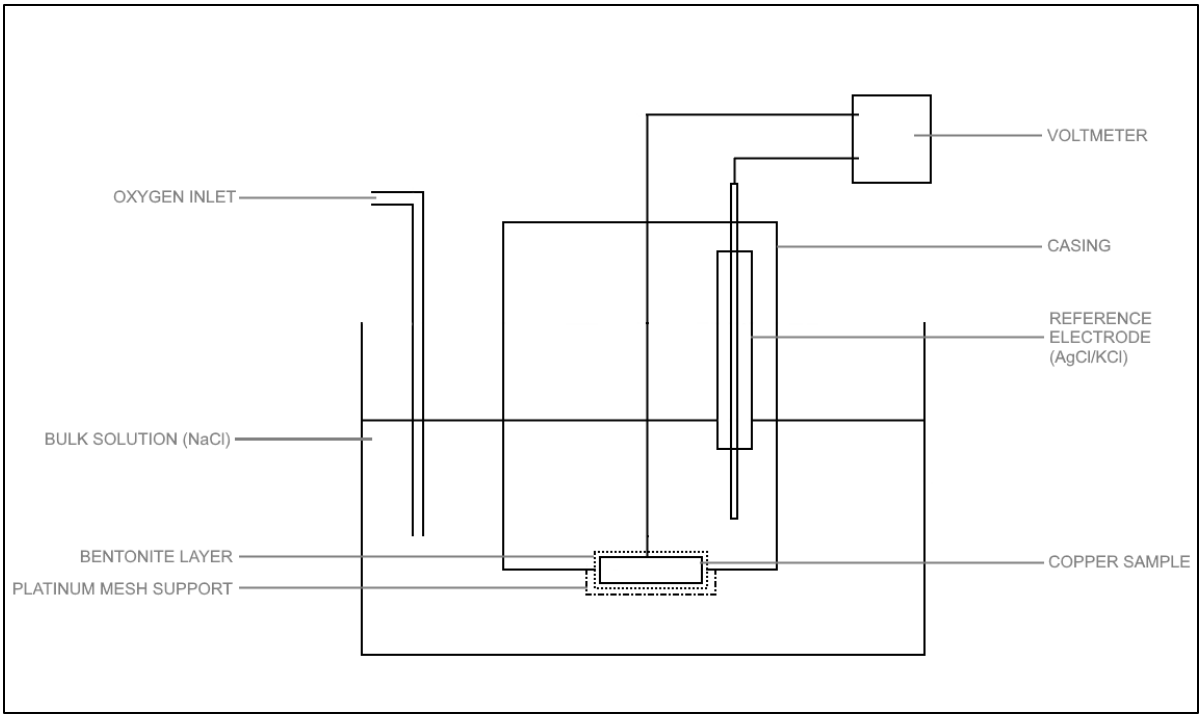

Figure 5.1: Schematic diagram of the experimental setup (King et al., 1995)

The variation of potential with time is shown on Figure 5.2. The graphs' trend shows considerable fluctuations in later time which was due to oxygen purging problem during the experiment. The potential can be used to calculate the corrosion current which could be used to calculate the extent of corrosion as explained in Section 3.2.3.

The COMSOL mixed potential model was able to predict the trends associated with the corrosion potential reported in the experiment when the reactions of Step 3d are considered. The model captured the steady state conditions reached before each change in oxygen concentration and the change in potential following a drop in oxygen concentration. The COMSOL model captured steady state corrosion potential within 10% of the experiment for the 10 mm case. The steady state corrosion potentials in the 1 mm case are more difficult to compare due to the experimental errors discussed above, however the overall fit of the COMSOL model to the experimental observations are comparable as they follow the same trend.

The initial two graphs (Figure 5.3 and Figure 5.4) show the variation of trend in COMSOL with increasing steps (Step 2 to Step 3d) for 1 mm and 10 mm layer of bentonite. There is relatively low variation in case of 1 mm layer compared to 10mm

indicating that the diffusion distance has a significant effect on corrosion potential. This will be later discussed in Chapter 6.

The comparison of experimental plots with COMSOL is the following section.

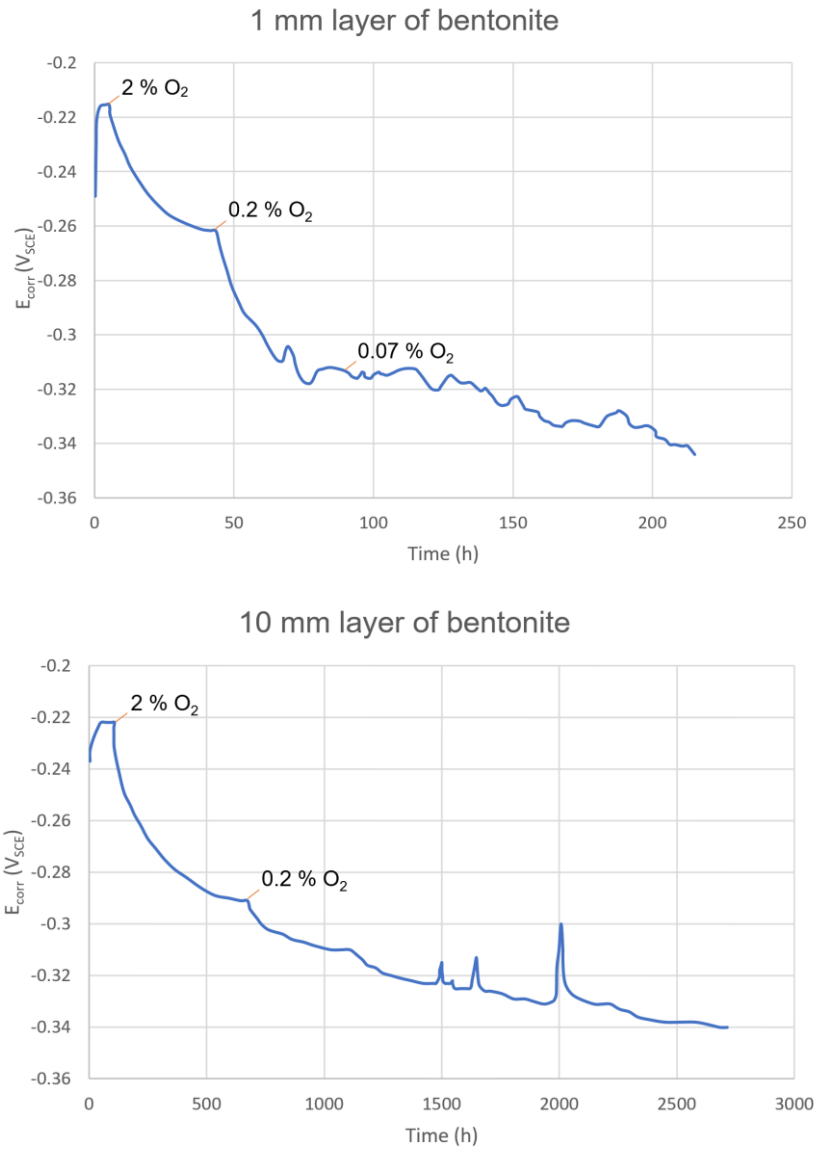

Figure 5.2: Experimental corrosion potential with time for 1 mm (top) and 10mm (bottom) bentonite thickness on copper.

5.2 Comparison of COMSOL Model with Experiments

The following section shows the comparison of the COMSOL model with the experiments. Figure 5.3 and Figure 5.4 shows the variation of potential (E_{corr}) for different steps of the CCM-UC model implemented in COMSOL. It can be seen that the trend for 1 mm layer of bentonite seems to follow the outputs of the experiment more closely relative to the 10 mm layer. This indicates that the time period, as well as, the diffusion distance can play a major role in the variation of corrosion potential.

One of the assumption used in the simulation was on the value of k_d which is originally indicated in King (2016) as 2 x 10^{-6} dm/s was taken as 1/100th of this value as the original value was based on limited experiments and studies (e.g. Al-Qunaibit et al. (2005)) show that desorption is negligible. This is further investigated in Chapter 6.

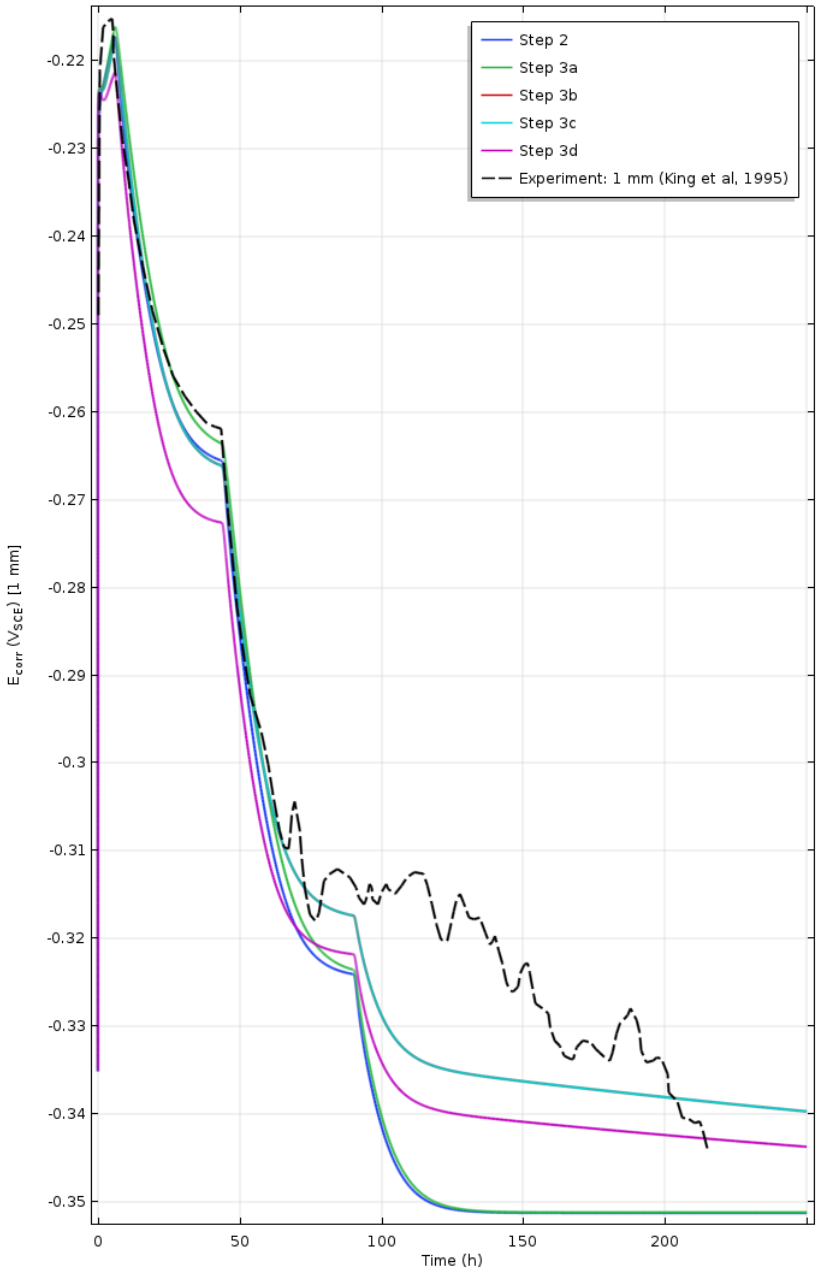

Figure 5.3: Variation of corrosion potential with time for 1 mm bentonite layer, with changing oxygen concentration for Step 2 to 3d in comparison with experimental results (King et. al, 1995)

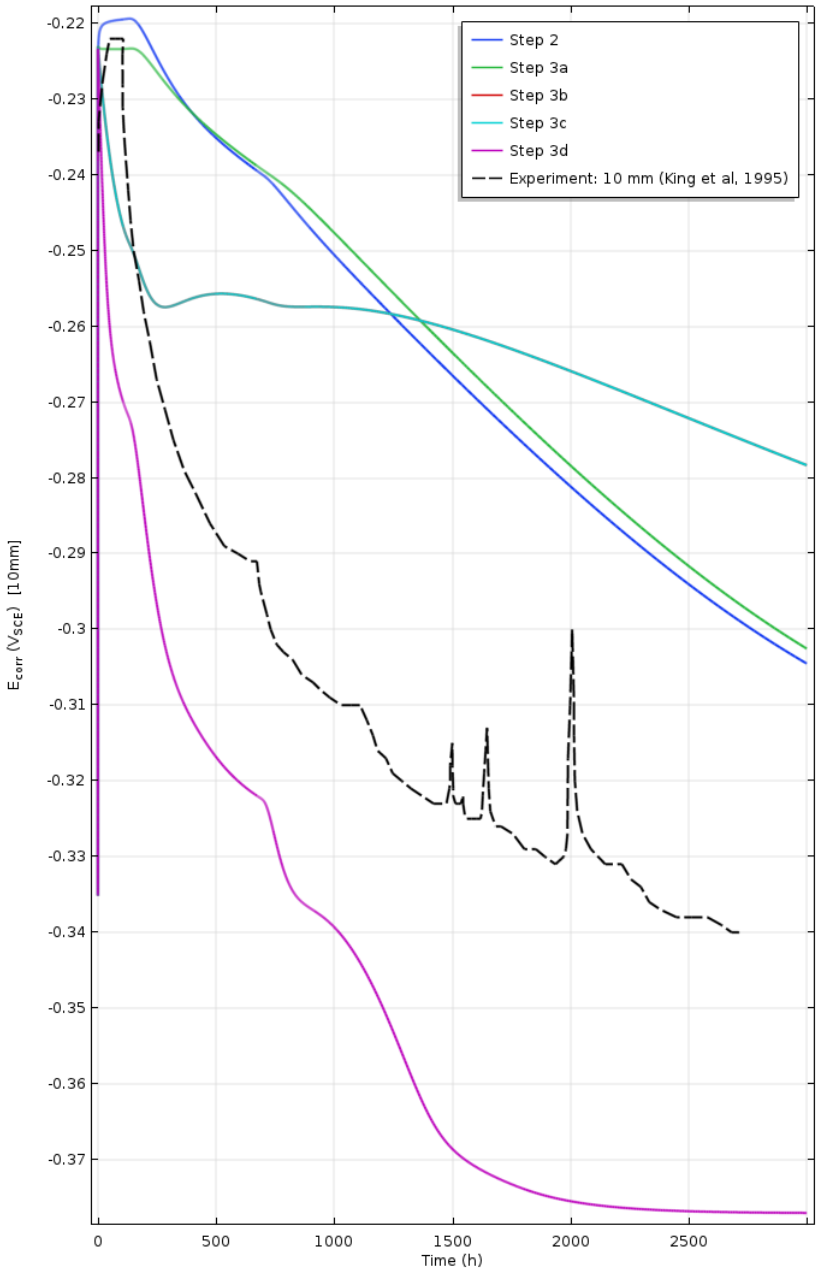

Figure 5.4: Variation of corrosion potential with time for 10 mm bentonite layer, with changing oxygen concentration for Step 2 to 3d in comparison with experimental results (King et. al, 1995)

5.3 Conclusion

The profile of corrosion potential obtained from COMSOL was compared with an experiment (King et al., 1995) conducted with 1 mm and 10 mm layer of bentonite covering a copper sample. The COMSOL model was able to capture the trend of the experiment for 1 mm bentonite layer fairly well. However, there is a deviation observed for the 10 mm experiment indicating that diffusion distance and time can be a major factor influencing corrosion potential.

CHAPTER SIX: SENSITIVITY ANALYSIS

6.1 Description

A sensitivity analysis was performed using COMSOL for different factors, f_x, that correspond to different rate constants, k_x obtained from (King, 2016). Initial chloride concentration was also included in the analysis as it is a significant contributor to corrosion. The analysis was run for Step 3d for both the 1 and 10 mm scenario. All rate constants were varied with different orders of magnitude corresponding to a range of values typically seen in literature (Chapter 2) or values seen as appropriate, if literature ranges did not exist. When one rate was changing, the others were kept at their original values. These values, as well as, the ranges are listed in Table 6.1. The sensitivity analysis was conducted to observe if any changes these parameters would significantly affect the overall corrosion potential.

Table 6.1: Factors used in sensitivity study

S. No	Variable (k_x)	Description	Original Value	Factors (f_x)
1	k_1	Homogenous oxidation of $CuCl_2^-$ by oxygen	Expression based*	0, 1/100, 1, 100
2	k_2	Precipitation of Solid Cuprite	1 s^{-1}	0, 1/100, 1, 100
3	k_3	Precipitation of paratacamite	1 x 10^{-5} s^{-1}	0, 1/100, 1, 100
4	k_4	Adsorption of copper ions	2 x 10^{-6} m^3/mol-s	0, 1/100, 1, 100
5	k_{-4}	Desorption of copper ions	1 x 10^{-6} s^{-1}	0, 1/100, 1, 100
6	k_a	Interfacial reaction for formation of $CuCl_2^-$	3.3 x 10^{-8} m^4/mol-s	1/1000, 1/100, 1, 10
7	k_{bb}	Conversion of $CuCl_2^-$ to CuCl	1.42 x 10^{-4} m/s	1/10, 1/2, 1, 2
8	k_c	Interfacial reaction for reduction of O_2	1.7 x 10^{-10} m/s	1/1000, 1/100, 1, 100
9	k_d	Interfacial reaction for reduction of Cu^{2+}	2 x 10^{-9} m/s	0, 1/100, 1, 100
10	$[Cl^-]$	Concentration of chloride	1000 mol/m^3 [657 mol/m^3 was taken as the default value for all the above previous rate variable]	0.657, 7, 1, 2

*$\log k_1 = 11.38 - 2064/T - 3.69\sqrt{\frac{c_6}{1-0.1103\,c_6}} + 0.73\sqrt{\frac{c_6}{1-0.1103\,c_6}}$

where c_6 is the chloride concentration.

6.2 k_1 (Homogenous oxidation of $CuCl_2^-$ by oxygen)

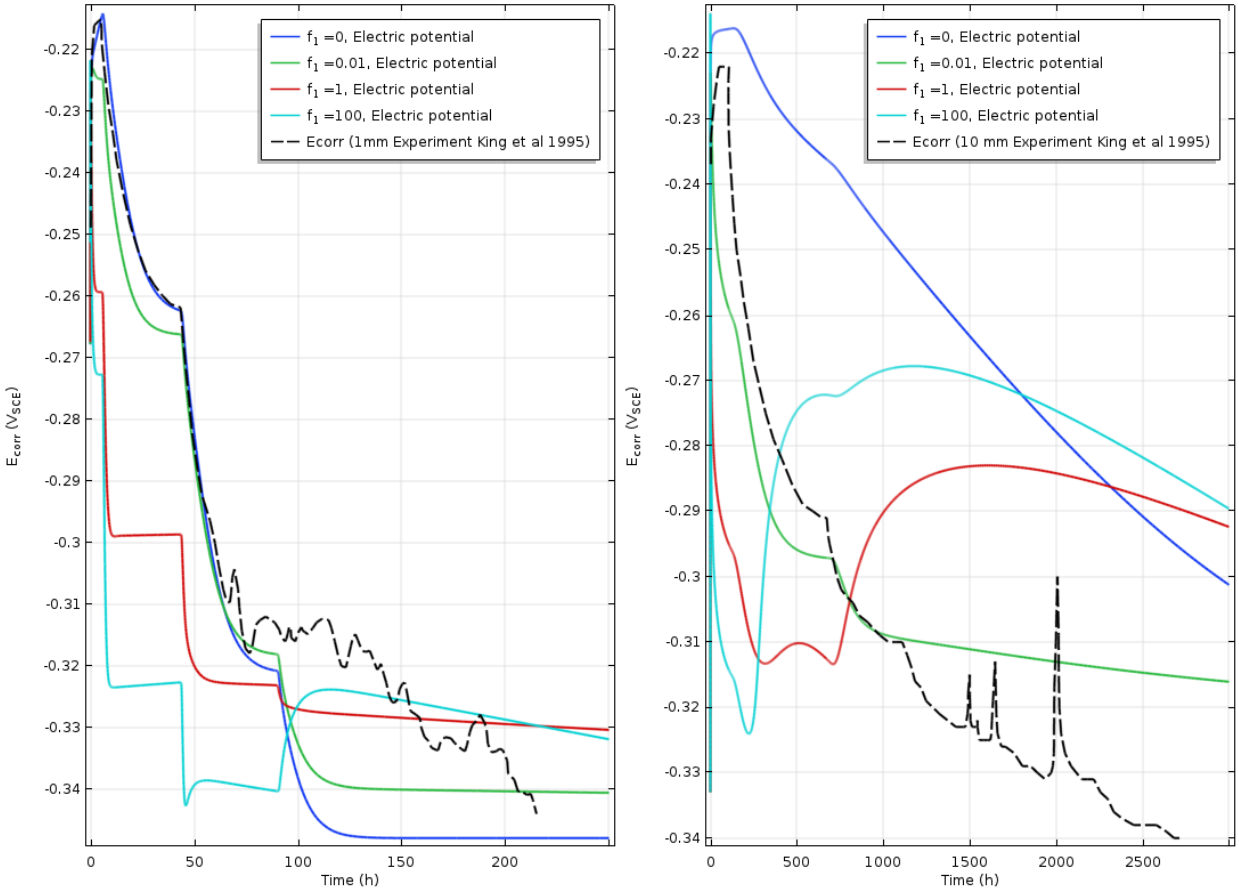

Figure 6.1: Sensitivity of corrosion potential with changing rate constant, k_1 by multiplying with factor, f_1 for 1 mm (left) and 10 mm (right) bentonite

Figure 6.1 shows the effect of changing k_1 on E_{corr} for both bentonite thicknesses. It can be seen that the rate at which $CuCl_2^-$ is oxidized has a significant effect on the corrosion potential. In most cases, an increase in k_1 decreases E_{corr}. This is due to the greater consumption of cuprous chloride ions to form cupric ions and releasing chloride ions (Equation 6.1). For the case of 1 mm bentonite, E_{corr} decreases as k_1 increases, except when k_1 becomes significantly large (f_1 =100) and corresponding oxygen level is low (time > 90 h). In this case, the potential starts increasing.

For 10 mm bentonite thickness, it can be seen that not including k_1 (f_1 =0) keeps the corrosion potential high and a low value of k_1 (f_1 = 0.01) shows a trend similar to the 1 mm bentonite case. However, as k_1 increases, the trend deviates and the corrosion potential increases as oxygen is decreased. From equations 6.1 and 6.2, it can be seen

that k_1 affects both chloride and oxygen concentration which are among the main factors which produces significant changes in corrosion potential.

$$4CuCl_2^- + O_2 + 2H_2O \xrightarrow{k_1} 4Cu^{2+} + 8Cl^- + 4OH^- \qquad 6.1$$

$$\log k_1 = 11.38 - 2064/T - 3.69\sqrt{\frac{c_6}{1-0.1103\,c_6}} + 0.73\sqrt{\frac{c_6}{1-0.1103\,c_6}} \qquad 6.2$$

6.3 k_2 (Precipitation of solid cuprite)

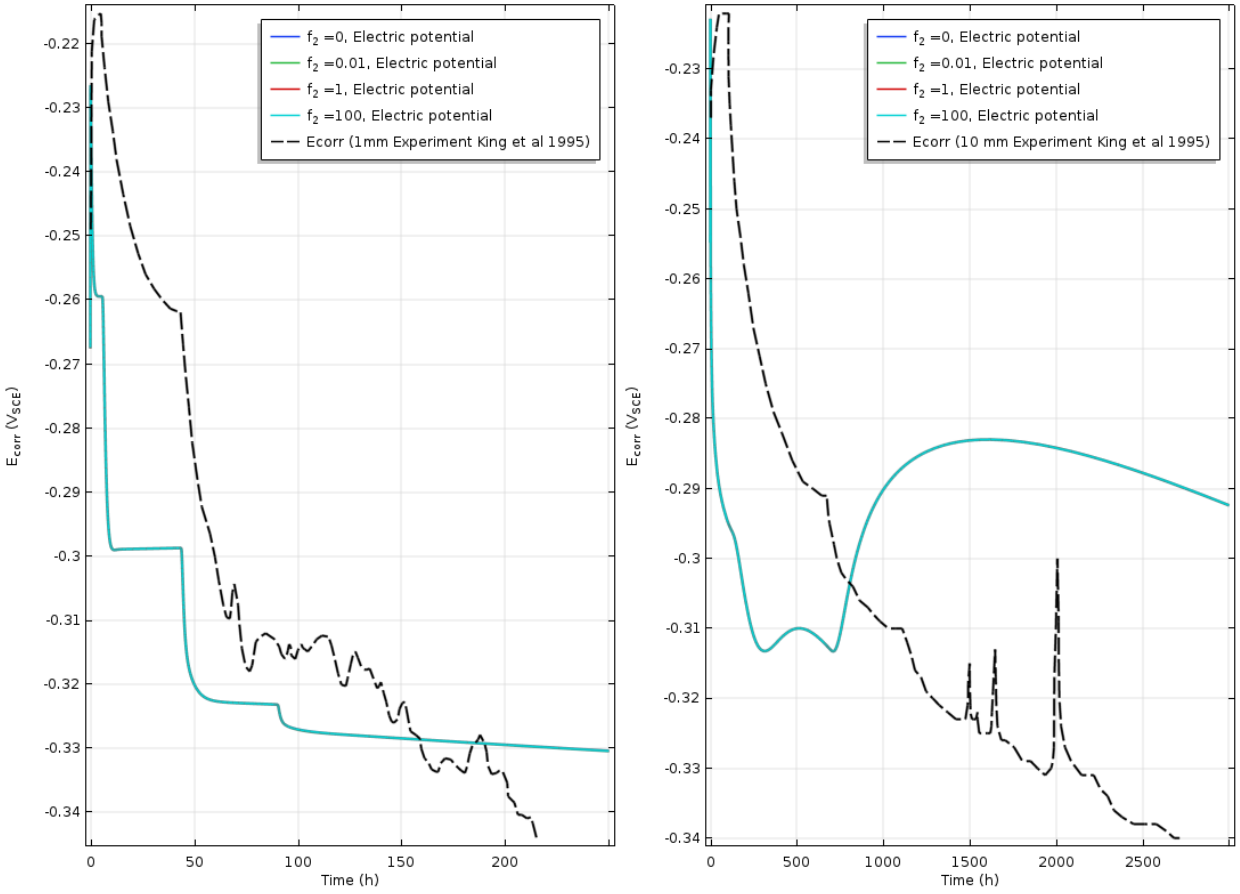

Figure 6.2: Sensitivity of corrosion potential with changing rate constant, k_2 by multiplying with factor, f_2 for 1 mm (left) and 10 mm (right) bentonite

$$2CuCl_2^- + H_2O \underset{k_{-2}}{\overset{k_2}{\rightleftharpoons}} Cu_2O + 4Cl^- + 2H^+ \qquad 6.3$$

There is no effect on corrosion potential with variation of k_2 / k_{-2} as seen in Figure 6.2 (k_{-2} trends not shown here). The formation of cuprous oxide is dependent on the pH which is not considered in this study (Cano et al., 2005).

6.4 k_3 (Precipitation of paratacamite)

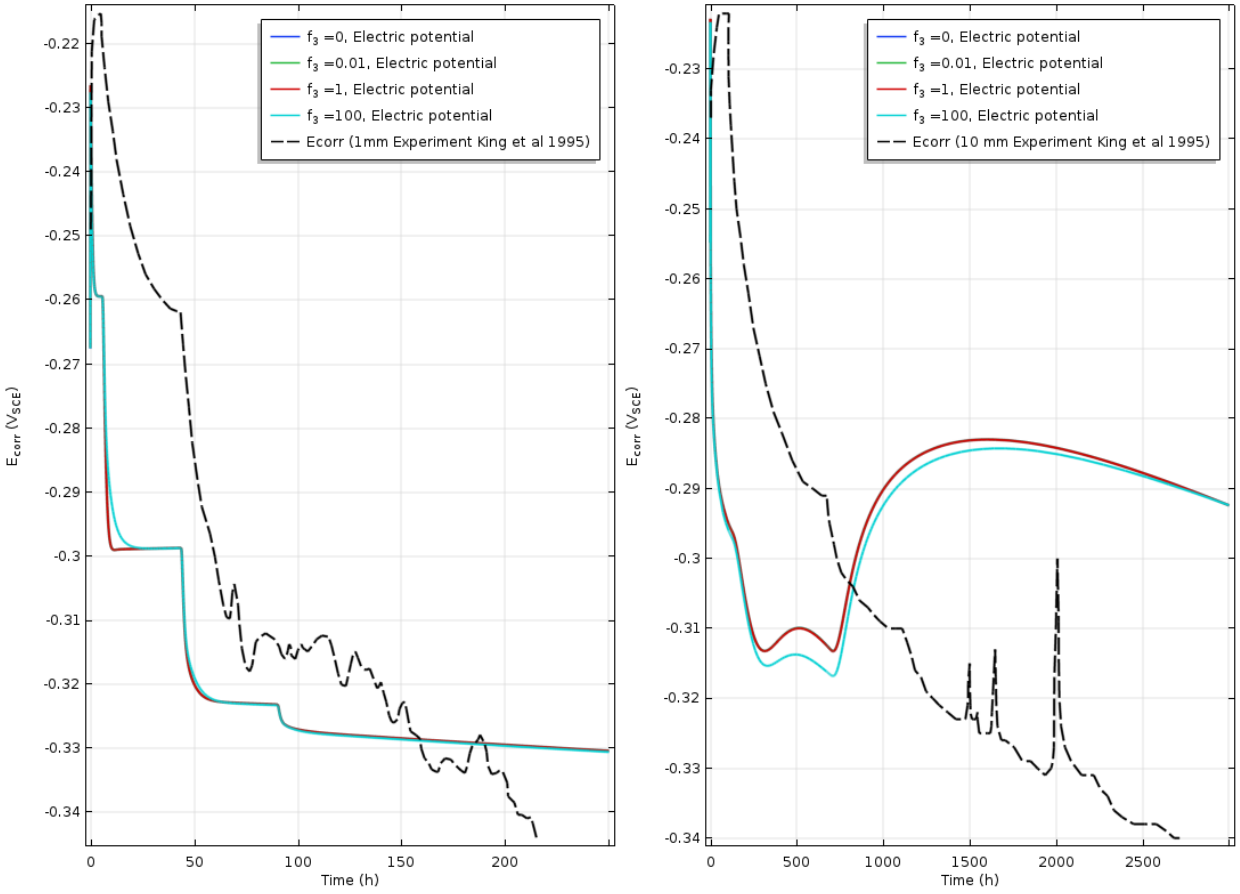

Figure 6.3: Sensitivity of corrosion potential with changing rate constant, k_3 by multiplying with factor, f_3 for 1 mm (left) and 10 mm (right) bentonite

The formation/dissolution of paratacamite does not have a significant effect on corrosion potential as shown in the above figures (Figure 6.3). This might be attributed to the fact that in the simulation the amount of paratacamite generated is nearly one-tenth lower than cupric ions or cuprous chloride thereby leading to less significant effects compared to other ions.

6.5 k_4/k_{-4} (Adsorption and desorption of copper ions)

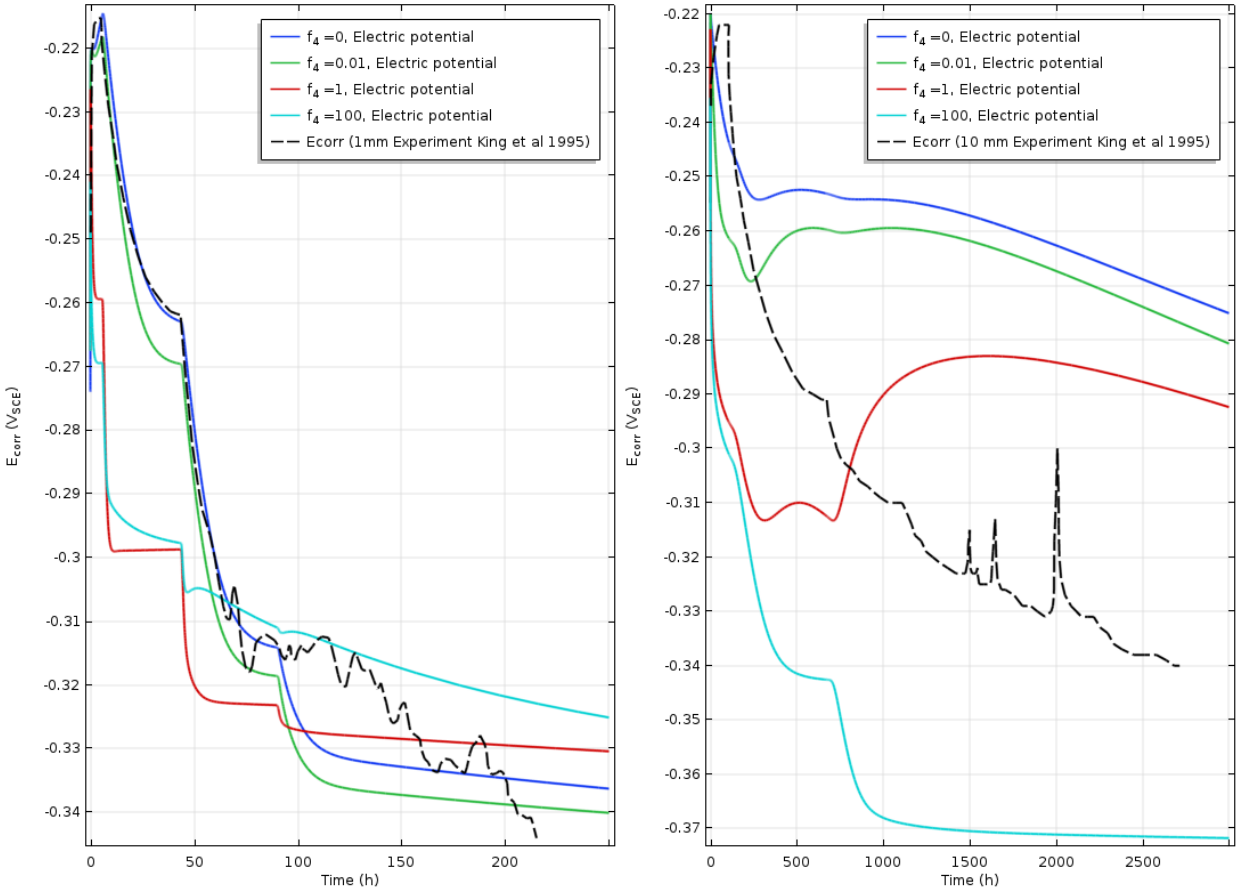

Figure 6.4: Sensitivity of corrosion potential with changing rate constant, k_4 by multiplying with factor, f_4 for 1 mm (left) and 10 mm (right) bentonite

The adsorption and desorption of cupric ions has a significant effect on the corrosion process as can be seen from Figure 6.4, as it determines the availability of cupric ions in the system. The scenario with the thicker bentonite layer (Figure 6.4, right) seems to have a more significant effect compared to the 1 mm layer of bentonite. Since adsorption is dependent on the number of vacant surface sites, a thicker bentonite layer will have more sites for adsorption.

In the 10 mm case, the increase in k_4 leads to a general decrease in E_{corr}. However, in the 1 mm case, the trend is not as straight forward as the impact of k_4 seems to also be a function of oxygen content. It can be seen from Figure 6.4 (left) that at high oxygen

levels, a higher adsorption value decreases E_{corr}. As oxygen is reduced, (time = 50 hours), higher adsorption values (f_4 = 100), actually have higher E_{corr} values than lower k_4 values.

$$Cu^{2+} + 2Y^{-} \underset{k_{-4}}{\overset{k_4}{\rightleftharpoons}} CuY_2 \qquad 6.4$$

Although adsorption by bentonite is high with increased pH (Veli and Alyüz, 2007), this factor was not considered in this study.

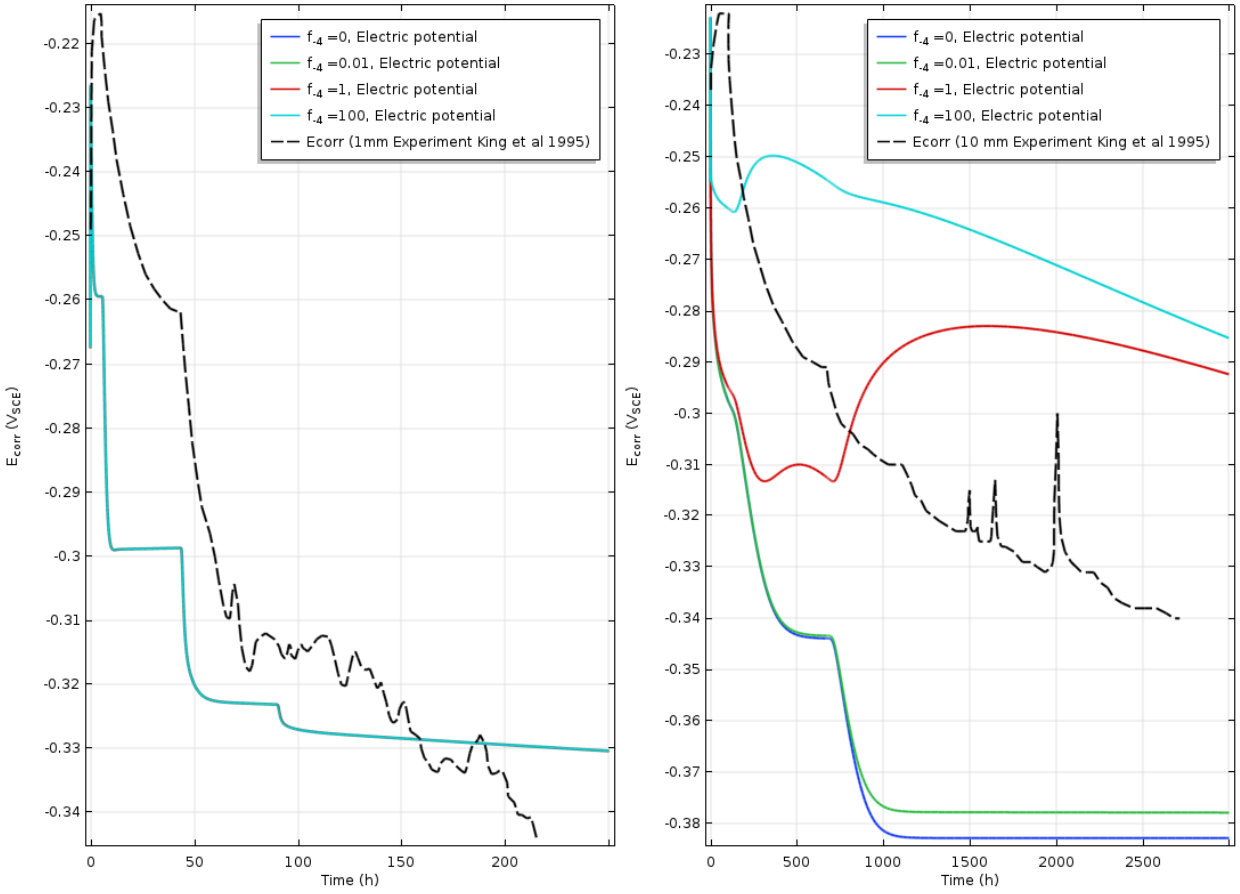

Figure 6.5: Sensitivity of corrosion potential with changing rate constant, k_{-4} by multiplying with factor, f_{-4} for 1 mm (left) and 10 mm (right) bentonite

The desorption of adsorbed copper tends to have no effect on the corrosion potential for 1 mm (Figure 6.5, left). However, in case of 10 mm layer of bentonite, an increase in desorption tends to increase the corrosion potential for lower oxygen concentrations (Figure 6.5, right). This might be attributed to more cupric ions being available for influencing cathodic current thereby increasing the potential.

6.6 k_a (Interfacial reaction for formation of $CuCl_2^-$)

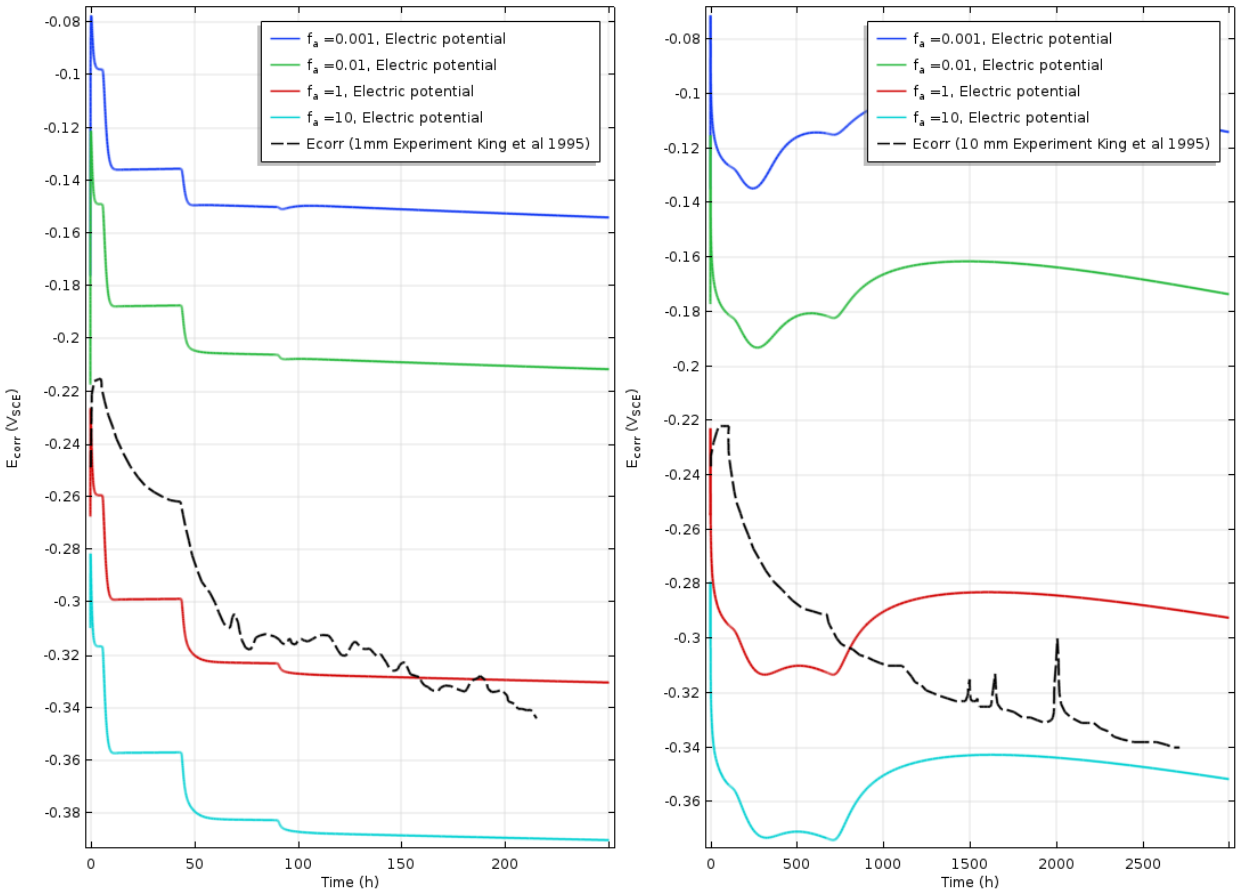

Figure 6.6: Sensitivity of corrosion potential with changing rate constant, k_a by multiplying with factor, f_a for 1 mm (left) and 10 mm (right) bentonite

Figure 6.6 shows that an increase in k_a leads to an increase in adsorption of chloride by copper.

$$Cu + Cl^- \underset{k_{ab}}{\overset{k_{af}}{\rightleftharpoons}} CuCl_{ADS} + e^- \qquad 6.5$$

$$CuCl_{ADS} + Cl^- \underset{k_{bb}}{\overset{k_{bf}}{\rightleftharpoons}} CuCl_2^- \qquad 6.6$$

where

$$k_a = \frac{k_{af} k_{bf}}{k_{ab}} \qquad 6.7$$

Increasing k_a leads to increase in anodic current (Equation 6.8), which will lead to decrease in potential i.e. potential moving towards more negative.

$$i_a = n_a F \left\{ k_a [Cl^-]^2 \exp \frac{F}{RT} (E - E_a) - k_{bb} [CuCl_2^-] \right\} \quad 6.8$$

This trend is observed in case of both 1 mm and 10 mm bentonite layers on copper. Unlike the homogeneous kinetics, it can be seen that changing k_a results in a shift in the E_{corr} value and not a change in figure shape, signifying that the anodic dissolution of copper only effects the initial corrosion potential.

6.7 k_{bb} (Conversion of $CuCl_2^-$ to CuCl)

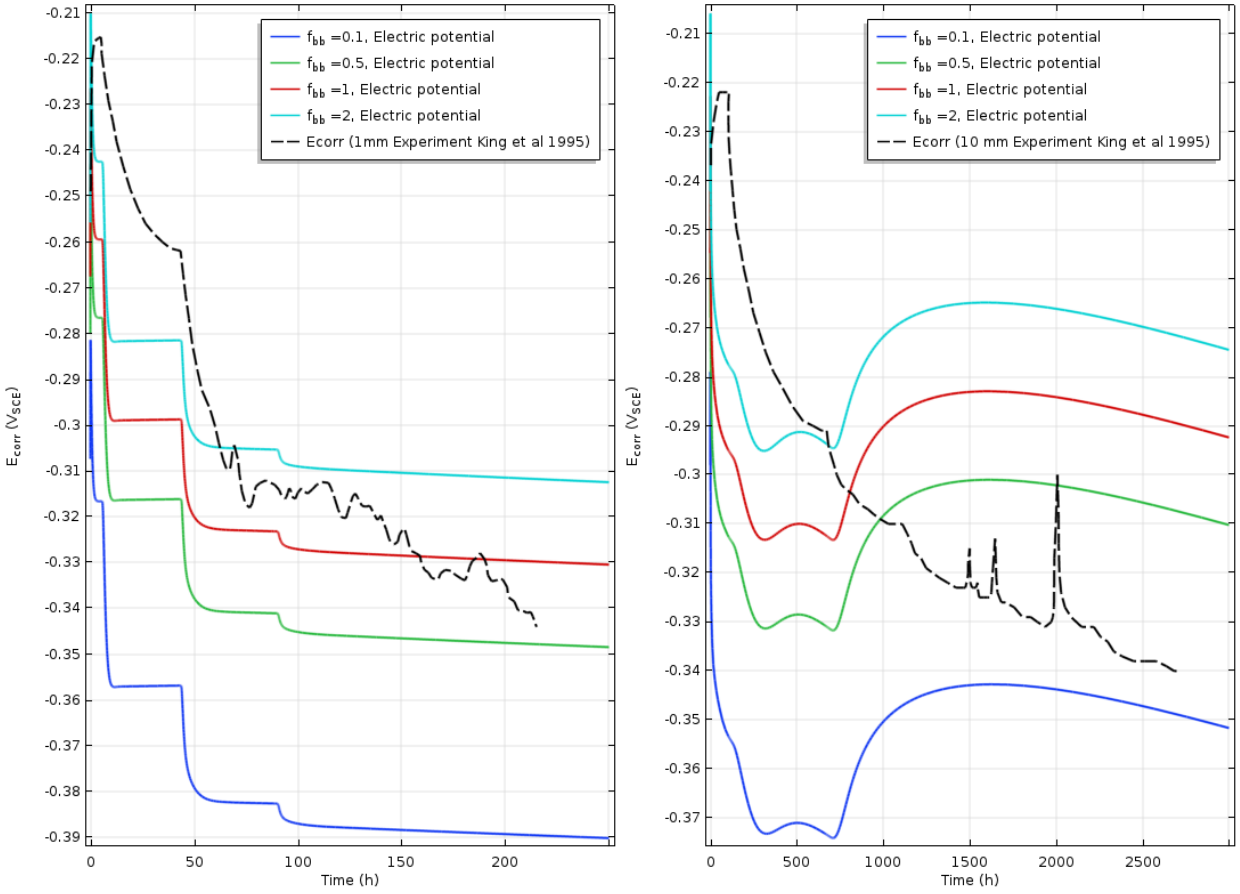

Figure 6.7: Sensitivity of corrosion potential with changing rate constant, k_{bb} by multiplying with factor, f_{bb} for 1 mm (left) and 10 mm (right) bentonite

High k_{bb} indicates that the reverse reaction involving cuprous chloride ions is occurring, as per Equation *6.6*. k_{bf} is included in the expression of k_a as indicated in Equation *6.7* With increasing k_{bb}, the corrosion potential tends to move towards the positive value. This is because the anodic current will decrease leading to increase in potential as expressed by Equation *6.8*.

As seen in Figure 6.7, a similar trend is observed for both 1 mm and 10 mm bentonite layers on copper. Similar to k_a, the change in k_{bb} only affects the initial corrosion potential.

6.8 k_c (Interfacial reaction for reduction of oxygen)

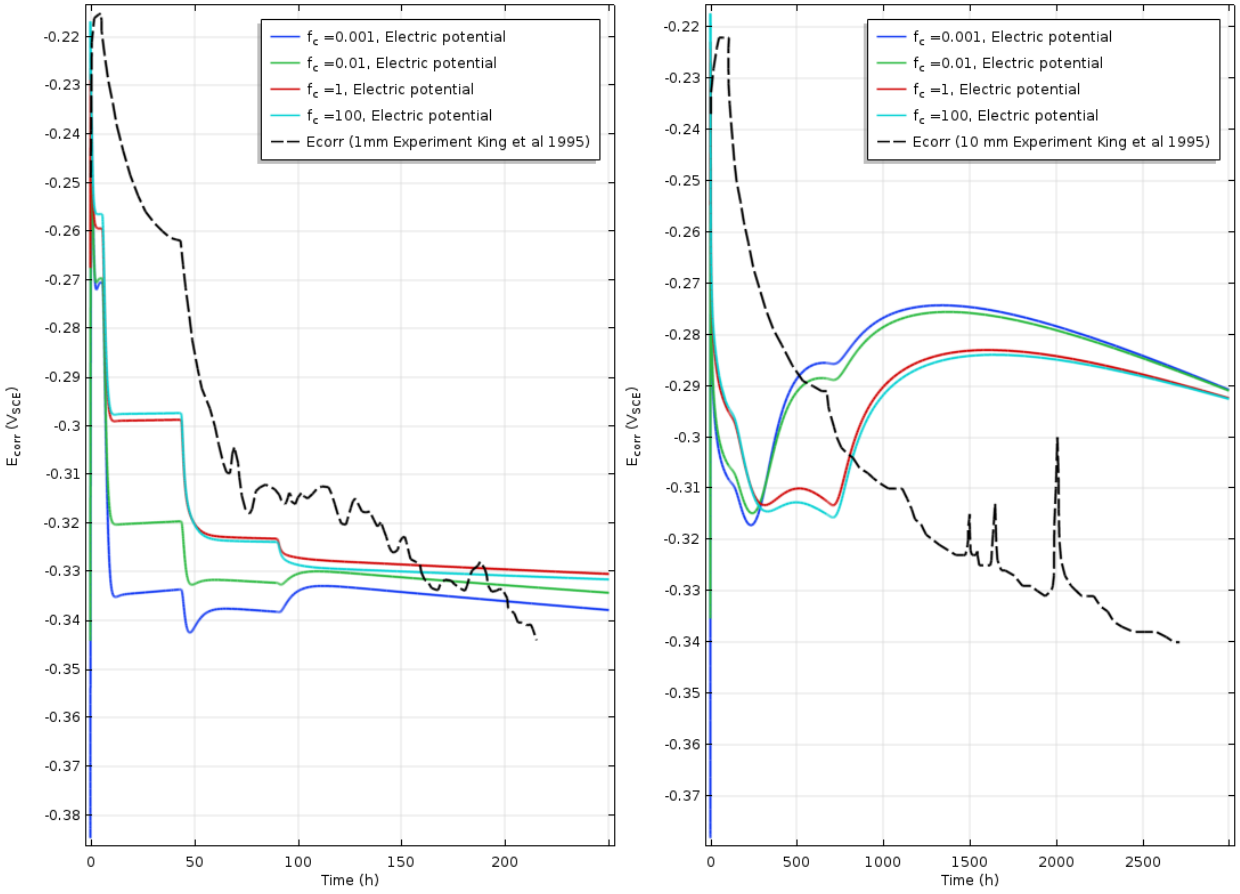

Figure 6.8: Sensitivity of corrosion potential with changing rate constant, k_c by multiplying with factor, f_c for 1 mm (left) and 10 mm (right) bentonite

The change in corrosion potential with varying k_c is not significant except in cases of low values of k_c (f_c =0.01, 0.001) (Figure 6.8). In this case, the trend deviates slightly and is magnified in case of 10 mm at time 107 h where the oxygen concentration is reduced by one-tenth of its original amount. Here the potential moves towards the positive direction. This indicates that when the reduction of oxygen decreases or is low, the cathodic influence is higher.

$$O_2 + 2\,H_2O + 4\,e^- \xrightarrow{k_c} 4\,OH^- \qquad 6.9$$

6.9 k_d (Interfacial reaction for reduction of Cu^{2+})

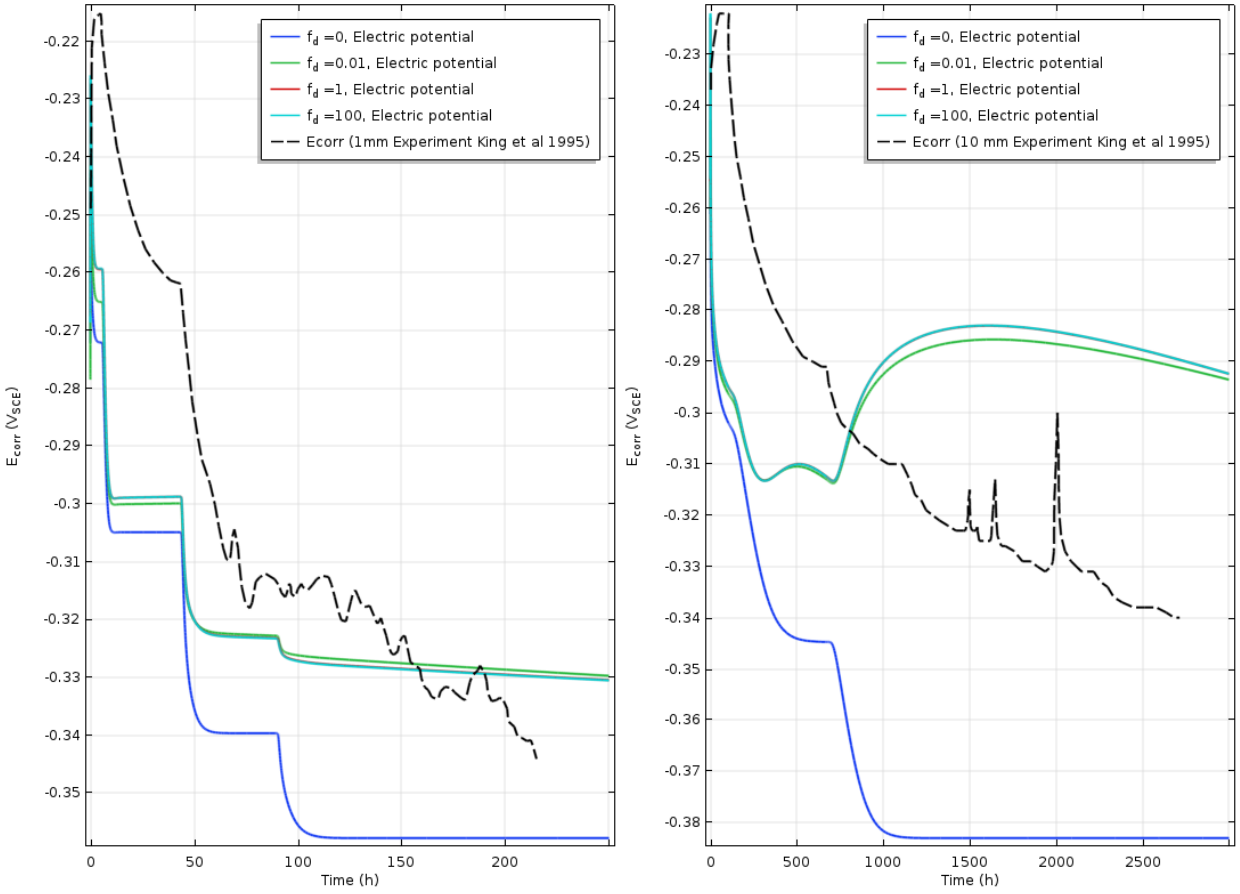

Figure 6.9: Sensitivity of corrosion potential with changing rate constant, k_d by multiplying with factor, f_d for 1 mm (left) and 10 mm (right) bentonite

Increase in the value of k_d leads to an increase in the formation of copper chloride ions (from cupric ions) at the interface. As seen in Figure 6.9, the result of f_d = 1 and f_d = 100 overlap, indicating that higher k_d have no significant effect on corrosion rates.

$$Cu^{2+} + 2\,Cl^- + e^- \xrightarrow{k_d} CuCl_2^- \qquad 6.10$$

The cathodic current is directly associated with the value of k_d in accordance with Equation *6.11*. When k_d increases, the cathodic current increases leading to moving of corrosion potential towards the positive direction.

$$i_d = -n_d F k_d [Cu^{2+}] \exp\left(-\frac{\alpha_d F}{RT}(E - E_d)\right) \quad 6.11$$

In case of 1 mm, the potential moves towards the positive direction initially which changes for f_d = 0.01 (time = 43.5 h) where it coincides and then moves below as shown (time = 90). In case of 10 mm, when the cathodic reaction is absent (k_d = 0), the trend does not move upward. High value of k_d (f_d = 100) leads to E_{corr} moving towards positive.

6.10 [Cl^-] (Concentration of chloride)

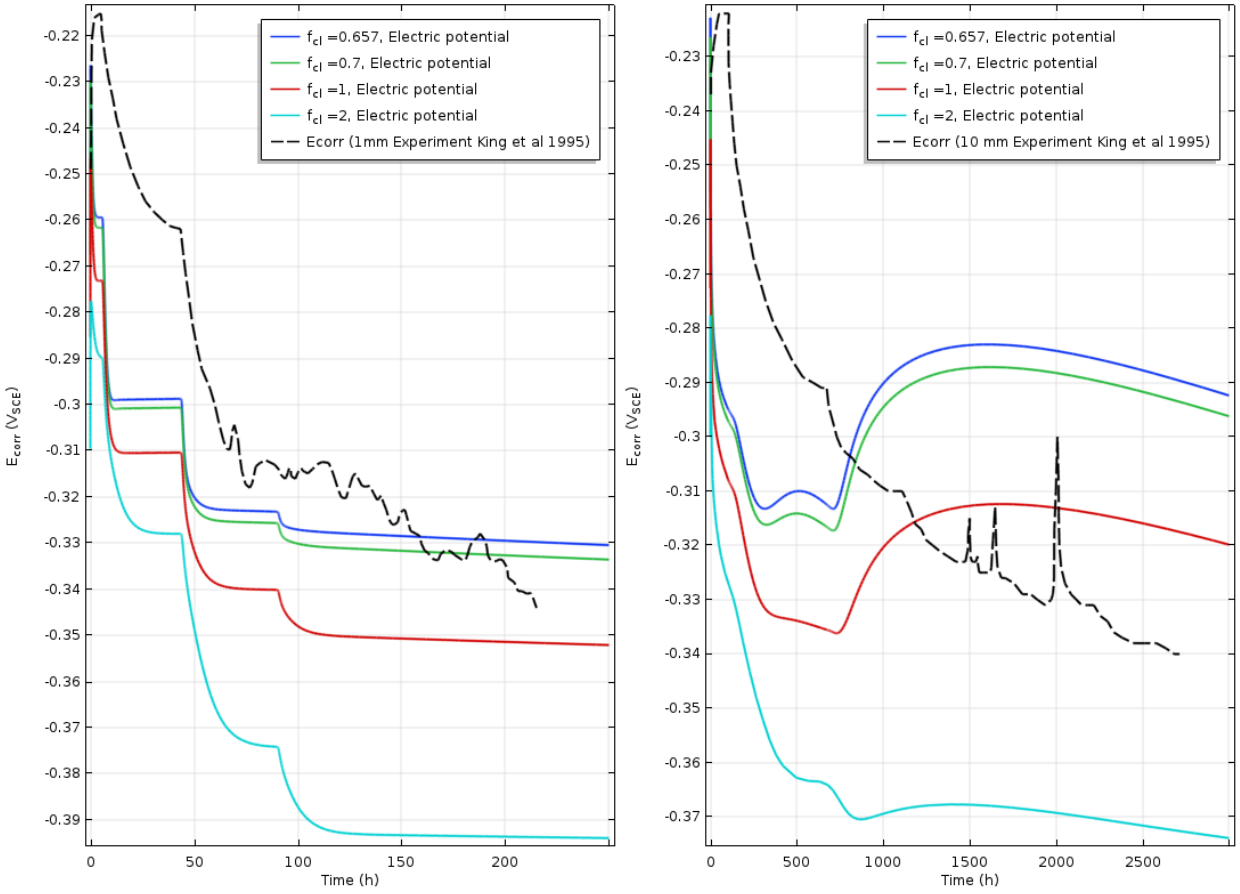

Figure 6.10: Sensitivity of corrosion potential with changing chloride concentration, [Cl^-] by multiplying with factor, f_{cl} for 1 mm (left) and 10 mm (right) bentonite

The increasing concentration of chloride decreases the corrosion potential as the anodic current is directly dependent on the chloride concentration (Equation *6.8*). With increase in chloride concentration, the anodic current will increase. This in turn will decrease the electrode potential in accordance to Evans diagrams. This trend is observed in the above figure (Figure 6.10).

6.11 Current Density plots

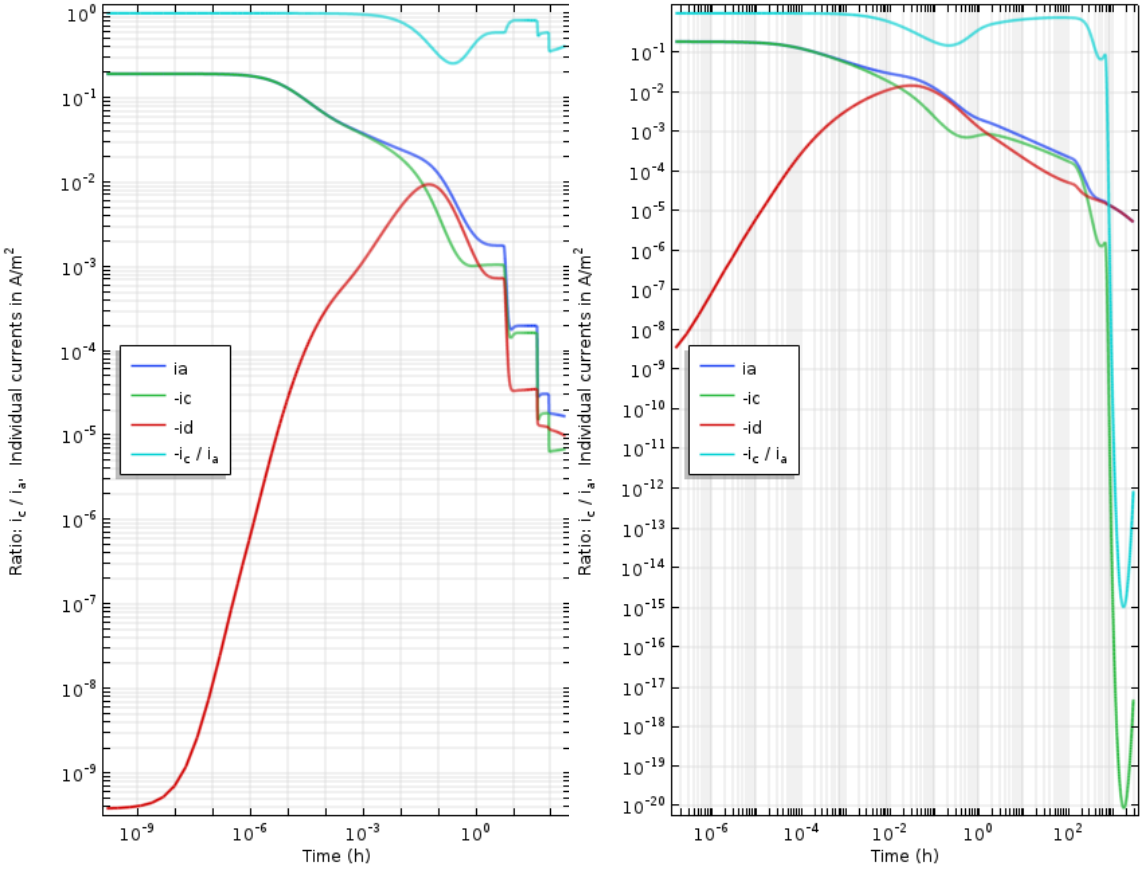

Figure 6.11: Current densities and ratio of i_c/i_a for 1 mm (left) and 10 mm (right) bentonite for Step 3d. The cathodic currents have been multiplied with -1 for visual ease

The above graphs (Figure 6.11) show that the oxygen concentration is a significant factor in influencing corrosion potential. Oxygen being a major cathodic reactant can lead to 'bumps' in which is observed with changing oxygen concentration.

$$i_c = -n_c F k_c [O_2] \exp\frac{\alpha_c F}{RT}(E - E_c) \qquad 6.12$$

6.12 Conclusion

A sensitivity analysis for different rate constants and chloride concentrations was done using the COMSOL model. This was performed by keeping various constants the same and changing one factor at a time. The analysis was run for Step 3d for both 1 and 10 mm scenarios.

The following trends were found for both the 1 mm and 10mm bentonite thickness:

- homogenous oxidation of $CuCl_2^-$ (k_1) had a large impact on the corrosion rate; for the 10 mm case the effect of k_1 was more significant at lower values of oxygen
- precipitation of solid cuprite (k_2) and paratcamite (k_3) had little effect the corrosion potential
- adsorption of Cu^{2+} (k_4) had a significant effect on both cases while desorption of copper (k_{-4}) only effected the corrosion potential in the 10 mm case
- interfacial reactions (k_a, k_{bb}) only affected the initial corrosion potential
- interfacial reaction for reduction of oxygen (k_c) has a slight effect on the copper potentials but only at lower values
- the corrosion potential changes at low values of k_d (reduction of Cu^{2+})

Overall, k_1, k_4 and k_c are the factors most sensitive in the copper corrosion process. Since there is significant uncertainty regarding these factors and little information is found in literature regarding their values, it would be recommended that further studies or experiments be performed to identify these factor under DGR conditions. Doing so would allow for a better estimation of the corrosion depth.

CHAPTER SEVEN: CONCLUSION AND FUTURE WORK

To ensure safe and reliable disposal, NWMO has implemented APM, the approach selected by the Government of Canada in 2007 for long-term management of used nuclear fuel. In support of APM, NWMO is pursuing an active Technical Program addressing a wide range of relevant topics in collaboration with Canadian universities, consultants and other countries pursuing the development of DGRs for used nuclear fuel. This project is part of one of Technical Programs that is currently refining generic engineering designs and safety cases in support of APM.

One uncertainty of the current NWMO plan is how prevalent UFC corrosion will be in the DGR. Corrosion can lead to deterioration of the copper layer due to interaction with the surrounding environment. Once corroded, the UFC may be compromised. To ensure this doesn't happen, models of the subsurface environment are often used. The model that has been commonly used by NWMO is the Copper Corrosion Model (CCM) developed by King et al. (1995). Due to some of the limitations imposed by CCM, including dimensionality and usability, a new corrosion model was developed in this study. The model was developed using COMSOL and represents a mixed potential model for the corrosion of copper. This model is capable of predicting corrosion potentials in a simplified 1D DGR environment.

The model is based on the copper corrosion mixed potential model (CCM) developed by King and Kolar (2000). The COMSOL model was verified against CCM to ensure that all equations were implemented accurately and it was found that the COMSOL model was able to reproduce the expected trends and behaviors. The COMSOL model was also validated against reproduced results from a copper corrosion experiment by King et al (1995).

Once validated, the model was used to run various sensitivity studies to assess the effect of different parameters on UFC corrosion. The analysis indicated that some of the rate constants involving adsorption of Cu^{2+}, homogenous oxidation of $CuCl_2^-$ and interfacial reduction of oxygen are among the main factors which can influence corrosion potential, and thereby to corrosion, to a significant level relative to other rate constants.

Future works may involve:

- continuation of steps of CCM-UC from Step 3e to Step 6 to include other conditions expected in a deep geological repository.
- experimental program to identify the parameters that are most uncertain (k_1, k_4 and k_c)
- implementation of CCM in two dimensions
- integration of CCM with other programs (transport or reactive) to give a complete picture of the DGR repository

BIBLIOGRAPHY

Aalto, H., Rajainmäki, H. and Laakso, L. (1996). Production methods and costs of oxygen free copper canisters for nuclear waste disposal, Posiva.

Abollino, O., Aceto, M., Malandrino, M., Sarzanini, C. and Mentasti, E. (2003). "Adsorption of heavy metals on Na-montmorillonite. Effect of pH and organic substances" *Water Research*, Vol. 37, No. 7, pp. 1619–1627.

Al-Qunaibit, M.H., Mekhemer, W.K. and Zaghloul, A.A. (2005). "The adsorption of Cu(II) ions on bentonite—a kinetic study" *Journal of Colloid and Interface Science*, Vol. 283, No. 2, pp. 316–321.

Anna, B., Kleopas, M., Constantine, S., Anestis, F. and Maria, B. (2015). "Adsorption of Cd(II), Cu(II), Ni(II) and Pb(II) onto natural bentonite: study in mono- and multi-metal systems" *Environmental Earth Sciences*, Vol. 73, No. 9, pp. 5435–5444.

Avis, J., Suckling, P., Calder, N., Walsh, R., Humphreys, P. and King, F. (2014). "T2GGM: A Coupled Gas Generation Model for Deep Geologic Disposal of Radioactive Waste" *Nuclear Technology*, Vol. 187, No. 2, pp. 175–187.

Bacarella, A.L. and Griess, J.C. (1973). "The Anodic Dissolution of Copper in Flowing Sodium Chloride Solutions Between 25° and 175°C" *Journal of The Electrochemical Society*, Vol. 120, No. 4, pp. 459–465.

Bereket, G., Arog, A.Z. and Özel, M.Z. (1997). "Removal of Pb(II), Cd(II), Cu(II), and Zn(II) from Aqueous Solutions by Adsorption on Bentonite" *Journal of Colloid And Interface Science*, Vol. 187, No. 2, pp. 338–343.

BfS (2016). Morsleben, Available at: http://www.endlager-morsleben.de/Morsleben/EN/topics/repository/repository-overview/repository-overview_node.html (Accessed: November 21, 2017).

BfS (2017). Asse - Saline solutions, Available at: http://www.asse.bund.de/Asse/EN/topics/what-is/saline-solutions/saline-solutions_node.html;jsessionid=F03DFC136AFC71F7610E421C087C37C6.1_cid382 (Accessed: November 21, 2017).

Bhattacharyya, K.G. and Gupta, S.S. (2006). "Kaolinite, montmorillonite, and their modified derivatives as adsorbents for removal of Cu(II) from aqueous solution" *Separation and Purification Technology*, Vol. 50, No. 3, pp. 388–397.

Boman, M., Berger, R., Andersson, Y., Hahlin, M., Björefors, F., Gustafsson, T. and Ottosson, M. (2014). "Corrosion of copper in water free from molecular oxygen" *Corrosion Engineering, Science and Technology*, Vol. 49, No. 6, pp. 431–434.

Boulay, N. and Edwards, M. (2001). “Role of temperature, chlorine, and organic matter in copper corrosion by-product release in soft water” *Water Research*, Vol. 35, No. 3, pp. 683–690.

Broomby (2014). How France is disposing of its nuclear waste, BBC World Service, Available at: http://www.bbc.com/news/science-environment-26425674 (Accessed: April 20, 2018).

Bube, C., Metz, V., Bohnert, E., Garbev, K., Schild, D. and Kienzler, B. (2013). “Long-term cement corrosion in chloride-rich solutions relevant to radioactive waste disposal in rock salt – Leaching experiments and thermodynamic simulations” *Physics and Chemistry of the Earth, Parts A/B/C*, Vol. 64, pp. 87–94.

Cano, E., Polo, J.L., La Iglesia, A. and Bastidas, J.M. (2005). “Rate control for copper tarnishing” *Corrosion Science*, Vol. 47, No. 4, pp. 977–987.

Carvalho, J.L., Steed, C.M., Birch, K. and Russell, S. (2013). Near-Field and far-Field Thermo-Mechanical Modelling of Conceptual Deep Geological Repositories for used Nuclear Fuel in Crystalline Rock. Geomechanics Symposium, June 2013, California, ARMA-2013-351, American Rock Mechanics Association.

Chen, Y.-G., He, Y., Ye, W.-M. and Jia, L.-Y. (2015). “Competitive adsorption characteristics of Na(I)/Cr(III) and Cu(II)/Cr(III) on GMZ bentonite in their binary solution” *Journal of Industrial and Engineering Chemistry*, Vol. 26, No. Complete, pp. 335–339.

Clarelli, F., De Filippo, B. and Natalini, R. (2014). “Mathematical model of copper corrosion” *Applied Mathematical Modelling*, Vol. 38, No. 19, pp. 4804–4816.

Cornwell, F.J., Wildsmith, G. and Gilbert, P.T. (1973). “Pitting Corrosion in Copper Tubes in Cold Water Service” *British Corrosion Journal*, Vol. 8, No. 5, pp. 202–209.

Corrosionpedia (2018). Evans, Corrosionpedia, Available at: https://www.corrosionpedia.com/definition/6210/evans-diagram (Accessed: January 25, 2018).

De Ryck, I., Adriaens, A. and Adams, F. (2005). “An overview of Mesopotamian bronze metallurgy during the 3rd millennium BC” *Journal of Cultural Heritage*, Vol. 6, No. 3, pp. 261–268.

Diffen (2014). Hard and Soft water, Available at: https://www.diffen.com/difference/Hard_Water_vs_Soft_Water (Accessed: March 23, 2018).

Elsner, C.I., Salvarezza, R.C. and Arvia, A.J. (1988). “The influence of halide ions at submonolayer levels on the formation of oxide layer and electrodissolution of copper in neutral solutions” *Electrochimica Acta*, Vol. 33, No. 12, pp. 1735–1741.

Eureka (2017). Yucca, Available at: http://www.yuccamountain.org/time.htm (Accessed: November 21, 2017).

Furrer, G., Westall, J. and Sollins, P. (1989). “The study of soil chemistry through quasi-steady-state models: I. Mathematical definition of model” *Geochimica et Cosmochimica Acta*, Vol. 53, No. 3, pp. 595–601.

Glatstein, D.A. and Francisca, F.M. (2015). “Influence of pH and ionic strength on Cd, Cu and Pb removal from water by adsorption in Na-bentonite” *Applied Clay Science*, Vol. 118, pp. 61–67.

Gok, O., Ozcan, A., Erdem, B. and Ozcan, A.S. (2008). “Prediction of the kinetics, equilibrium and thermodynamic parameters of adsorption of copper(II) ions onto 8-hydroxy quinoline immobilized bentonite” *Colloids and Surfaces A: Physicochemical and Engineering Aspects*, Vol. 317, No. 1–3, pp. 174–185.

González-Dávila, M., Santana-Casiano, J.M., González, A.G., Pérez, N. and Millero, F.J. (2009). “Oxidation of copper(I) in seawater at nanomolar levels” *Marine Chemistry*, Vol. 115, No. 1, pp. 118–124.

Guo, R. (2011). “Thermohydromechanical modelling of the buffer/container experiment” *Engineering Geology*, Vol. 122, No. 3, pp. 303–315.

Gupta, S.S. and G. Bhattacharyya, K. (2012). “Adsorption of heavy metals on kaolinite and montmorillonite: a review” *Physical Chemistry Chemical Physics*, Vol. 14, No. 19, pp. 6698–6723.

Hsueh, K.-L., Chin, D.-T. and Srinivasan, S. (1983). “Electrode kinetics of oxygen reduction: A theoretical and experimental analysis of the rotating ring-disc electrode method” *Journal of Electroanalytical Chemistry and Interfacial Electrochemistry*, Vol. 153, No. 1, pp. 79–95.

Huh, J.-H., Hyun Kim, S., Hwan Chu, J., Youb Kim, S., Hyun Kim, J. and Kwon, S.-Y. (2014). “Enhancement of seawater corrosion resistance in copper using acetone-derived graphene coating” *Nanoscale*, Vol. 6, No. 8, pp. 4379–4386.

Humphreys, P., McGarry, R., Hoffmann, A. and Binks, P. (1997). “DRINK: a biogeochemical source term model for low level radioactive waste disposal sites” *FEMS Microbiology Reviews*, Vol. 20, No. 3–4, pp. 557–571.

Hurlen, T. (1961). “Dissolution of copper by oxidation agents in acid chloride solution” *Acta. Chem. Scand*, Vol. 15, No. 6, pp. 1239–1245.

Hutchison, M.J., Zhou, P., Ogle, K. and Scully, J.R. (2017). “Enhanced Electrochemical Cu Release from Commercial Cu-Sn Alloys: Fate of the Alloying Elements in Artificial Perspiration” *Electrochimica Acta*, Vol. 241, pp. 73–88.

Huttunen-Saarivirta, E., Rajala, P. and Carpén, L. (2016). “Corrosion behaviour of copper under biotic and abiotic conditions in anoxic ground water: electrochemical study” *Electrochimica Acta*, Vol. 203, pp. 350–365.

Ives, D.J.G. and Rawson, A.E. (1962). “Copper corrosion III. Electrochemical theory of general corrosion” *Journal of the Electrochemical Society*, Vol. 109, No. 6, pp. 458–462.

Jason Nisse (2005). BNFL told to combat threat of nuclear contamination on Cumbrian, The Independent, Available at: http://www.independent.co.uk/news/business/news/bnfl-told-to-combat-threat-of-nuclear-contamination-on-cumbrian-beaches-494576.html (Accessed: March 24, 2018).

Jhaveri, A.S. and Sharma, M.M. (1967). “Kinetics of absorption of oxygen in aqueous solutions of cuprous chloride” *Chemical Engineering Science*, Vol. 22, No. 1, pp. 1–6.

Johansson, A.J., Lilja, C., Sjögren, L., Gordon, A., Hallbeck, L. and Johansson, L. (2017). “Insights from post-test examination of three packages from the MiniCan test series of copper-cast iron canisters for geological disposal of spent nuclear fuel: impact of the presence and density of bentonite clay” *Corrosion Engineering, Science and Technology*, Vol. 52, No. sup1, pp. 54–60.

KAERI. Korea Atomic Energy Research Institute -> Reactor System Tech. Development Dept., Available at: https://www.kaeri.re.kr/english/sub/sub01_04_02_02_04.jsp (Accessed: March 23, 2018).

Kallio, H. (1997). “Grimsel and planning of the nuclear waste management in Switzerland” *ATS Ydintekniikka*, Vol. 26, No. 4, pp. 27–29.

King, F. (2005). Overview of the corrosion behaviour of copper and steel used fuel containers in a deep geologic repository in the sedimentary rock of the Michigan Basin, Ontario.: OPG, NWMO.

King, F. (2016). Notes for the Stepwise Implementation of a COMSOL Version of the Copper Corrosion Model (CCMC): NWMO.

King, F., Ahonen, L., Taxén, C., Vuorinen, U. and Werme, L. (2001). Copper corrosion under expected conditions in a deep geologic repository: SKB TR-01-23.

King, F., Ahonen, L., Taxen, C., Vuorinen, U. and Werme, L. (2002a). Copper corrosion under expected conditions in a deep geologic repository: POSIVA 2002-01.

King, F. and Kolar, M. (1996). “Mechanistic Modelling of the Corrosion Behaviour of Copper Nuclear Fuel Waste Containers” *AECL*.

King, F. and Kolar, M. (2000). The copper container corrosion model used in AECL's second case study, Ontario Power Generation, Nuclear Waste Management Division: Report 06819-REP-01200-10041-R00 Toronto.

King, F. and Kolar, M. (2005). Preliminary assessment of the stress corrosion cracking of used fuel disposal containers using the CCM-SCC.0 model. Ontario Power Generation, Nuclear Waste Management Division Report 06819-REP-01300-10103-R00. Toronto, Canada.

King, F., Kolář, M. and Keech, P.G. (2014). "Simulations of long-term anaerobic corrosion of carbon steel containers in Canadian deep geological repository" *Corrosion Engineering, Science and Technology*, Vol. 49, No. 6, pp. 455–459.

King, F., Kolar, M. and Maak, P. (2008). "Reactive-transport model for the prediction of the uniform corrosion behaviour of copper used fuel containers" *Journal of Nuclear Materials*, Vol. 379, No. 1, pp. 133–141.

King, F., Kolar, M. and Stroes-Gascoyne, S. (2002b). Theory manual for the microbiological copper corrosion model CCM-MIC.0. 06819-REP-0120010091-R00.

King, F., Kolar, M., Vähänen, M. and Lilja, C. (2011). "Modelling long term corrosion behaviour of copper canisters in KBS-3 repository" *Corrosion Engineering, Science and Technology*, Vol. 46, No. 2, pp. 217–222.

King, F. and Lilja, C. (2014). "Localised corrosion of copper canisters" *Corrosion Engineering, Science and Technology*, Vol. 49, No. 6, pp. 420–424.

King, F., Lilja, C., Pedersen, K., Pitkänen, P. and Vähänen, M. (2012). POSIVA - 2012 - State of the art corrosion: SKB TR-10-67.

King, F., Litke, C.D., Quinn, M.J. and LeNeveu, D.M. (1995). "The measurement and prediction of the corrosion potential of copper in chloride solutions as a function of oxygen concentration and mass-transfer coefficient" *Corrosion Science*, Vol. 37, No. 5, pp. 833–851.

King, F., Quinn, M.J. and Litke, C.D. (1994). A Potentiostatic Study of the Reduction of Oxygen on Copper in 1 mol/dm3 NaCl: AECL COG-94-123.

Kitamura, A., Takase, H., Metcalfe, R. and Penfold, J. (2016). "Effects of α-radiation on a direct disposal system for spent nuclear fuel – (2) review of research into safety assessments of direct disposal of spent nuclear fuel in Europe and North America" *Journal of Nuclear Science and Technology*, Vol. 53, No. 1, pp. 19–33.

Kosec, T., Kranjc, A., Rosborg, B. and Legat, A. (2015). "Post examination of copper ER sensors exposed to bentonite" *Journal of Nuclear Materials*, No. 459, pp. 306–312.

Koyuncu, H. and Kul, A.R. (2014). “An investigation of Cu(II) adsorption by native and activated bentonite: Kinetic, equilibrium and thermodynamic study” *Journal of Environmental Chemical Engineering*, Vol. 2, No. 3, pp. 1722–1730.

Kwong, G.M. (2011). Status of Corrosion Studies for Copper Used Fuel Containers Under Low Salinity Conditions: NWMO Technical Report, TR-2011-14, Toronto, ON.

Lal, H. and Thirsk, H.R. (1953). “The anodic behaviour of copper in neutral and alkaline chloride solutions” *Journal of the Chemical Society (Resumed)*, pp. 2638–2644.

Le News (2017). Swiss, Le News, Available at: https://lenews.ch/2017/12/13/swiss-fact-switzerland-has-enough-nuclear-waste-to-fill-zurich-train-station/ (Accessed: March 11, 2018).

Le Roux, S.G., Miller, J.A., Dunford, A.J. and Clarke, C.E. (2016). “The dissolution kinetics of atacamite in the acid range and the stability of atacamite containing soils from Namaqualand, South Africa” *Applied Geochemistry*, Vol. 64, pp. 22–29.

Mattsson, E. (1980). “Corrosion of Copper and Brass: Practical Experience in relation to Basic Data” *British Corrosion Journal*, Vol. 15, No. 1, pp. 6–13.

McDonald, R.G. and Muir, D.M. (2007). “Pressure oxidation leaching of chalcopyrite. Part I. Comparison of high and low temperature reaction kinetics and products” *Hydrometallurgy*, Vol. 86, No. 3–4, pp. 191–205.

Melichová, Z. and Hromada, L. (2013). “Adsorption of Pb2+ and Cu2+ Ions from Aqueous Solutions on Natural Bentonite” *Polish Journal of Environmental Studies*, Vol. 22, No. 2, pp. 457–464.

Mendoza, A.R., Corvo, F., Gómez, A. and Gómez, J. (2004). “Influence of the corrosion products of copper on its atmospheric corrosion kinetics in tropical climate” *Corrosion Science*, Vol. 46, No. 5, pp. 1189–1200.

Merkel, T.H., Groß, H.-J., Werner, W., Dahlke, T., Reicherter, S., Beuchle, G. and Eberle, S.H. (2002). “Copper corrosion by-product release in long-term stagnation experiments” *Water Research*, Vol. 36, No. 6, pp. 1547–1555.

Morel, F.M.M., Westall, J.C. and Hume, D.N. (1979). “Chloride Interference in Cupric Ion Selective Electrode Measurements” *Analytical Chemistry*, Vol. 51, No. 11, pp. 1792–1798.

Nagra (2014). Experiment on safe disposal of radioactive waste, Available at: https://www.nagra.ch/en/news/mediareleasedetail/experimentonsafedisposalofradioactivewaste.htm (Accessed: February 21, 2018).

Nagra (2018). Retrievability, Available at: https://www.nagra.ch/en/retrievability.htm (Accessed: March 11, 2018).

Necib, S., Diomidis, N., Keech, P. and Nakayama, M. (2017). “Corrosion of carbon steel in clay environments relevant to radioactive waste geological disposals, Mont Terri rock laboratory (Switzerland)” *Swiss Journal of Geosciences*, Vol. 110, No. 1, pp. 329–342.

NEI (2014). Waste, Available at: https://www.nei.org/Master-Document-Folder/Backgrounders/Fact-Sheets/Disposal-Of-Commercial-Low-Level-Radioactive-Waste (Accessed: January 9, 2018).

NEI (2017). Statistics, Available at: https://www.nei.org/Knowledge-Center/Nuclear-Statistics/World-Statistics (Accessed: June 22, 2017).

NMWO (2018). What Other Countries Are Doing | NWMO, Available at: https://www.nwmo.ca/en/Canadas-Plan/What-Other-Countries-Are-Doing (Accessed: March 23, 2018).

NRC (1996). The Waste Isolation Pilot Plant: A Potential Solution for the Disposal of Transuranic Waste, National Research Council, The National Academies Press, 174 pgs.

NWMO (2016). NWMO, Available at: https://www.nwmo.ca/en/Canadas-Plan/Canadas-Used-Nuclear-Fuel/How-Much-Is-There (Accessed: September 7, 2017).

NWMO (2017a). NWMO, Available at: https://www.nwmo.ca/en/Canadas-Plan/Canadas-Used-Nuclear-Fuel/How-Is-It-Stored-Today (Accessed: September 7, 2017).

NWMO (2017b). NWMO, Available at: https://www.nwmo.ca/en/A-Safe-Approach/Facilities/Deep-Geological-Repository/Multiple-Barrier-System (Accessed: September 14, 2017).

NWMO (2018). Multiple-Barrier System, Available at: https://www.nwmo.ca/en/A-Safe-Approach/Facilities/Deep-Geological-Repository/Multiple-Barrier-System (Accessed: January 1, 2018).

Odnevall, I. and Leygraf, C. (1995). “Atmospheric Corrosion of Copper in a Rural Atmosphere” *Journal of The Electrochemical Society*, Vol. 142, No. 11, pp. 3682–3689.

Oglesby, G.B., Duer, W.C. and Millero, F.J. (1977). “Effect of chloride ion and ionic strength on the response of a copper(II) ion-selective electrode” *Analytical Chemistry*, Vol. 49, No. 6, pp. 877–879.

Ooma, T., Tamura, N., Shimizu, T., Takazawa, M., Yamaguchi, K., Takase, T., Nakai, K., Nakagami, M. and Wada, H. (2014). “Evaluation of pH and redox conditions in subsurface disposal system for assessing influence of metal corrosion” *Corrosion Engineering, Science and Technology*, Vol. 49, No. 6, pp. 492–497.

OPG (2017). Available at: http://www.opg.com/generating-power/nuclear/Pages/nuclear.aspx (Accessed: September 7, 2017).

Palit, A. and Pehkonen, S.O. (2000). “Copper corrosion in distribution systems: evaluation of a homogeneous Cu 2 O film and a natural corrosion scale as corrosion inhibitors” *Corrosion Science*, Vol. 42, No. 10, pp. 1801–1822.

Pettersson, K. (2010). “A study of grain boundary sliding in copper with and without an addition of phosphorus” *Journal of Nuclear Materials*, Vol. 405, No. 2, pp. 131–137.

Poluektov, P.P., Schmidt, O.V., Kascheev, V.A. and Ojovan, M.I. (2017). “Modelling aqueous corrosion of nuclear waste phosphate glass” *Journal of Nuclear Materials*, Vol. 484, No. Supplement C, pp. 357–366.

Posiva (2018). Basics of the final disposal, Posiva, Available at: http://www.posiva.fi/en/final_disposal/basics_of_the_final_disposal (Accessed: February 21, 2018).

Rani, N. and Shrivastava, J. (2016). “Long-Term Performance Assessment of Nuclear Waste and Natural Glasses in the Geological Repository: a Geochemical Modelling” *Current Science*, Vol. 110.2, No. 214.

Ryan, S.R. and King, F. (1994). The adsorption of Cu(II) on sodium bentonite in a synthetic saline groundwater: AECL COG-I--94-125.

Sandy, Maramis, V., Kurniawan, A., Ayucitra, A., Sunarso, J. and Ismadji, S. (2012). “Removal of copper ions from aqueous solution by adsorption using LABORATORIES-modified bentonite (organo-bentonite)” *Frontiers of Chemical Science and Engineering*, Vol. 6, No. 1, pp. 58–66.

Scott, D.A. (2000). “A Review of Copper Chlorides and Related Salts in Bronze Corrosion and as Painting Pigments” *Studies in Conservation*, Vol. 45, No. 1, pp. 39–53.

Scully, J.R. and Edwards, M. (2013). Review of the NWMO Copper Corrosion Allowance. Technical Report: NWMO TR-2013-04.

Scully, J.R., Féron, D. and Hänninen, H. (2016). Review of the NWMO Copper Corrosion Program. Technical Report: NWMO-TR-2016-11.

Sharma, V.K. and Millero, F.J. (1988a). “The oxidation of Cu (I) in electrolyte solutions” *Journal of solution chemistry*, Vol. 17, No. 6, pp. 581–599.

Sharma, V.K. and Millero, F.J. (1988b). “Effect of ionic interactions on the rates of oxidation of Cu(I) with O2 in natural waters” *Marine Chemistry*, Vol. 25, No. 2, pp. 141–161.

Shim, J.J. and Kim, J.G. (2004). “Copper corrosion in potable water distribution systems: influence of copper products on the corrosion behavior” *Materials Letters*, Vol. 58, No. 14, pp. 2002–2006.

SKB (2018). The Spent Fuel Repository, Available at: http://www.skb.com/future-projects/the-spent-fuel-repository/ (Accessed: April 18, 2018).

Standish, T., Chen, J., Jacklin, R., Jakupi, P., Ramamurthy, S., Zagidulin, D., Keech, P. and Shoesmith, D. (2016). “Corrosion of copper-coated steel high level nuclear waste containers under permanent disposal conditions” *Electrochimica Acta*, Vol. 211, pp. 331–342.

Sugawara, H., Iron, T.R.I. for and Metals, S. and O. (1965). “Formation of Anodic Film on Copper in 3% NaCl Aqueous Solution” *Science reports of the Research Institutes, Tohoku University. Ser. A, Physics, chemistry and metallurgy*, Vol. 17/18, pp. 95b-104b.

Suorsa, M. (2017). *Effect of clay colloids on radionuclide migration*, Masters Thesis, University of Helsinki.

Tavakoli, B., Weidner, J., Garcia-Diaz, B., Martinez-Rodriguez, M., C. Olsen, L. and Shimpalee, S. (2017). “Modeling the Effect of Cathodic Protection on Superalloys inside High Temperature Molten Salt Systems” *Journal of The Electrochemical Society*, Vol. 164, pp. C171–C179.

Thury, M. and Bossart, P. (1999). “The Mont Terri rock laboratory, a new international research project in a Mesozoic shale formation, in Switzerland” *Engineering Geology*, Vol. 52, No. 3, pp. 347–359.

Tran, T.T.M., Fiaud, C., Sutter, E.M.M. and Villanova, A. (2003). “The atmospheric corrosion of copper by hydrogen sulphide in underground conditions” *Corrosion Science*, Vol. 45, No. 12, pp. 2787–2802.

Uddin, M.K. (2017). “A review on the adsorption of heavy metals by clay minerals, with special focus on the past decade” *Chemical Engineering Journal*, Vol. 308, pp. 438–462.

Vargas, I.T., Alsina, M.A., Pastén, P.A. and Pizarro, G.E. (2009). “Influence of solid corrosion by-products on the consumption of dissolved oxygen in copper pipes” *Corrosion Science*, Vol. 51, No. 5, pp. 1030–1037.

Vargas, I.T., Pastén, P.A. and Pizarro, G.E. (2010). “Empirical model for dissolved oxygen depletion during corrosion of drinking water copper pipes” *Corrosion Science*, Vol. 52, No. 7, pp. 2250–2257.

Veleva, L. and Farro, W. (2012). “Influence of seawater and its aerosols on copper patina composition” *Applied Surface Science*, Vol. 258, No. 24, pp. 10072–10076.

Veleva, L., Quintana, P., Ramanauskas, R., Pomes, R. and Maldonado, L. (1996). “Mechanism of copper patina formation in marine environments” *Electrochimica Acta*, Vol. 41, No. 10, pp. 1641–1646.

Veli, S. and Alyüz, B. (2007). “Adsorption of copper and zinc from aqueous solutions by using natural clay” *Journal of Hazardous Materials*, Vol. 149, No. 1, pp. 226–233.

Watanabe, M., Handa, T., Ichino, T., Kuwaki, N. and Sakai, J. (2009a). “Characterization of patinas that formed on copper exposed in different environments for one month” *Zairyo to Kankyo/ Corrosion Engineering*, Vol. 58, No. 4, pp. 143–157.

Watanabe, M., Matsumoto, M., Kuwaki, N. and Sakai, J. (2009b). “Formation of basic copper sulfates and chlorides during atmospheric copper corrosion” *Zairyo to Kankyo/ Corrosion Engineering*, Vol. 58, No. 9, pp. 328–334.

Wehrli, B. (1990). “Redox reactions of metal ions at mineral surfaces” *IN: Aquatic Chemical Kinetics: Reaction Rates of Processes in Natural Waters. Environmental Science and Technology Series. John Wiley & Sons, New York. 1990. p 311-336. 9 fig, 4 tab, 58 ref.*

Werme, L.O., Sellin, P. and Kjellbert, N. (1992). Copper canisters for nuclear high level waste disposal: corrosion aspects, Svensk kärnbränslehantering.

Wersin, P., Bruno, J. and Spahiu, K. (1993). Kinetic modelling of bentonite-canister interaction. Implications for Cu, Fe and Pb corrosion in a repository for spent nuclear fuel. Technical Report: SKB TR 93-16

Wersin, P., Spahiu, K. and Bruno, J. (1994). Kinetic modelling of bentonite-canister interaction. Long-term predictions of copper canister corrosion under oxic and anoxic conditions. Technical Report: SKB TR-94-25.

WISE (1991). Morsleben closed | Wise International, Available at: https://www.wiseinternational.org/nuclear-monitor/364/morsleben-closed (Accessed: February 21, 2018).

WNA (2017). Available at: http://www.world-nuclear.org/information-library/country-profiles/countries-a-f/canada-nuclear-power.aspx (Accessed: August 2, 2017).

Zhang, Q., Zheng, M., Huang, Y., Nishikata, A., Lu, D., Zhang, J., Wang, X., Wen, J., Li, Y. and Liu, Y. (2017). “Corrosion behaviour of carbon steel, titanium and titanium alloy in simulated underground water in Beishan area preselected for nuclear waste repository in China” *Corrosion Engineering, Science and Technology*, Vol. 52, No. 6, pp. 425–431.

Zhou, P., Hutchison, M.J., Scully, J.R. and Ogle, K. (2016). “The anodic dissolution of copper alloys: Pure copper in synthetic tap water” *Electrochimica Acta*, Vol. 191, pp. 548–557.

GLOSSARY

Notation	Species
i_{corr}	Corrosion current
i_a	Current for anodic dissolution of Cu
i_c	Current for reduction of O_2
i_d	Current for reduction of Cu^{2+}
M_{Cu}	Atomic mass of Cu (63.546 g/mol)
F	Faraday's constant (96487 C/mol)
ρ_{Cu}	Density of Cu (8.96 x 10^6 g/m^3)
c_A	Gaseous O_2
c_0	Dissolved O_2
c_1	Dissolved $CuCl_2^-$
c_2	Precipitated Cu_2O
c_3	Dissolved Cu^{2+}
c_4	Precipitated $CuCl_2 \cdot 3Cu(OH)_2$
c_5	Adsorbed Cu(II)
c_6	Dissolved Cl^-
c_7	Dissolved Fe(II)
c_8	Precipitated Fe(II)
T	Temperature
S	Saturation (100%)
ε_a	Accessible porosity
ε_e	Effective porosity
τ_f	Tortuosity
D_0	Bulk-solution diffusion coefficient of O_2
D_1	Bulk-solution diffusion coefficient of $CuCl_{2^-}$

Notation	Species
D_3	Bulk-solution diffusion coefficient of Cu^{2+}
D_6	Bulk-solution diffusion coefficient of Cl^-
k_1	Rate constant for homogenous oxidation of $CuCl_2^-$
k_2/k_{-2}	Rate constant for precipitation/dissolution of Cu_2O
k_3/k_{-3}	Rate constant for precipitation/dissolution of $CuCl_2.3Cu(OH)_2$
k_4/k_{-4}	Rate constant for adsorption/desorption of Cu^{2+}
k_{af}/k_{ab}	Rate constant for Cu conversion to $CuCl_{ADS}$/ Reverse rate constant
k_{bf}/k_{bb}	Rate constant for conversion of $CuCl_{ADS}$ to $CuCl_2^-$ /Reverse rate constant
k_a	Combined electrochemical constant for anodic dissolution of Cu (k_{af} x k_{bf})/k_{ab}
k_c	Electrochemical rate constant for the reduction of oxygen
k_d	Electrochemical rate constant for the reduction of Cu^{2+}

APPENDIX A: CORROSION RATE EXPRESSION

Corrosion Rate (CR) = $\frac{i_{corr}\, M_{Cu}}{F \rho_{Cu}}$

Derivation:

From Faraday's law of electrolysis:

$$\frac{\omega}{M} = \frac{It}{zF}$$

Rearranging

$$I = \omega \frac{F}{t} \frac{z}{M}$$

As Mass = Density x Volume:

$$I = V\rho \frac{F}{t} \frac{z}{M}$$

As Volume = Area x Length

$$I = (Al)\rho \frac{F}{t} \frac{z}{M}$$

$$\frac{I}{A} = \frac{l}{t} \rho \frac{Fz}{M}$$

$$i_{corr} = CR\rho \frac{Fz}{M}$$

Rearranging:

$$CR = \frac{i_{corr} M}{F\rho}$$

Where z=1 as the interfacial copper ions involve one electron

APPENDIX B: VERIFICATION

B1. Verification

COMSOL outputs are compared with that of CCM as shown in Chapter 4. Section B2 shows the profile of plots obtained for 1 mm layer of bentonite and Section B3 for 10 mm layer. As stated in Chapter 4, it can be seen that all the plots, except the current density, overlap each other.

B2. 1 mm bentonite thickness

Figure B1 to Figure B7 shows the plots obtained for **Step 3a** which involves reduction of Cu^{2+} and homogenous oxidation of $CuCl_2^-$ in addition to the previous steps.

Outputs obtained for **Step 3b** (precipitation and dissolution of solid Cu(II) in addition to previous steps) is indicated by Figure B8 to Figure B15.

Step 3c which involves the precipitation and dissolution of Cu_2O is shown by Figure B16 to Figure B23.

Step 2 and **Step 3d** are included with Chapter 4

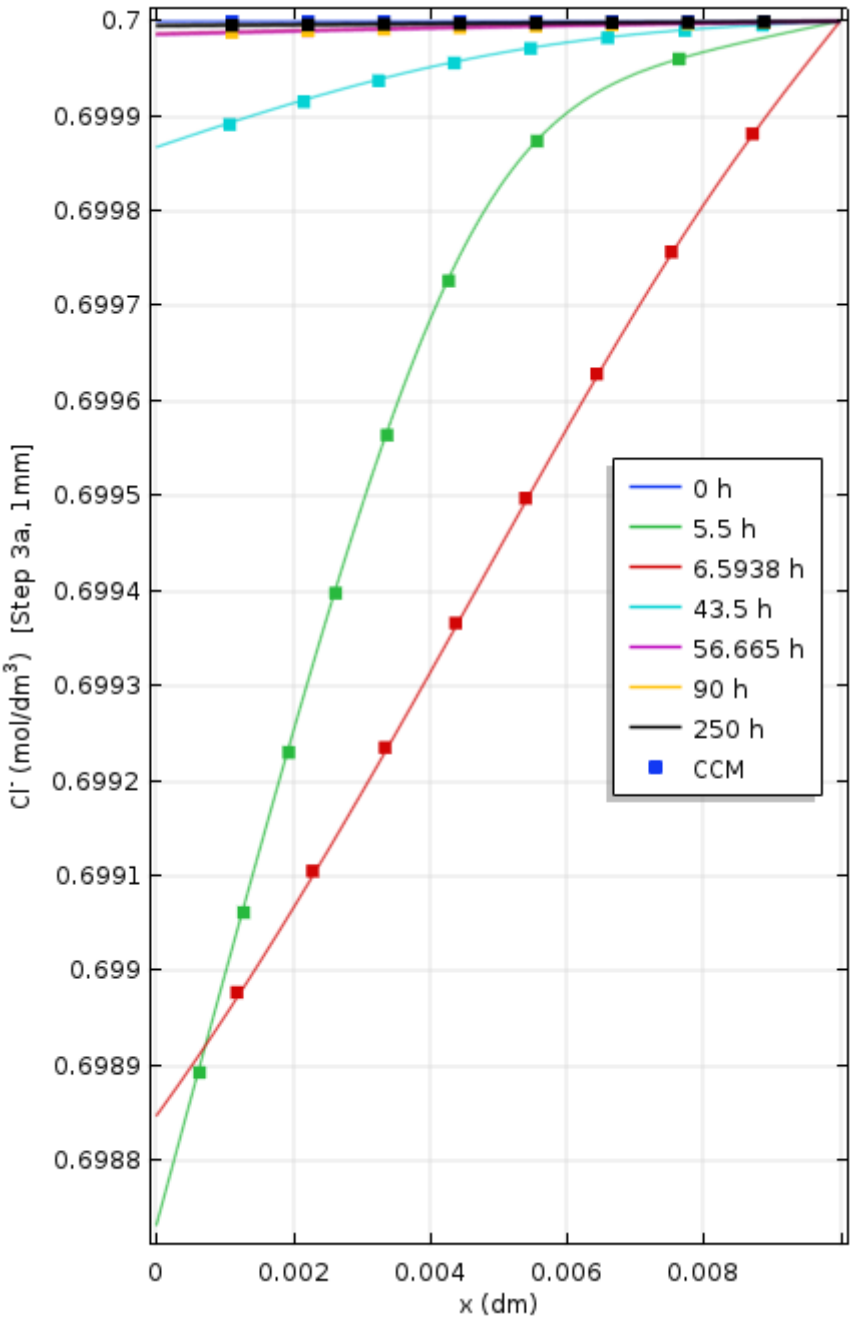

Figure B1: Concentration profile of chloride with distance for 1 mm, Step 3a

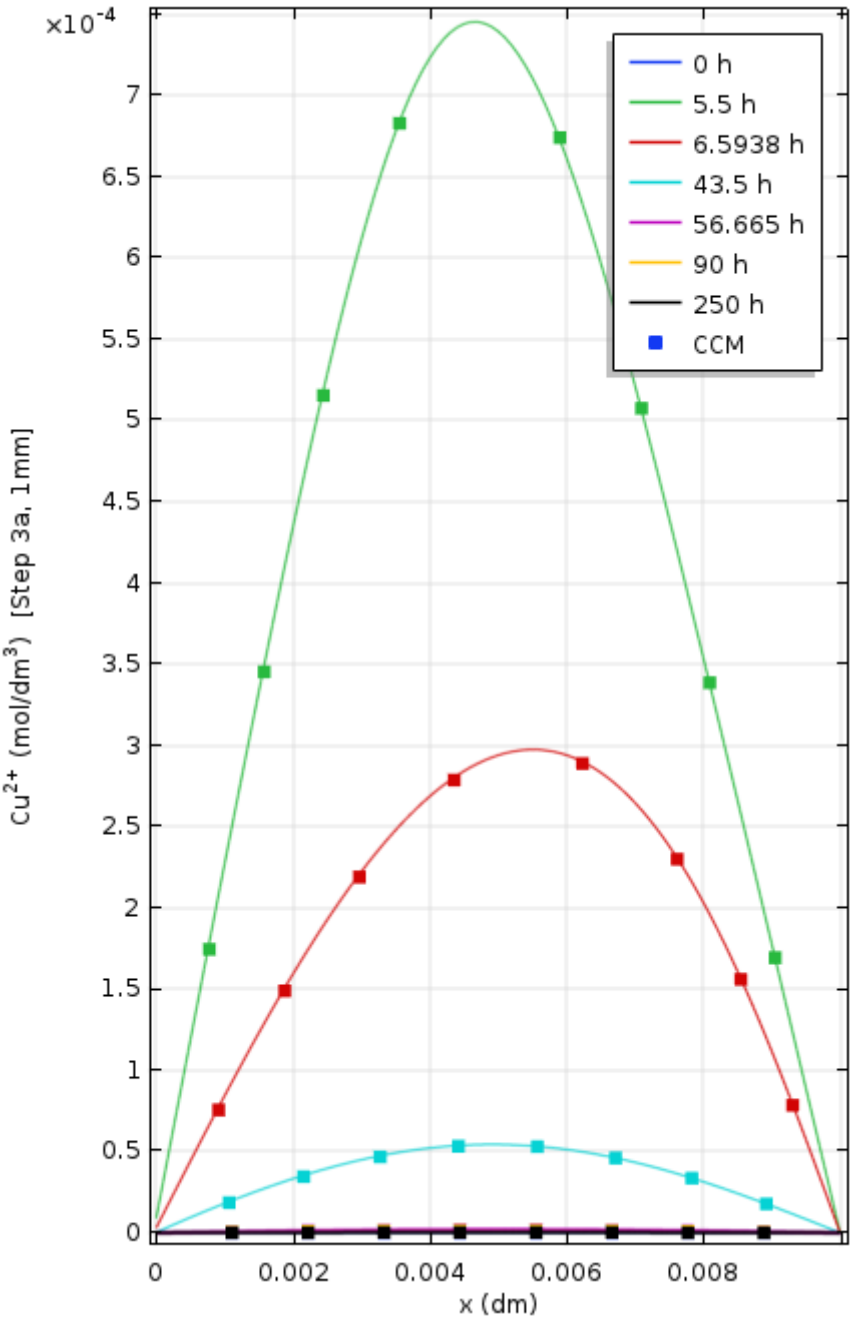

Figure B2: Concentration profile of copper ions with distance for 1 mm, Step 3a

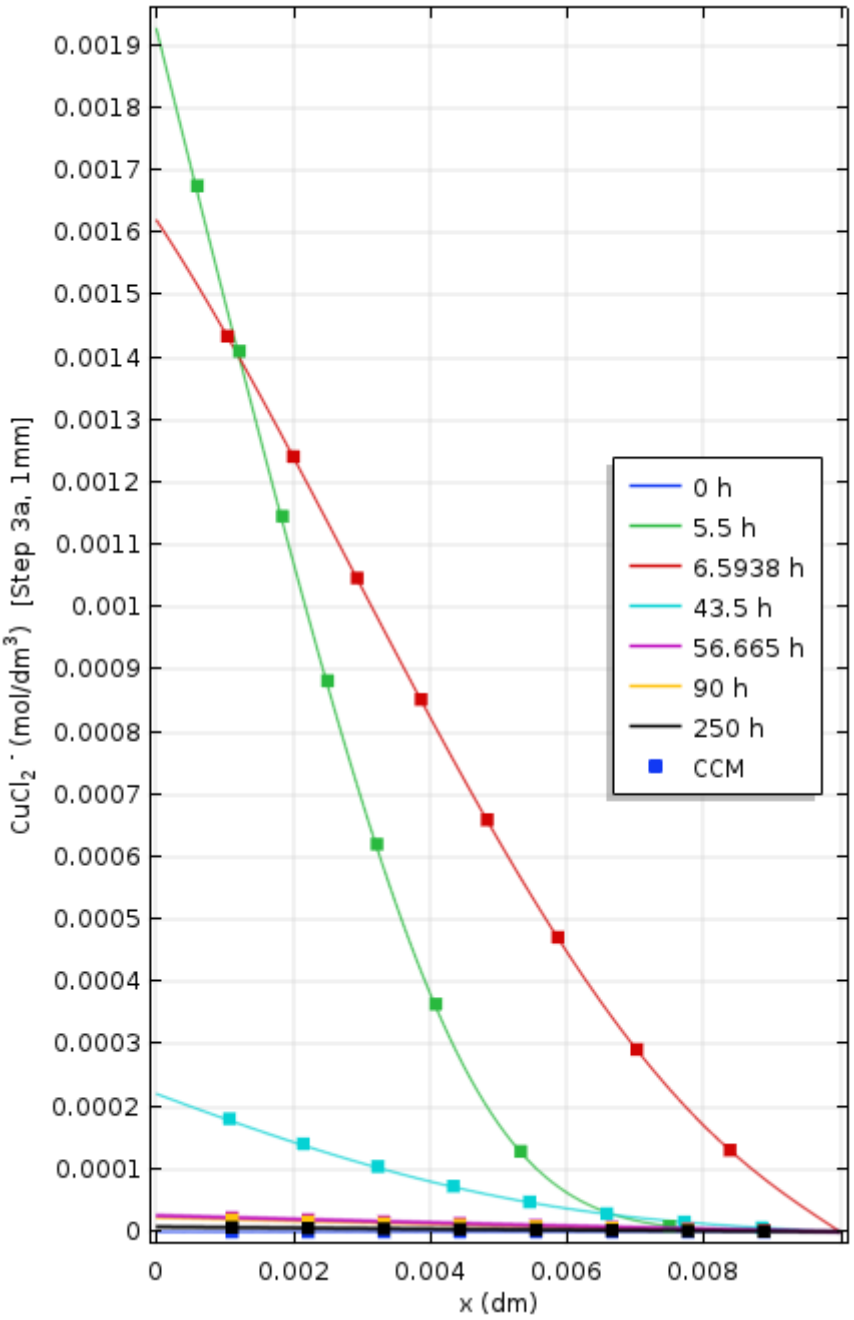

Figure B3: Concentration profile of copper chloride ions with distance for 1 mm, Step 3a

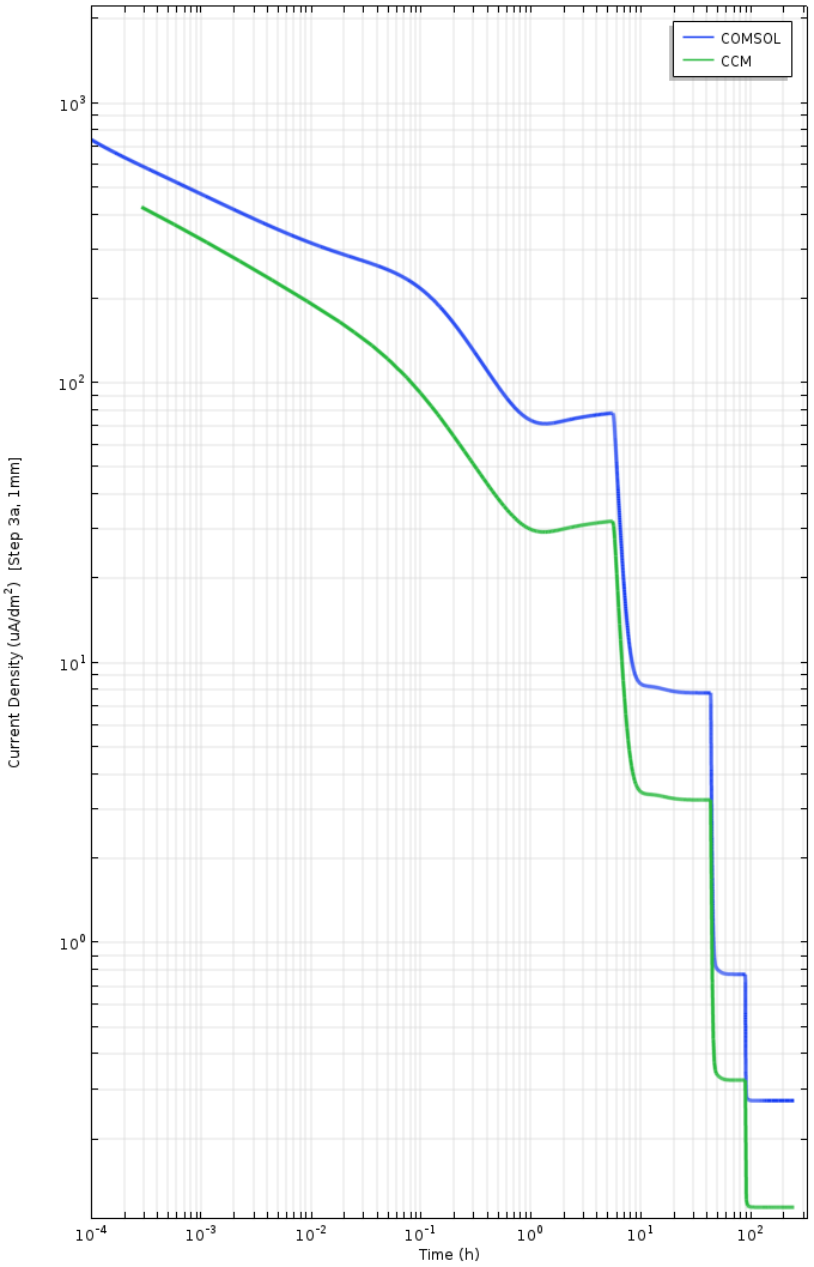

Figure B4: Current density profile over time for 1 mm bentonite thickness, Step 3a

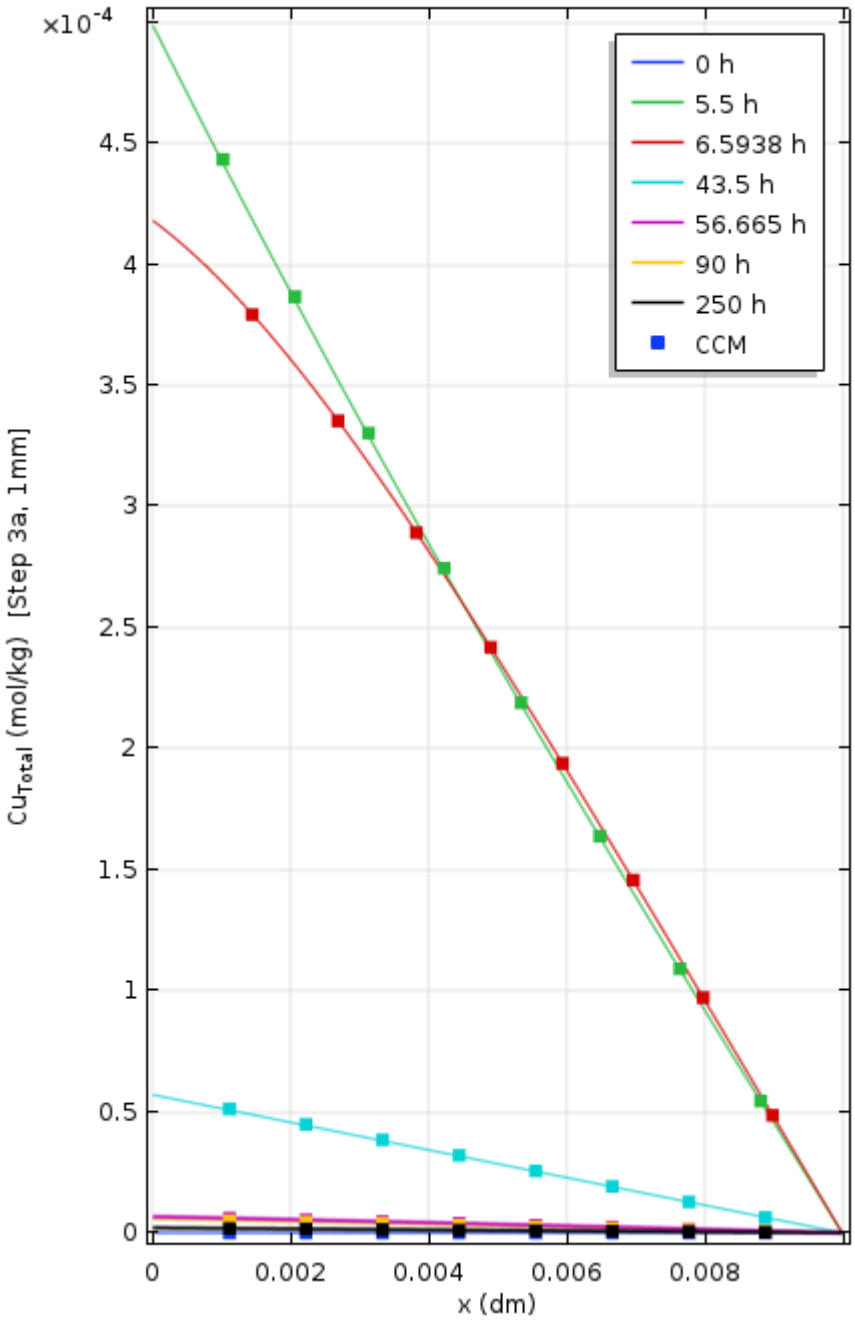

Figure B5: Concentration profile of total amount of copper ($CuCl_2^-$, Cu^{2+}, Cu_2O, $CuCl_2.3Cu(OH)_2$) with distance for 1 mm, Step 3a

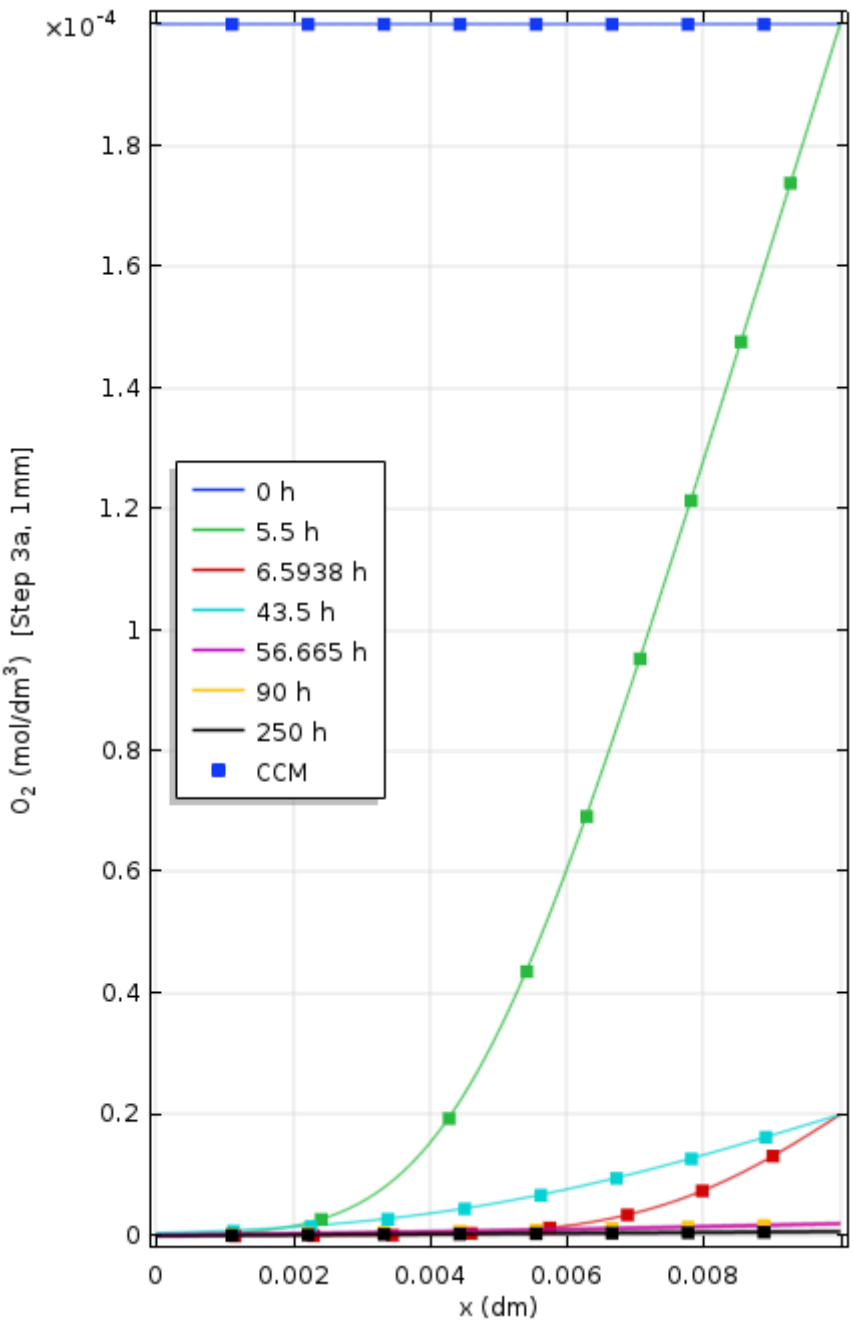

Figure B6: Concentration profile of oxygen with distance for 1 mm, Step 3a

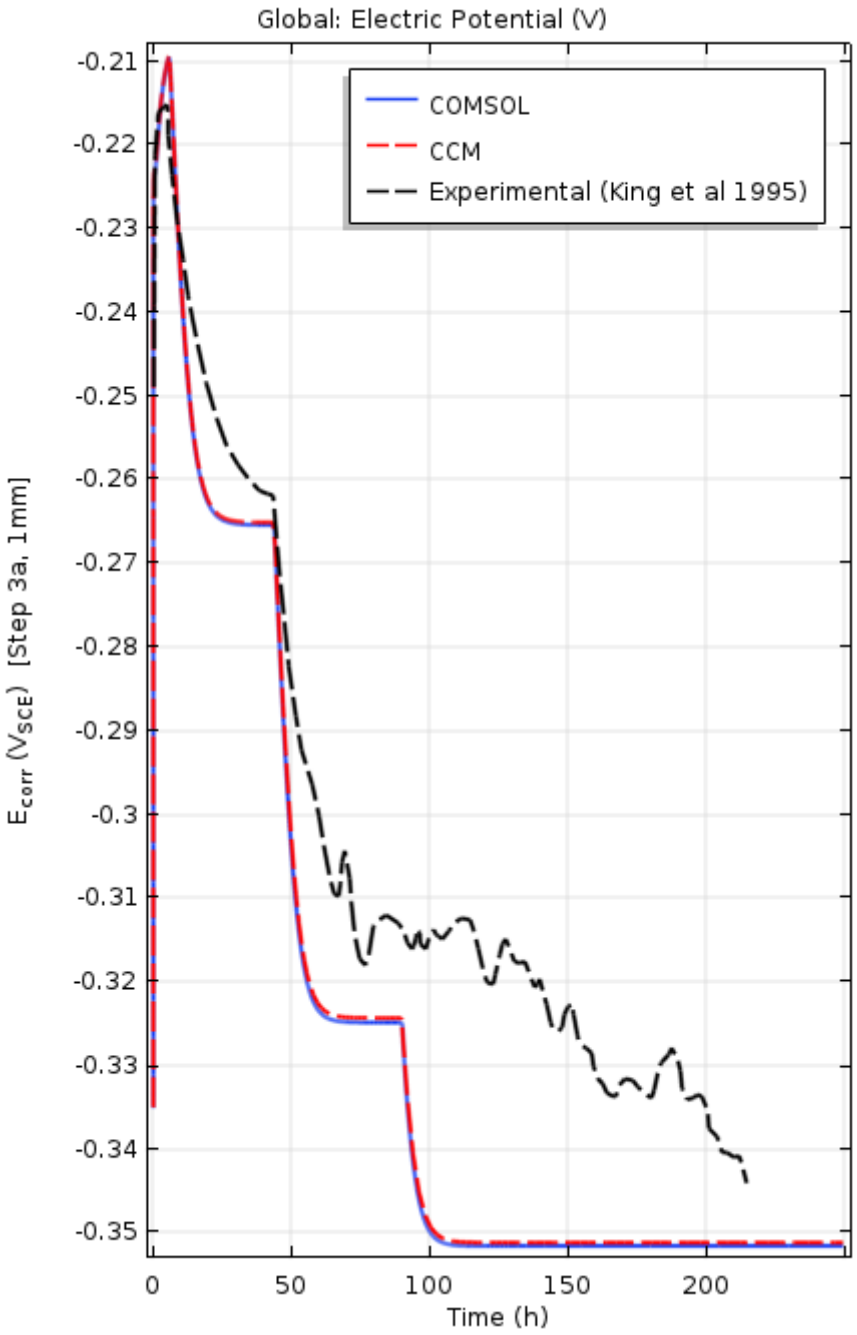

Figure B7: Variation of corrosion potential with time for 1 mm bentonite thickness with changing oxygen concentration for Step 3a

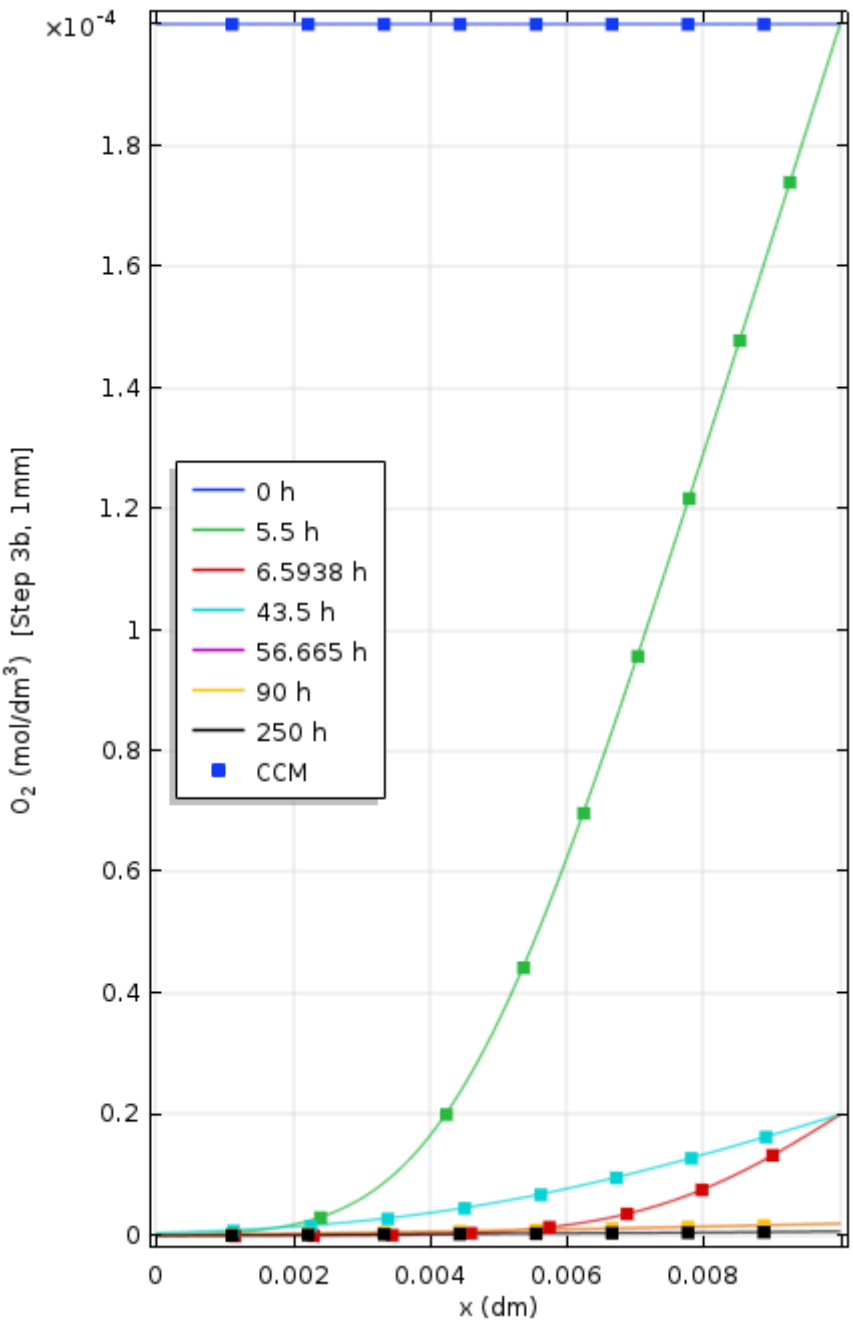

Figure B8: Concentration profile of oxygen with distance for 1 mm, Step 3b

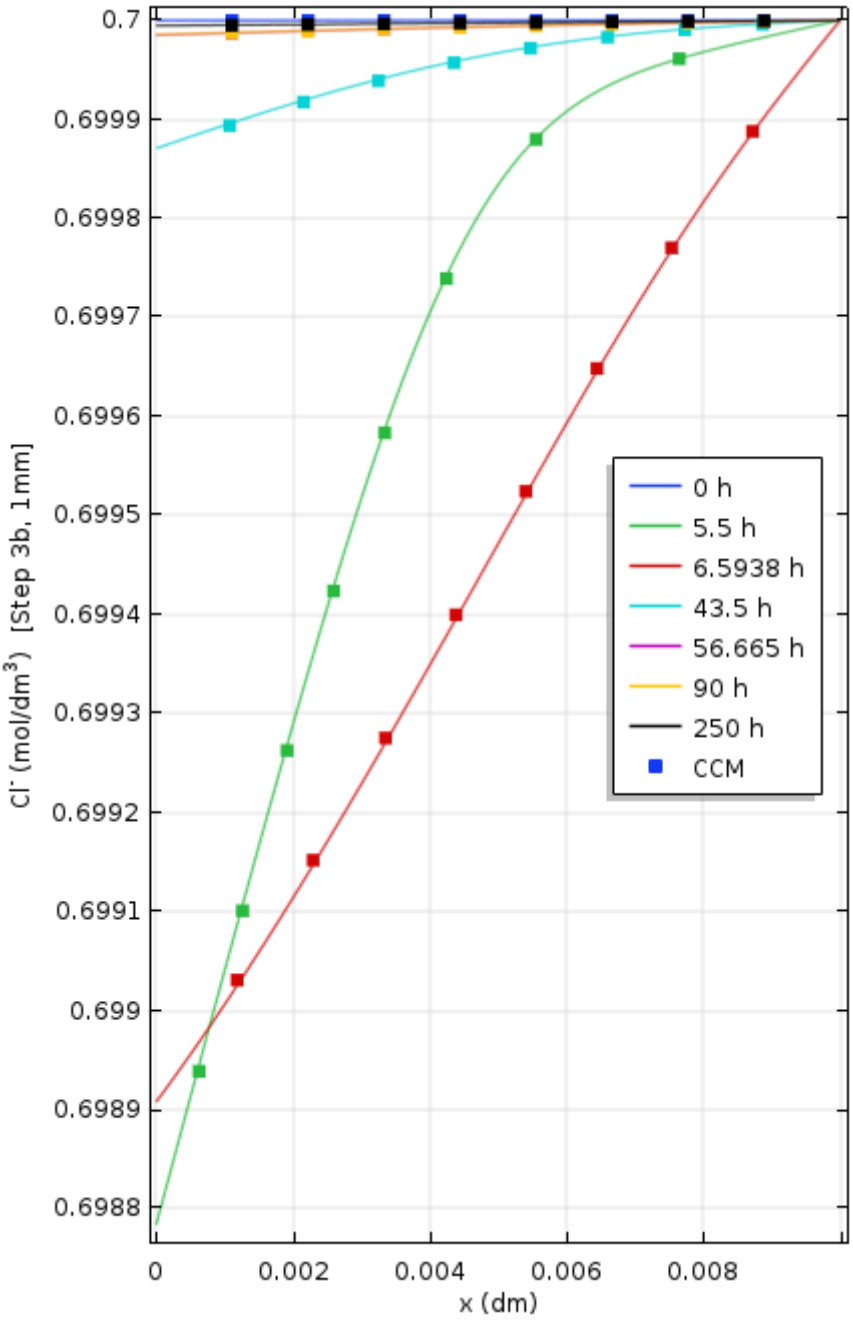

Figure B9: Concentration profile of chloride with distance for 1 mm, Step 3b

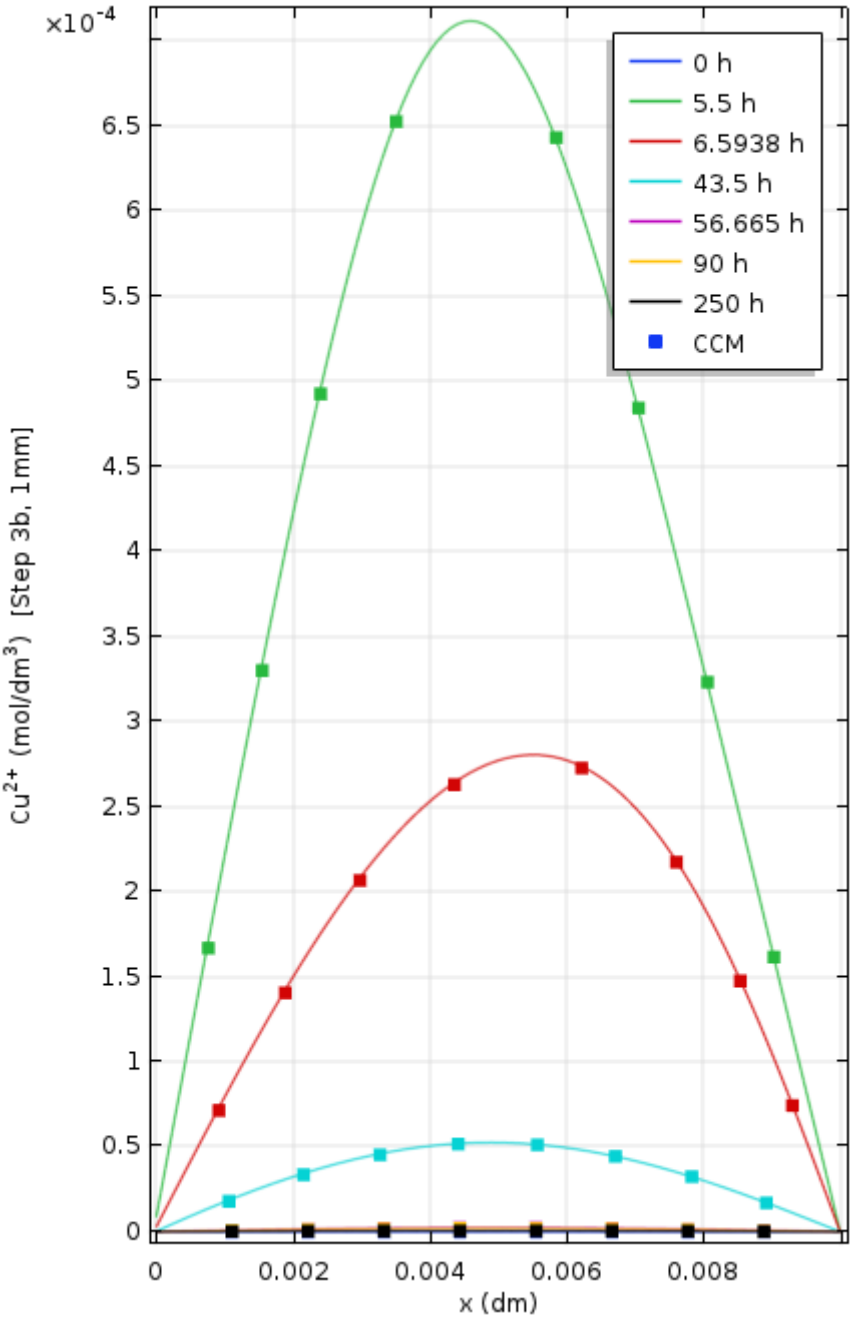

Figure B10: Concentration profile of copper ions with distance for 1 mm, Step 3b

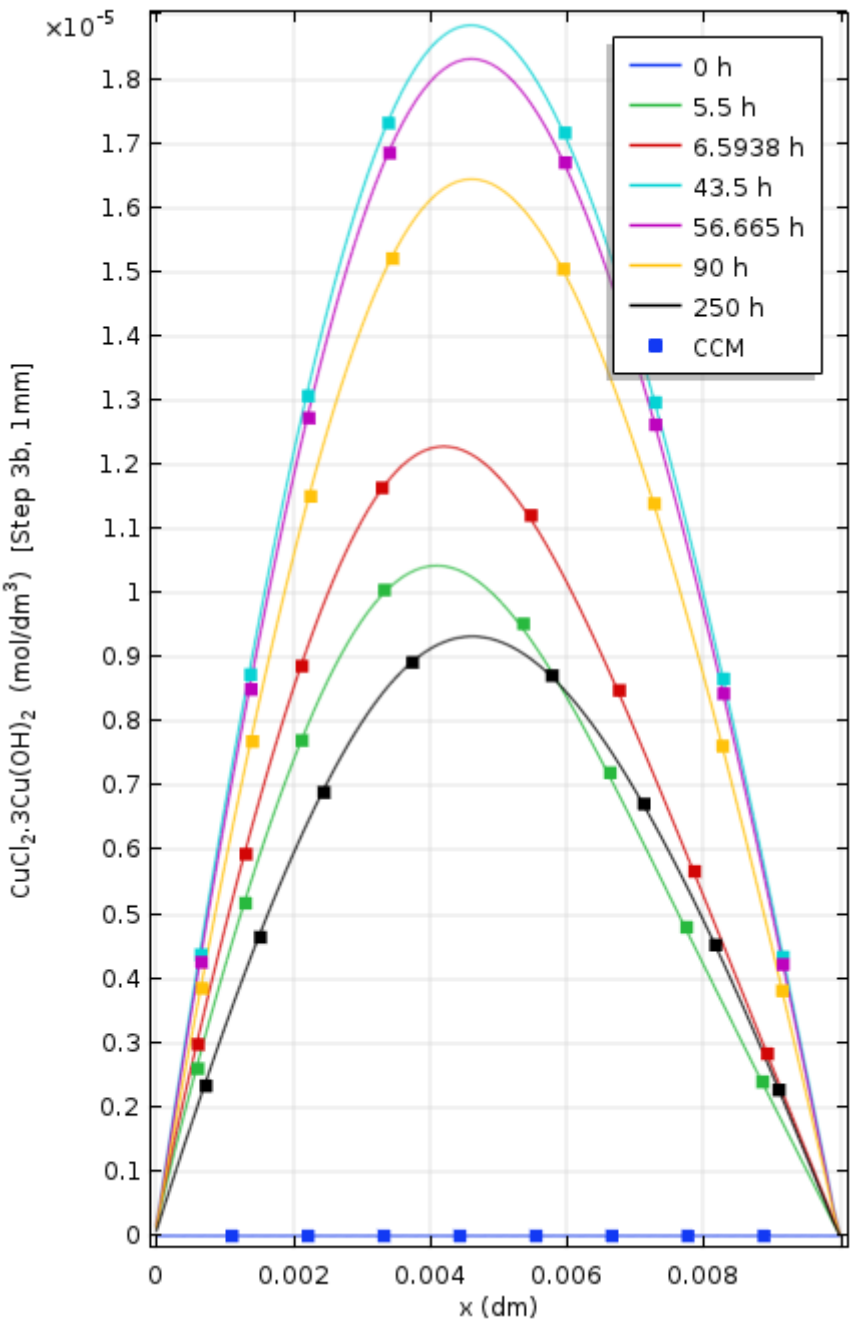

Figure B11: Concentration profile of paratacamite with distance for 1 mm, Step 3b

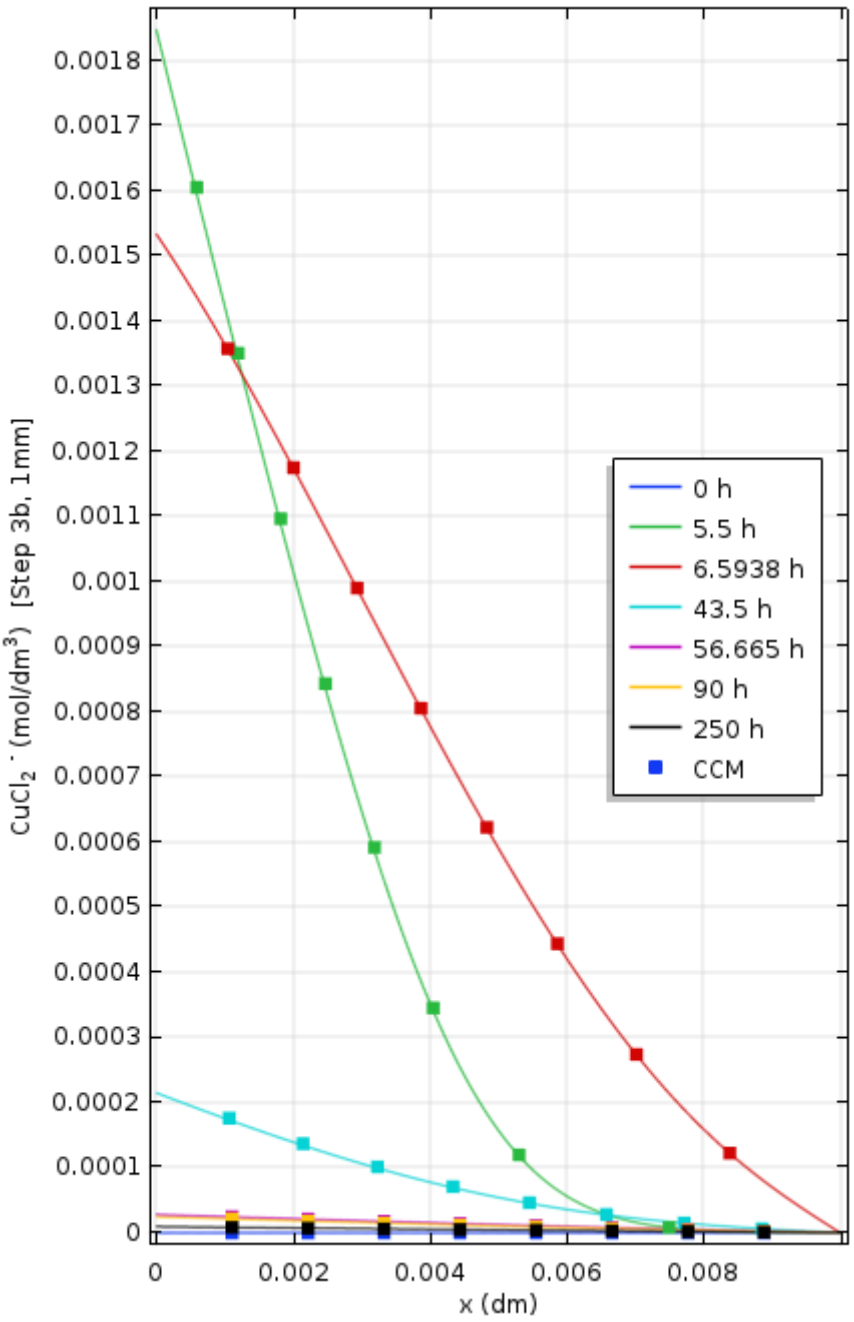

Figure B12: Concentration profile of copper chloride ions with distance for 1 mm, Step 3b

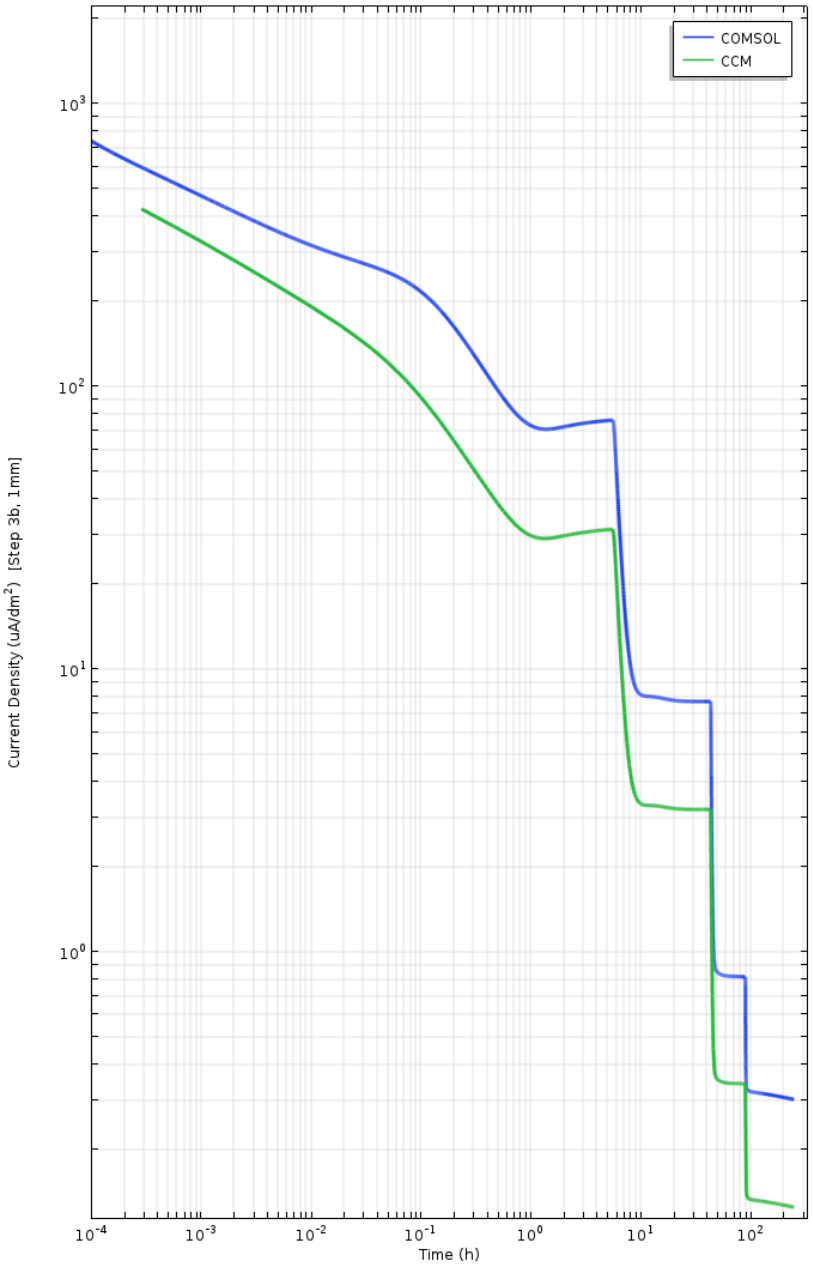

Figure B13: Current density profile over time for 1 mm bentonite thickness, Step 3b

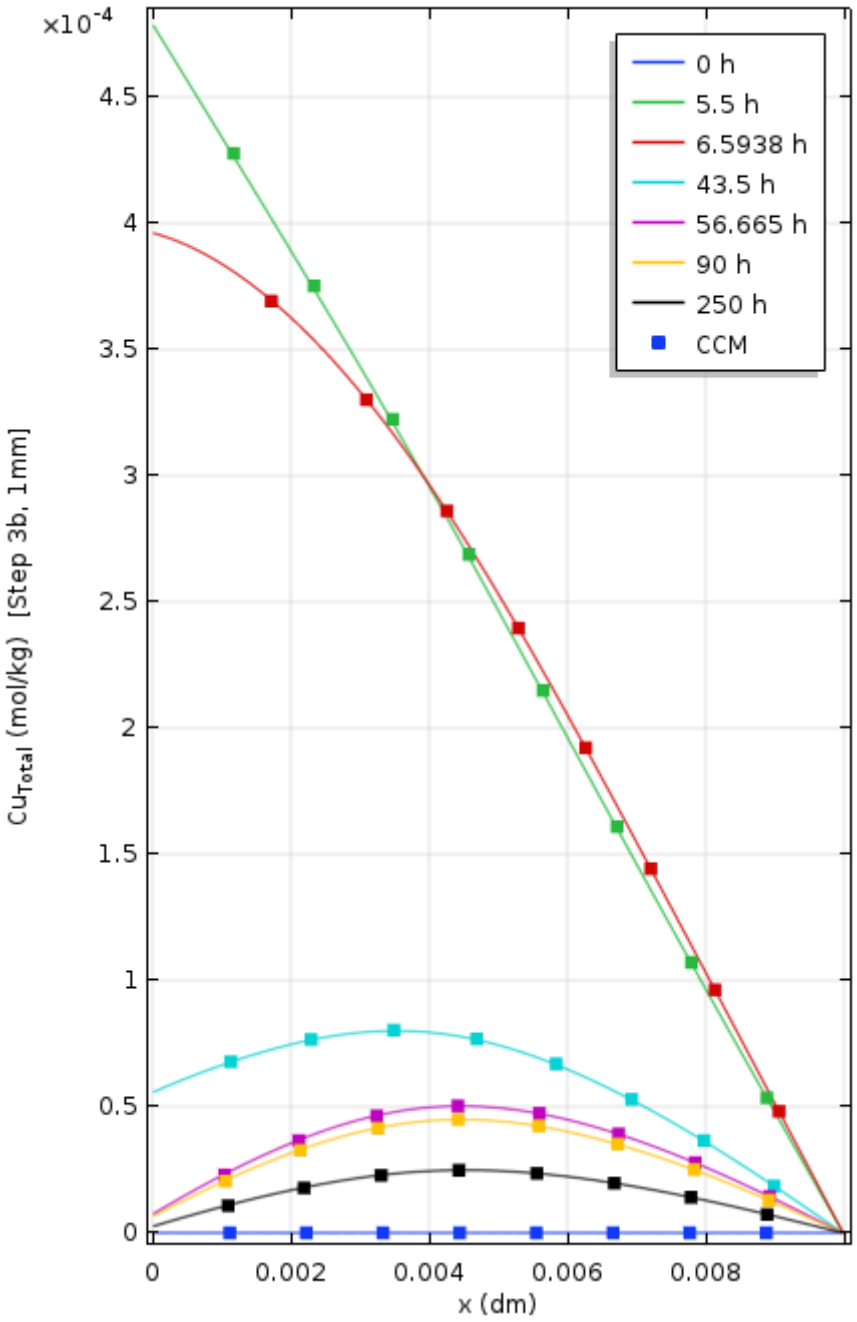

Figure B14: Concentration profile of total amount of copper ($CuCl_2^-$, Cu^{2+}, Cu_2O, $CuCl_2.3Cu(OH)_2$) with distance for 1 mm, Step 3b

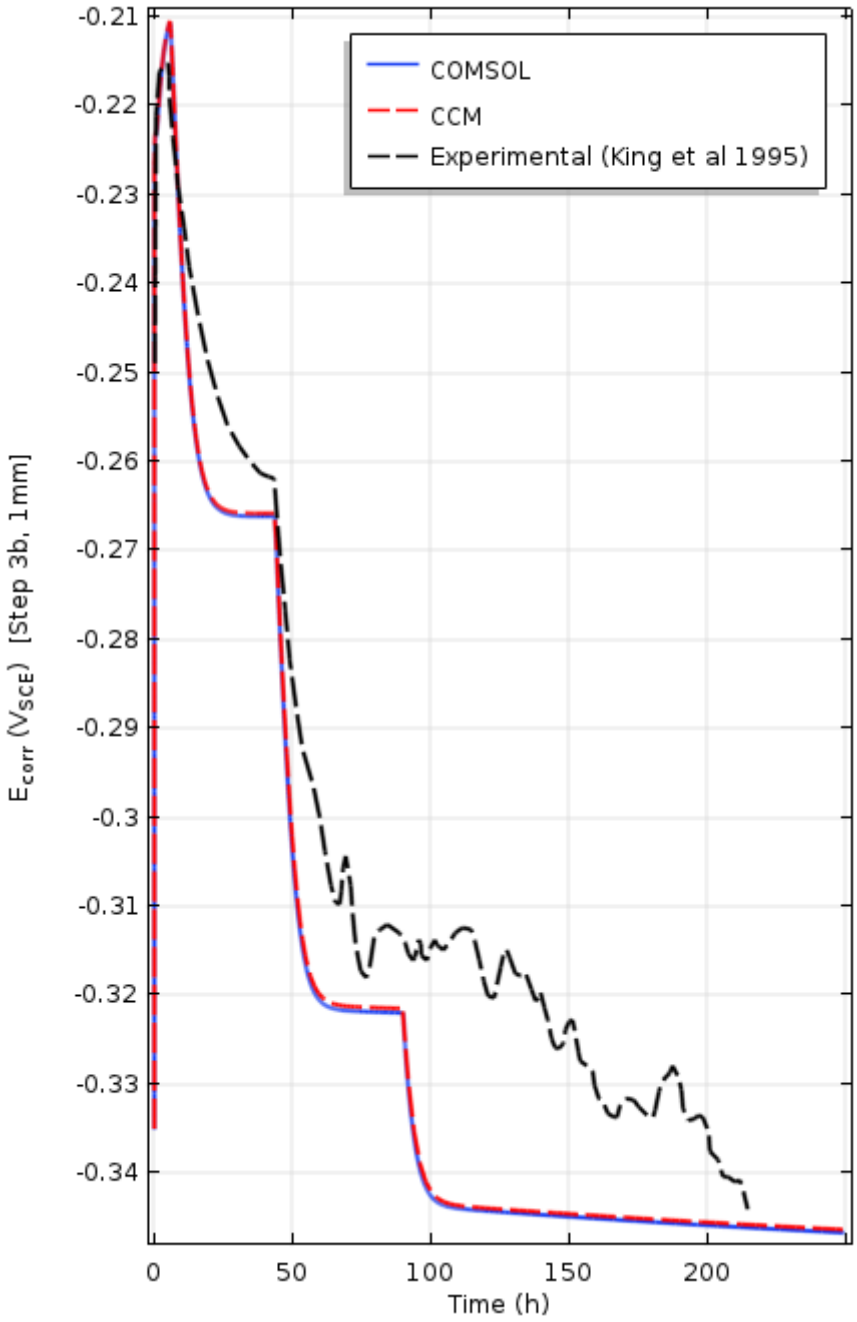

Figure B15: Variation of corrosion potential with time for 1 mm bentonite thickness with changing oxygen concentration for Step 3b

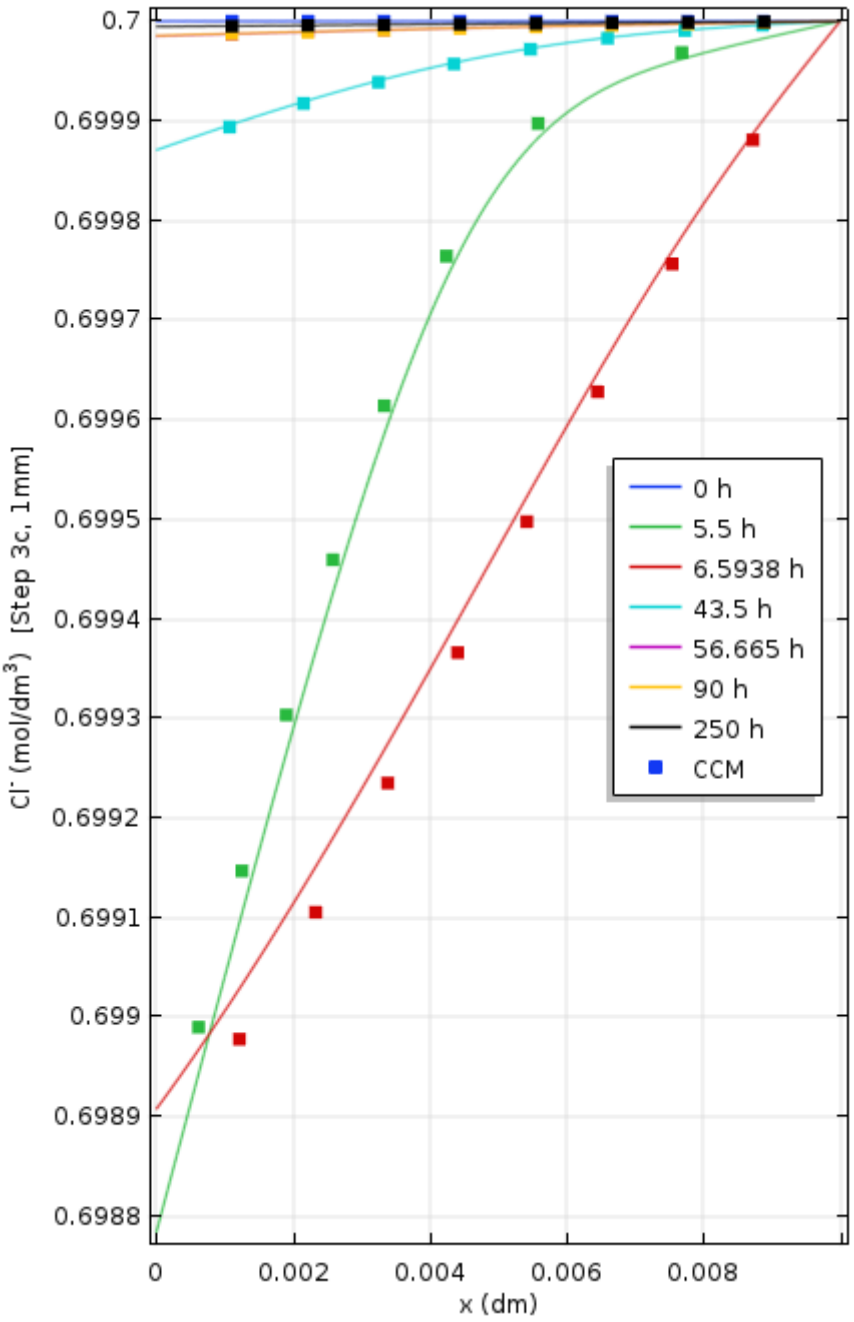

Figure B16: Concentration profile of chloride with distance for 1 mm, Step 3c

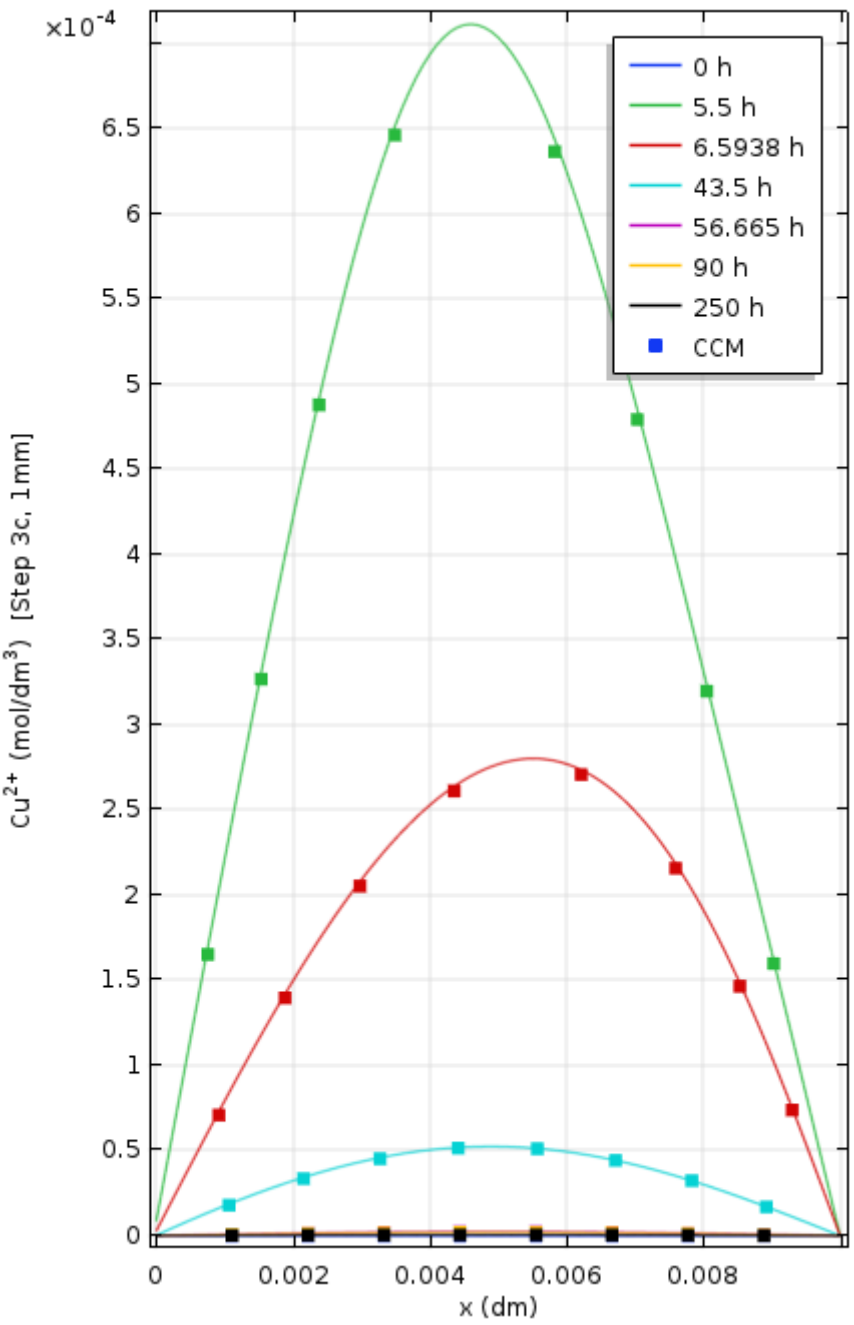

Figure B17: Concentration profile of copper ions with distance for 1 mm, Step 3c

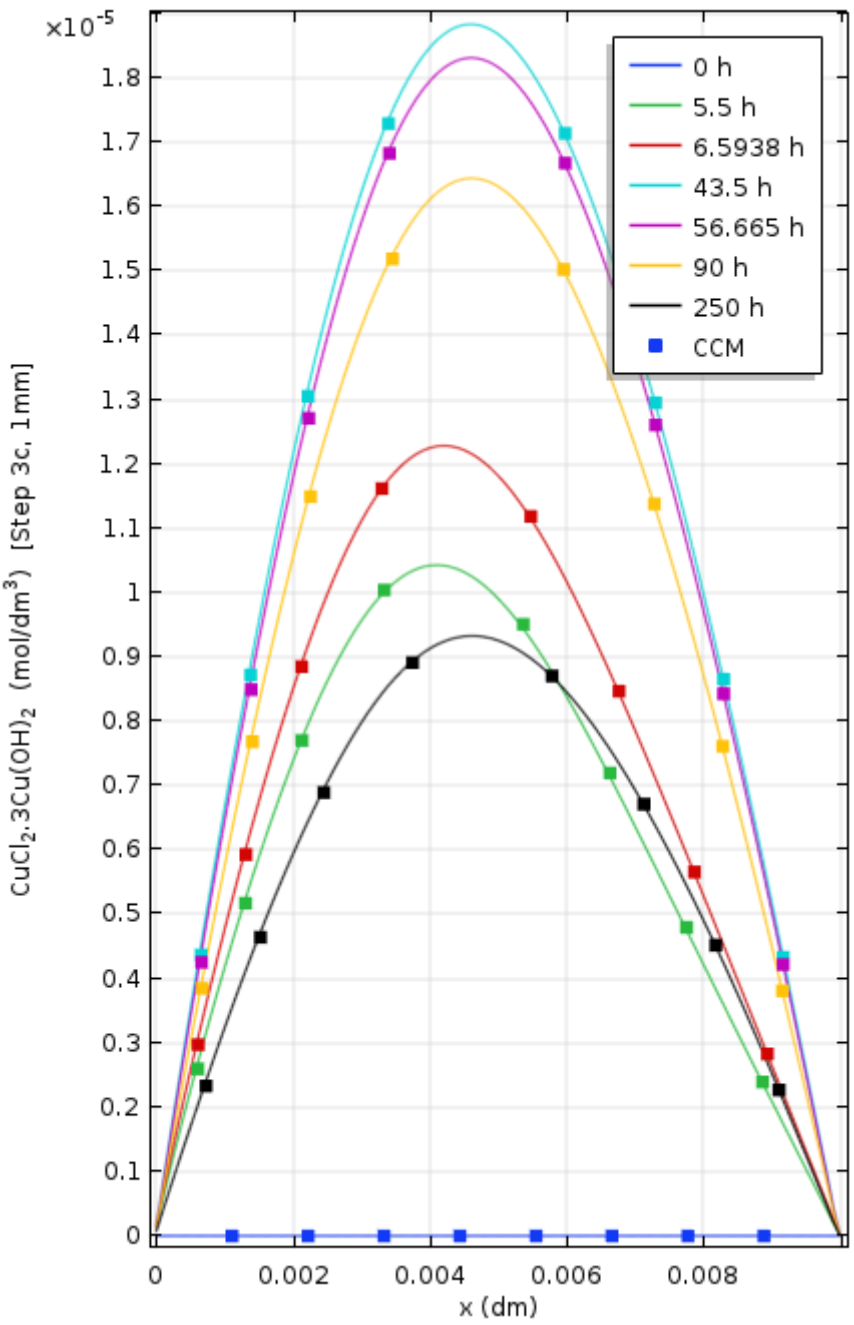

Figure B18: Concentration profile of paratacamite with distance for 1 mm, Step 3c

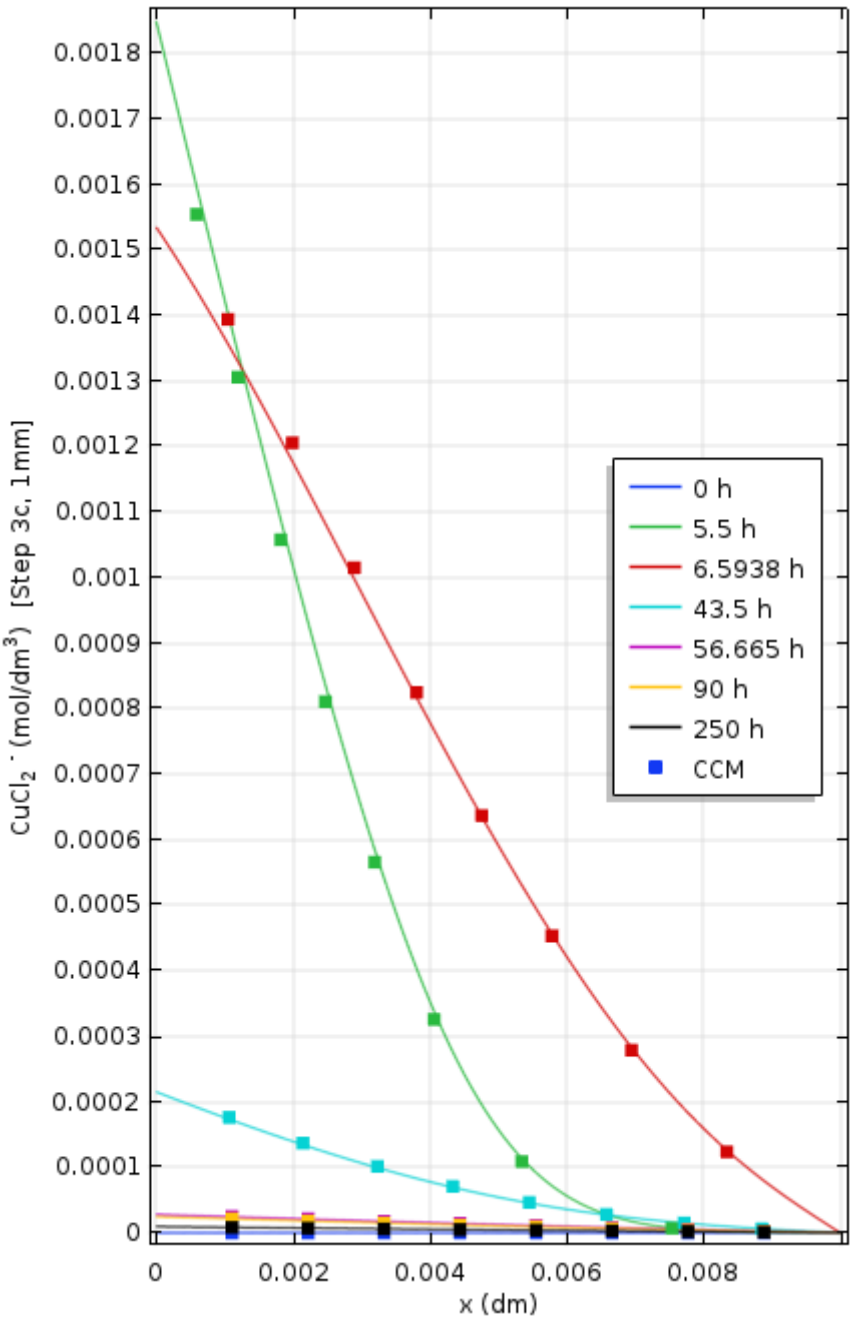

Figure B19: Concentration profile of copper chloride ions with distance for 1 mm, Step 3c

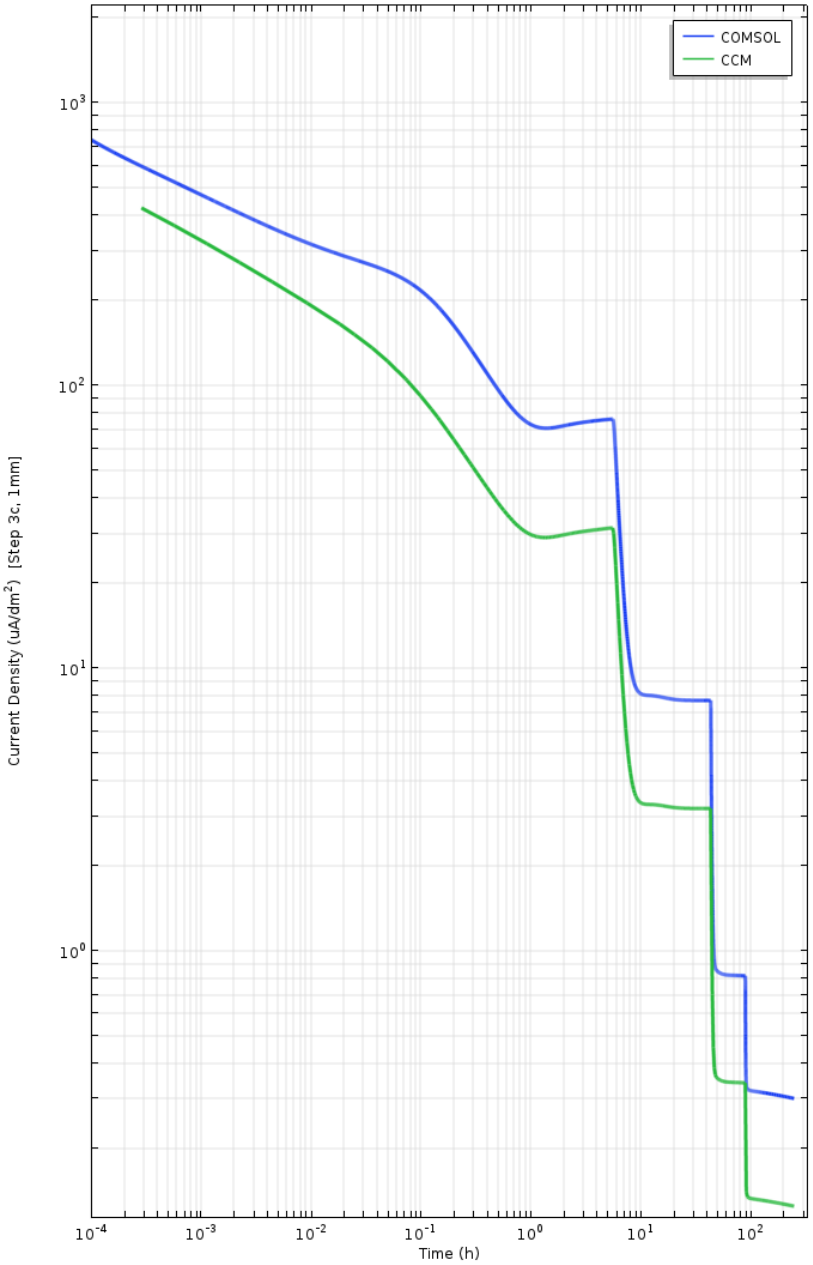

Figure B20: Current density profile over time for 1 mm bentonite thickness, Step 3c

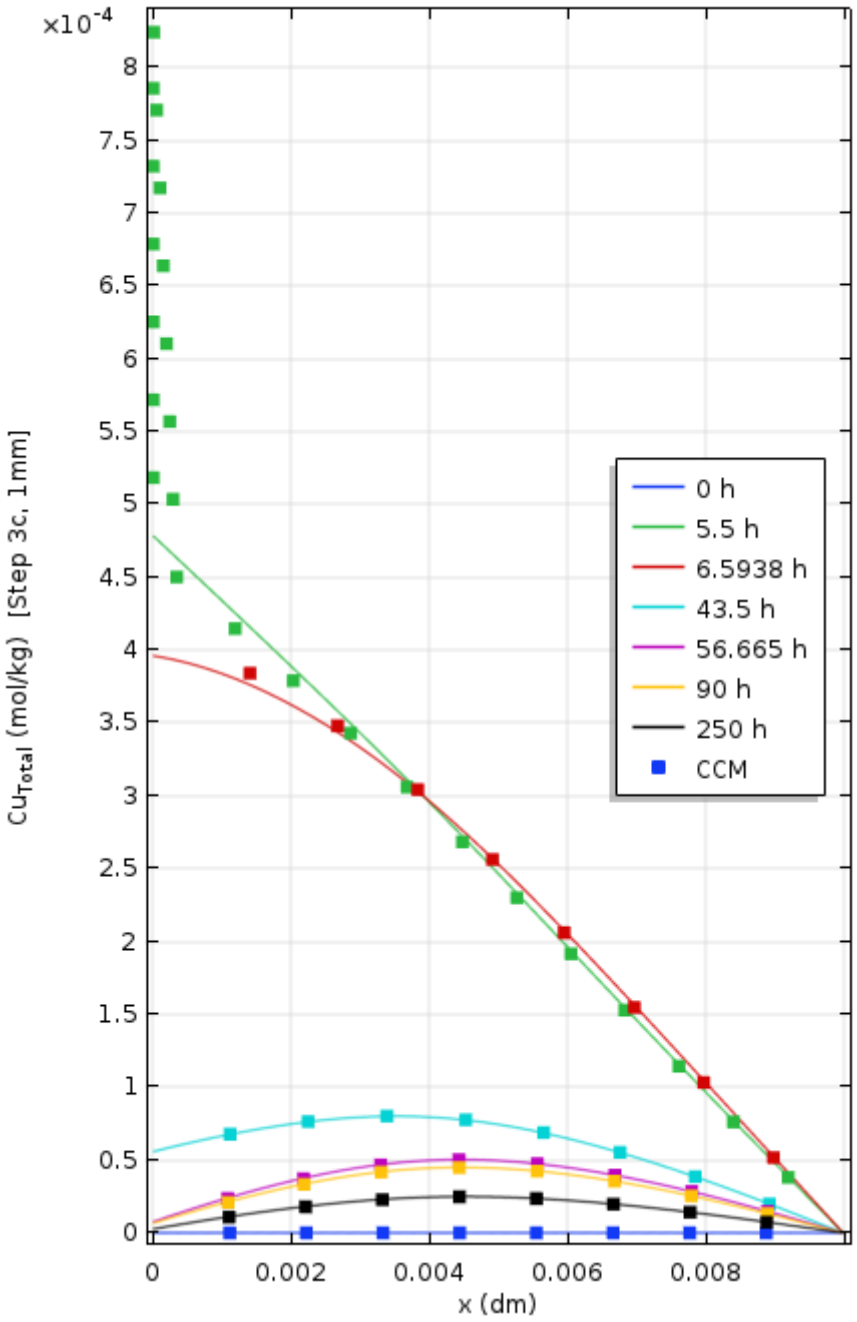

Figure B21: Concentration profile of total amount of copper ($CuCl_2^-$, Cu^{2+}, Cu_2O, $CuCl_2.3Cu(OH)_2$) with distance for 1 mm, Step 3c

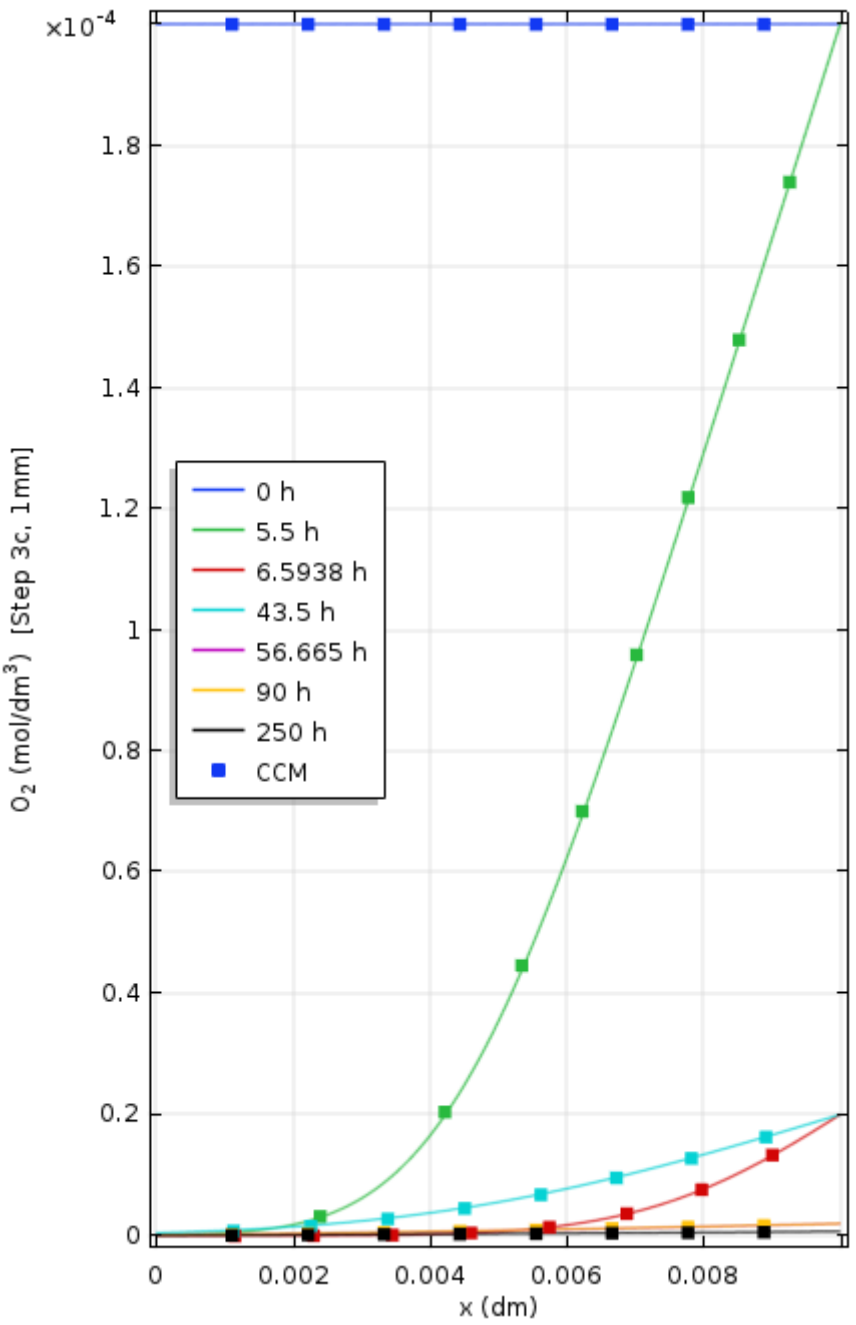

Figure B22: Concentration profile of oxygen with distance for 1 mm, Step 3c

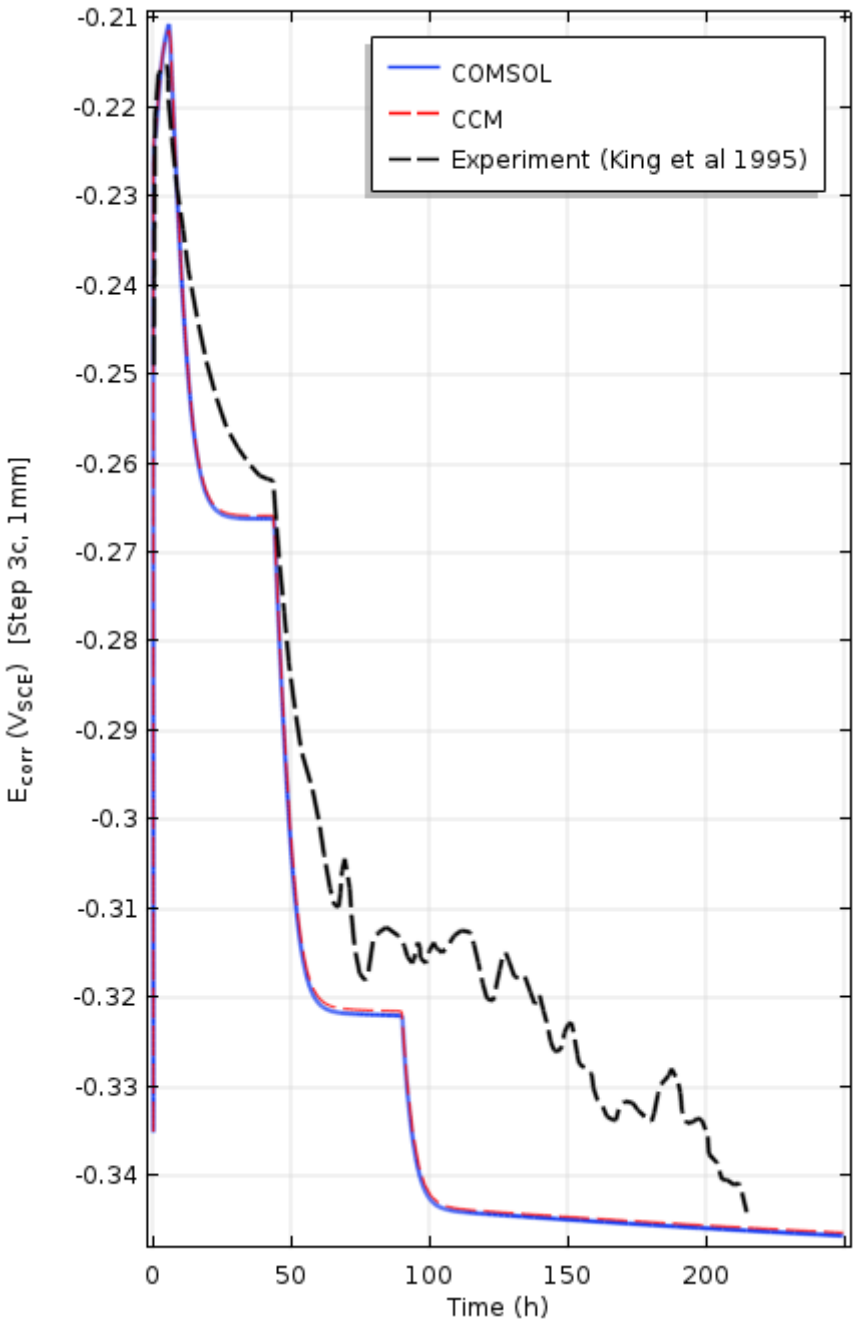

Figure B23: Variation of corrosion potential with time for 1 mm bentonite thickness with changing oxygen concentration for Step 3c

B3. 10 mm bentonite thickness

Similar to 1 mm layer (Section 0), 10 mm profiles of COMSOL are compared to that of CCM outputs.

Figure B24 to Figure B29 show the initial transient state (**Step 2**).

Figure B30 to Figure B36 indicate **Step 3a** outputs comparison

Figure B37 to Figure B44 show the outputs obtained for **Step 3b**

Figure B45 to Figure B52 indicate comparison of outputs obtained for **Step 3c**

Step 3d comparisons are included in Chapter 4

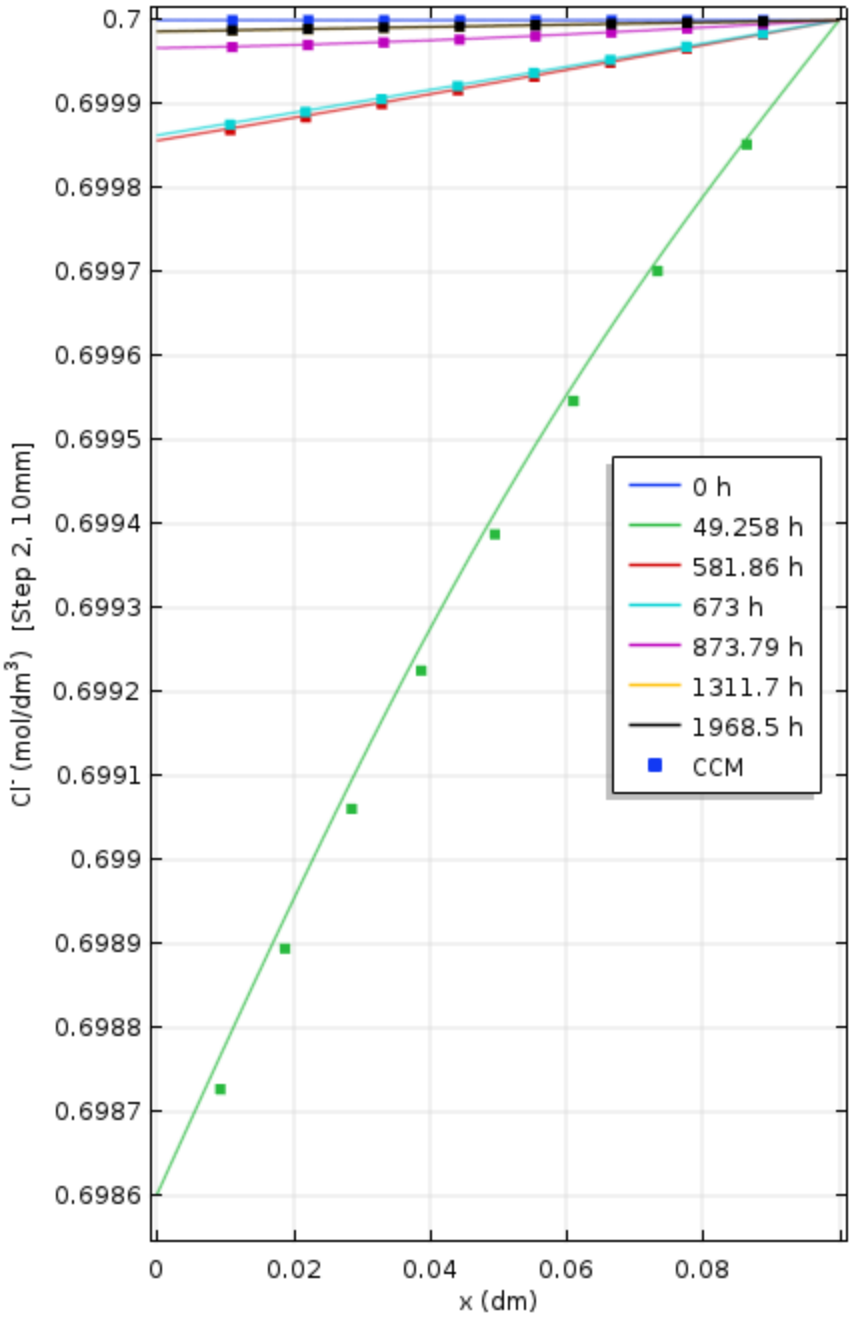

Figure B24: Concentration profile of chloride with distance for 10 mm, Step 2

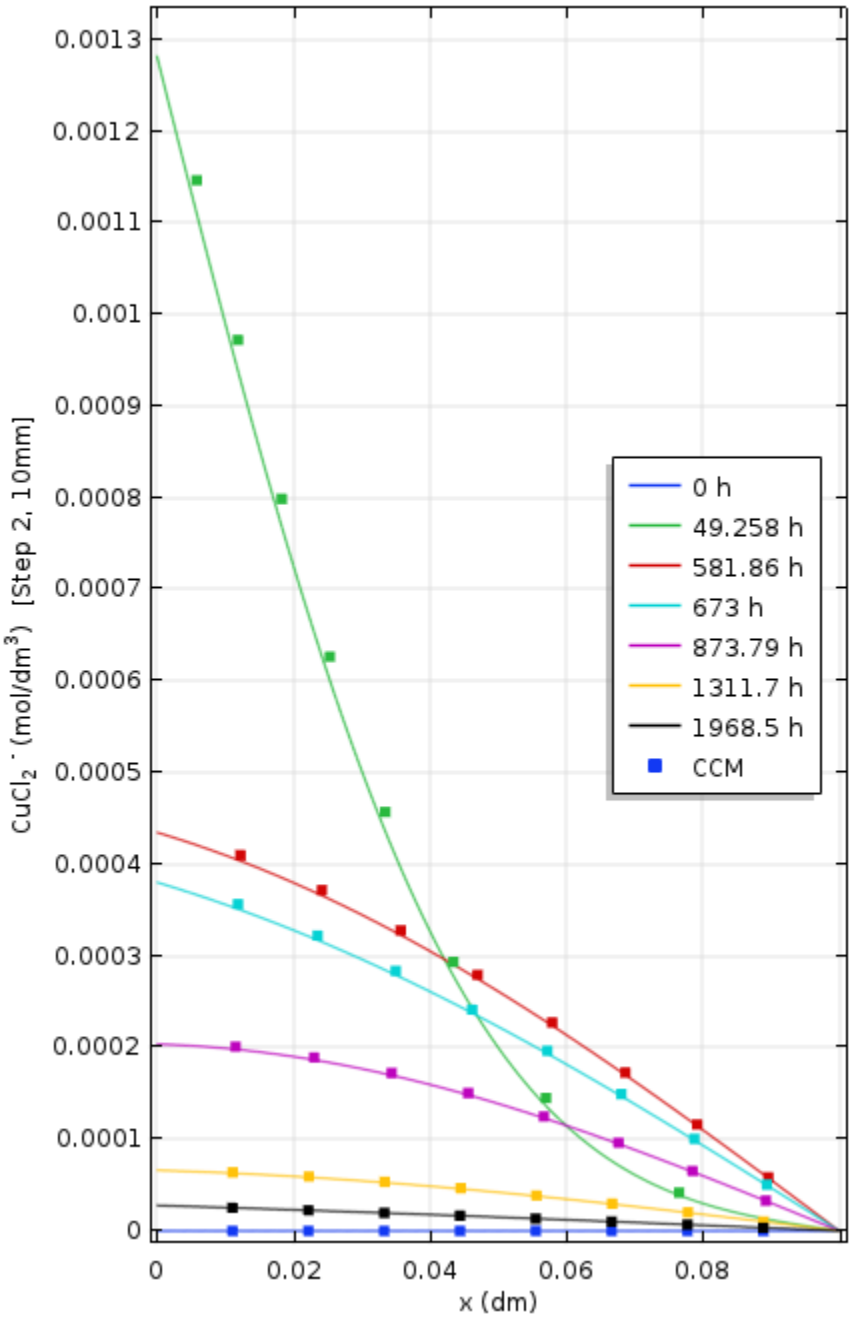

Figure B25: Concentration profile of copper chloride ions with distance for 10 mm, Step 2

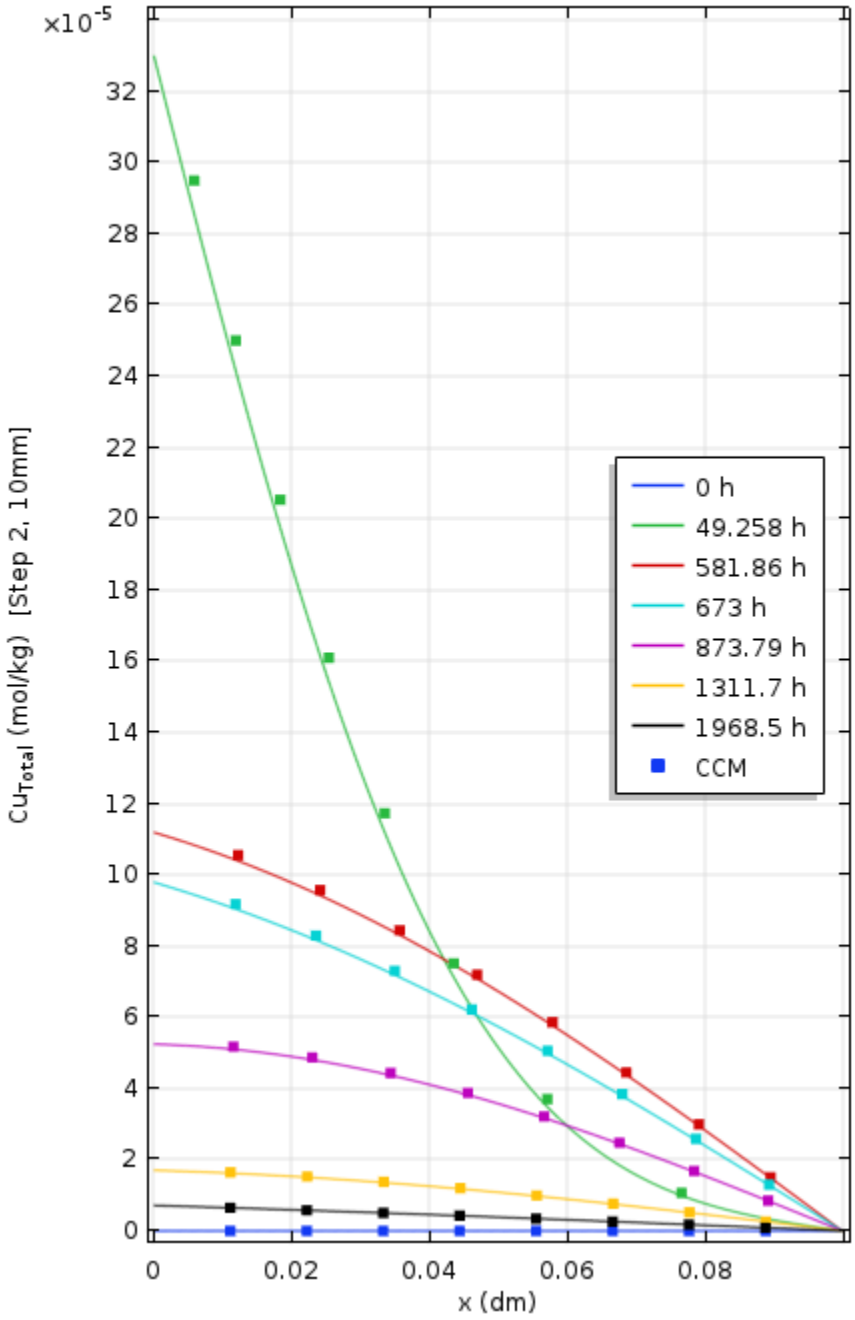

Figure B26: Concentration profile of total amount of copper ($CuCl_2^-$, Cu^{2+}, Cu_2O, $CuCl_2.3Cu(OH)_2$) with distance for 10 mm, Step 2

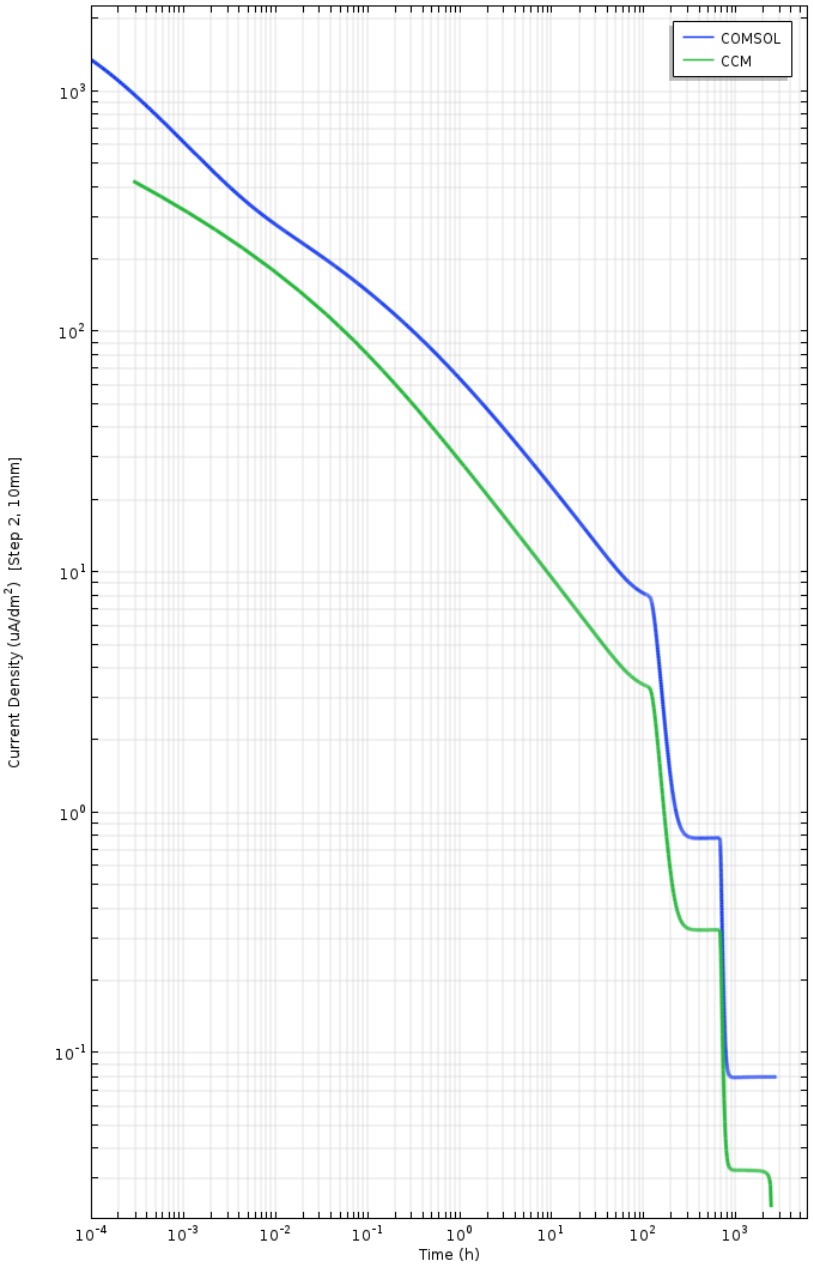

Figure B27: Current density profile over time for 10 mm bentonite thickness, Step 2

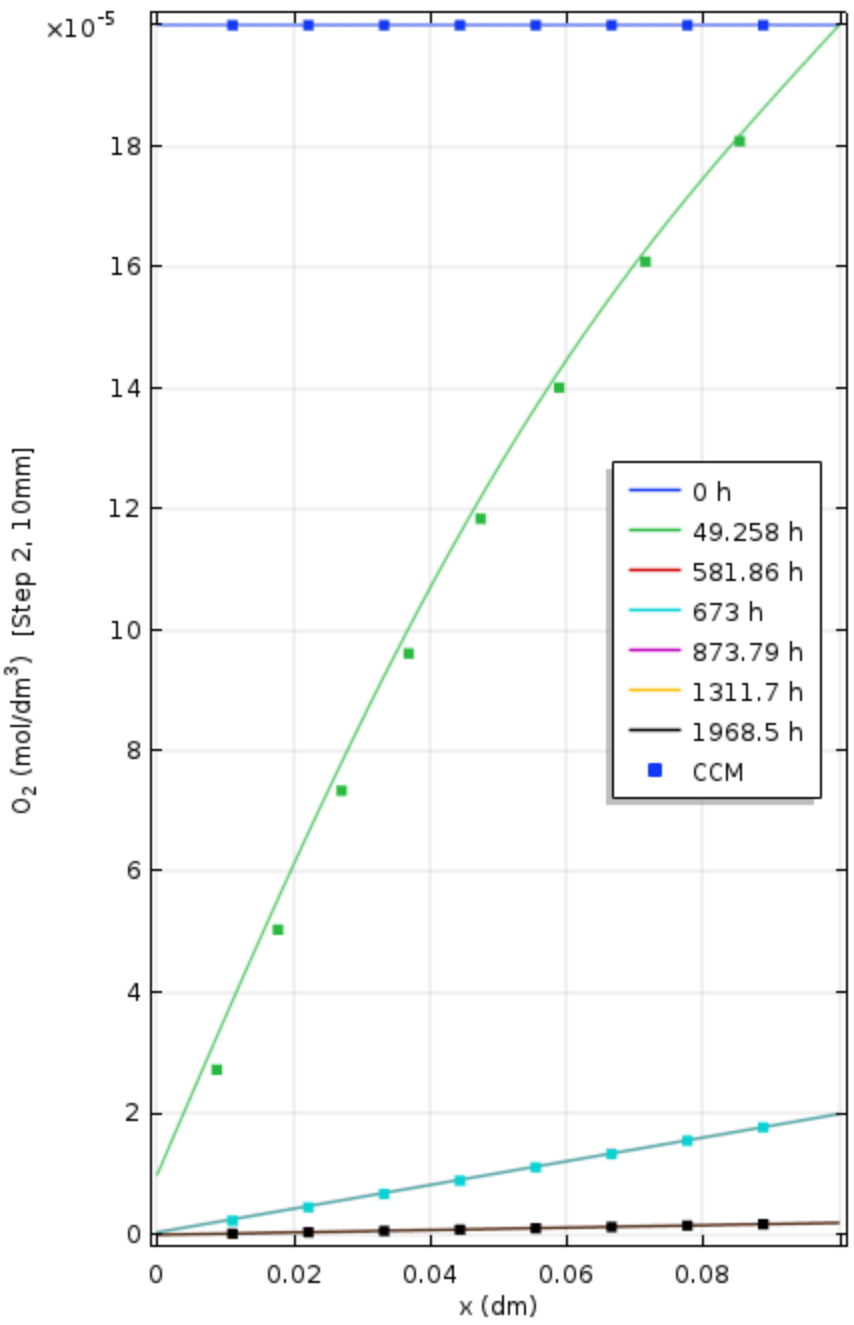

Figure B28: Concentration profile of oxygen with distance for 10 mm, Step 2

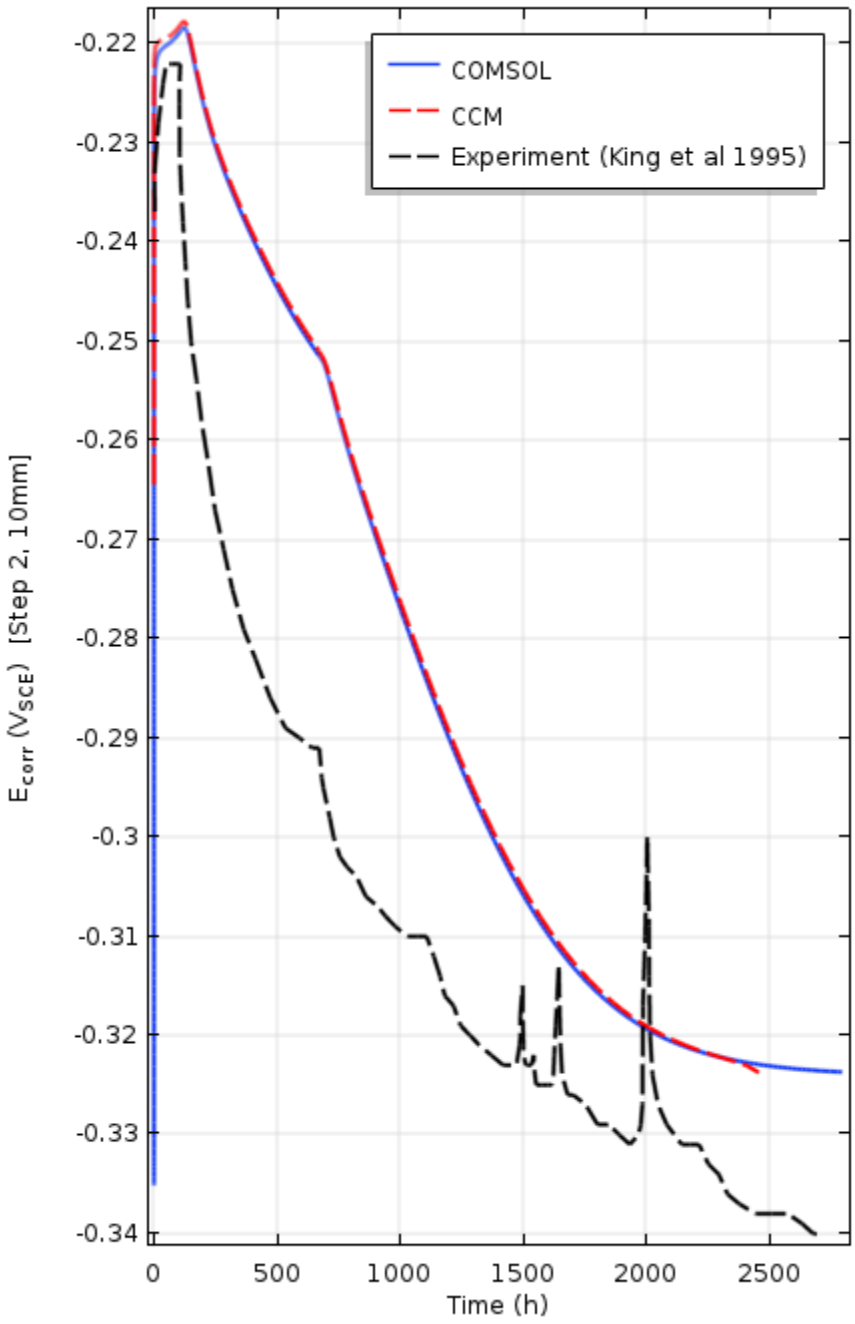

Figure B29: Variation of corrosion potential with time for 10 mm bentonite thickness with changing oxygen concentration for Step 2

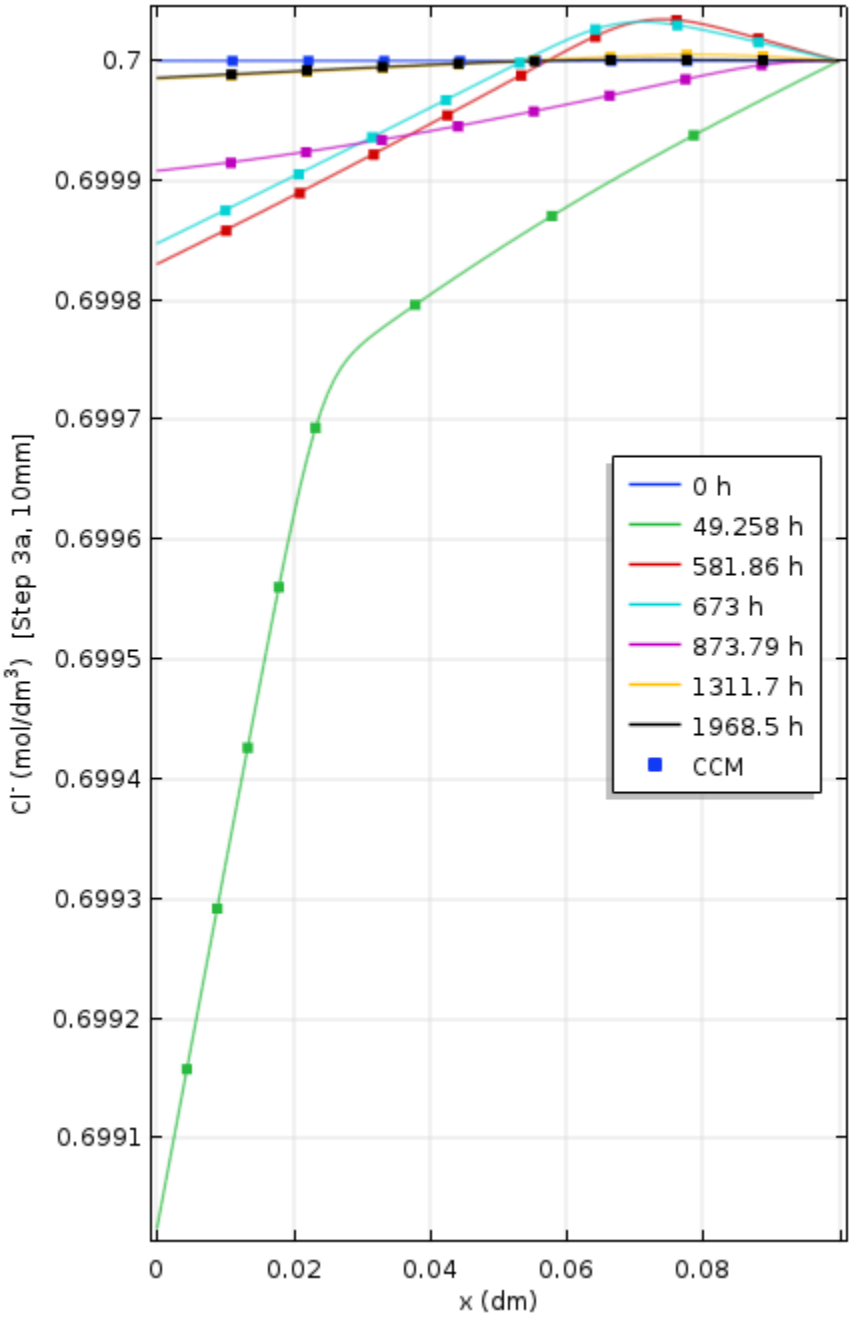

Figure B30: Concentration profile of chloride ions with distance for 10 mm, Step 3a

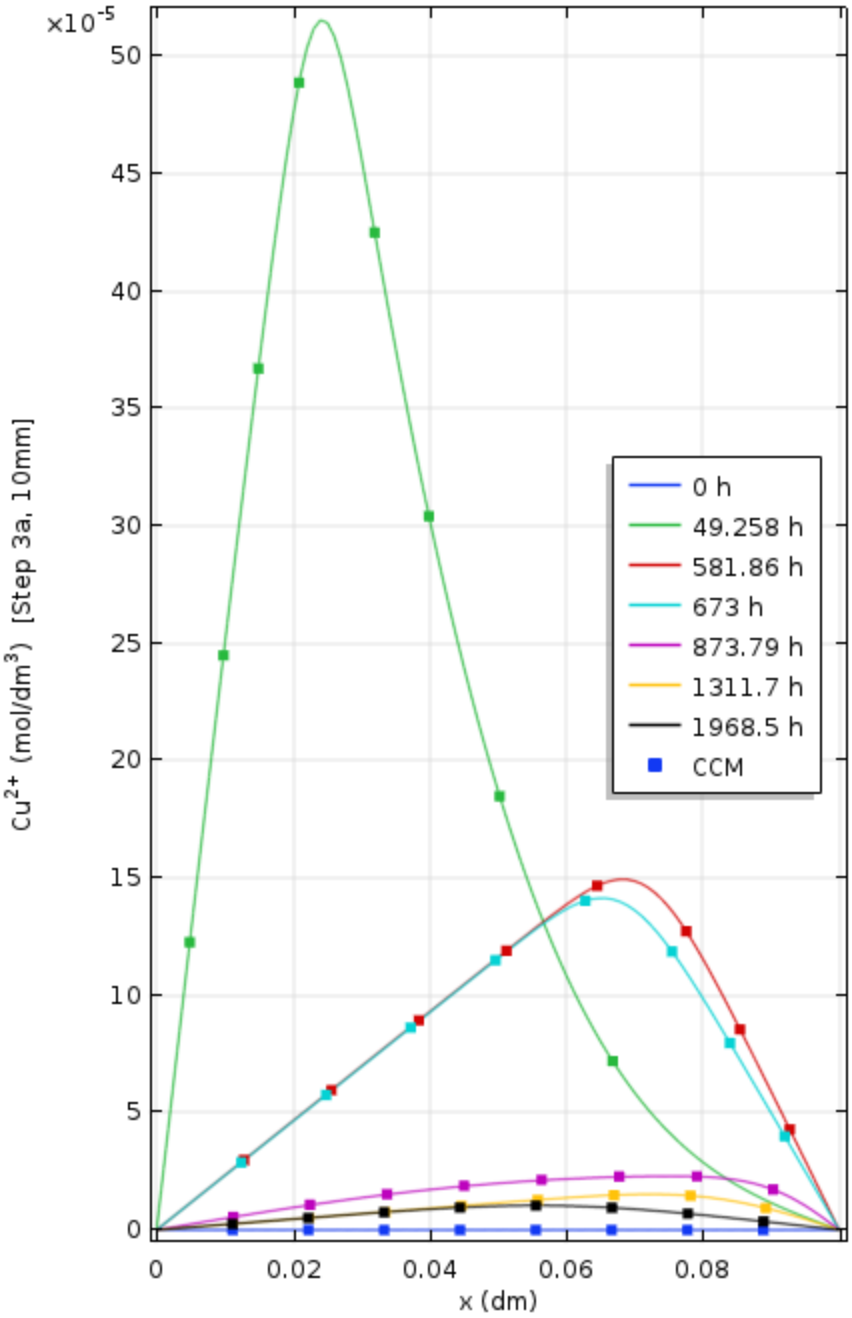

Figure B31: Concentration profile of copper ions with distance for 10 mm, Step 3a

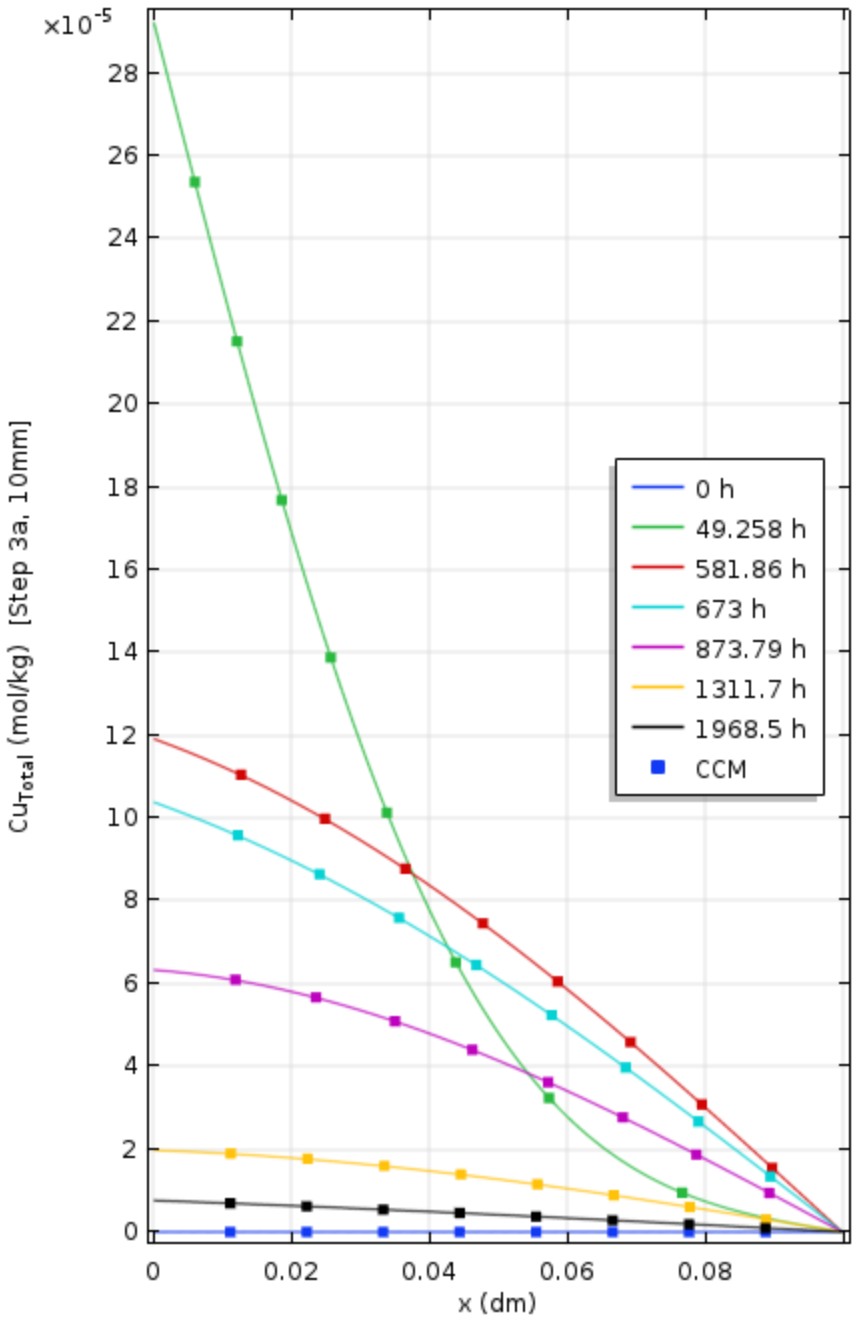

Figure B32: Concentration profile of total amount of copper ($CuCl_2^-$, Cu^{2+}, Cu_2O, $CuCl_2.3Cu(OH)_2$) with distance for 10 mm, Step 3a

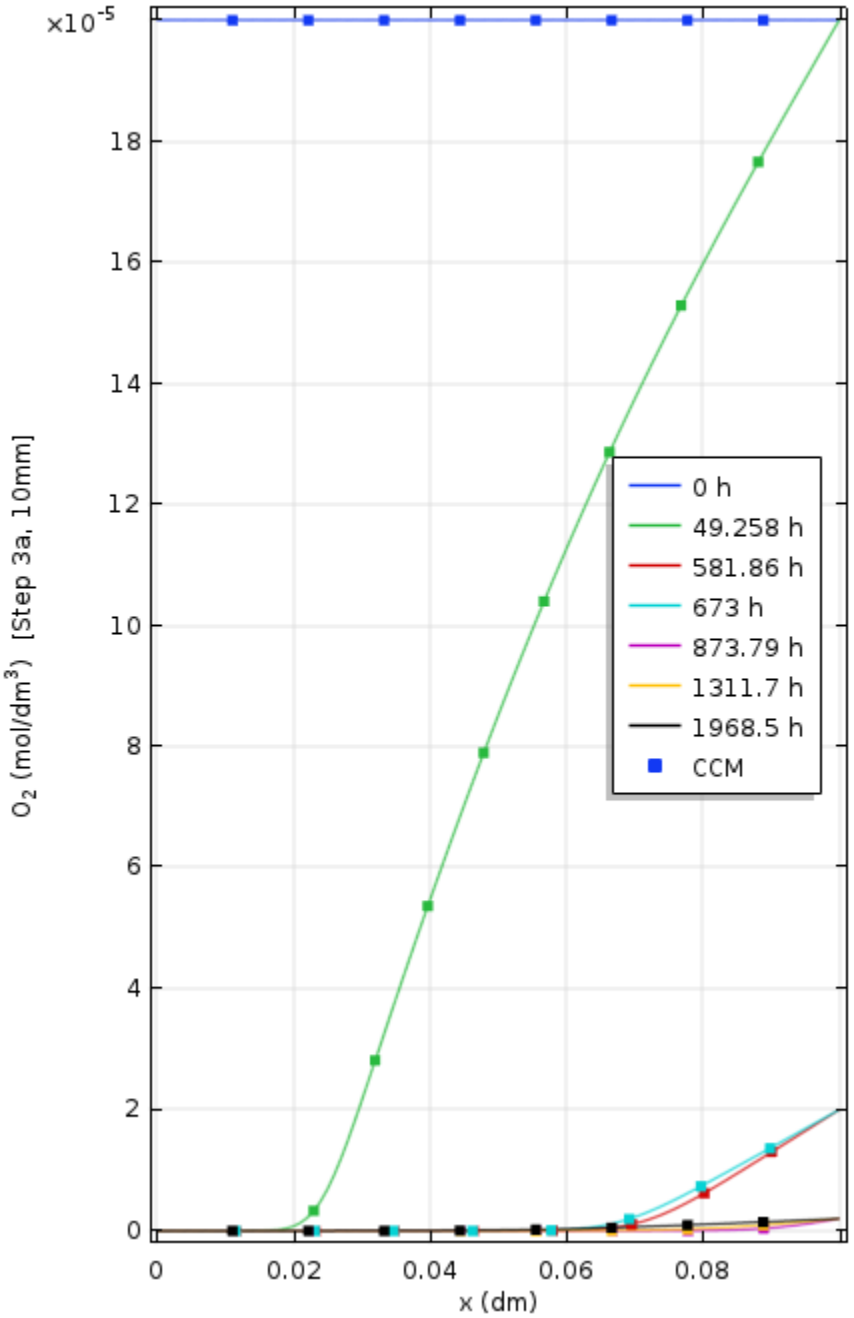

Figure B33: Concentration profile of oxygen with distance for 10 mm, Step 3a

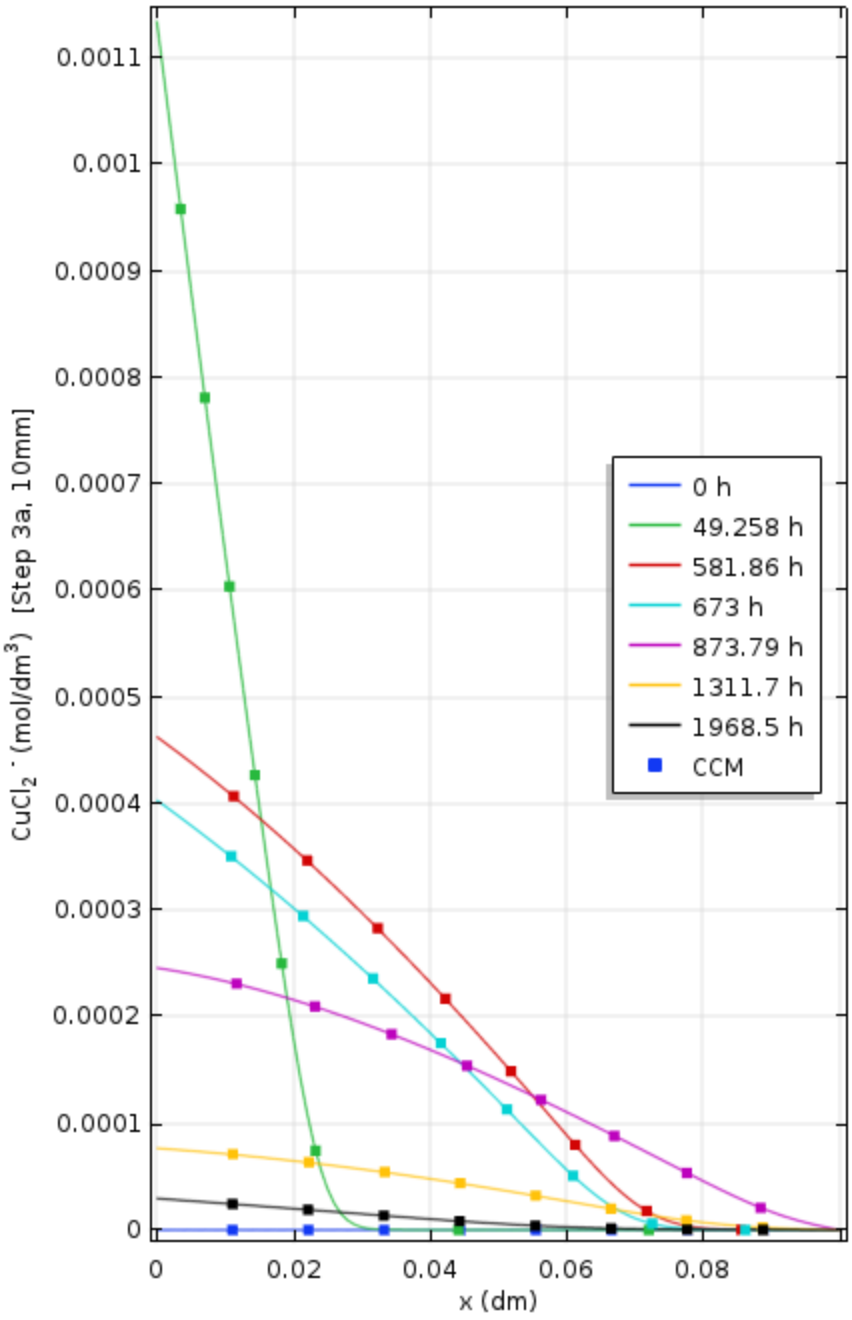

Figure B34: Concentration profile of copper chloride ions with distance for 10 mm, Step 3a

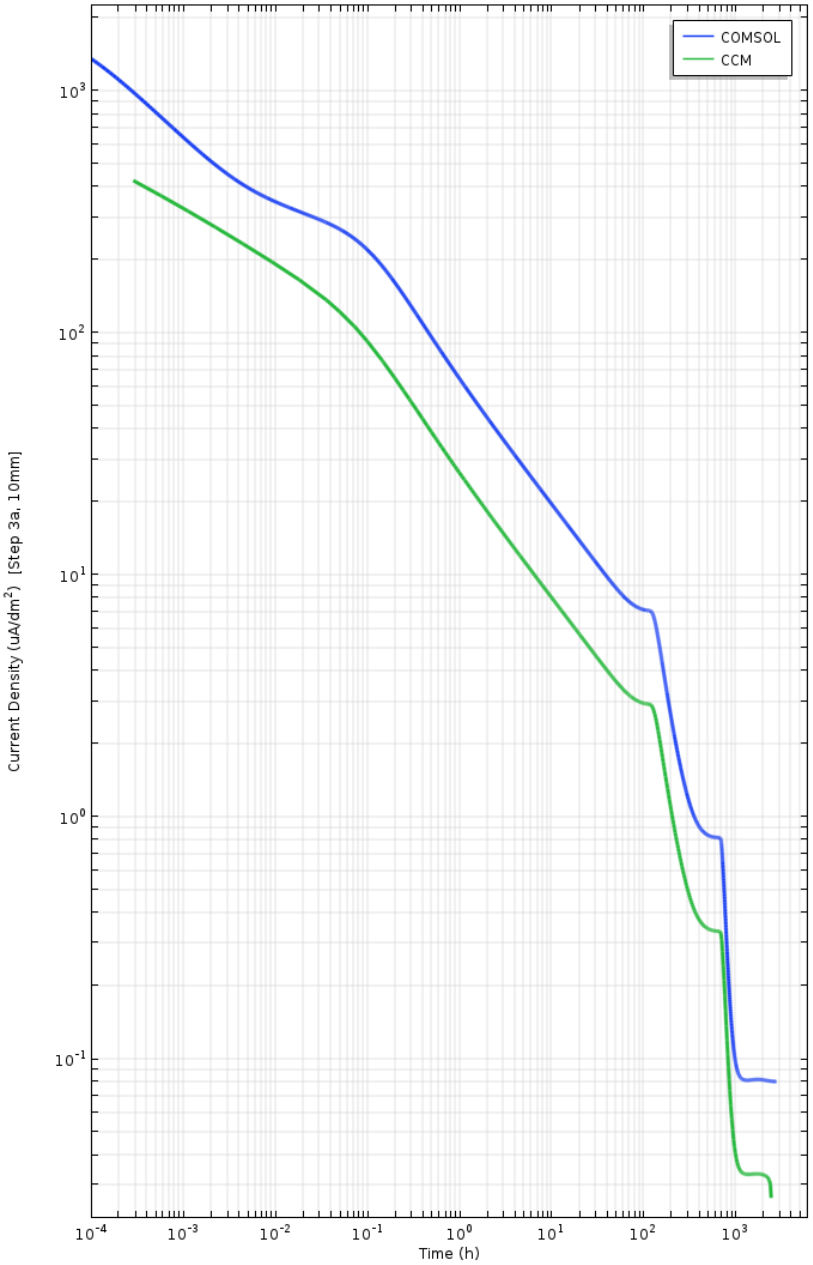

Figure B35: Current density profile over time for 10 mm bentonite thickness, Step 3a

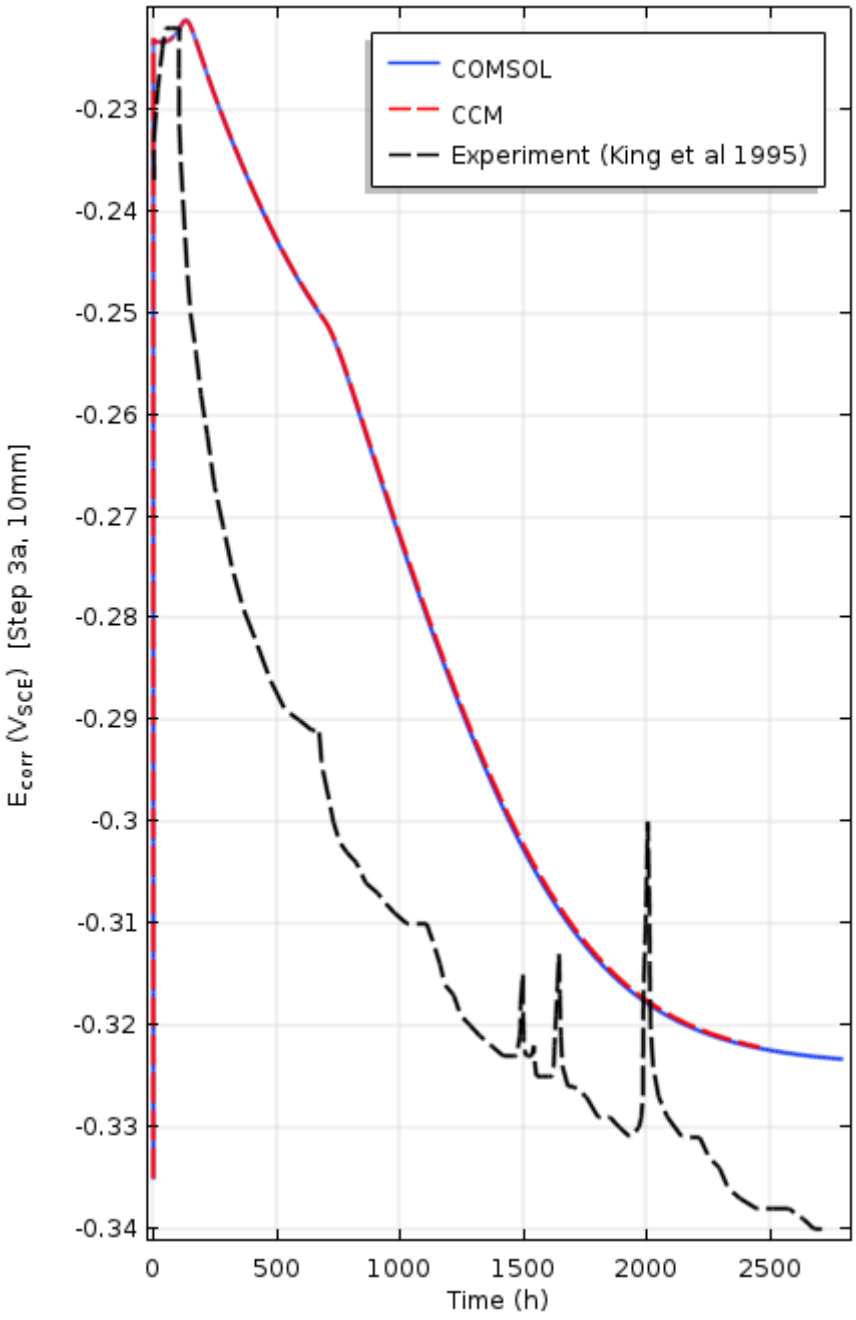

Figure B36: Variation of corrosion potential with time for 10 mm bentonite thickness with changing oxygen concentration for Step 3a

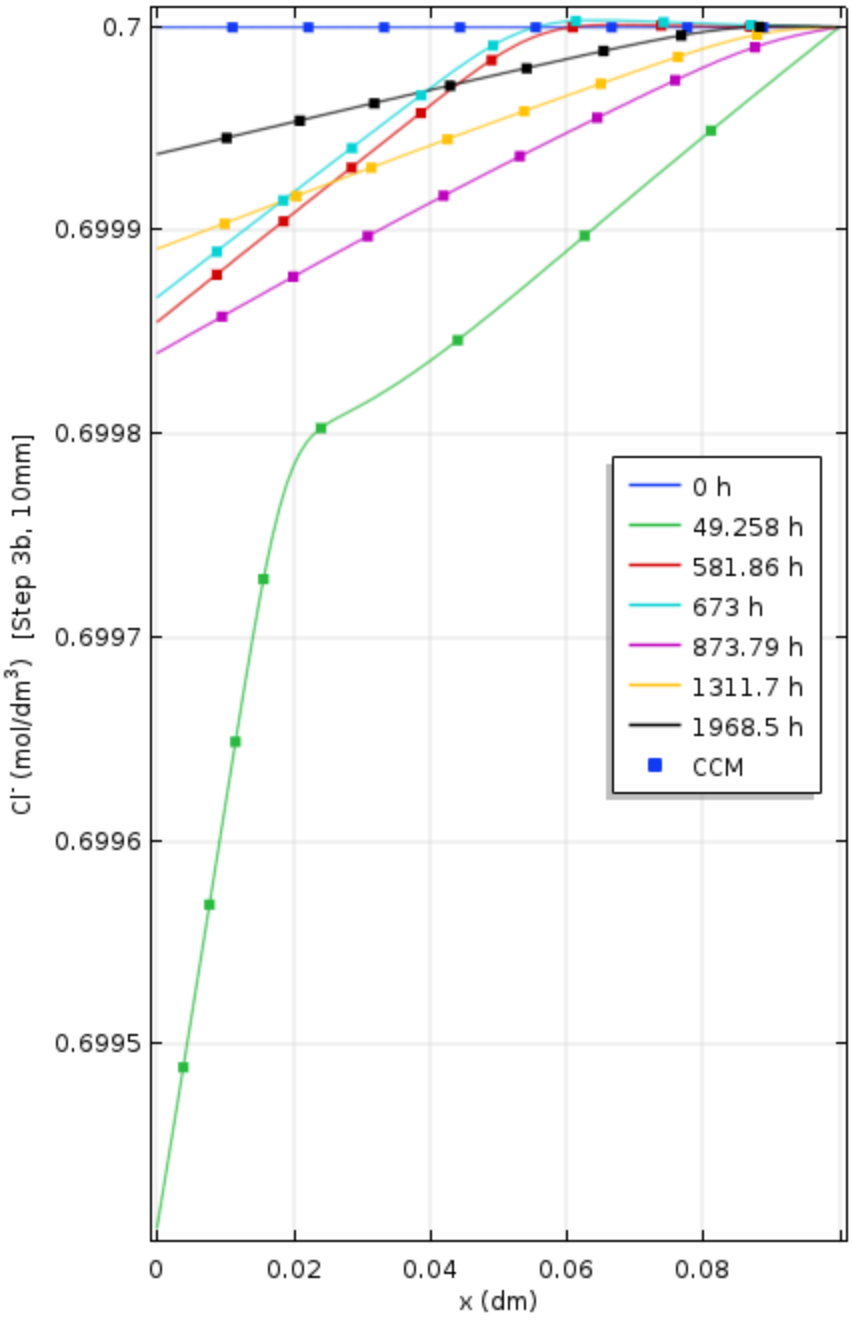

Figure B37: Concentration profile of chloride ions with distance for 10 mm, Step 3b

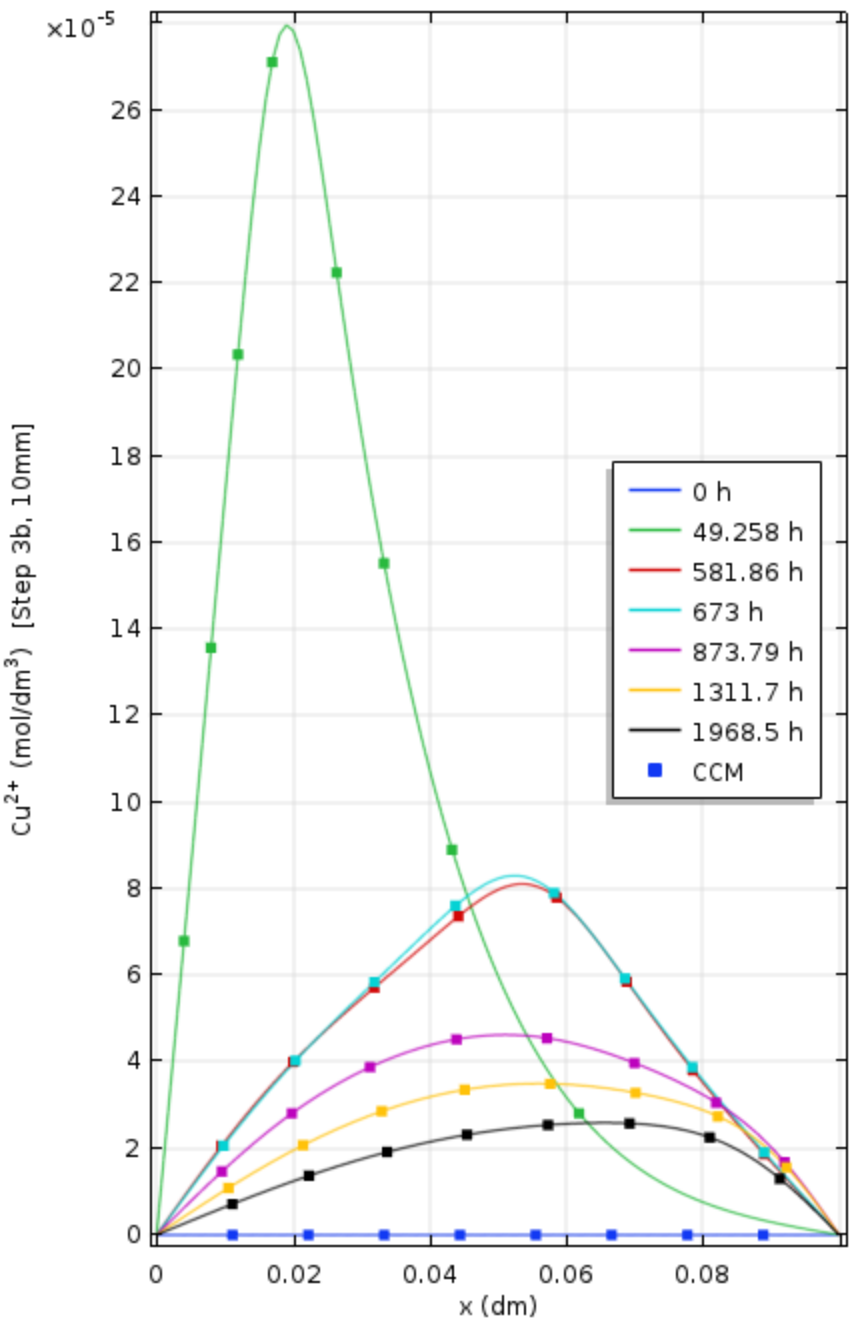

Figure B38: Concentration profile of copper ions with distance for 10 mm, Step 3b

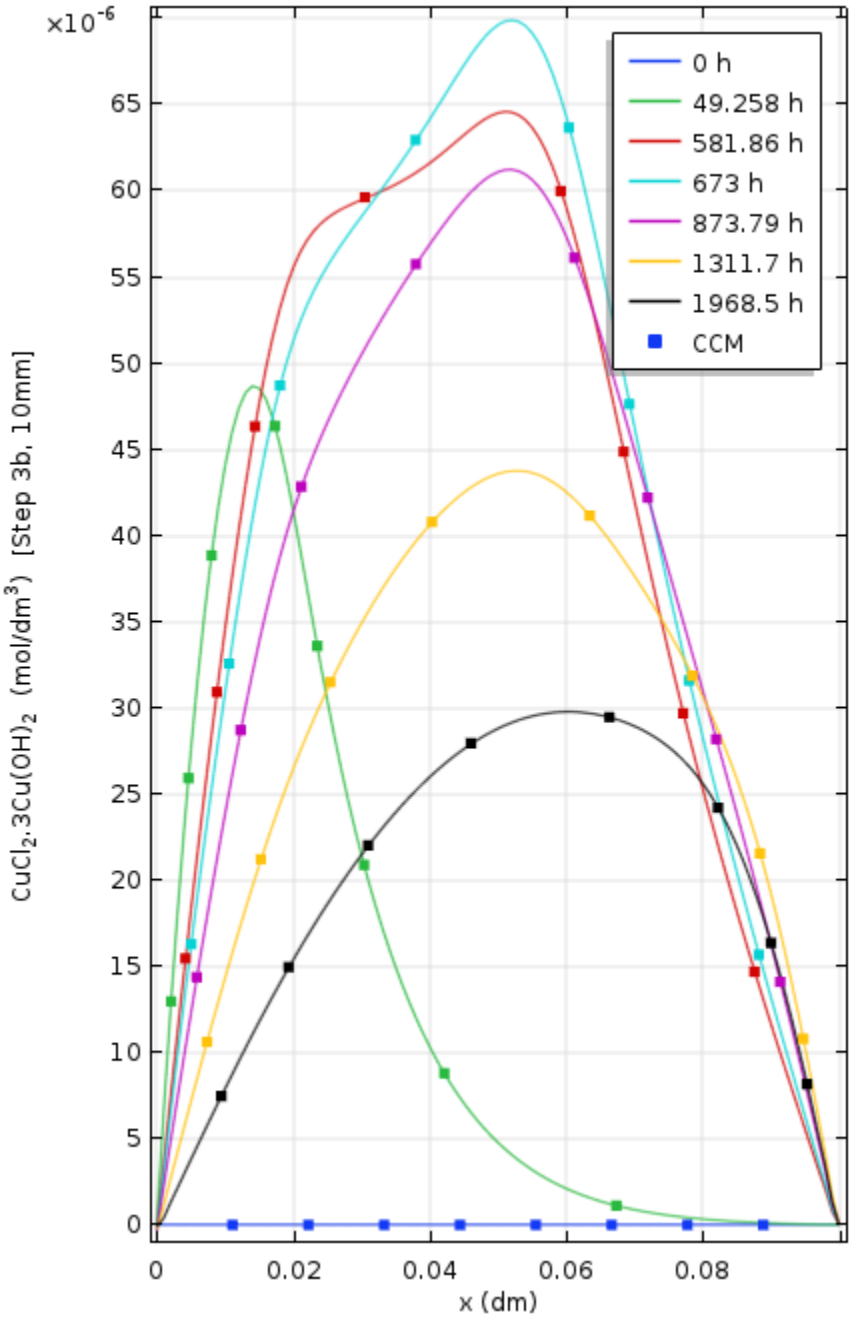

Figure B39: Concentration profile of paratacamite with distance for 10 mm, Step 3b

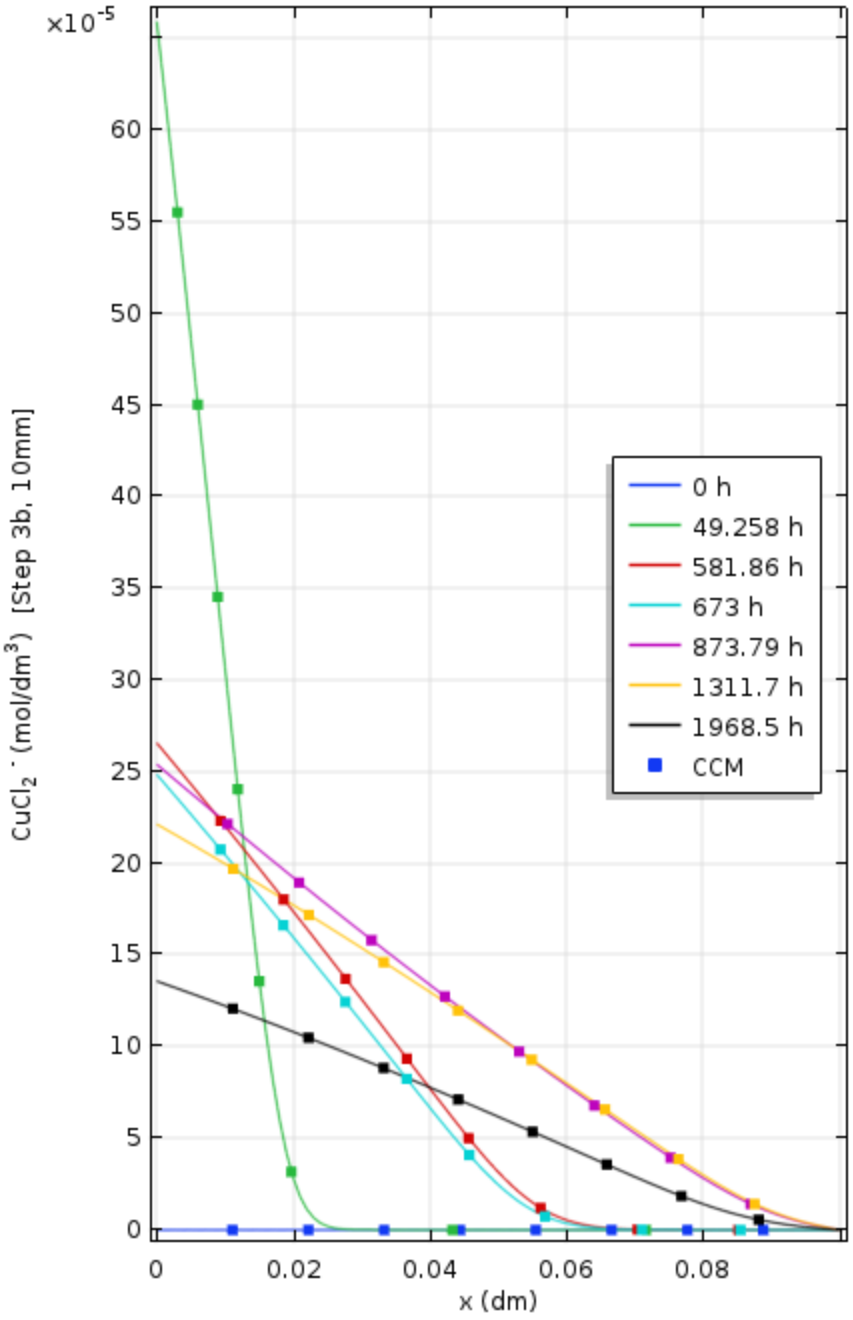

Figure B40: Concentration profile of copper chloride ions with distance for 10 mm, Step 3b

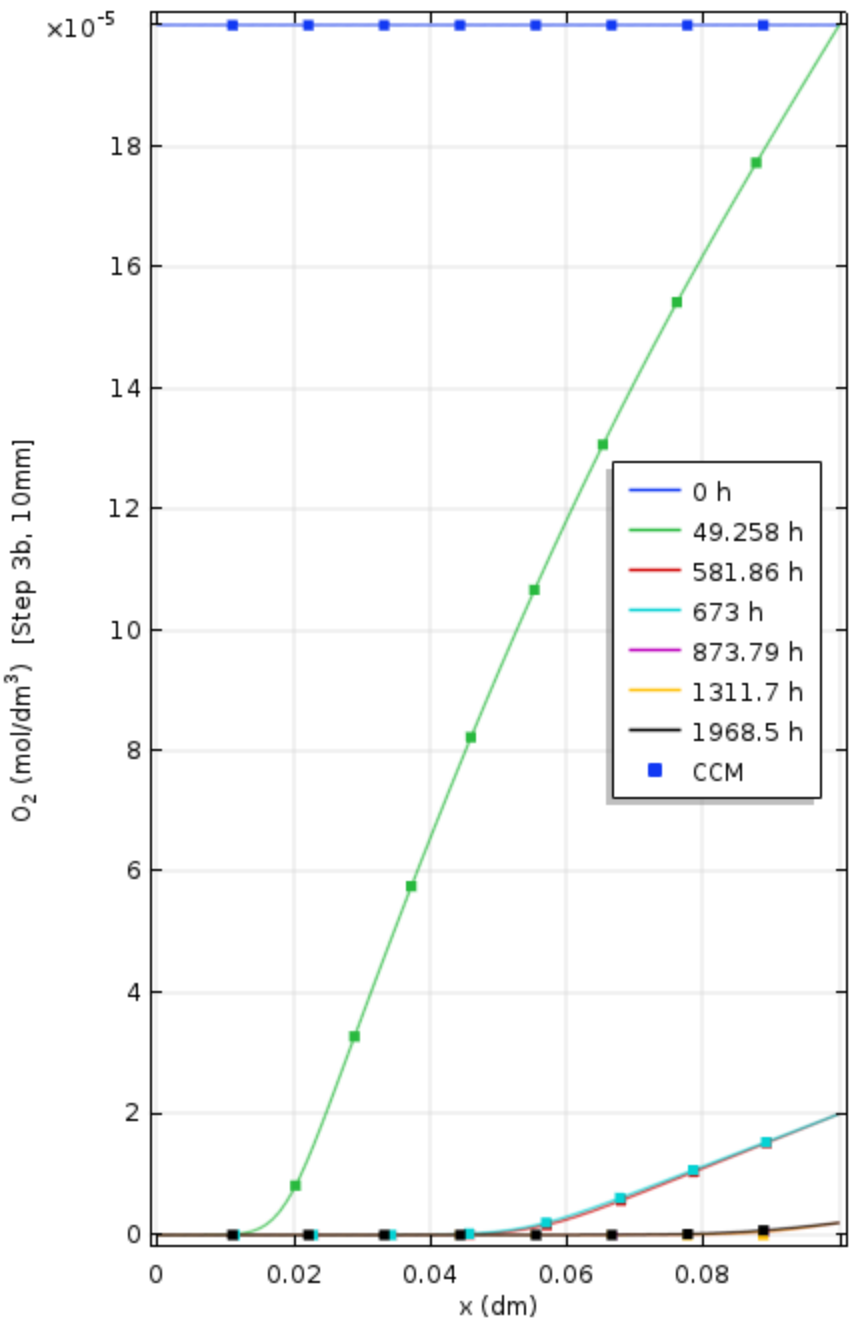

Figure B41: Concentration profile of oxygen with distance for 10 mm, Step 3b

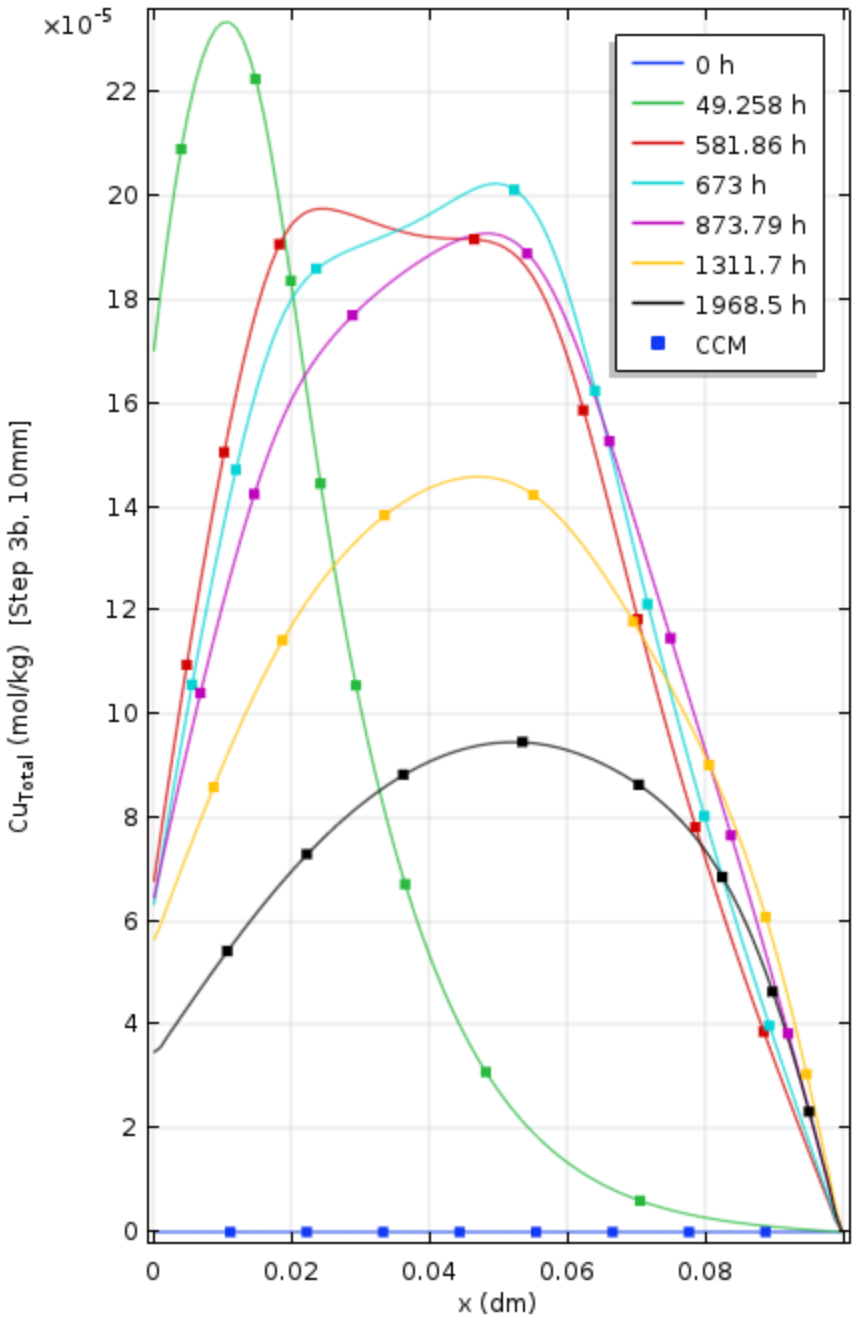

Figure B42: Concentration profile of total amount of copper ($CuCl_2^-$, Cu^{2+}, Cu_2O, $CuCl_2.3Cu(OH)_2$) with distance for 10 mm, Step 3b

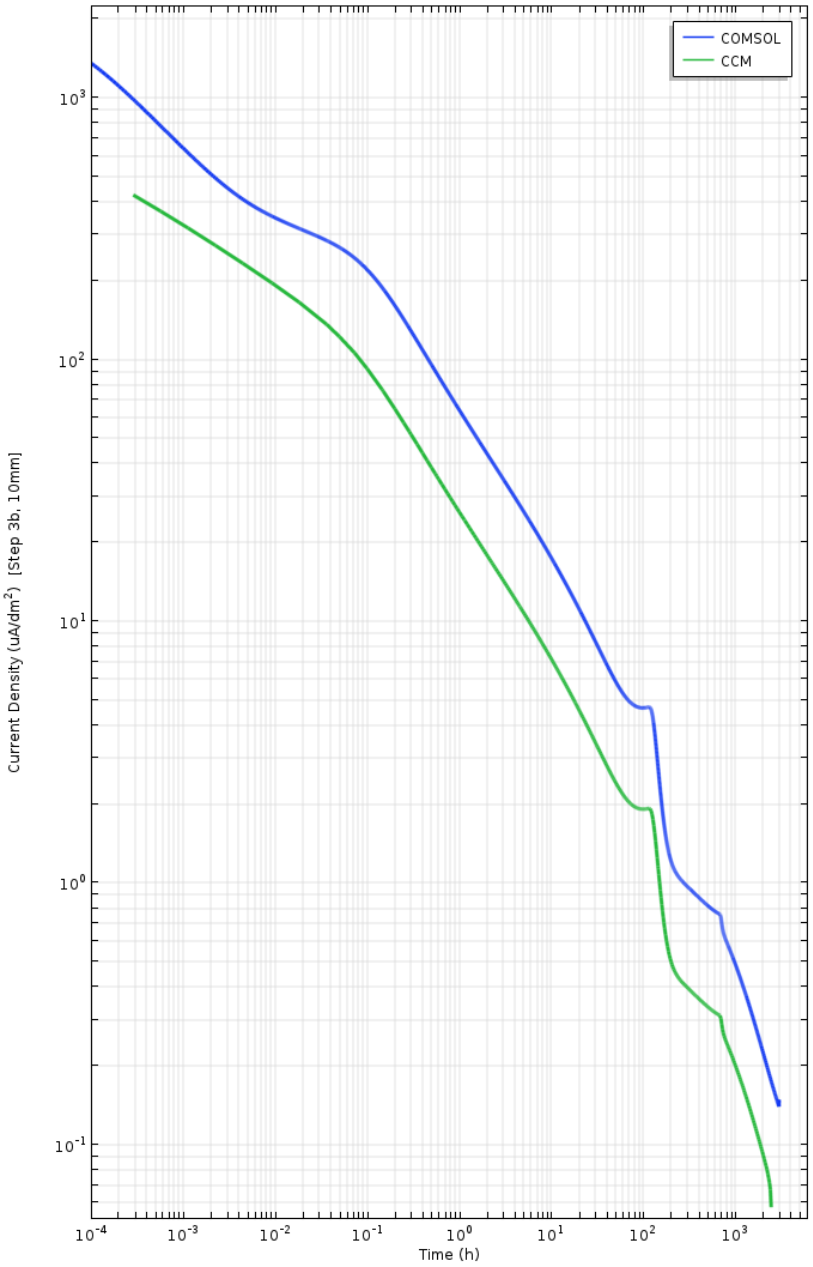

Figure B43: Current density profile over time for 10 mm bentonite thickness, Step 3b

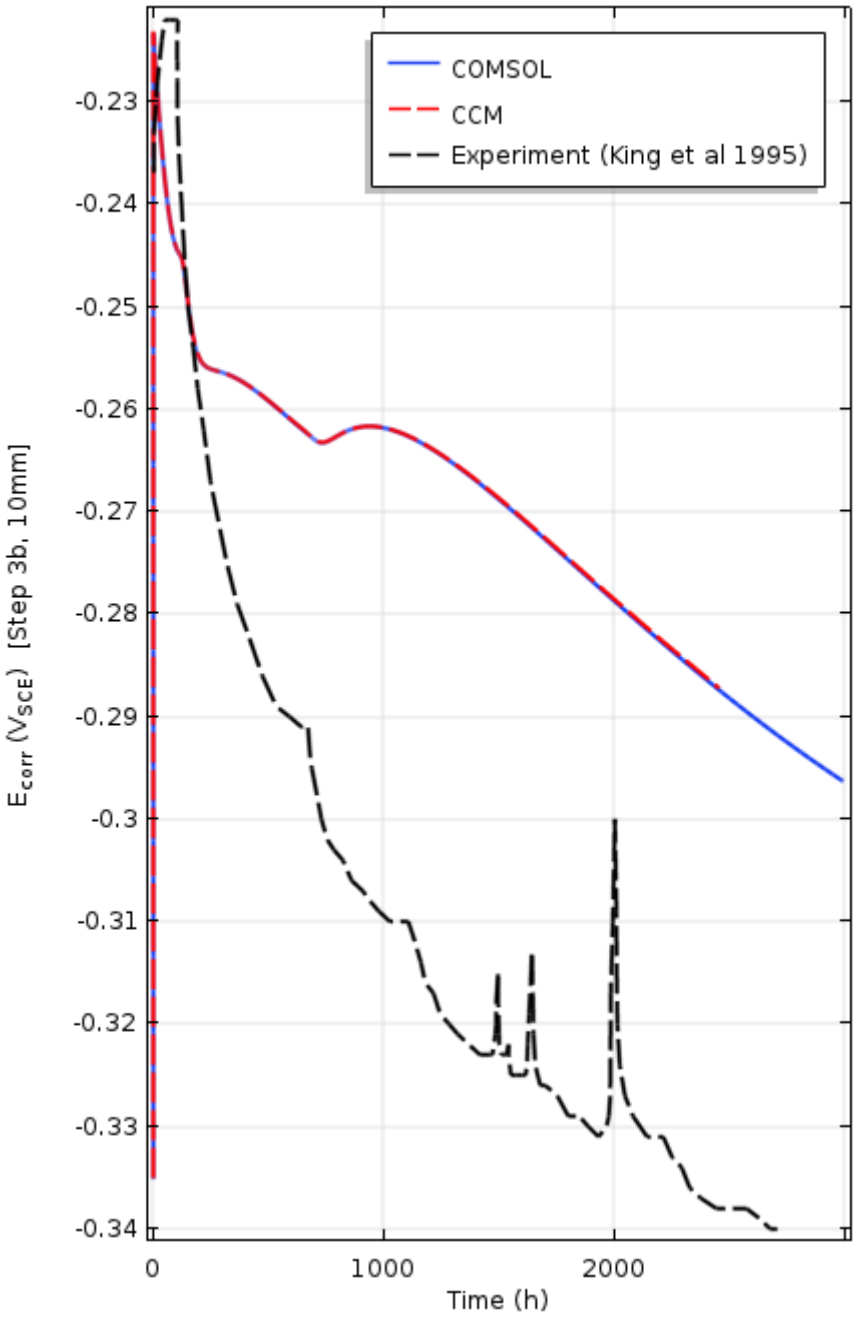

Figure B44: Variation of corrosion potential with time for 10 mm bentonite thickness with changing oxygen concentration for Step 3b

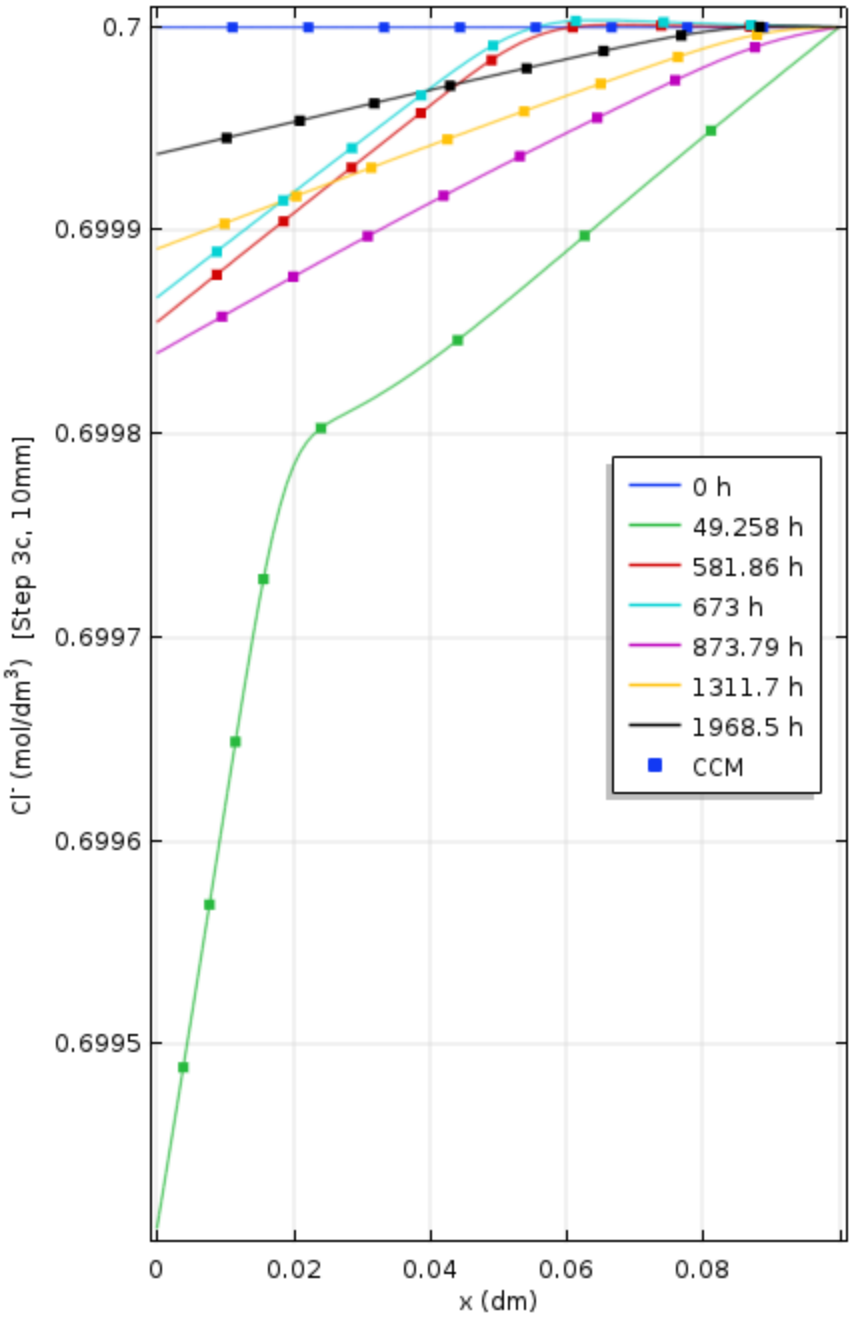

Figure B45: Concentration profile of chloride ions with distance for 10 mm, Step 3c

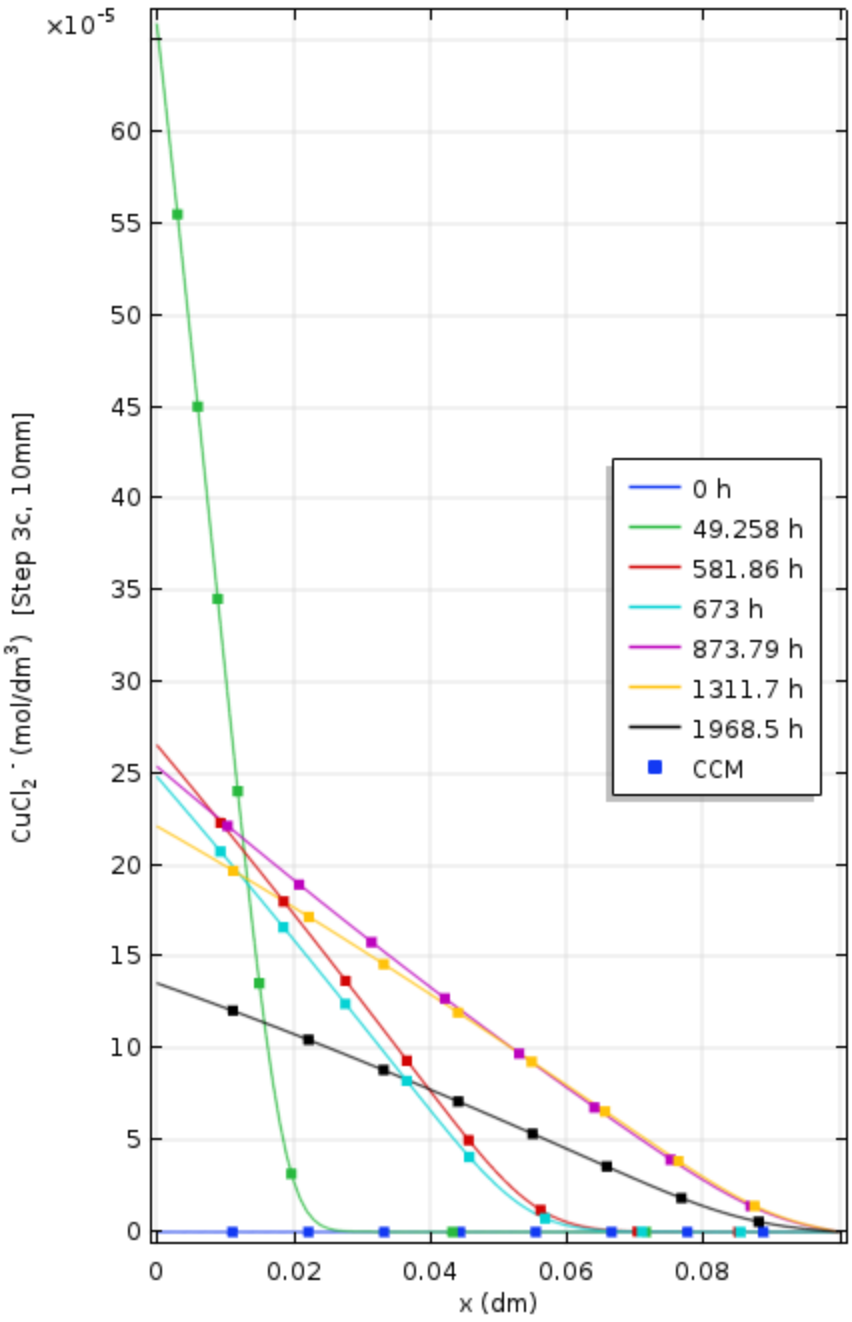

Figure B46: Concentration profile of copper chloride ions with distance for 10 mm, Step 3c

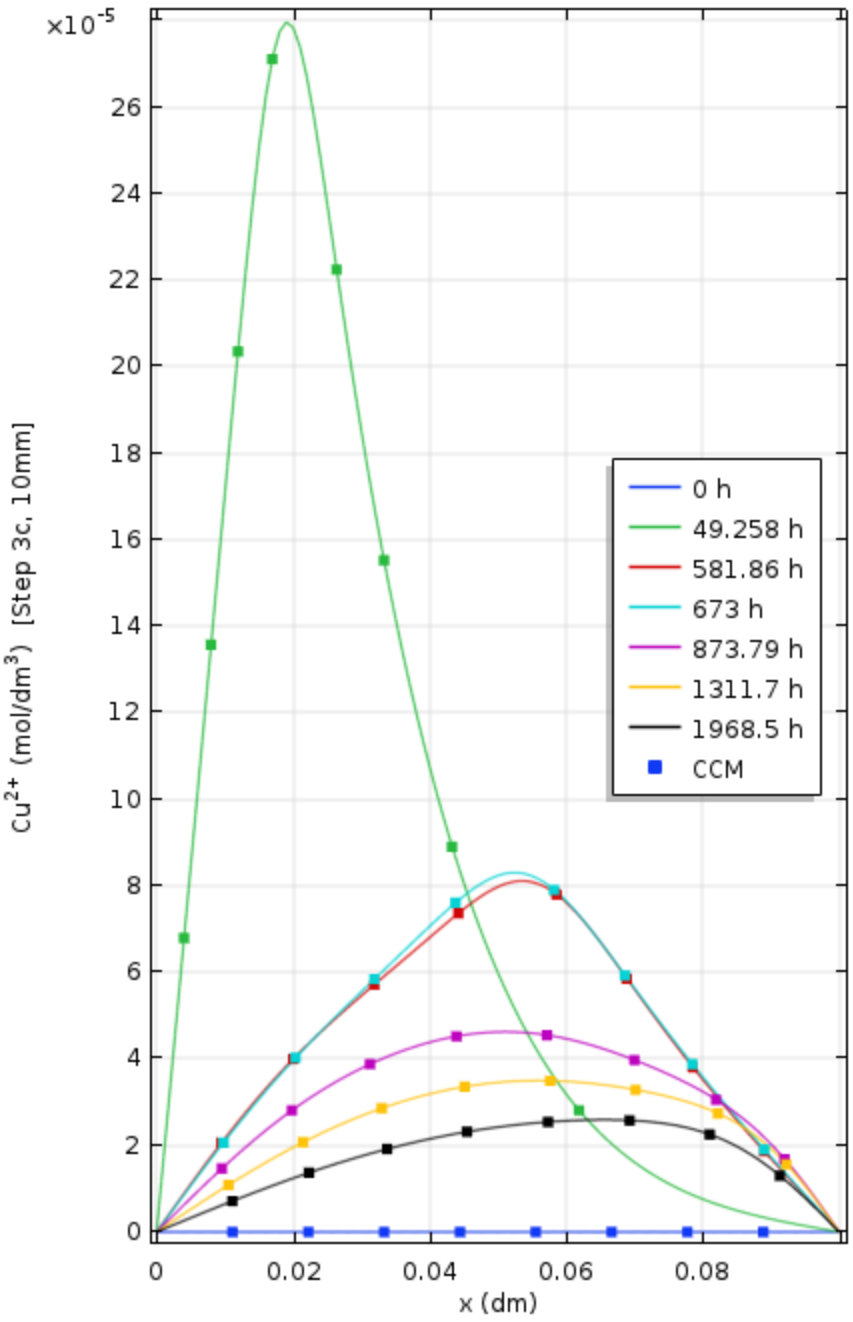

Figure B47: Concentration profile of copper ions with distance for 10 mm, Step 3c

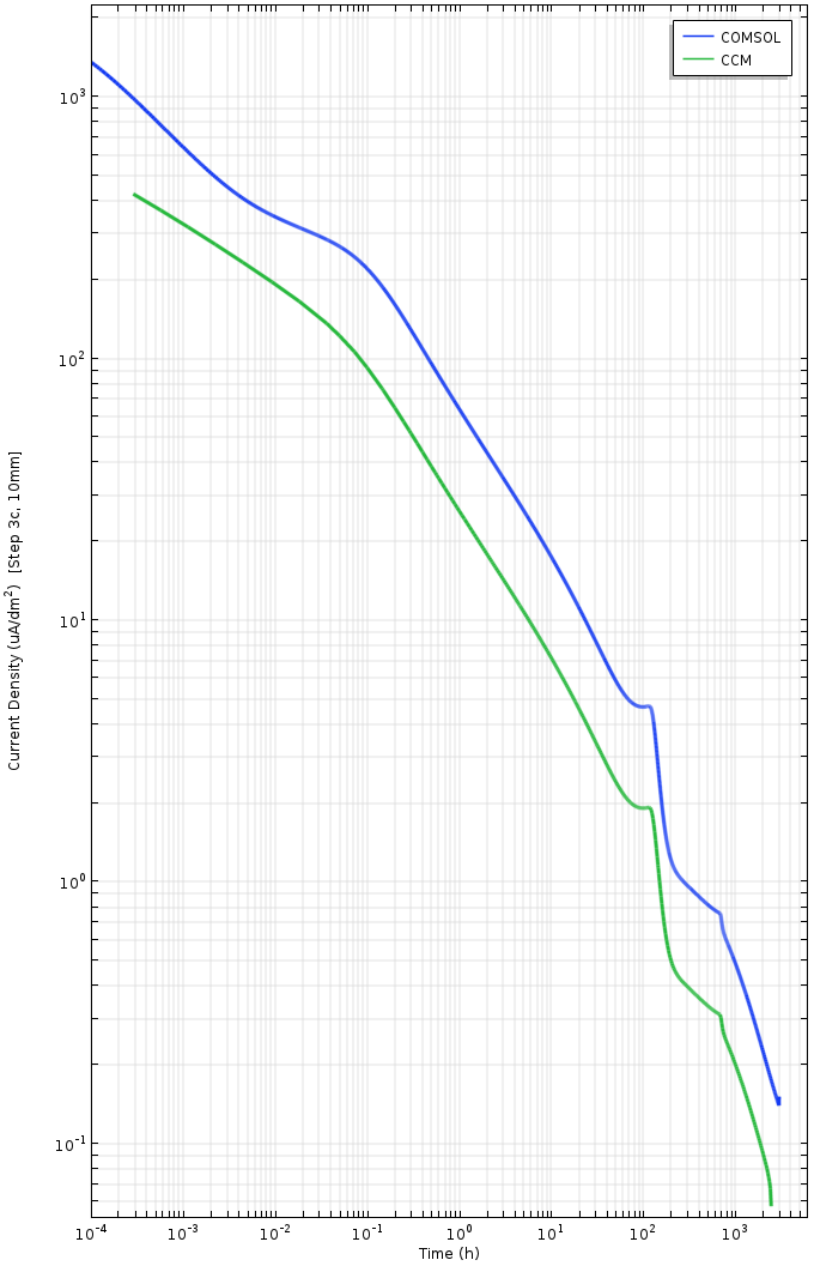

Figure B48: Current density profile over time for 10 mm bentonite thickness, Step 3c

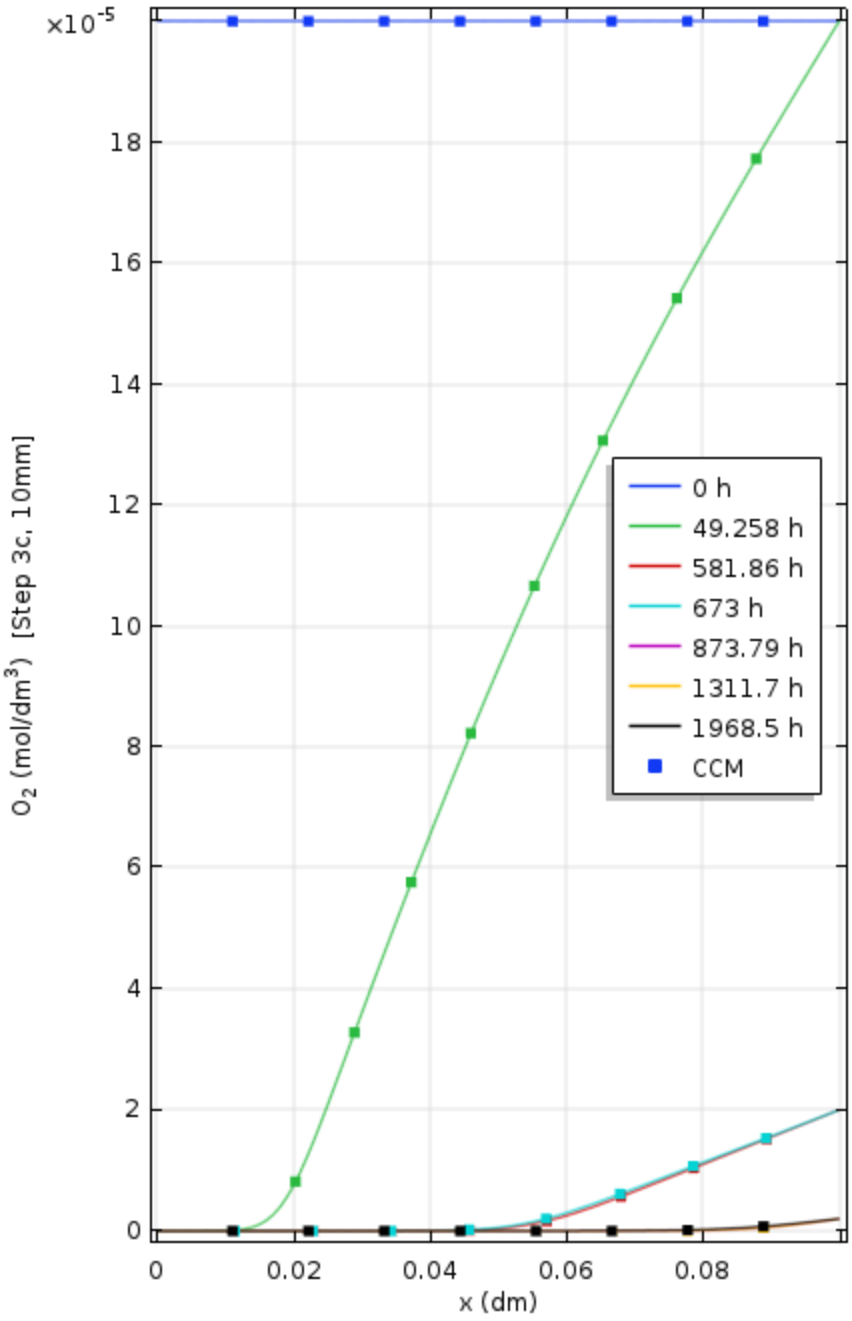

Figure B49: Concentration profile of oxygen with distance for 10 mm, Step 3c

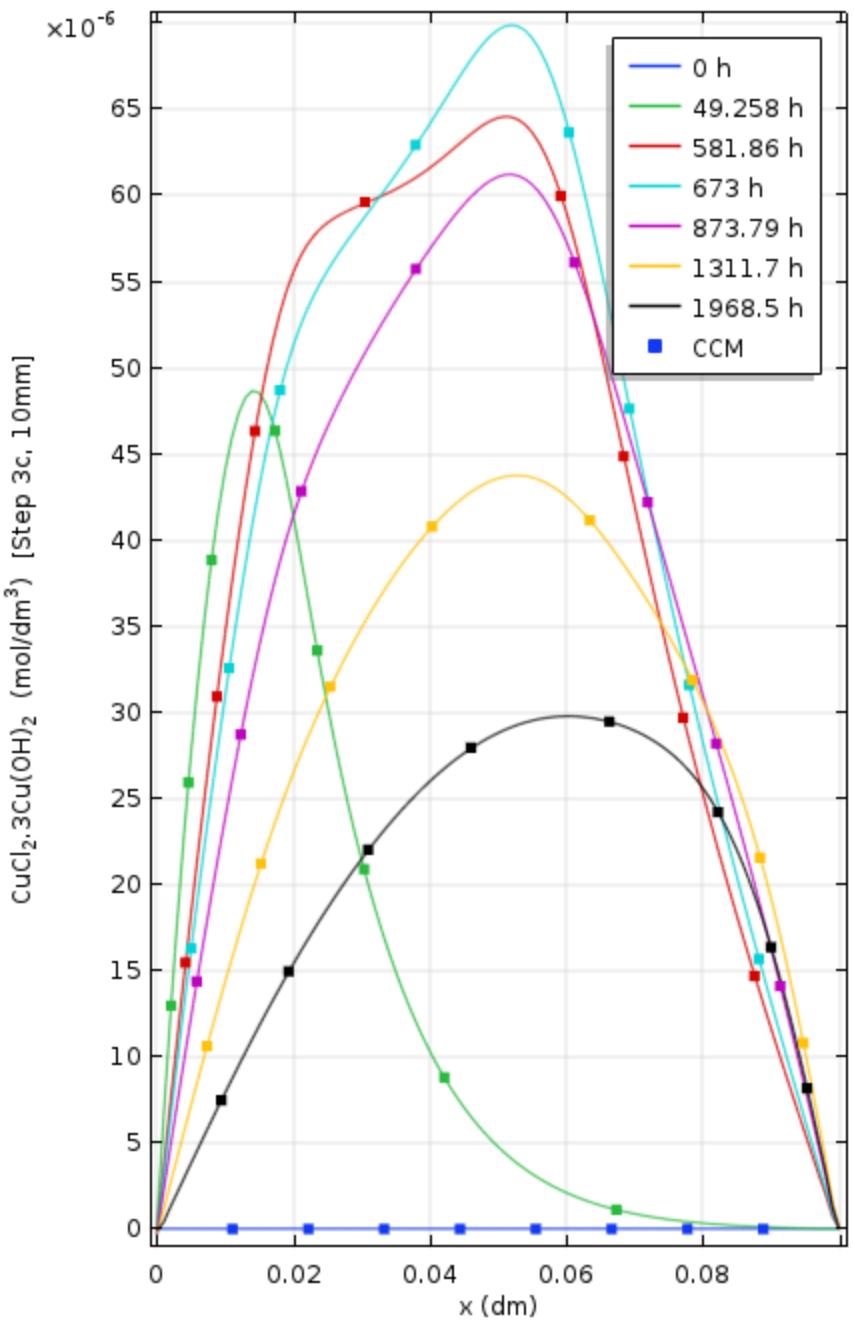

Figure B50: Concentration profile of paratacamite with distance for 10 mm, Step 3c

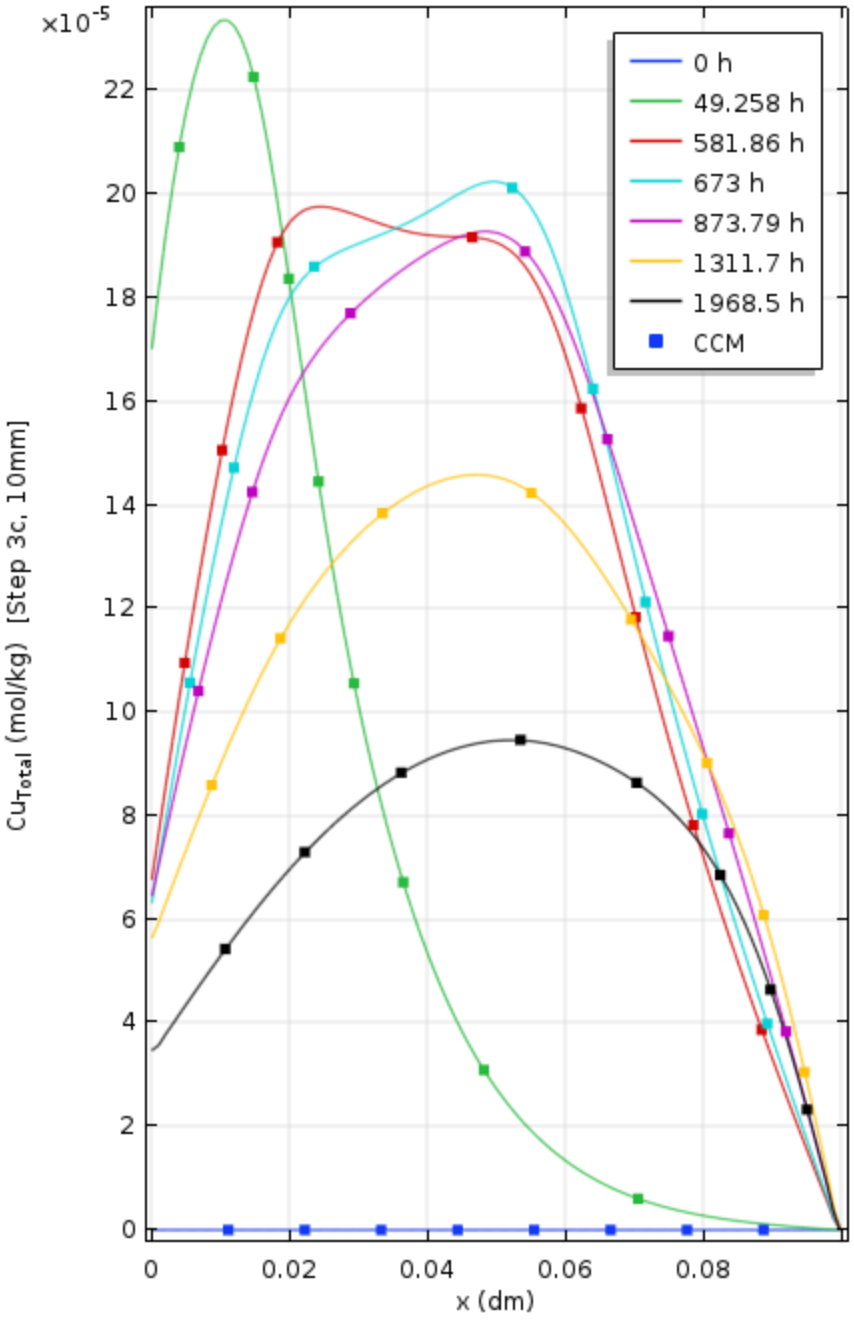

Figure B51: Concentration profile of total amount of copper ($CuCl_2^-$, Cu^{2+}, Cu_2O, $CuCl_2.3Cu(OH)_2$) with distance for 10 mm, Step 3c

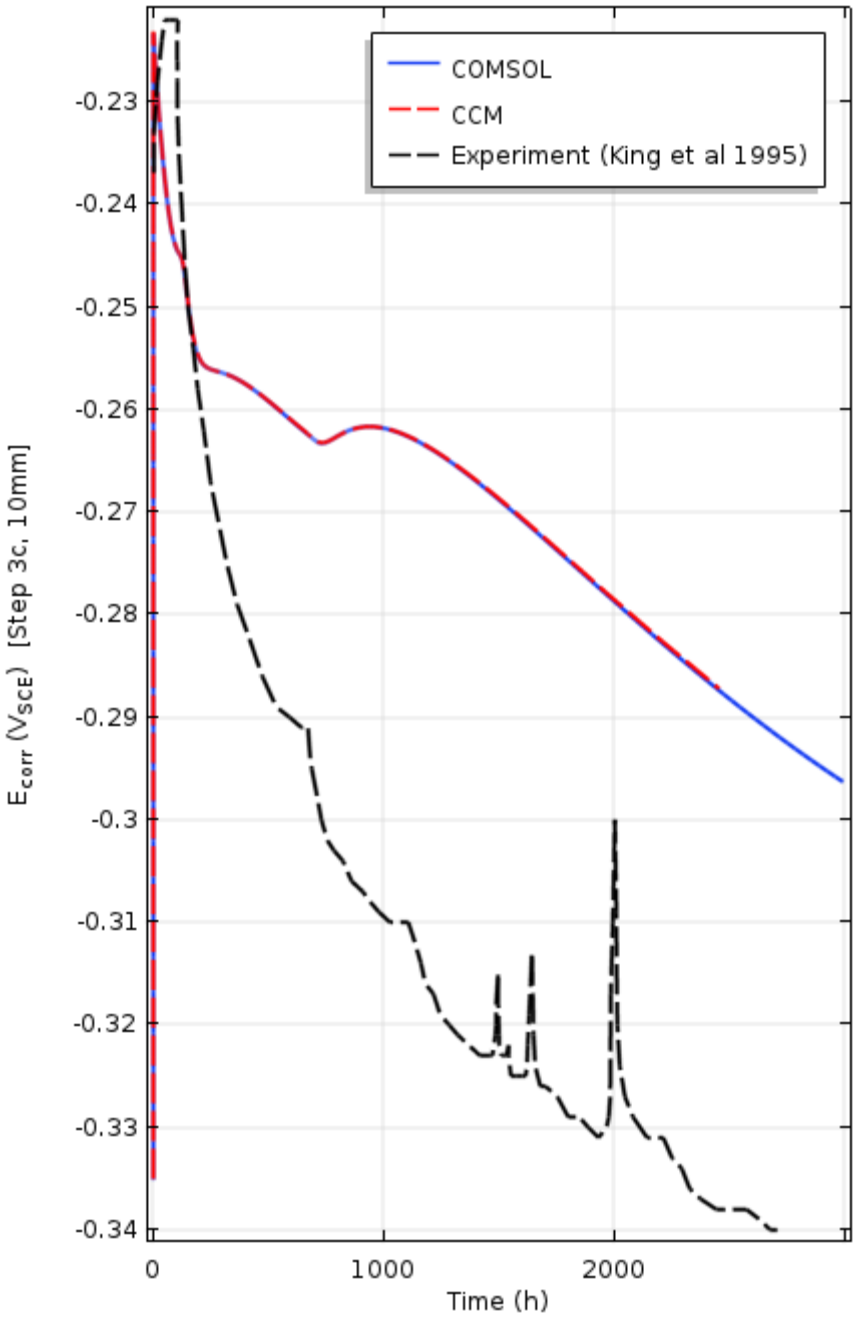

Figure B52: Variation of corrosion potential with time for 10 mm with changing oxygen concentration for Step 3c

APPENDIX C: SCREEN SHOTS OF MODEL DATA AND COMSOL

Parameter	Value or Expression	Description
alpha_c	0.5	cathodic transfer coefficient for the reduction of O2
alpha_d	0.5	cathodic transfer coefficient for the reduction of Cu2+
cCl_0	clf*1000[mol/m^3]	Initial concentration of Cl
cCu_ads_max_L1	0.3[mol/kg]*rho_d/epsA_L1	Maximum adsorbtion of copper
cCu2_ion_sat	4.3e-7[mol/dm^3]	Saturated concentration of Cu2+
cCuCl2_sat	3.4e-3 [mol/dm^3]	Concentration of CuCl2- in equilibrium with Cu2O
cFe2_ion	0 [mol/dm^3]	Fe concentration
cFe2_ion_sat	1e-5 [mol/dm^3]	Concentration of dissolved Fe(II) in equilibrium with Fe(II) ppt at 25 C
clf	0.657	Chloride activity coefficient
cO2_0	2e-4 [mol/dm^3]	Initial concentration of O2
D_Cl	2E-7 [dm^2/s]	Bulk diffusion coefficient of chloride
D_Cu2_ion	6e-8 [dm^2/s]	Bulk diffusion coefficient of Cu2+
D_CuCl2	6E-8 [dm^2/s]	Bulk diffusion coefficient of CuCl2
D_Fe2_ion	5e-8 [dm^2/s]	Bulk Diffusion coef of Fe(II) at 25 C
D_O2	1.7e-7 [dm^2/s]	Bulk diffusion coefficient of oxygen
E_a_0	-0.105 [V]	Standard potential for anodic dissolution of copper as CuCl2-
E_c_0	0.16 [V]	Standard potential for oxygen reduction
E_d_0	0.223[V]	Standard potential for Cu2+ reduction
Ecorr_initial	-0.25[V]	Initial value given for easier convergence
epsA_L1	epsE_L1+epsS_L1	Accessible porosity
epsE_L1	0.205	Effective porosity for Layer 1 or immediate layer
epsS_L1	0.205	Storage porosity for Layer 1 or immediate layer
k_a	3.3e-4 [dm^4/mol/s]	Combined electrochemical reate constant for the anodic dissolution of
k_bb	1.42e-3[dm/s]	Rate constant for the conversion of CuCl2- to CuCl
k_c	1.7e-9 [dm/s]	electrochemical rate constant for the reduction of O2
k_d	2e-8 [dm/s]	Rate constant for interfacial reduction of Cu2+
k_f2	1 [1/s]	Rate of hydrolysis of CuCl2- at 25 C
k_f3	1e-5 [1/s]	Forwared rate const for precipitation of paratacamite
k_f4	2e-6 [m^3/(mol*s)]	Rate constant for the adsorption of Cu2+ on Na bentonite at 25 C
k_f7	1 [1/s]	Rate constant for ppt. of Fe(II) solid at 25 C
k_r2	0.1 [1/s]	Rate constant for the dissolution of Cu2O at 25 C
k_r3	1e-6[1/s]	Reverse rate const for precipitation of paratacamite
k_r4	1e-8 [1/s]	Rate constant for the desoption of Cu2+ [Taken 1/100 th of original value in King (2016)]
k_r7	0.1 [1/s]	Rate constant for the dissolution of Fe(II) at 25 C
Length	10 [mm]	system length
M_Cu	63.546 [g/mol]	atomic mass of copper
max_element_size	6.7E-7[m]	m (default from "extremely fine")
n_0	4	number of electrons in reduction of O2
n_a	1	Number of electrons transferred during anodic dissolution of Cu
n_d	1	Number of electrons transferred during reduction of Cu2+
n_mew	1	porosity
rho_Cu	8.96e6 [g/m^3]	density of copper
rho_d	(1-epsA_L1)*rho_p	dry density
rho_p	2.7 [kg/dm^3]	particle density
S	1	Saturation
T	298.15 [K]	operating temperature
tau_L1	0.05	tortuosity for Layer 1 or immediate layer
tauEps	tau_L1*epsE_L1/epsA_L1	0.025 (Product used)

*Figure C1: Raw parameters used in the COMSOL model (**Most of the parameters are obtained from King (2016))***

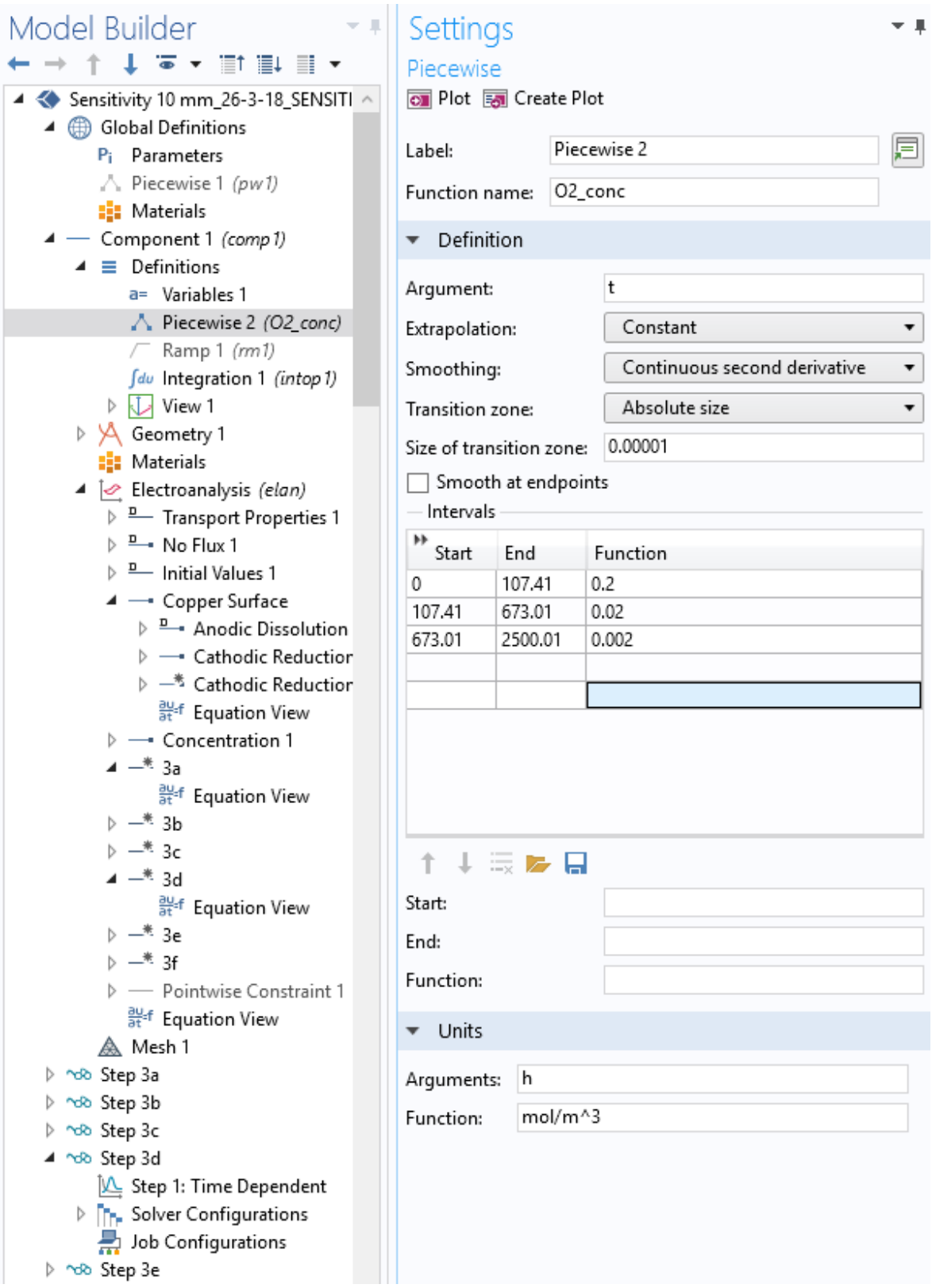

Figure C2: Oxygen concentration variation (10 mm)

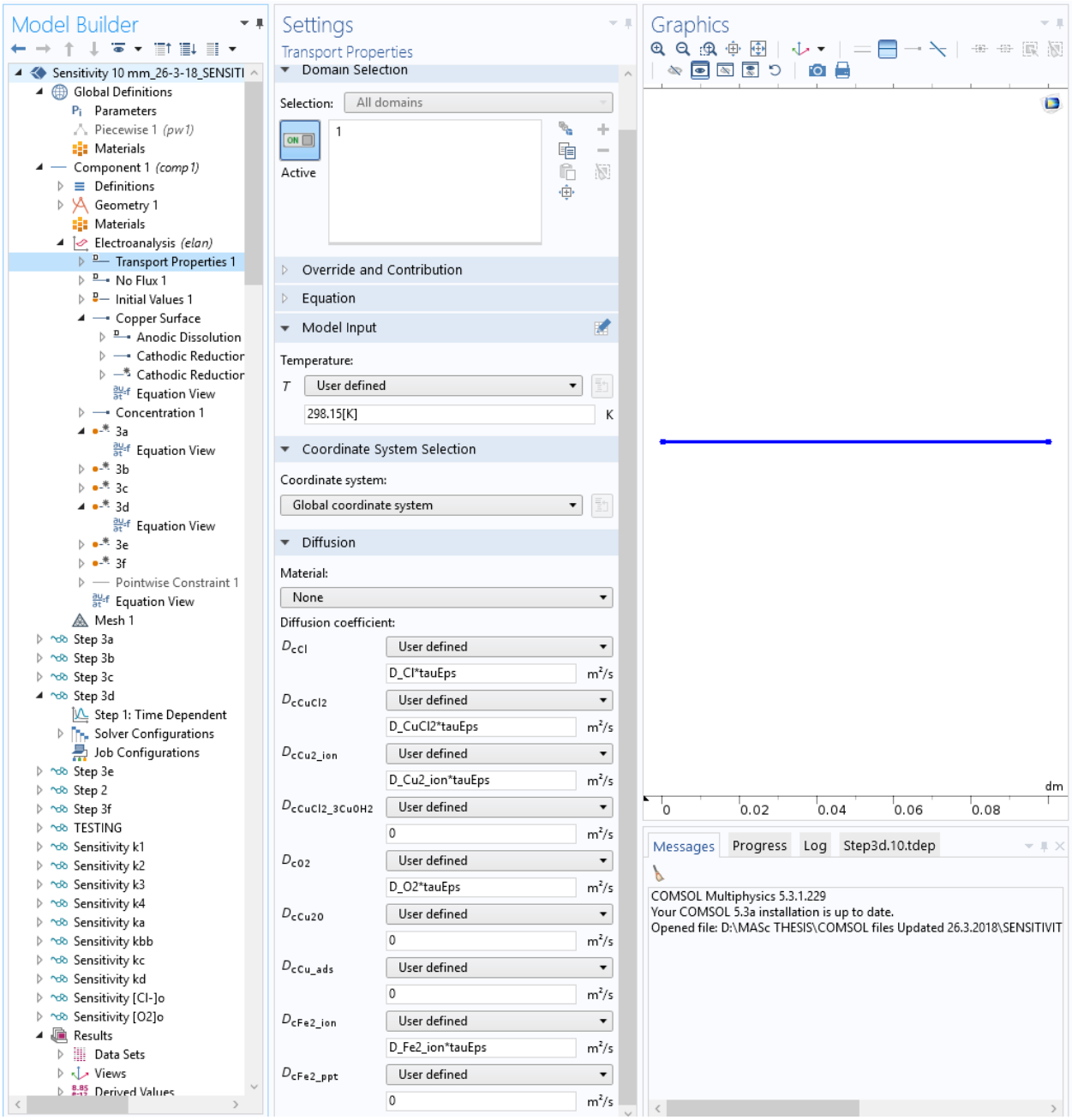

Figure C3: Diffusion constants incorporation

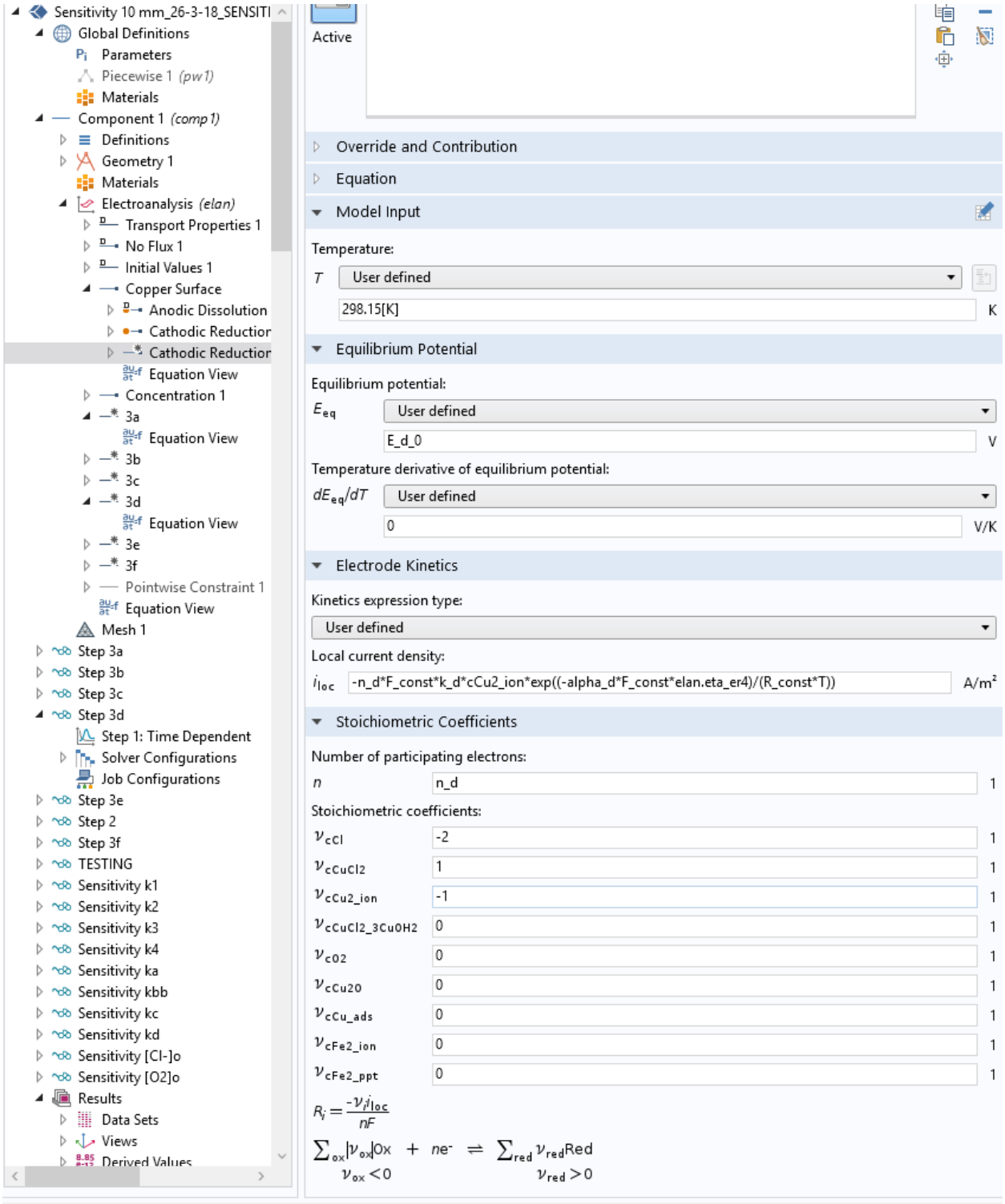

Figure C4: Butler-Volmer equations incorporation